Fundamental Studies of Selective Oxidation Reactions on Gold and Silver Surfaces

Fundamental Studies of Selective Oxidation Reactions on Gold and Silver Surfaces

A thesis presented
by

Cassandra Grace Freyschlag Siler

to
The School of Engineering and Applied Sciences
in partial fulfillment of the requirements
for the degree of
Doctor of Philosophy
in the subject of

Engineering Sciences

Harvard University
Cambridge, Massachusetts
June 2014

Thesis advisor

Cynthia Friend

Author

Cassandra Grace Freyschlag Siler

Fundamental Studies of Selective Oxidation Reactions on Gold and Silver Surfaces

Abstract

This thesis explores the fundamental chemistry of selective oxidation reactions on gold and silver surfaces, developing a predictive framework for oxidative catalysis, which is crucial for rational design of catalytic systems. We begin with an introduction covering the history of precious metal catalyst development, with emphasis on the roles of silver and gold (Chapter 1). Next, we explore selectivity control for oxidative reactions on gold. Specifically, we address the role of coadsorbed oxygen with respect to stability and selectivity control in the reaction of adsorbed acetate (Chapters 2 and 3), the importance of van der Waals forces in controlling the selectivity for cross-coupling reactions (Chapter 4), and the influence of $-CF_3$ on alkoxide stability on gold (Chapter 5). Further, we study various oxidative coupling and partial oxidation reactions on silver. In each case we elucidate reaction mechanisms, with attention to control of reaction selectivity. First, we establish oxidative coupling between dimethylamine and formaldehyde to form dimethylformamide (Chapter 6). Then we explore the role of hydroxyl in oxidative reactions silver, establishing its reactivity as a nucleophile in reaction with formaldehyde (Chapter 7). Finally, we directly compare the reactivity of gold and silver, in the acetylation of dimethylamine using acetaldehyde (Chapter 8). Appendices are included which investigate the ox-

idation of dimethylamine on silver (Appendix A), selectivity control for alcohol and aldehyde coupling on silver (Appendix B), and reactivity of hydroxyl on silver as a Brønsted base (Appendix C). A MATLAB code, which was developed for quantitative analysis of temperature program reaction spectroscopy experiments is also presented (Appendix D), as well as Supporting Material (Appendix E).

Contents

Citations to Previously Published Work

Parts of this dissertation cover research reported in the following articles:

1. Siler, C. G. F.; Cremer, T.; Rodriguez-Reyes, J. C. F.; Friend, C. M., Madix, R. J. "Switching Selectivity in Oxidation Reactions on Gold: The Mechanism of C-C vs C-H Bond Activation in the Acetate Intermediate on Au(111)," *ACS Catalysis*, **2014**, *4*, 3281-3288.

2. Rodriguez-Reyes, J. C. F.; Siler, C. G. F.; Liu, W.; Tkatchenko, A.; Friend, C. M.; Madix, R. J. "van der Waals Interactions Determine Selectivity in Catalysis by Metallic Gold," *Journal of the American Chemical Society [Just Accepted]*, DOI:10.1021/ja506447y. Published online, Aug. 28, 2014.

3. Cremer, T.; Siler, C. G. F.; Rodriguez-Reyes, J. C. F.; Friend, C. M., Madix, R. J. "Tuning the Stability of Surface Intermediates Using Adsorbed Oxygen: Acetate on Au(111)" *Journal of Physical Chemistry Letters*, **2014**, *5*, 1126-1130.

4. Siler, C. G. F.; Xu, B.; Madix, R. J.; Friend, C. M. "Role of Surface-Bound Intermediates in the Oxygen-Assisted Synthesis of Amides by Metallic Silver and Gold" *Journal of the American Chemical Society*, **2012**, *134*, 12604-12610.

5. Freyschlag, C. G.; Madix, R. J.; "Precious Metal Magic: Catalytic Wizardry" *Materials Today*, **2011**, *14*, 134-142.

6. Zhou, L.; Freyschlag, C. G.; Xu, B.; Friend, C. M.; Madix, R. J. "Direct selective oxygen-assisted acylation of amines driven by metallic silver surfaces: dimethylamine with formaldehyde" *Chemical Communications*, **2010**, *46*, 704-706.

The author also contributed to the following articles, which are not included in this thesis:

1. Xu, B.; Siler, C. G. F.; Madix, R. J; Friend, C. M. "Ag/Au Mixed Sites Promote Oxidative Coupling of Methanol on the Alloy Surface" *Chemistry– A European Journal*, **2014**, *16*, 4646-4652.

2. Xu, B.; Haubrich, J.; Freyschlag, C. G.; Madix, R. J; Friend, C. M. "Oxygen-assisted cross-coupling of methanol with alkyl alcohols on metallic gold" *Chemical Science*, **2010**, *310*, 310-314.

Acknowledgments

First, I want to thank my advisor, Cynthia Friend, who has been an immense support and guide in all matters toward becoming an independent scientist. I also thank Robert Madix, who was in practice a second advisor to me. His depth of knowledge and insight have been an invaluable resource. It has been a privilege to work with them and with the Friend group as a whole.

Thank you to my committee, Professors Ted Betley, Joanna Aizenberg, and Mike Aziz. Thank you for your support, feedback, and for taking the time to read this thesis and evaluate my defense.

Thanks to the other members of the Friend group, particularly those with whom I collaborated early on– Dr. Ling Zhou, Dr. Bingjun Xu, Dr. Derek Butcher, and Mr. Josh Klobas. Thanks to Dr. Kara Stowers for her pep talks and friendship. Completion of this thesis officially marks "success!" Thanks to Dr. Stephen Jensen, for friendship and advice over countless hours together in the lab. And to the other Friend group members over the years for making it an enjoyable place to work and develop new ideas.

I could not have made this journey without the support of my family and friends. Thanks to my parents and sisters, for their support and encouragement, especially in my first year and in times of broken instrumentation. Thanks to the non-chemist Harvard friends, keeping me sane. Especially to Clarissa and Andy for not only being such great friends but also for often housing us as we traveled between Cambridge and Seattle. And thanks to my Highrock Church family, for keeping me grounded and giving me perspective.

Last, but certainly not least, I want to thank my husband, Nick. I can't thank you enough– For taking care of our son for the last several months so I could finish, for help writing code and type-setting this thesis, and for always believing in me. And thank you to my son, Anson, for being such a source of joy in the last year.

I also gratefully acknowledge financial support from the Department of Energy Graduate Fellowship Program (DOE-SCGF) administered by ORISE-ORAU under contract no. DE-AC05-06OR2310, and the Harvard University Center for the Environment. Both were fantastic programs that significantly enriched my graduate experience.

To Nick and Anson– you are my favorites.

Chapter 1

Precious Metal Magic: Catalytic Wizardry

1.1 Abstract

Magic: 'Influencing the course of events by using mysterious or supernatural forces.' Precious metals are alluring and somewhat 'magical' because of their inactivity toward chemical reactions. Since the industrial revolution, however, mankind has realized that precious metals have power to influence the course of chemical events–through catalysis. A catalyst is defined as a substance that facilitates a chemical transformation without itself being consumed in the process; this power has a mysterious, almost magic-wand character. In this review we explore precious metals catalysis through the wide-angle lens of historical development and the atomic scale microscope of recent discoveries. Fundamental understanding of underlying mechanisms for catalytic oxidation processes reveals the magic and transforms the

use of precious metals from instruments of adornment, trade and Edisonian industrialization, to key players in a new era of catalysis by design with potential for environmentally benign chemical processing.

This paper was published in *Materials Today*, **2011**, *14*, 134-142.

1.2 From then to now

New eras have dawned and the course of history has changed, simply due to mastery of the elements. The Iron Age, Bronze Age, and Nuclear Age are obvious examples, but the rise of industry through synthetic manipulation of the elements and more recent advances in medicine and nanotechnology bring us to yet another source point in history, brimming with potential. Surprisingly, by clever utilization of their chemical "inertness," chemistry of precious metals has emerged as one of the exciting frontiers for advanced understanding and applications, particularly in catalysis.

Shiny, malleable, and resistant to corrosion, gold has been the most coveted precious metal since the time of the Pharaohs. In addition to its well-known uses in currency and jewelry, metalworkers found that the properties of gold were more than meets the eye. For example, gold alloy nanoparticles (defined as particles from 1-100 nm in size) in the glass of the famous Lycurgus cup, c.a. 4th century AD, cause the color to change from green for reflected light (Fig. 1.1a) to red for transmitted light (Fig. 1.1b) [1]. Nanoparticles of another precious metal, silver, are responsible for the gold luster of medieval middle-eastern and renaissance Italian pottery [2]. Gold nanoparticles lend red color to medieval stained glass, and gold has even been consumed for its alleged healing effects, the earliest occurrence being in ancient China,

c.a. 2500 BC [3].

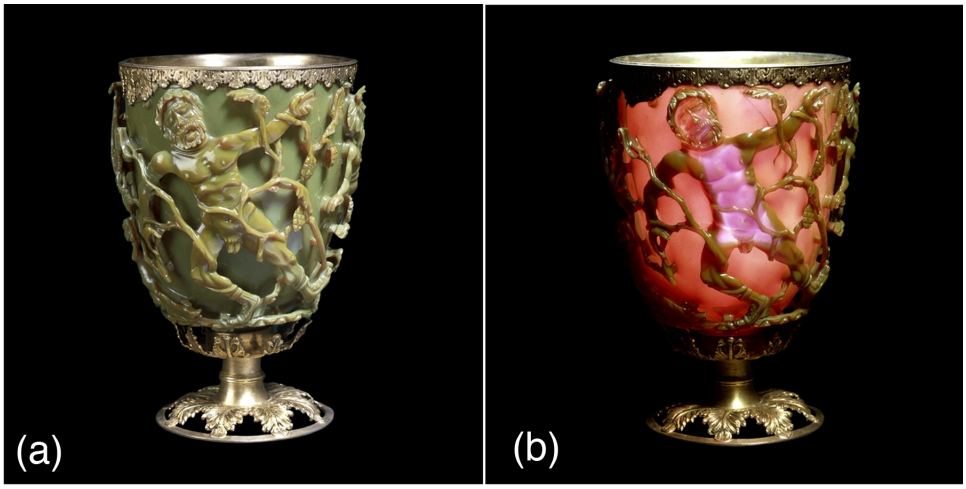

Figure 1.1: The Lycurgus cup is green when viewed with reflected light (a), and red when light is transmitted through it (b), due to precious metal (Au/Ag alloy) nanoparticles within the glass. ©Trustees of the British Museum.

1.2.1 First player: Platinum

Despite being one of the last precious metals to be manipulated (due to its higher melting point), platinum was nevertheless one of the first to be used for catalysis. Platinum has been a common catalyst since the 1820s, when Dobereiner invented a small "tinderbox" [4]. In this pre-match device, hydrogen was generated in situ and reacted with oxygen over a small supported platinum catalyst to yield a flame. In 1831, Peregrin Phillips patented the use of platinum as a catalyst for production of sulfuric acid via the oxidation of SO_2 in the "contact process" [5]. This innovation replaced the "lead chamber process" and enabled economical production of more concentrated sufuric acid, which was critical for the growing chemical industry [6]. However, platinum catalysts suffered from poisoning and were replaced in the

early 1900s by vanadium oxides with alkali metal oxide promoters, which are now the standard catalyst for the contact process [7].

With the advent of the internal combustion engine and the need for refining crude oil for fuel in massive quantities, catalytic cracking (breakdown of heavy hydrocarbons to readily combustible molecules) became widespread. Platinum nanoparticles supported on alumina became the catalytic material of choice for transforming alkanes into branched alkenes and aromatics–a process known as "catalytic reforming" [4]. This technological advance provided cheap transportation that has reshaped cultures throughout technologically advanced societies. The platinum enables dehydrogenation of the larger organic species and the acidic alumina on which it rests facilitates isomerization to form the higher octane organic molecules. Adding either rhenium or iridium to the platinum enhances activity, because the added element breaks the C-C bonds in carbonaceous deposits, which would otherwise poison the platinum surface [4]. As platinum was used in this fashion to increase the octane rating of fuel entering the engine, it would also be used as the basis of the catalytic converter to clean up the gases exiting the engine–a veritable "jack of all trades." This use represents a first step for catalysts for environmental purposes.

The catalytic converter is one of the best-known uses of catalysis in modern society. Due to incomplete combustion of the fuel, its sulfur content, and the equilibrium between oxygen and nitrogen attained at the high temperature of the internal combustion engine, the exhaust includes a toxic mixture of CO, hydrocarbons (C_xH_x), NO_x, and SO_x, along with H_2O and CO_2. The sulfur oxides are eliminated by desulfurization of the fuel in its manufacture. However, removal of the remaining gases posed

a seemingly insurmountable problem. Fortunately, the CO and C_xH_x can be oxidized and NO_x simultaneously reduced using a so-called "three way" catalyst, yielding CO_2, H_2O, H_2, and N_2 [5]. Bonds are broken on the precious metals, and then the atoms recombine to form CO_2, H_2, N_2, and H_2O (reactions 1.1-1.4) [8].

$$NO \longrightarrow N + O \quad (Rh) \tag{1.1}$$

$$O_2 \longrightarrow O + O \quad (Rh/Pd/Pt) \tag{1.2}$$

$$CH \longrightarrow C + H \quad (Pd/Pt) \tag{1.3}$$

$$CO + O \longrightarrow CO_2 \quad (Pd/Pt) \tag{1.4}$$

The standard three-way catalyst consists of precious metals Rh and Pt and/or Pd on an oxide or mixed-oxide monolith support. The Rh acts to promote NO dissociation, leading to N_2 formation, while Pt and Pd combust CO and C_xH_x to CO_2 and water [8]. To the layman this technological advance is apparently "magical." It is a triumph of the science of catalysis. One remaining challenge is the 'cold-start' problem: controlling the unwanted emissions produced before the catalytic converter reaches operational temperatures [8].

1.2.2 Silver comes in second

Because we live in an oxygen-rich atmosphere, the conversion of natural gas and other hydrocarbon sources to useful materials via chemical intermediates produced by partial oxidation was a "natural" pursuit. Partial oxidation and epoxidation catalysis using metallic silver emerged in the early 1900s. Silver catalysts are used industrially in the oxidation of methanol to formaldehyde and in the epoxidation of ethylene [4].

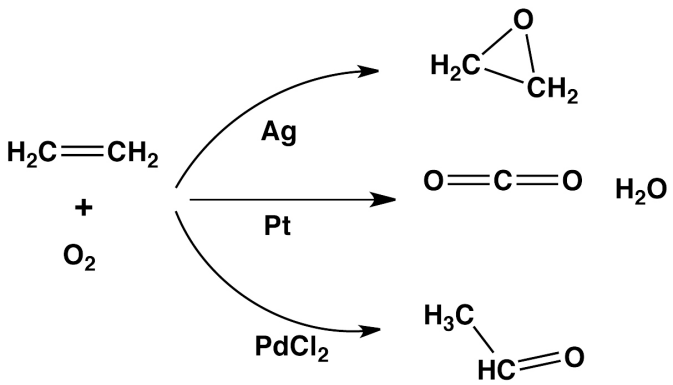

Figure 1.2: Ethylene oxidation over Ag, Pt, and with $PdCl_2$ has extremely different selectivities, resulting in the major products being ethylene oxide, CO_2 and H_2O, and acetaldehyde, respectively. Based on a figure appearing in [4].

Oxidation of ethylene is a good example of the importance of catalyst selectivity, as a different catalyst yields a dramatically different major product (Fig. 1.2) [4]. When ethylene is oxidized over platinum, since platinum facilely cleaves C-H bonds, full combustion occurs, and the products are CO_2 and H_2O. Palladium salts afford the partial oxidation product, acetaldehyde. Silver, however, uniquely yields ethylene oxide, a precursor to polyester materials and ethylene glycol for antifreeze. The origin of this singular capacity of metallic silver lies in the inability of silver itself to break the C-H bond in ethylene, the relatively weak binding of adsorbed atomic oxygen to the silver surface and the ability of this surface-bound oxygen to attach itself to the C-C double bond in ethylene–a unique confluence of circumstances. Moreover, this balance is so delicate that propylene (adding one more carbon to ethylene) undergoes complete combustion [9]. Modern model studies under well controlled conditions employing methods of surface physics in ultra high vacuum studies have led to understanding of the kinetics and mechanisms of the reactions on silver surfaces [10,11].

Both the methanol oxidation [12] and ethylene epoxidation [13] systems have been microkinetically modeled, as well as that of the active oxygen on silver [14], aiding in understanding of the molecular-level processes in industrial conditions. As research has continued, the range of catalytic reactions that precious metals facilitate has increased dramatically, particularly with metallic gold, the relative newcomer to catalysis.

1.3 Gold is now green: a more current environmental currency

The recent interest in gold as a catalyst was ignited by the discovery of Haruta et al. that gold nanoparticles on reducible oxides were effective catalysts for CO oxidation at low temperatures [15]. While gold, silver, and platinum will presumably always be used to make jewelry, their abilities as chemical agents to direct reactions via catalysis has potential for immense impact. The chemical industry produces large amounts of waste and consumes about 20% of the energy in the U.S. industrial sector [16], and the average chemical company emits more CO_2 than companies in the other six S&P sectors combined [17]. The demand for green catalysis–utilizing catalysts that reduce the environmental impact of chemical processes–requires selective, stable catalysts that function in a benign medium and can be easily recovered [18]. It has been suggested that low-temperature reactions on precious metals–gold in particular–may be part of the solution [19, 20]. Here, we will give an overview of the catalytic applications and strengths of the precious metals, with emphasis on heterogeneous

catalysis. Then we will focus particularly on fundamental understanding of the metals that have captured man's attention from the beginning: gold, and its fellow coinage metal, silver.

1.3.1 Magicians with different tricks

The catalytic 'bag of tricks' is revealed by modern research to be somewhat different for each precious metal, and they exhibit distinct patterns that can be used to predict and design new catalytic systems. Because such a myriad of transformations is desired in the field of catalysis, this process requires varying levels of selectivity and specificity of the catalyst to cleave bonds of one type and reform others. One useful way to think about the differences between precious metals is to classify them in terms of bond-breaking capability, as demonstrated for the clean metals in Fig. 1.3. This list is meant to be representative, not exhaustive.

The supposedly 'inert' gold catalyzes a surprising variety of reactions [20], which include hydrogenation, selective partial oxidation reactions [21] and nucleophilic addition to pi systems. As depicted in Fig. 1.4, selective oxidation of alcohols by gold leads to formation of aldehydes and ketones, as well as esters [22, 23]; and selective oxidation of amines yields nitriles and aldehydes [24]. Gold nano-clusters catalyze the intra-molecular cyclization of amines and alkenes [25]. On metallic gold, coupling reactions between alcohols and aldehydes (either externally introduced or made in situ) result in ester formation [22,26,27]. In addition to epoxidation of propylene [28] and styrene [29], gold also facilitates the aziridination of olefins by the direct addition of adsorbed NH [30]. The capabilities of gold for selective oxidation processes using

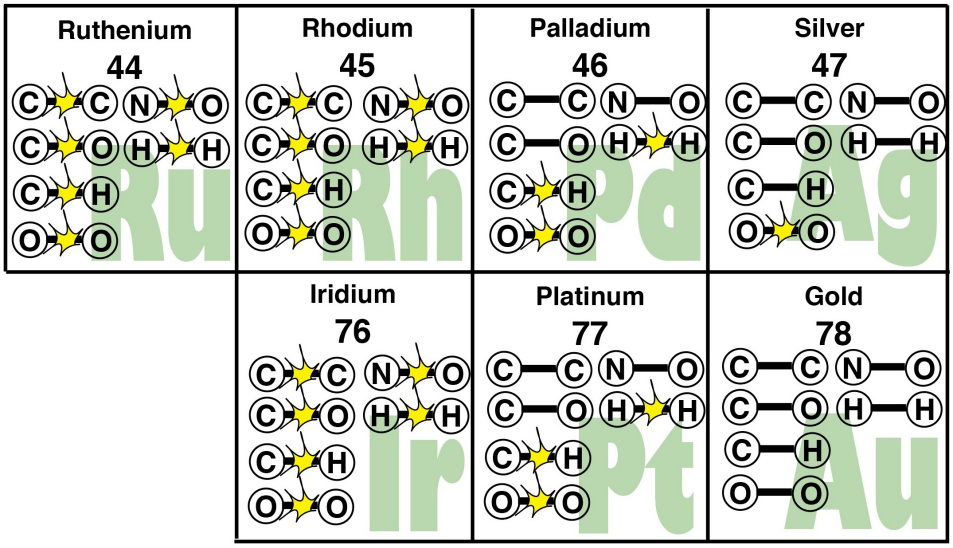

Figure 1.3: The precious metals used in catalysis can be "ranked" by their bond-breaking abilities. The capacity for each metal for breaking specific chemical bonds is indicated. Note the increasing "inertness" in progressing from left to right in this series.

O_2 as the oxidant make it a green competitor for production of commodity chemicals such as sodium glycolate, sodium lactate, and sodium gluconate from cheap starting reagents, avoiding the use of chlorinated reagents and hydrogen cyanide [21]. Gold outperforms both palladium and platinum catalysts for diol partial oxidation, with 98% selectivity and 1000-35000 TOF (h^{-1}) for the oxidation of ethylene glycol to ethyl glycolate [21].

1.4 De-mystifying the magic

Just as magic tricks captivate and intrigue audiences who desire to understand how the illusions are performed, so catalysis raises the questions 'how?' and 'why?' from the chemist. Since the mid-late 20th century, the development of new surface

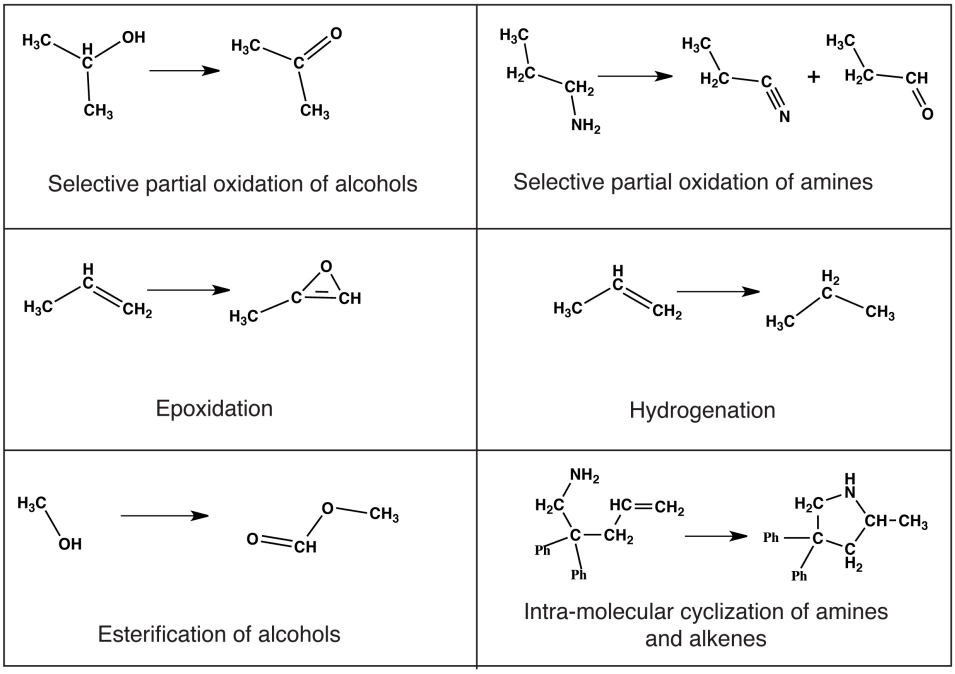

Figure 1.4: Gold facilitates a wide variety of reactions, the examples below are representative of this variety, and have been observed in solution and gas phase catalysis.

science and materials research techniques has enabled researchers to provide fundamental answers to those questions and to gain greater understanding not only of precious metals as materials themselves and what they do, but how they do it. This understanding can lead to the design of new tricks with ever more impressive results.

One of the most powerful tools for dissecting this chemical "magic" is that of temperature programmed reaction spectroscopy (TPRS). In this technique, the desired reactants are placed on a metal crystal surface of controlled structure and composition in ultra high vacuum at a temperature sufficiently low that initially no reactions take place. Then, with the crystal in front of a multichannel mass spectrometer, the crystal is heated linearly with time, leading to the activation of the various reaction channels available to the reactants. Products evolve from the surface at temperatures characteristic of the activation energies of their formation [31, 32]. Multiple products can be monitored at the same time, enabling deciphering of the entire reaction. In combination with isotopic labeling, this method reveals step by step the processes of bond rupture and reformation of the catalytic transformation. It can be complemented by spectroscopic techniques such as vibrational [33] and photoelectron spectroscopies [34] in order to identify intermediates on the surface, and follow the course of the molecular rearrangements during the reaction. In some cases reactants, products and reaction intermediates can be directly imaged using scanning tunneling microscopy (STM) [34, 35].

1.4.1 Oxygen: the 'breath' of precious metal catalysts for synthesis

Many important precious metal catalytic processes are oxidative, so oxygen, both atomic and diatomic, has been the subject of much fruitful academic debate and discovery in the surface science of catalysis. On Pd, Pt, and Ag molecular oxygen readily dissociates to form surface-bound atomic oxygen. When supplied from another source, such as a metal oxide or a stronger oxidant, such as ozone, atomic oxygen binds to Au surfaces. On specific single crystals surfaces of these metals, this oxygen assumes different structures and has different binding strengths (Fig. 1.5).

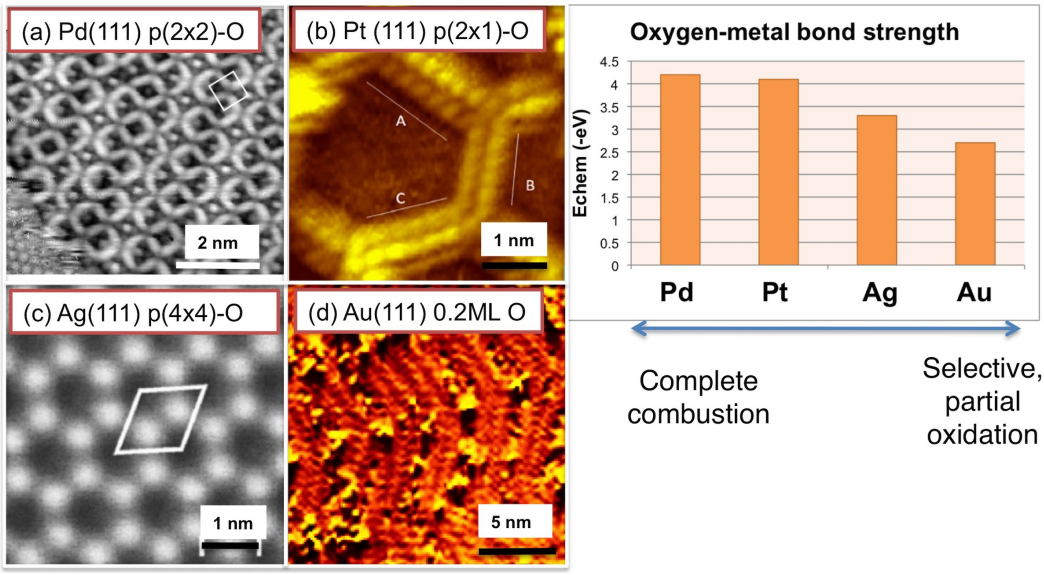

Figure 1.5: Representative atomically resolved structures of oxygen on (a) Pd [36], (b) Pt [37], (c) Ag, and (d) Au [38] that are active for oxidation catalysis. In most cases atoms from the metal surface are enlisted to form a two-dimensional metal oxide. The energy for the chemisorption of oxygen is taken from [39]. Fig. (a) reprinted with permission from [36]. ©2002 by the American Physical Society. Fig. (b) reprinted from [37] with permission from Elsevier. Fig. (d) reprinted with permission [38]. ©2006 American Chemical Society.

The oxygen/precious metal interaction is one of great complexity and importance, as the oxidative catalysis of precious metals requires binding of oxygen to the surface. For an in-depth discussion of the theory of adsorption of oxygen on precious metals, see Hammer and Norskov [39]. On Pt and Pd dioxygen dissociates and binds readily, forming well-ordered structures [36,37,40]. Since these metals readily activate C-H bonds in hydrocarbons, this oxygen can react with hydrocarbon fragments on the surface, usually leading to complete combustion. Oxidation occurs readily when the oxygen surface concentration is less than one monolayer, but enhanced reactivity has also been reported for a thin surface oxide of palladium [41]. On Au and Ag oxygen is bound less strongly. Oxygen dissociation occurs on both Ag(110) and Ag(111) single crystal surfaces, forming an ordered, less dense over-layer than on Pt and Pd. On both of these surfaces, silver atoms are recruited by the oxygen in order to form a 2D surface oxide with its own specific stoichiometry [42, 43].

Gold is more 'inert' to reaction because of the low oxygen dissociation probability of molecular oxygen with the surface ($\ll 10^{-6}$). However, O_2 is used as the oxidant in reactions with gold nanoparticles with [44] and without [45] an oxide support, and it has been shown that identical reactions occur due to atomic oxygen on gold single crystal surfaces. Hence, there is prima facia evidence that the reactive species is adsorbed atomic oxyen. Using ozone exposure to achieve $O_{(a)}$ on gold in ultra high vacuum [46] the structure of $O_{(a)}$ on gold is disordered, with the oxygen adatoms resulting in a release of gold atoms and small nanoparticle structures on the surface. When oxidized at a higher temperature, less active, more highly structured "2D-oxide" structures form [38]. In the presence of adsorbed surface oxygen on gold,

a new world of chemistry unfolds, as we will see below.

1.4.2 CO oxidation:

Catalytic CO oxidation by precious metals is particularly important for environmental protection, in ameliorating truck and auto exhaust and for the prevention of poisoning of fuel cell electrodes. As one of the simplest test reactions, it has also played a significant role in the development of the fundamentals of reactions on precious metal surfaces. First, we will address CO oxidation on Pt, which is the basis of the automotive catalytic converter, and then we will discuss the remarkable development in the oxidation of CO on gold nanoparticles supported on reducible oxides, which opened the door to radically new directions in catalysis by gold.

CO oxidation on Pt proceeds by reaction of coadsorbed CO and atomic oxygen. Below a critical steady state reaction temperature the surface can become saturated with CO, so that dissociation of dioxygen cannot proceed, and the adsorbed CO poisons the surface. Above this minimum temperature, which depends on the metal, the reaction proceeds readily [49]. By any measure this reaction is extremely facile, because platinum readily dissociates dioxygen, and binds CO in molecular form, bringing the atomic oxygen and CO in close proximity to facilitate reaction with a very low energy barrier (Fig.1.6a) [47]. Under certain conditions of pressure and temperature dramatic periodic oscillations in the rate occur, leading to time varying rates of formation of CO_2(Fig. 1.6b) [48]. These oscillations are the result of two dimensional concentration inhomogeneities across the surface. Their experimental elucidation was a significant aspect of the research of Prof. Gerhard Ertl, the Nobel Laureate in

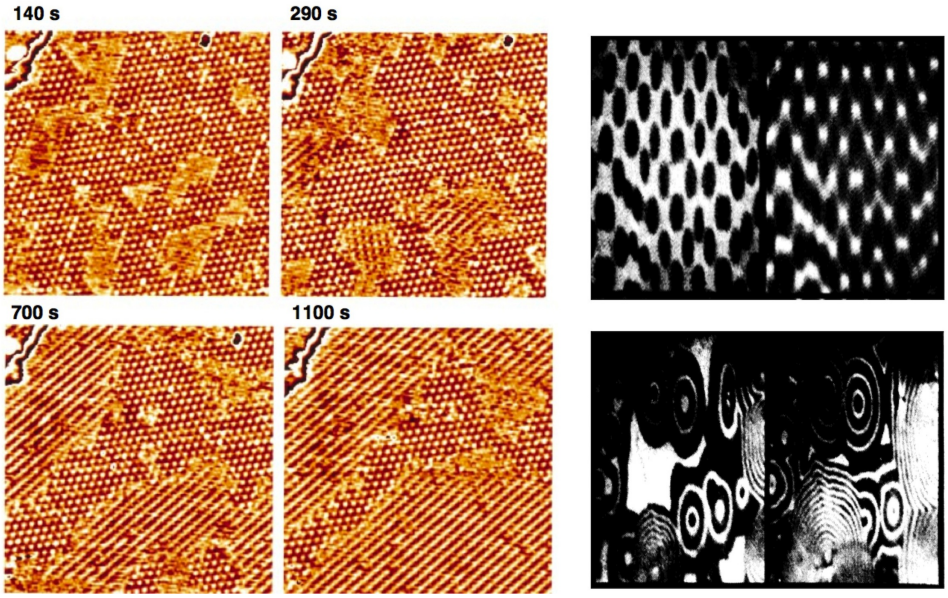

Figure 1.6: (a) STM shows CO oxidation on O/Pt(111) over time. The (2x2)-O (darker areas) and the c(4x2)-CO (lighter areas) reconstructions come into contact to oxidize CO to CO_2 at the interface between structures [47]. (b) Photoemission electron microscopy (PEEM), shows reaction wave fronts, in which the oxygen-covered areas are dark, and the CO covered areas are bright. These wave fronts can take both propagating (bottom) and standing (top) wave forms, depending on the conditions [48]. Fig. (a) from [47]. Reprinted with permission from AAAS. Fig. (b) reprinted with permission from [48]. ©1990 by the American Physical Society.

Chemistry in 2007.

CO can also be oxidized by metallic gold on oxide supports. Though this fact was well documented in the 1970's, it was not until the mid 90's that it was shown that CO could be oxidized at temperatures as low as -70^{o}C using reducible oxides as supports for gold nanoparticles [15]. While it is clear that changing the support changes the rate of this reaction, the mechanism for oxygen activation and spillover is still under investigation. Gold nanoparticles were also shown to be active for NO reduction by hydrocarbons.

1.4.3 Epoxidation:

As discussed above, ethylene epoxidation is not only an important industrial process, but also a delicate one. It has been extensively studied, but under ultra high vacuum conditions, ethylene desorbs at temperatures below which reaction proceeds, prohibiting the reaction from being studied traditionally. This obstacle was circumvented by the use of norbornene, which possesses a C-C double bond with the appropriate structure to allow reaction with adsorbed atomic oxygen, confirming that direct epoxidation of alkenes by adsorbed atomic oxygen is the important reaction, even for ethylene [50]. It is possible, however, to interrogate the nature of the reactive intermediates formed in the ethylene epoxidation by looking at the reaction in reverse. By adsorbing ethylene oxide at 250 K, an intermediate forms on the surface and re-desorbs as ethylene oxide at 300 K [51]. This intermediate is proposed to be an oxametallacycle intermediate, where the metal, oxygen, and carbon atoms form a cyclic structure [51]. In order to further study this intermediate as well as the oxida-

tion of higher molecular weight olefins on silver, styrene oxidation has been studied on both the Ag(110) and Ag(111) surfaces (Fig. 1.7) [52]. On Ag(111) it was found that upon addition of styrene to an oxygen-covered silver surface, an oxametallacycle intermediate forms, which leads to styrene oxide formation [53]. On Ag(110) the dominant path is to form a combustion intermediate which leads to other products. However, when Cs is added as a promoter, styrene oxide is the dominant product [54].

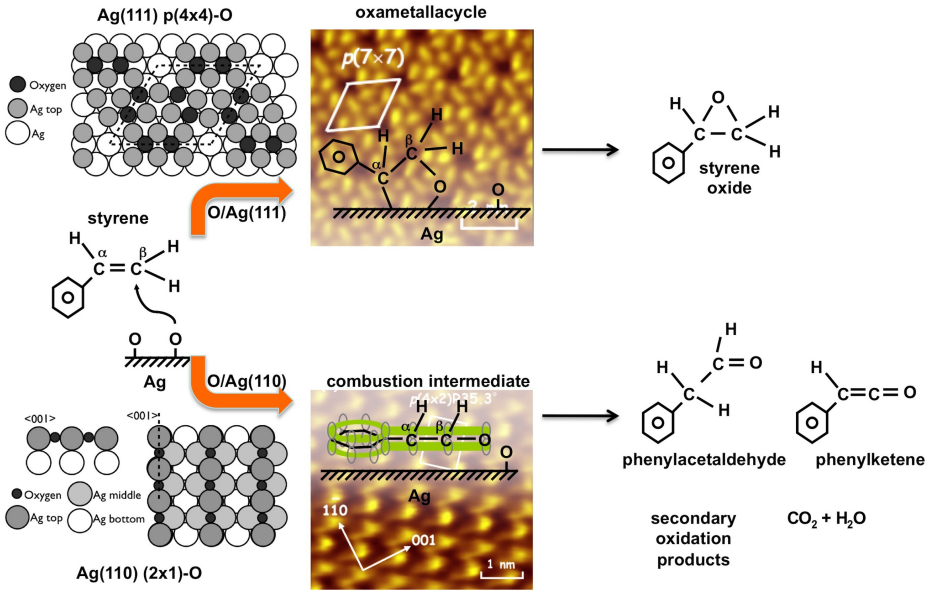

Figure 1.7: The dominant pathways for styrene oxidation on O/Ag(111) and O/Ag(110). The O/Ag (111) and (110) structures are shown to the left, after [42, 43], respectively. STM images from [52]

Selective epoxidation of propene is also very desirable for chemical and pharmaceutical industry, and cannot be performed by silver, because the C-H bonds of the methyl group are readily attacked by surface-bound oxygen. Industrially, propene oxide is produced in a wasteful two-stage process [28]. A direct catalytic oxidation route had not been possible until a discovery by Hayashi et al [55]. They found that in the presence of both H_2 and O_2, gold supported on TiO_2 can facilitate a direct

oxidation in the vapor phase, with selectivity of over 90%. It was found that TiO_2 must be used as the support, and that H_2 enhanced the selectivity. It is essential that more fundamental research be done to separate the mechanistic roles of the nanoparticles and the supports, so that a better understanding of principles needed to design operating conditions for the reaction can be realized.

1.5 Novel coupling reactions on Au and Ag:

Though molecularly simple reactions such as CO oxidation and epoxidation reactions are of technological importance to our society, more complex synthesis reactions create the chemical intermediates that are used to form a vast number of useful retail products. Again the precious metals, particularly Au and Ag can play a substantial role as catalysts for such reactions, because, perhaps paradoxically, they are basically inert toward reactions with most molecules. However, for oxidative reactions on Ag and Au, surface-bound atomic oxygen activates the surface for selective partial oxidation with remarkable precision [56]. Surface-bound oxygen atoms, $O_{(a)}$, act as a Brønsted base and selectively clip O-H, N-H, and S-H bonds in larger molecules, forming a surface-bound molecular fragment and an adsorbed OH group [57–60]. This reactivity pattern was originally established on metallic silver for a wide variety of molecules [10] and extended in principle to gold surfaces [61]. Recent studies have shown a much more extensive pattern of oxygen activation on gold [29,30,62–64], including most recently, the self and cross-coupling of alcohols [23,65] and the coupling of alcohols with aldehydes [27] to form esters (Fig. 1.8a).

In general terms, after activation of the alcohol by surface-bound oxygen to

form adsorbed RO–, cleavage of the C-H bond by the surface produces an aldehyde, in which the carbon bound to the oxygen has a slight positive charge. This carbon is then readily attacked by the oxygen of the RO (Fig. 1.8a,2), and a C-O bond forms. The resulting intermediate then loses a hydrogen to the surface to form the ester product. This reaction also proceeds readily if the aldehyde is added directly to the surface RO– species. Friend et al. find that when cross coupling two alcohols, the cross-coupled product is always the methyl-ester of the longer chain alcohol. By balancing the β-H elimination abilities from the alkoxy to form the aldehyde with the gas phase acidity of methanol, ethanol, and butanol, they optimize the conditions under which the cross-coupling product will be dominant [26]. Alcohol cross coupling has been achieved over supported gold nanoparticles as well, and the mechanistic insight gained in ultra high vacuum correlates well with solution phase reactions. For example, Nielsen et al. report high selectivity for the coupling of hexanol with methanol under similar conditions, ~90% methanol molar fraction [44]. Ethanol self-coupling to ethyl acetate has also been observed [66].

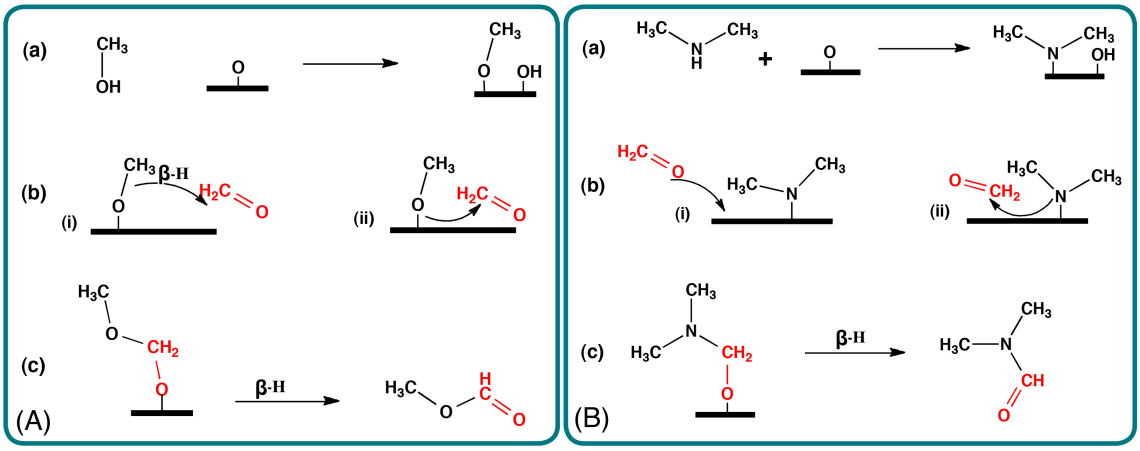

Figure 1.8: The mechanistic pathway for coupling of (a) alcohols and aldehydes and (b) amines and aldehydes on oxygen covered silver or gold.

Using these fundamental studies of oxidative coupling of alcohols on gold single crystals, it was envisioned that alcohols could self-couple to selectively form esters in a steady state catalytic reactor [22, 23]. Using a new novel nanoporous gold material, which contains a very small concentration of silver, high selectivity for oxygen-assisted ester formation from methanol self-coupling was realized by flowing a mixture of oxygen and methanol over the nanoporous gold at relatively low temperatures (Fig. 1.9) [67]. This non-supported catalyst is intriguing for a number of reasons, including the fact that oxygen dissociates and reacts without the aid of an oxide support, the catalyst is not prone to sintering at operational temperatures, and the exact amount of silver in the gold changes the selectivity and optimal temperature of operation [67].

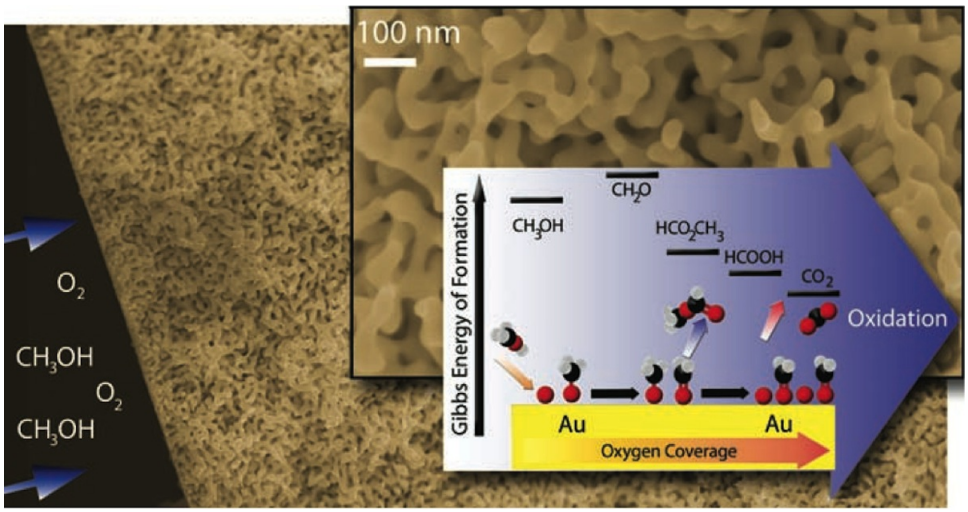

Figure 1.9: Unsupported nanoporous gold facilitates the same methanol cross coupling to methylformate (HCO_2CH_3) as seen on gold single crystals in ultra high vacuum. High selectivity is favored at low surface oxygen coverages. From [67]. Reprinted with permission from AAAS.

The general similarity of the electron charge distribution surrounding oxygen and nitrogen atoms in molecules suggests that similar reactions might occur with amines, where essentially the OH functionality in the alcohol is replaced by an NH

group in the amine (Fig. 1.8b). Indeed the N-H bond in the amine is activated by surface oxygen, and the resulting species adds facilely to the electron deficient center in aldehydes. These similar reactions provide an excellent example of the use of general patterns of reactivity to anticipate new synthesis pathways–enabling catalysis by design, as opposed to trial and error.

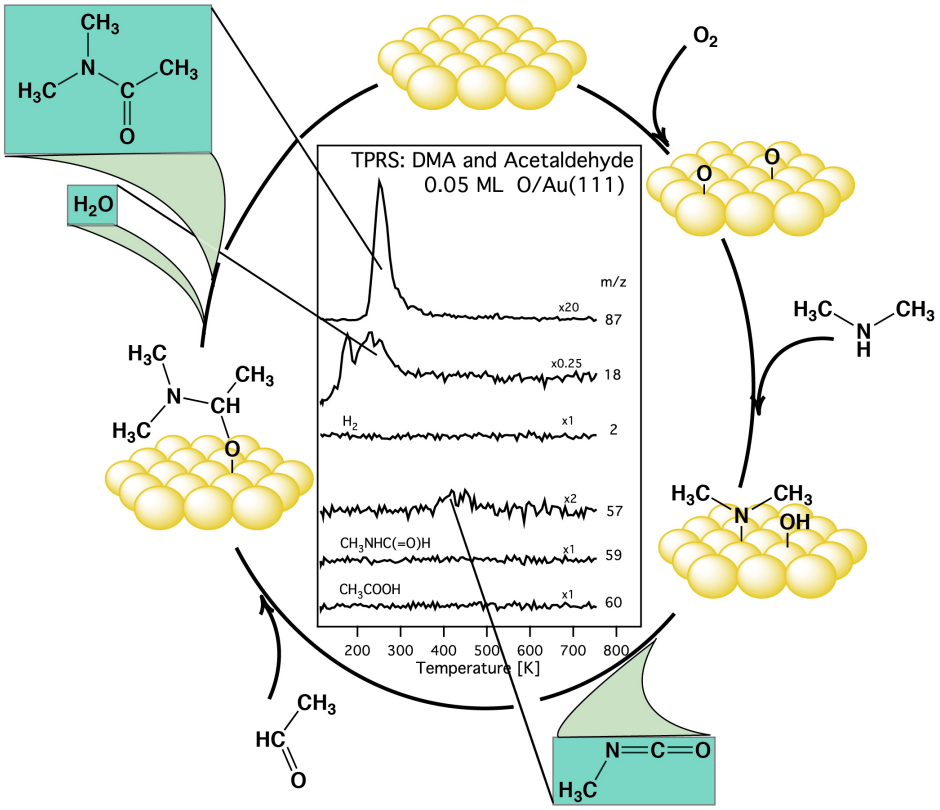

Figure 1.10: Temperature programmed reaction spectroscopy allows the deciphering of the mechanism for catalytic production of amides by amine/aldehyde coupling on an oxygen covered gold surface. The external cycle shows the sequence of reactions that transform dimethyl amine and acetaldehyde into dimethylacetamide (upper left). Competing partial oxidation of dimethyl amine leads to methyl isocyanate (lower right) Lines from each product to the temperature programmed reaction traces in the center indicate the mass spectrometric identification of the products. Modified from [68].

As was predicted by the mechanism shown in Fig. 1.8b, silver and gold surfaces have been shown to facilitate amide synthesis from aldehydes and amines in ultra high vacuum. Using TPRS and isotopic labeling, the reaction mechanism has been clearly delineated (Fig. 1.10). At low oxygen coverages, this reaction approaches 100% selectivity for the formation of the coupling product, dimethylacetamide, on both silver and gold surfaces; the route to methyl isocyanate and combustion products is practically eliminated. Differences in selectivity and reaction mechanism have been investigated by comparative study of acetlyation of dimethlyamine with acetaldehyde on the both oxygen-covered Au and Ag surfaces under ultra high vacuum [68]. In this study and the previous studies of dimethylamine acylation by formaldehyde on gold [69] and silver [70], it was observed that the oxygen-assisted reaction proceeds on the surface via activation of N-H to form adsorbed amides. Coupling then occurs via nucleophilic attack of the amide on the carbonyl carbon of the aldehyde. This mechanism expands the known reactivity patterns of adsorbed oxygen on silver and gold [56], providing insight into similar chemistry on gold nanoparticles [71, 72]. For example, Christensen et al. observe coupling of an alcohol and an amine to form an amide over a supported gold catalyst [72]. The observed chemistry makes sense when viewed in light of the mechanism proposed here. Oxygen on gold activates both the O-H and N-H bond, the alkoxy then β-H eliminates to form an aldehyde, which can be nucleophilically attacked by the activated amide. The partial oxidation and coupling reactions in solution phase catalysis using molecular oxygen as the oxidant follow the same acid base reaction and coupling patterns as seen in ultra high vacuum using atomic oxygen on gold. Further study into these rich partial oxidation and coupling

reactions will surely be expanded, and hopefully industrial implementation will be realized in the near future.

1.6 Summary

Although catalysis has been increasingly well understood over the ages, it was not until the last 60 years that clear and detailed reaction mechanisms emerged to change understanding and design of more complex reactions. The last two examples of novel coupling chemistry on oxygen-covered silver and gold surfaces may represent a turning point in catalysis design–we have reached a confluence of catalyst process design by reactivity principles derived in ultra high vacuum advanced by ambient and high pressure catalysis research to open new possibilities for green catalysis by precious metals.

Chapter 2

Tuning the Stability of Surface Intermediates Using Adsorbed Oxygen: Acetate on Au(111)

2.1 Abstract

Selective oxidative reactions promoted by gold depend critically on controlling the coverage and stability of adsorbed intermediates, as well as promoting specific bond activations of those intermediates. We demonstrate that acetate, a common intermediate in oxidation of olefins, aldehydes, and alcohols, is destabilized by 7-10 kcal/mol by co-adsorbed oxygen relative to its stability on the clean gold surface. The amount of destabilization depends on the oxygen coverage. Peak temperatures of products indicative of oxygen-assisted and clean-surface bond activation differ by up to 130 K. Experiments with d_3-acetate show a kinetic isotope effect of 6.9 at 400 K,

indicating that the rate-limiting step of the low temperature oxygen-assisted reaction is γ-CH bond breaking. This clearly demonstrates that co-adsorbed oxygen activates γ-CH bonds on gold and suggests that an oxygen-assisted activation may also occur for β-CH bonds crucial in oxygen-assisted alcohol coupling on metallic gold catalysts, as predicted by theory.

This paper was published in *Journal of Physical Chemistry Letters*, **2014**, *5*, 1126-1130.

2.2 Introduction

Identifying and understanding factors that control the stability of reactive intermediates is a central issue in heterogeneous catalysis because it affects the reaction kinetics and overall reaction selectivity. Understanding of these factors provides guidance on how to adjust reaction conditions to improve reaction selectivity or to reactivate catalysts by tuning the surface concentrations of key intermediates.

Herein, we demonstrate a dramatic change in the thermal stability of adsorbed acetate on Au(111) due to the presence of adsorbed O as a prototype for oxidation reactions and C-H bond activation. Acetate is of specific interest because it is a strongly-bound carboxylate intermediate that is formed from secondary oxidation reactions that can inhibit other reactions via site-blocking [73–75]. Acetate has been proposed to lead to nonselective oxidation of ethylene on Ag [76], and acetaldehyde and ethanol on Au [23]. Therefore, understanding how to alter the stability of acetate is an important issue. On gold, adsorbed O has a high potential to facilitate the activation of specific types of C-H bonds that may lead to a desired reaction because

of the inherently low capability of metallic gold to activate C-H bonds [77].

Gold is of interest because of its high activity and selectivity for a broad range of molecular transformations at low temperature on both single crystal models [78] and on working catalysts [20, 79], including partial oxidation of alkenes [19, 80], and selective oxidation [81] and oxidative coupling of alcohols [44,82]. Gold has been found to be active for oxygen-assisted coupling of methanol with alcohols [26, 44, 61, 65], CO [83], and amines [68, 69, 72, 84–86] to form methyl esters, dimethylcarbonate, and amides or amines, respectively. Adsorbed atomic oxygen plays an essential role in these reactions, ranging from being the active site for activation of alcohols and amines to a direct reactant in alkene oxidation.

It is already established that adsorbed oxygen activates the O-H bonds in alcohols and N-H bonds in amines [61,87,88] to produce reactive intermediates, with the $O_{(a)}$ acting as a Brønsted base:

$$O_{(a)} + ROH_{(g)} -> OH_{(a)} + RO_{(a)} \tag{2.1}$$

On Au(111), $OH_{(a)}$ is a transient species [60] and quickly disproportionates, generating water and adsorbed oxygen:

$$OH_{(a)} + OH_{(a)} \longrightarrow O_{(a)} + H_2O_{(g)} \cdot \tag{2.2}$$

If the subsequent reaction of the alkoxy forms an aldehyde (oxidation) or ester (oxidative coupling), there must be C-H bond activation of the hydrogen beta to the surface (denoted β-CH), which is now 'activated' due to its proximity to the surface-bound oxygen (Fig. 2.1). Work using density functional theory indicates that co-adsorbed atomic oxygen–or even a neighboring OH or alkoxy–facilitates this process by directly

accepting the H atom with a lower energy barrier than direct C-H bond activation by the gold surface [77, 89]. Because β-CH elimination is facile, this potential role of co-adsorbed O remains experimentally unproven. It is generally observed, however, that with increased amounts of excess oxygen more decomposition/combustion occurs [22,23]. Secondary oxidation of hydrocarbons such as alcohols leads to formation of carboxylates [23, 76], which can result in unwanted product formation or degradation of catalyst selectivity and activity. Carboxylate formation is also suggested as a pathway for nonselective oxidation in olefin expoxidation [90, 91].

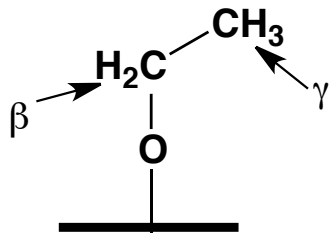

Figure 2.1: Illustration of β-and γ-hydrogen positions in surface-bound ethoxy.

Hydrogen atoms γ to the surface (denoted γ-CH) are generally more stable than the β-CH bonds found in methanol or ethanol and are 'unactivated' in the sense that they are not adjacent to an electron-withdrawing heteroatom (Fig. 2.1) [92]. This type of C-H bond is found in carboxylates and tertiary alcohols, as well as cyclic molecules. In this work, we show that adsorbed atomic oxygen enables a reaction pathway for γ-CH activation on gold, which is not observed in its absence. Without co-adsorbed O a different reaction pathway with much higher activation energy is exclusively observed, with both C-C and C-H bond cleavage. Acetate was studied because it has both C-H and C-C bonds, is a model carboxylate, is formed as an intermediate in alcohol and aldehyde oxidation reactions [23], and can be isolated on

the surface by reaction of acetic acid with adsorbed atomic oxygen.

2.3 Results and Discussion

Adsorbed acetate was prepared by dosing acetic acid at 200 K on a Au (111) surface pre-covered with atomic oxygen (O/Au(111)). The acetic acid undergoes reaction with the adsorbed oxygen (reaction 2.1) generating adsorbed acetate and water:

$$O_{(a)} + 2\,CH_3COOH \longrightarrow H_2O_{(g)} + 2\,CH_3COO_{(a)}\,. \tag{2.3}$$

By changing the acetic acid dose, the relative amount of adsorbed acetate and oxygen was controlled; e.g., for high acetic acid doses and low pre-coverages of adsorbed O, all of the oxygen reacts away as water leaving only adsorbed acetate on the surface.

Two entirely different reaction pathways, separated in temperature by 130 K, appear for acetate decomposition on Au(111) depending upon whether co-adsorbed oxygen is present or not (Fig. 2.2). For both reaction pathways the dominant product is CO_2, so the evolution of the two pathways with increasing oxygen coverage is easily discerned. Following a dose of excess acid on 0.2 ML O (Fig. 2.2a), no adsorbed oxygen remains, and the decomposition of the acetate occurs at 530 K (rate of CO_2 formation is maximum). The complete consumption of adsorbed O is established by the fact that there is no O_2 evolved in the temperature programmed reaction spectrum (Fig. 2.2). Low acid doses at the same O coverage produce excess adsorbed O, and the decomposition occurs at 440 K (Fig 2.2c). At an intermediate acid dose both reaction routes are observed (Fig. 2.2b). At even higher excess oxygen coverage (initial concentration of O = 0.55 ML) the decomposition occurs at 400 K (Fig. 2.2d).

The reactions at 400 K and 440 K probably occur via similar reaction pathways and the peak at 440 K peak clearly remains as a shoulder as reaction conditions change.

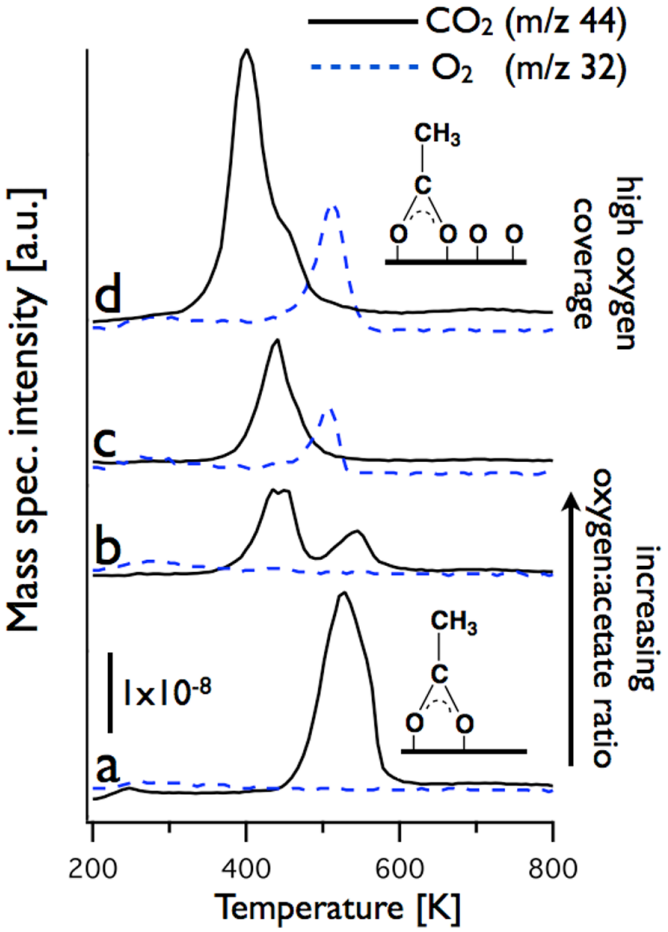

Figure 2.2: CO_2 (m/z 44) evolution (black) and excess oxygen (m/z 32) desorption (dashed blue, x5) from acetate decomposition on Au(111) with oxygen/acetate ratio as follows: a) 0.2 ML O, excess acid, b) 0.2 ML O, intermediate acid dose, c) 0.2 ML O, low acid dose, d) 0.55 ML O, excess acid. Dosing of both ozone to generate O/Au(111) and acid to generate the acetate was done at 200 K. Schematics of acetate on the clean surface and in the presence of co-adsorbed oxygen are shown to illustrate the reaction conditions and are not meant as molecular models.

There are at least two possible origins for the shift to lower temperature at higher oxygen coverage: (1) different oxygen species that arise at higher coverage [93]

and (2) a coverage effect involving repulsive lateral interactions between the closely packed acetates and co-adsorbed oxygen. Because the oxygen-covered gold surface is known to restructure while heating (i.e. during the course of reaction), separating these effects is difficult.

The oxygen-rich and oxygen-free pathways lead to different products concomitant with CO_2, supporting the hypothesis that co-adsorbed O facilitates γ-CH bond activation. For the oxygen-assisted pathway (400-440 K) formaldehyde, water, ketene, acetic acid and CO are formed. Water is evolved from reaction of adsorbed oxygen with C-H bonds in the acetate. The oxygen-free pathway (530 K) evolves methyl (CH_3), CO, methylacetate, formaldehyde, ketene, acetic acid, C_2H_6, and H_3CCO (Fig. 2.2). No water is evolved with the high temperature peak, nor is there O_2 recombination; thus, the complete consumption of the adsorbed oxygen prior to the onset of this reaction pathway is demonstrated. Even though the spectrum of products is complex, the primary product, CO_2, is a proxy for determining the stability of the acetate. In neither case did post-dosing of ozone result in CO_2 evolution, indicating that no carbon remains on the surface after acetate decomposition. Products were identified using the NIST database and fragmentation patterns determined from desorption of neat samples where possible. A full study of the reaction mechanisms and selectivity for both pathways is currently underway.

There is a substantial difference in the peak temperatures for CO_2 formation from d_3- vs d_0-acetate in the low-temperature pathway that occurs when excess adsorbed O is present, signifying a substantial kinetic isotope effect (KIE) (Fig. 2.3). Hence, the rate-limiting step for the low temperature pathway involves γ-CH bond

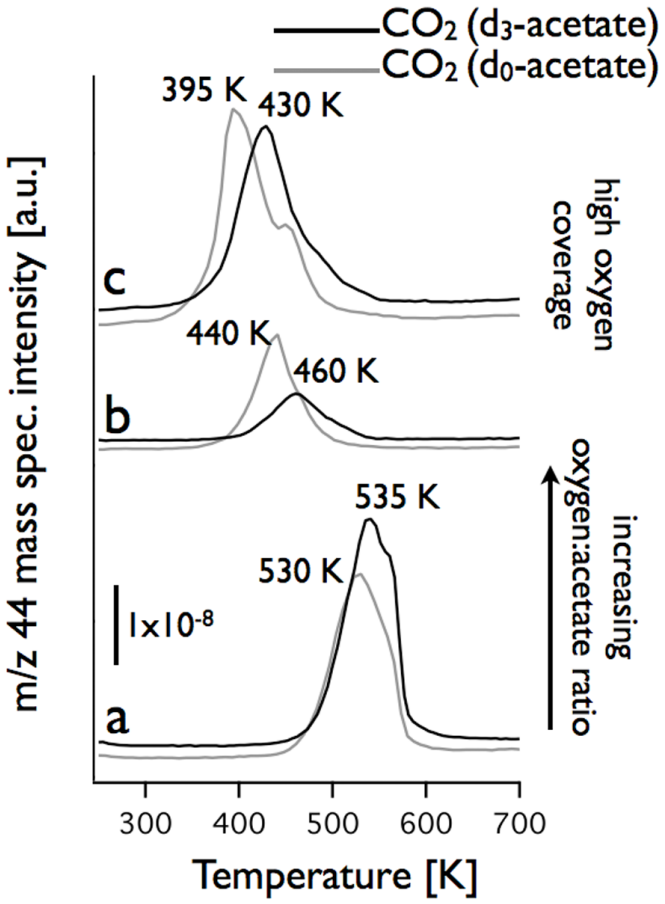

Figure 2.3: CO_2 (m/z 44) evolution from d_3-acetate decomposition (black) on Au(111) with varying acetate/oxygen ratios: a) 0.2 ML O, excess acid, b) 0.2 ML O, intermediate acid dose, c) 0.5 ML O, excess acid. Dosing of both ozone to generate O/Au(111) and acid to generate the acetate was done at 200 K. For comparison, CO_2 from the non-deuterated case in the same conditions is shown in gray.

breaking. Decomposition of d_3-acetate in the presence of excess adsorbed O (initial oxygen coverages of 0.5 ML and 0.2 ML) occurs at 430 K and 460 K, respectively (Fig. 2.3b, c), compared to 395 and 440 K for d_0-acetate, clearly demonstrating that C-D bond breaking is rate-limiting when co-adsorbed oxygen is present [94]. CO_2 is produced either from C-C bond breaking or via C-H(D) bond scission in the methyl group. Even though three C-H bonds are ultimately lost from CH_3 to yield CO_2, the evolution of formaldehyde indicates that they are broken stepwise and not in a concerted manner. In contrast, there is no measureable temperature shift in the onset of CO_2 production for the high-temperature route. (The peak temperature is the same within experimental error (~5 K), and is also quite sensitive to small changes in reaction conditions, such as oxygen coverage).

The activation energies for the decomposition pathways and the magnitude of the KIE were estimated from the peak temperatures of the reactions for the two isotopes using a pre-exponential factor of 10^{16} and assuming the reaction to be first order (Table 2.1) [31, 95, 96]. The pre-exponential factor of 10^{16} was chosen because it is the experimentally determined value for γ-CH activation ethylidyne, a similar intermediate, on Pt(111) [95]. Varying the pre-exponential factor from 10^{13}-10^{16} yields a range of activation energies of approximately 3 kcal/mol. The choice of the pre-exponential factor does not change the measured magnitude of the KIE.

The KIE measured for acetate decomposition on Au(111) in the presence of excess O_{ad} is similar to KIE values for dehydrogenation of methyl groups in other molecular intermediates bound to several different surfaces (Table 2.2). For example, the difference in activation energies for decomposition of d_0-acetate and d_3-acetate,

Conditions	Peak Temp (K) (d_0-acetate)	$E_{(a)}$ (d_0-acetate) (kcal/mol)	Peak Temp (K) (d_3-acetate)	$E_{(a)}$ (d_3-acetate) (kcal/mol)	k_H/k_D at 400 K (300 K)
0.55 ML O, excess oxygen	400	29.9	430	32.2	–
0.2 ML O, excess oxygen	440	32.9	460	34.5	6.9 (13.2)
0.2 ML O "clean surface"	530	39.9	535	40.3	–

Table 2.1: Peak temperatures, activation energies, and kinetic isotope effect for acetate decomposition in the presence or absence of co-adsorbed oxygen, using a pre-exponential factor of 10^{16} and assuming the reaction to be first order.

Reaction	Peak Temp (K) (excess adsorbed O)	Peak Temp (K) ("clean surface")	Kinetic Isotope Effect
Acetate on Ag(110) [97]	400	580	20 K shift for excess O_{ads}
t-butoxy on Ag(110) [92, 98]	440	510	k_H/k_D(300 K)=7 for excess O_{ads}
t-butoxy on Cu [99]	600	600	k_H/k_D(300 K)=11.5 for excess O_{ads}

Table 2.2: Decomposition by activation of γ-hydrogens in the presence and absence of co-adsorbed oxygen. In order to avoid possible complications due to lateral interactions at higher acetate coverage, initial oxygen coverage of 0.2 ML O were used when calculating the KIE.

1.5 kcal/mol, is similar to the difference of 1.1 kcal/mol measured for d_3-methoxy dehydrogenation on Cu(110) [94]. The KIE of k_H/k_D at 400 K (6.9) is similar to that for decomposition of d_3-methoxy on Cu(110) (6.3) [94]. Although a KIE was not reported for acetate on Ag(110), there was a similar shift in the decomposition temperature (20 K) d_3-acetate vs. d_0-acetate in the presence of excess oxygen [97]. The KIE for dehydrogenation of d_3-ethylidyne on Pt(111) is 3.1 [95]. In the presence of excess adsorbed O, the KIE for t-butoxy decomposition is high, ~11.5. The origin of the range of KIEs is not known and requires theoretical modeling of the transition states for these various processes.

γ-Carbon-hydrogen activation in t-butoxy and acetate has only been previously studied on silver [92,98] and copper [99] (Table 2.2). On Ag(110) excess oxygen assists the decomposition of adsorbed acetate at 400 K, whereas in the absence of oxygen decomposition occurs at 580 K [97]. Likewise oxygen-assisted activation of the γ-CH bond in adsorbed t-butoxy occurs at 440 K, whereas C-H bond cleavage occurs well above 500 K on the clean surface [92,98]. In contrast, on Cu(110) reaction of t-butoxy occurs at 600 K, with only a slight shift to lower temperatures when excess oxygen is present [99]. In all cases, a KIE is observed when co-adsorbed oxygen is present.

Excess oxygen on gold opens a low-energy reaction pathway for carboxylate decomposition via γ-CH bond activation–up to 10 kcal/mol lower than the competing pathway on clean gold. This fact suggests that similarly adsorbed O may facilitate β-CH in critical steps in oxygen-assisted alcohol coupling on metallic gold catalysts, as predicted by theory. This result also has direct implications for the prevention of poisoning of gold catalysts due to the buildup of carboxylates in oxidation reac-

tions. Depending on the specific reaction, it may be desirable to operate (or purge the catalyst) with a slight excess of oxygen to facilitate a lower temperature pathway for further oxidation (combustion) of the carboxylate, so as to remove carboxylate species that populate the catalyst surface at the relatively low temperatures employed in selective oxidative chemistry using gold-based catalysts. Investigation of the respective mechanisms for the two different pathways is currently underway.

The stability and coverage of surface intermediates can be controlled by co-adsorbed O, resulting in two important effects. (1) Co-adsorbed O can be used to change reaction selectivity–in an obvious way, it will promote secondary oxidation; less obvious is the possibility of opening new reaction pathways. (2) O can be used to prevent or reverse poisoning due to carboxylate accumulation–at the least, it can be used to regenerate poisoned catalysts.

2.4 Experimental Methods

All reactions were done in ultra high vacuum with a base pressure of $\sim 2 \times 10^{-10}$ torr using a Hiden quadrupole mass spectrometer (HAL-Hiden/3F) for temperature programmed reaction spectroscopy (TPRS), which has been described in detail elsewhere [100]. Heating rates of 5 K/s were employed in all TPRS measurements. The surface was cleaned by argon ion sputtering and annealing to 900 K, followed by multiple oxidation cycles using ozone until no CO_2 desorbed. A bias of -100 V was applied to the sample during TPRS experiments to prevent electron-stimulated reactions from the mass spectrometer filament. Ozone was generated using a LG-7 CD Laboratory Ozone Generator. Approximately 15 g/Nm^3 ozone in oxygen was

constantly flowed through a gas line from which the ozone was dosed in order to create adsorbed atomic oxygen on the surface. Each day, the ozone dose was calibrated using saturation coverage (O_{ad} coverage=1.1 ML) as a reference for the area of O_2 evolution peak for oxygen saturation. The O coverages for lower exposures of ozone were determined by measuring the O_2 peak area and referencing to the area for saturation. When acetic acid was dosed in excess, the dose was sufficient to build up multilayers of acid at 150 K. When dosing acid on 0.2 ML O and maintaining co-adsorbed oxygen, the dose was simply decreased until excess oxygen was observed after the reaction, ensuring that not all of the oxygen was consumed. Doses of acid were done using a direct doser and controlled by number of turns of the dosing valve; a background pressure rise was not observed during the acid doses.

Chapter 3

Switching Selectivity in Oxidation Reactions on Gold: The Mechanism of C-C vs C-H Bond Activation in the Acetate Intermediate on Au(111)

3.1 Abstract

Carboxylates are important intermediates in oxidative reactions on gold, as they are precursors to carboxylic acids and CO_2. They may also act as site-blockers in oxidative coupling of alcohols, thereby decreasing both catalyst activity and selectivity. We demonstrate that the reaction selectivity and pathways for a prototype carboxylate, acetate, adsorbed on Au(111), are dramatically altered by the presence of coadsorbed atomic O. Finely tuning the initial oxygen coverage affords control of

the product selectivity and the reaction pathway. Oxygen-assisted γ-C-H activation occurs with coadsorbed oxygen near 425 K, yielding mainly CO_2 and formaldehyde, and a kinetic isotope effect is observed for these products. In the absence of coadsorbed oxygen, acetate reacts at 530 K by C-C bond cleavage to form CO_2, methyl, and methyl acetate, as well as minor products. These studies have led to the identification of a new synthetic pathway for ester formation, in which methyl (either produced in the reaction or introduced externally using methyl iodide) reacts with surface acetate to form methyl acetate. Detailed isotopic labeling studies using d_3-acetate, ^{13}C-acetate, and ^{18}O show that the methyl carbon forms mainly formaldehyde in the oxygen assisted reaction and methyl in the clean surface reaction, and that surface oxygen is incorporated into products in the low temperature, oxygen-assisted pathway. A complete mechanism is proposed and compared to the reaction of acetate on silver. These studies provide a detailed fundamental understanding of acetate chemistry on gold and demonstrate how the oxygen concentration can be used to tune selectivity.

This paper was published in *ACS Catalysis*, **2014**, *4*, 3281-3288. Reprinted with permission, Copyright 2014 American Chemical Society.

3.2 Introduction

Selective oxygen-assisted catalysis on gold has developed into a rich area of research, encompassing both reactor-based studies and model studies of reaction mechanisms and principles on single crystals. Oxygen-activated gold catalyzes the oxidation of alkenes, alcohols, and amines, forming epoxides [19,29,80,101], aldehydes [102,103]

or acids [81, 104–108], and imines [109–112], respectively; oxidative coupling of alcohols yields esters [22, 23, 26, 44, 65, 67, 110, 113] and coupling of amines with aldehydes or methanol yields amides on gold [68, 69, 72, 84, 85, 111, 114]. Fundamental studies of these reactions have afforded insight into selectivity control as well as the prediction of new classes of reactions by gold catalysis [67, 83, 113–116]. In particular, mechanistic insight from ultra high vacuum (UHV) studies on Au(111) has been shown to directly correlate with activity seen on a nanoporous gold catalyst in a flow reactor [67, 113, 116]. Less well studied is the activation of adsorbed carboxylates, which are often formed in oxidative processes along the pathway to combustion.

Carboxylates are important intermediates on gold because they (1) form as intermediates in oxidation reactions and (2) may lead to poisoning of a catalyst surface. Carboxylates are strongly bound to the surface and often form via secondary oxidation of hydrocarbons or alcohols. Acetate in particular has been implicated as the intermediate in non-selective oxidation of ethylene on silver [51, 76] and of acetaldehyde and ethanol on gold [23]. Once formed, it has been proposed that carboxylates or similar intermediates may decrease catalyst selectivity by site-blocking [73–75], thereby preventing desired reactions. In order to tailor reaction conditions to avoid these complications it is imperative to understand carboxylate stability and surface reactivity.

In general, oxidation reactions on gold are facilitated by an adsorbed oxygen adatoms. Initially, oxygen atoms act as a Brønsted base toward OH, NH, and even CH hydrogens to form the corresponding activated intermediate and adsorbed OH [61, 117], eg., ethoxy forming from reaction with ethanol [23]. Further activation of

beta C-H bonds leads to products, for example acetaldehyde and ethyl acetate from ethanol oxidation [23, 105, 118]. Density functional theory has predicted that the β-CH bond cleavage of methoxy via an oxygenate (an oxygen adatom, hydroxyl, or neighboring alkoxy) has a lower energy barrier than direct C-H activation by the metal [77]. In order to test this principle, we here addresses oxygen activation of *gamma* C-H bonds (Fig. 3.1), finding that C-H bond cleavage is facilitated via co-adsorbed oxygen, and that activation by the metal results in C-C bond cleavage at a much higher temperature.

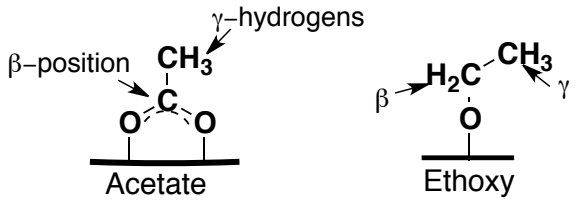

Figure 3.1: Acetate and ethoxy adsorbed on a surface. γ and β positions are according to their position with reference to the surface.

Herein, we demonstrate that coadsorbed oxygen opens new reaction pathways for acetate on Au(111), leading to a selectivity switch. In conjunction, the stability of acetate on Au(111) is dramatically decreased by coadsorbed oxygen due to the opening of pathways involving O attack [119]. A detailed mechanism for reaction of acetate both in the presence and absence of adsorbed atomic oxygen is established using temperature programmed reaction spectroscopy and isotopic labeling experiments. In addition, a new synthetic route for esters via carboxylates was discovered in which methyl introduced externally or produced during the reaction is added to acetate on the surface, forming methyl acetate. These studies demonstrate the key roles of adsorbed O in determining reactivity on gold and suggest a means of controlling

selectivity in catalytic systems that produce carboxylates.

3.3 Results

The effect of coadsorbed atomic oxygen on acetate reactivity was first investigated by varying the amount of acetic acid exposed to a surface with a fixed concentration of atomic oxygen of 0.2 monolayers (ML). Acetate is formed from reaction with O adsorbed on Au(111) through the well-established acid-base chemistry on oxygen-covered gold [61]:

$$\mathrm{O}_{(a)} + 2\,\mathrm{CH_3COOH}_{(g)} \longrightarrow \mathrm{H_2O}_{(a/g)} + 2\,\mathrm{CH_3COO}_{(a)} \tag{3.1}$$

Excess acetic acid was dosed onto a Au(111) surface with an initial oxygen coverage of 0.2 ML at 200 K–the conditions being chosen to prevent the buildup of either water or acid multilayers. With this procedure, the reaction goes to completion, and acetate was formed free of coadsorbed oxygen atoms. In contrast, with a small initial dose of acid at the same initial oxygen coverage, excess adsorbed oxygen remained (Fig. 3.2).

Coadsorbed oxygen initiates a reaction inaccessible in its absence, facilitating C-H bond cleavage and reaction at a much lower temperature with a decidedly different distribution of products compared to the oxygen-free surface. Reaction of acetate under the two conditions, as measured by temperature programmed reaction, occurred at 440 and 530 K, respectively, corresponding to activation energies of 29 kcal/mol and 35 kcal/mol (the anaylsis was simplified by assuming first order reaction and a pre-exponential factor of 10^{14}). The pre-exponential factor of 10^{14} was chosen

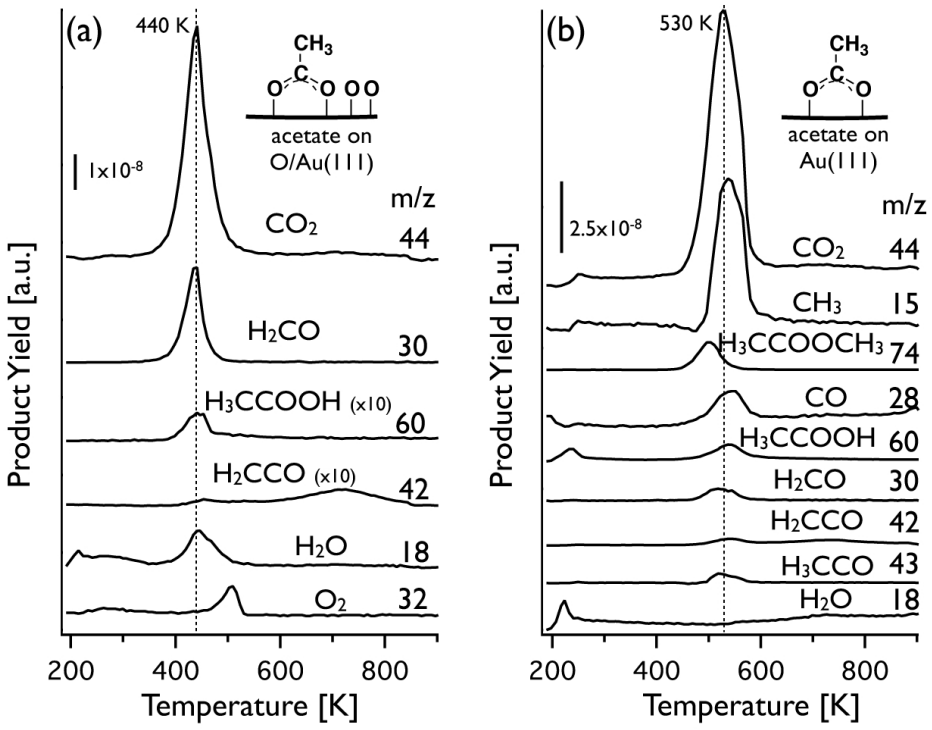

Figure 3.2: Temperature programmed reaction spectra of acetate in the presence and absence of coadsorbed oxygen. Initial oxygen coverage in both cases was 0.2 ML O. Acetic acid was dosed at 200 K (a) with the acid dose controlled to retain excess oxygen and (b) in excess acid to consume all oxygen. Unless otherwise noted, products are scaled to reflect their relative yields, calculated using quantitative mass spectrometry methods described in the experimental section and supporting information.

because it is typical of experimentally determined pre-exponential factors of similar intermediates [120, 121], lying in the middle of the range for similar H-elimination reactions, which range from $10^{12} - 10^{16}$ [95, 122, 123]. Previously, we used the value of 10^{16} in calculations for acetate on gold, which results in an upward shift of $\sim$ 3-5 kcal/mol [119]. The reaction temperature drops even further, to 400 K (E_a = 26 kcal/mol) occurs with initial oxygen coverages $\geq$ 0.3 ML (see Fig. 3.4). CO_2 is the main product for both reaction pathways, however, there are significant differences in the other products.

The product distributions are strongly dependent on the amount of excess oxygen on the surface (Fig. 3.3, Table E.1). With excess oxygen the major products are carbon dioxide and formaldehyde, with minor amounts of acetic acid, ketene (H_2CCO), water, and a small amount of carbon monoxide. Products are evolved concomitantly with the CO_2 (Fig. 3.2) with the exception of a broad ketene peak around 700 K. In the absence of excess oxygen several new products form: methyl, methyl acetate, and carbon monoxide along with minor amounts of formaldehyde, H_3CCO radical, acetic acid, ethane, and ketene. Yields for minor products and selectivities for all products are included in Table E.1. The production of methyl acetate indicates a new synthetic route for esters using acetate as a synthetic reactive intermediate (see Fig. 3.8). Quantitative analysis of the data was used to identify products and determine the relative amounts formed for both reaction conditions.

The changes in selectivity and kinetics can also be monitored by varying the initial oxygen coverage while consistently dosing an excess of acetic acid. This way, the capacity of the surface dictates when coadsorbed oxygen remains on the surface, which

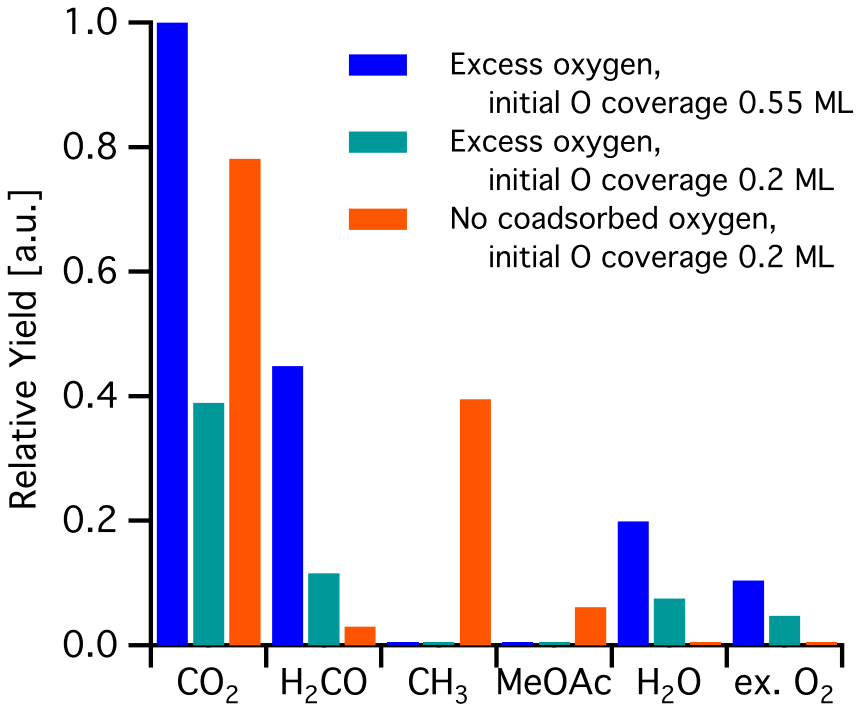

Figure 3.3: Relative yields for major products of acetate reaction (CO_2, H_2CO, CH_3, methyl acetate, H_2O, and excess oxygen) under varying reaction conditions, calculated using quantitative mass spectroscopy, with an enhancement factor of 3.2 included for CH_3. Yields are normalized to the amount of CO_2 produced for an initial oxygen coverage of 0.55 ML. Calculation details in experimental and supporting information.

in turn controls the reaction pathway. The preferred reaction pathway transitions in a narrow window of initial oxygen, 0.24-0.3 ML. (Fig. 3.4). Starting at the lowest oxygen coverage, the high temperature CO_2 peak (530 K) grows in; at 0.24 ML O the low temperature peak ($\sim$ 450 K) starts to form; at 0.3 ML O the lowest temperature peak (400 K) builds in and becomes dominant at 0.5 ML O, although the 450 K peak is still present as a shoulder. Although excess oxygen after the reaction is not seen, water forms with CO_2 during the reaction, which is evidence of coadsorbed oxygen reacting with hydrogen from the acetate. Above 0.5 ML O, unreacted oxygen recombines to form O_2 and the amount of CO_2 formed decreases; the latter effect is attributed to reduction in the binding capacity for the acetate.

The kinetics for CO_2 production is also strongly dependent on the initial O coverage and whether there is excess O adsorbed on the surface (Fig. 3.4). Specifically, the peak temperature for CO_2 is much higher when there is not excess adsorbed oxygen. Based on the decrease in peak temperature for CO_2, the 6 kcal/mol activation energy difference seen at 0.2 ML O with excess oxygen (see 3.2a) increases to 9 kcal/mol at initial oxygen coverages $\geq$ 0.3 ML.

The mechanisms for CO_2 formation are changed by the presence of adsorbed excess O, accounting for the different peaks in the temperature programmed reaction data (Fig. 3.4). The rate-limiting step for *oxygen-assisted* formation of CO_2 formation at low temperature involves C-H bond cleavage based on the kinetic isotope effect observed for reaction of d_3-acetate (Fig. 3.5). In contrast, the peak temperature of the higher temperature route that occurs in the absence of excess O is the same for d_0- and d_3-acetate (Fig. 3.5). At an initial oxygen coverage of 0.2 ML O and an acid

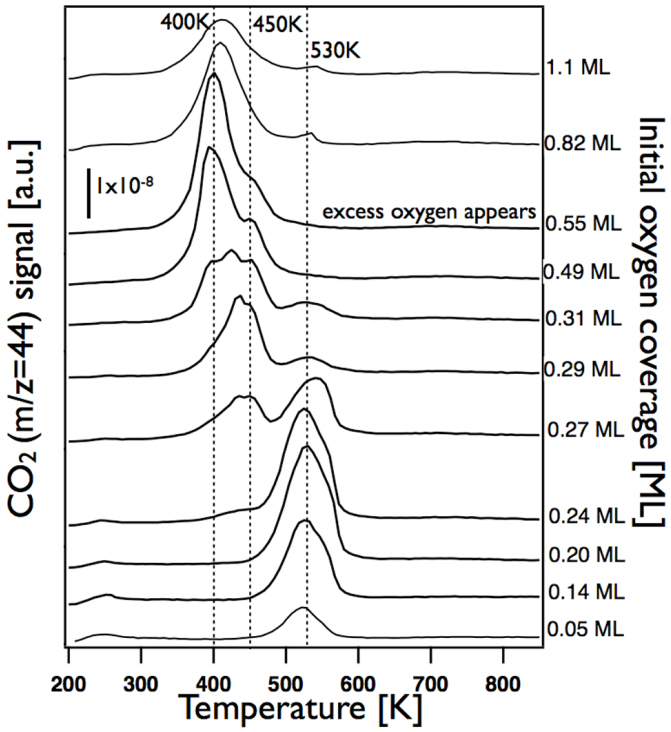

Figure 3.4: Multiple low temperature reaction pathways for acetate activation evolve with increasing amounts of coadsorbed oxygen on the surface, as marked by CO_2 traces for acetate reaction for excess acetic acid dosed at 200 K on varying O-precoverages on Au(111). CO_2 is the main product in all cases. Excess oxygen recombines at ~540 K and is present at initial oxygen coverages of 0.55 ML and higher.

dose for which both the low temperature and high temperature peaks are observed, the effect of isotopic substitution for both reaction channels can be observed (Fig. 3.5). For the oxygen-assisted reaction channel, a temperature shift of 15 K to higher temperature is observed for CO_2 and formaldehyde production from d_3-acetate relative to the perhydrido acetate, indicating that C-H bond activation is involved in the rate-limiting step. In the high temperature route there is no measurable temperature shift for CO_2 production and both methyl and methyl acetate are completely deuterated. These data are unequivocal evidence that the high temperature reaction pathway involves C-C bond cleavage, and that the methyl group (resulting from the C-C bond cleavage) can either react with another acetate to form methyl acetate or desorb intact from the surface.

Surface oxygen is incorporated into the products in the oxygen-assisted, low temperature route, as shown by ^{18}O-labeling of the surface oxygen (~35% ^{18}O, Fig. 3.6). The most significant amount of ^{18}O incorporation is into formaldehyde evolved at 400 K. The higher temperature formaldehyde peak (530 K), however, does not contain ^{18}O, indicating that it is formed via a different route. A small amount of ^{18}O appears in the higher temperature channel, incorporated into CO_2. A small amount of ^{18}O (~7% of products contain one ^{18}O) is incorporated into the acetic acid and methyl acetate (not shown), indicating that the adsorbed acetate undergoes a limited amount of exchange with oxygen on the surface, consistent with previous studies [60]. In neither the low or high temperature pathways is ^{18}O incorporated into the CO.

The differences in reaction pathways as a function of oxygen coverage are also demonstrated using ^{13}C-labeling of the methyl group to delineate which products

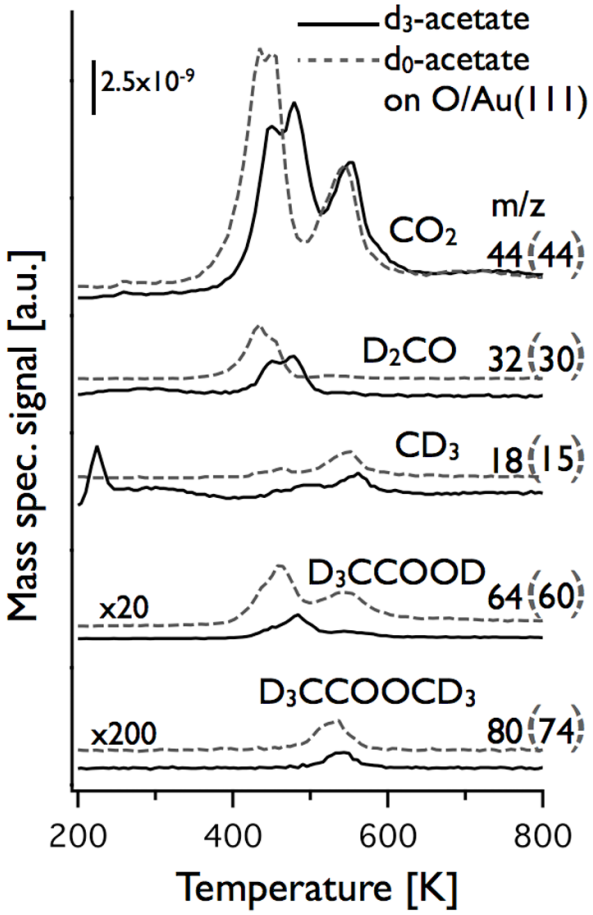

Figure 3.5: Deuterium isotopic labeling experiments for selected products on a 0.2 ML O/Au(111) surface using an acetic acid dose that allows both the low temperature and high temperature pathways to be observed. D_4-acetic acid was dosed at 200 K to form the d_3-acetate. D_3-acetate data is shown in black, grey dashed lines are data obtained separately for d_0-acetate.

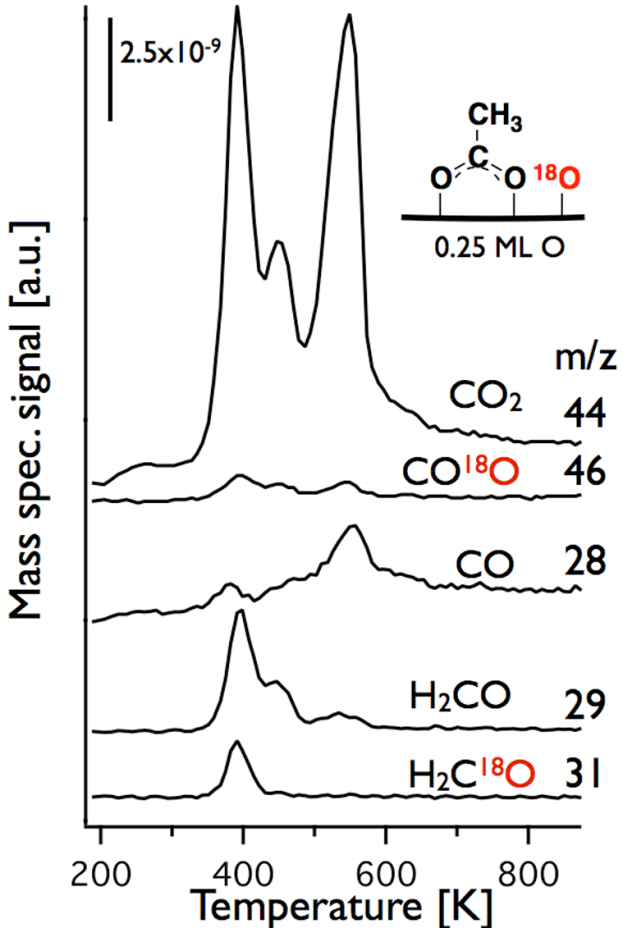

Figure 3.6: Surface oxygen incorporation into products is shown by reaction with ^{18}O/Au(111) (35%). ^{16}O is replaced by ^{18}O by dosing $H_2^{18}O$ for 30s at 180 K on 0.3 ML ^{16}O/Au, then flashing to 350 K to desorb the water. The final oxygen coverage is about 0.25 ML (35% ^{18}O). The acetic acid dose was controlled in order to observe both reaction channels.

originate from the methyl carbon (Fig. 3.7). In the O-assisted pathway ($\theta_{initial}$ = 0.5 ML), formaldehyde is 100% ^{13}C-labeled. This result in combination with the incorporation of ^{18}O from the surface (Fig. 3.6) shows that formaldehyde is produced from attack of the methyl carbon by adsorbed oxygen. Some total oxidation of the methyl group also occurs, based on the fact that ~18% of the CO_2 is also ^{13}C labeled. In the absence of excess O, $^{13}CH_3$ and $^{13}CH_3O{-}C(=O)^{13}CH_3$ (methyl acetate) are formed. The methyl acetate is 100% doubly labeled, which supports the conclusion that the methyl is also 100% labeled, although an exact number for the methyl is difficult to assess because of overlapping fragments with other products. Only ~3% of the CO_2 is ^{13}C -labeled. This experiment was also used to confirm that neither ethane nor ethylene was formed as a major product in the high temperature route (Fig. E.3).

We further probed the reaction to form methyl acetate by using an external source of methyl (CH_3I) to demonstrate that it is produced by addition of methyl to an intact acetate species. Acetate was first isolated on the gold surface by dosing acetic acid on 0.1 ML O at 200 K, followed by exposure to methyl iodide at 140 K. Methyl iodide is known to dissociate on Au(111) starting at 150 K, reacting a coverage of 0.054 ML upon heating to 300 K [124]. In these experiments, methyl acetate (monitored using the major fragment, m/z=43, as well as the parent ion, m/z=74) forms via reaction of acetate with adsorbed methyl from 200-300 K (Fig. 3.8). At higher temperature, methyl acetate is formed via acetate decomposition at 530 K. The m/z 28 and 30 peaks at 350 K are due to ethane formation from methyl recombination [125]. This experiment clearly demonstrates the principle for facile

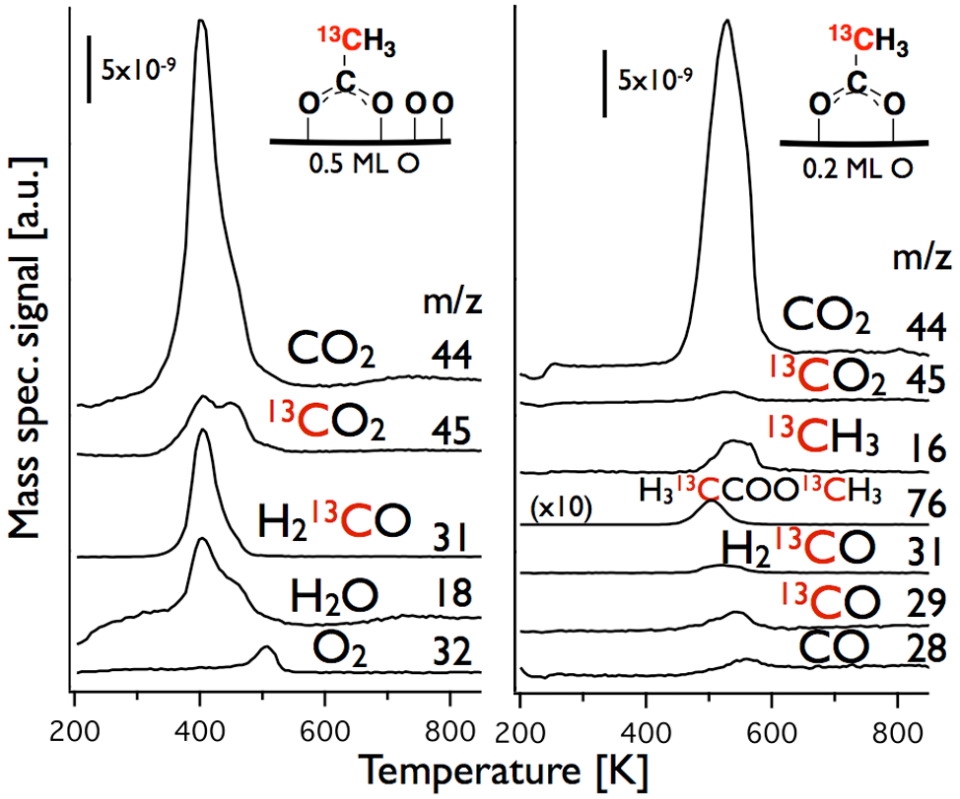

Figure 3.7: Reaction of ^{13}C-acetic acid ($^{13}CH_3COOH$) on Au(111) with initial oxygen coverages of 0.5 ML O (left) and 0.2 ML O (right). Multilayers of acetic acid were dosed at 200 K on both oxygen coverages.

ester formation using an alkyl source for addition to the adsorbed carboxylate.

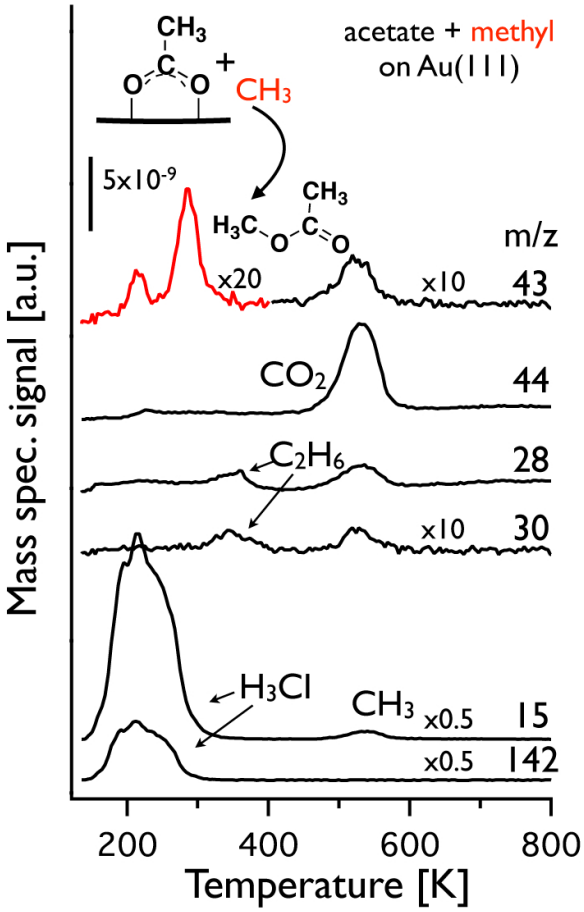

Figure 3.8: Acetate reacts with an external methyl from methyl iodide to form methyl acetate below room temperature. Acetic acid was dosed at 200 K on 0.1 ML O/Au(111), then annealed to 265 K and cooled back down to 140 K. Methyl iodide was introduced in excess at 140 K. The low temperature m/z 15 and 142 are molecular methyl idodide.

3.4 Discussion

Four fundamental principles important in heterogeneous oxidation catalysis emerge from this study: (1) The selectivity for acetate reaction is determined and

tuned by the presence or absence of coadsorbed oxygen; (2) adsorbed oxygen atoms activate the gamma-CH bond (Fig. 3.1) destabilizing the acetate intermediate; (3) in the absence of adsorbed oxygen, acetate decomposition is rate-limited by C-C bond rupture at higher temperature; (4) methyl addition to the acetate provides a direct route to formation of the corresponding ester. The reaction mechanisms for each pathway and effects of oxygen coverage are discussed below and compared to the carboxylate chemistry on silver and copper. These principles serve as a guide for selecting conditions for catalytic reactions that involve acetate as an intermediate. The correspondence between fundamental studies on O/Au(111) and reactions under flow conditions at atmospheric pressure using nanoporous gold catalysts has already been demonstrated in our lab [67, 113, 116].

3.4.1 Coadsorbed oxygen and C-H bond cleavage

The activation energies of the oxygen-assisted and gold surface mediated reaction differ by 6-9 kcal/mol, as the coadsorbed oxygen o[ens a new, lower-energy reaction pathway. This suggests possible strategies for operating or purging catalysts that may be poisoned by the buildup of adsorbed carboxylates, that is, maintaining a slight excess of oxygen in the feed stream in order to enable lower-temperature reaction of the carboxylate molecule.

The facile activation of the gamma C-H (γ-CH) bond in adsorbed acetate by coadsorbed oxygen suggests that a similar process may occur for the beta C-H bond (β-CH) in oxygen-assisted coupling reactions. β-H elimination takes place in most oxidative processes on gold, forming aldehydes and esters, among other products,

and has been predicted by theory to be facilitated by adsorbed oxygen, hydroxyl, or alkoxies [77]. However, because β-CH cleavage is so facile, it is difficult to prove experimentally whether this is the case. Gamma C-H bonds are more stable than those beta to the surface, because they lack proximity to an electron-withdrawing atom (Fig. 3.1). Indeed, as shown by the observed kinetic isotope effect of 6.9 [119], the oxygen-assisted route was indeed limited by γ-CH bond breaking. While it is theoretically possible that an even higher temperature may allow for direct γ-CH activation by the surface, it was not accessibly in our experiments, as C-C bond cleavage and complete removal of acetate took place before any direct γ-CH activation by the metal.

On coinage metals, adsorbed oxygen exhibits a pattern of facilitating γ-CH bond breaking. The most direct comparison to acetate on gold is acetate on silver. On Ag(110), acetate reacts with coadsorbed oxygen as low as 340 K to form formate, which decomposes to CO_2 and H_2 at 400 K [97]. Sault et al. invoke a mechanism that involves direct γ-H activation of the methyl carbon and subsequent reaction of the activated CH_2 group to form formate [97]. Interestingly, formaldehyde is not observed, whereas it is on O-covered Au(111). On clean Ag(110), acetate decomposition does not occur until 580 K, where CO_2, CH_4, acetic acid, and ketene form, similar to reaction on clean Au(111) [76]. *tert*-Butoxy, which also possesses only γ-C-H bonds, exhibits a similar pattern of oxygen-assisted reactivity on Ag(110); the oxygen assisted reaction takes place at 440 K, while reaction on the clean surface occurs at 510 K [92]. On copper, however, reactions of *tert*-butoxy occur around 600 K, with only a slight shift to lower temperature when oxygen is present [99]. In all cases the oxygen-assisted

reaction has a significant kinetic isotope effect, indicating that C-H bond breaking is the rate-limiting step. While copper, silver, and gold all have the mechanism of γ-C-H bond breaking by co-adsorbed oxygen, only silver and gold have the dramatic change in stability, manifested by the reaction temperature shift of over 100 K, between the clean and oxygen-covered surfaces.

3.4.2 Coverage effects

The product distributions depend strongly on the oxygen coverage, and a sudden switch in selectivity takes place due to a very slight change in initial oxygen coverage, just below 0.3 ML O (Fig. 3.9). CO_2 is the dominant product at all initial oxygen coverages, but the other products differ significantly. The products occurring exclusively in the high temperature channel, methyl and methyl acetate, reach their peak yield at 0.2 ML O (corresponding to 0.4 ML of acetate), indicating that above this coverage, coadsorbed oxygen begins to be present, in agreement with the CO_2 peak shift in Fig. 3.4. Formaldehyde, which is most uniquely characteristic of the oxygen-assisted reaction pathway, peaks at 0.55 ML O. Total conversion of acetic acid also depends on oxygen coverage, and peaks when the maximum amount of acetate is formed on the surface, at both ~0.2 and 0.55 ML initial oxygen coverages. At higher oxygen coverages the total product yield decreases, apparently due to site limitations for acetate formation, as reflected by the increase in oxygen recombination above this coverage.

The amount of oxygen coadsorbed with the acetate dictates the products formed at 530, 450 and 400 K, respectively, with a pronounced further lowering of the peak

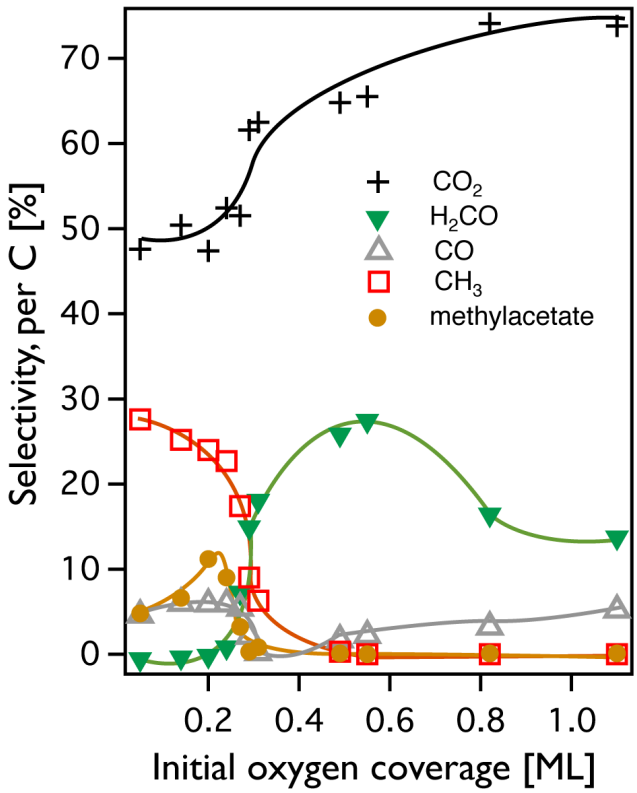

Figure 3.9: The selectivity (on a per carbon basis) for acetate reaction as a function of initial surface oxygen coverage shows a sharp change in product distribution at ~0.3 ML initial O coverage. Corresponding yield is shown in Fig. E.5. For details on the calculations on the yield and selectivity, see supporting information. The curves serve as a guide and do not correspond to a fit of the data.

Initial oxygen coverage (ML)	Dominant Reaction Temperature (K)	Coadsorbed O (ML)
0.05-0.24	530	none
0.27-0.31	440, 530	0.12-0.16
0.49-1.1	400	0.28-0.69

Table 3.1: Comparing surface coverage to reaction pathway.

temperature of the oxygen-assisted reaction at an initial coverage of ≥ 0.3 ML O (Table 3.1). Possible factors that could contribute to the further destabilization include the following: (1) a change in the dominant type of oxygen on the surface as the coverage increases, (2) repulsive lateral interactions among adsorbed acetate due to closer packing, and (3) a change in the binding of the acetate, perhaps to monodentate, causing it to react with oxygen at lower temperature. Because of the fact that both the oxygen structure and the coverage change as the surface is heated during the reaction, these effects are very difficult to separate. Notably, the shift of the lower temperature peak to 400 K only occurs when the combined coverage of acetate and co-adsorbed oxygen is high (above 0.8 ML, see Table E.2). This suggests that the shift arises from either a structural change or strong intermolecular interactions for a densely packed layer.

3.4.3 Reaction mechanisms

The switch in selectivity for acetate reaction on Au demonstrates how the product distributions can be tuned using by adjusting the steady-state oxygen coverage in a catalytic process (for example by changing the oxygen partial pressure) but also

suggests a new route for production of esters (Fig. 3.10).

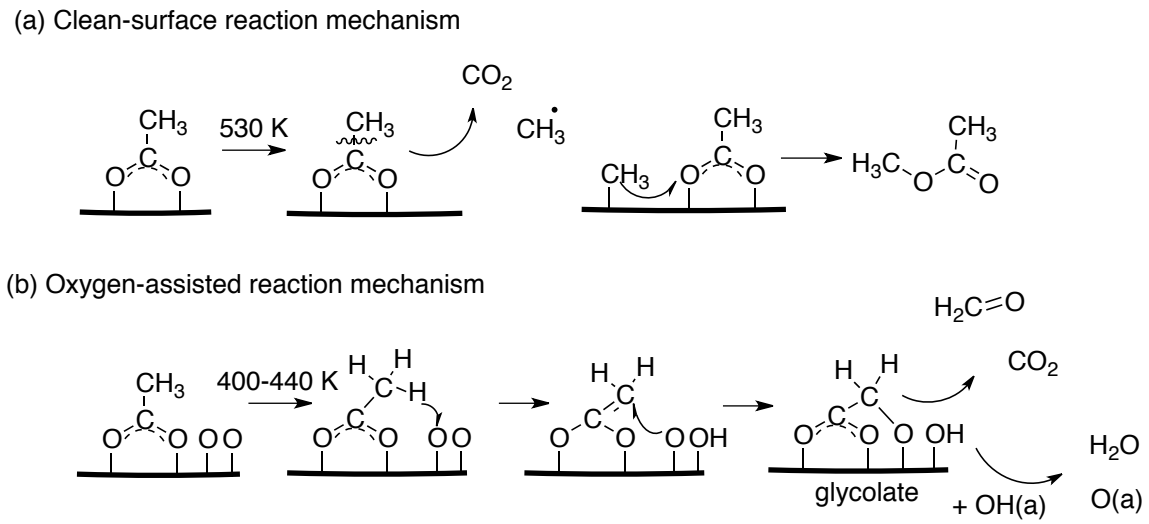

Figure 3.10: Reaction mechanisms for both the clean-surface and oxygen-assisted reaction pathways for acetate on Au(111).

Clean-surface pathway (530 K), Fig. 3.10a

In the absence of coadsorbed oxygen the decomposition of the acetate occurs through C-C bond activation by gold, yielding CO_2, methyl, methyl acetate and CO as the main products (Fig. 3.3). Because gold does not activate C-H bonds, the C-C scission occurs selectively at elevated temperatures. This led to the discovery of a different pathway for methyl ester formation–addition of methyl to one of the acetate oxygens. In the initial stages of reaction, there is intact acetate that reacts efficiently with the methyl to form methyl acetate. In a catalytic process, the conditions for selective C-C dissociation could be achieved by maintaining a low steady-state rate of O_2 dissociation relative to the rate of acetate formation by adjusting the partial pressures of reactants. The order of appearance of the products demonstrates clearly that C-C dissociation is the first step in the reaction of acetate on the clean gold surface (Fig. E.5). Specifically, CO_2 and methyl acetate form first at 460 K indicating

that C-C bond rupture is the first step, yielding CO_2 and CH_3 (Fig. 3.10a). Once the surface is depleted of acetate, gas phase methyl is evolved. Surface lifetimes of radical species have been measured to be the order of 10^{-8} s on Mo(110), giving sufficient time for reaction with nearby acetates initially [126]. The observation of a minor amount of ethane is also evidence for the finite lifetime of adsorbed methyl groups. The other products begin desorbing at 490 K, indicating the onset of C-O bond cleavage. Formation of H_3CCO is direct evidence for C-O bond dissociation, as well as minor products requiring $O_{(a)}$. Formed through the C-O bond cleavage, $O_{(a)}$ can attack a methyl group, resulting in γ-C-H bond activation to form small amounts of formaldehyde or even CO_2 in much the same way as the low temperature oxygen-assisted reaction. The minor products mechanisms are shown in Fig. E.6.

Oxygen-assisted pathway (400 - 440 K), Fig. 3.10b

Under O-rich conditions, adsorbed oxygen attacks the methyl group of the acetate leading to γ-CH activation and OH formation. This is demonstrated by the kinetic isotope effect observed for deuteration of the methyl group (Fig. 3.5). After γ-hydrogen activation another oxygen can react with the activated CH_2-moiety, ultimately forming formaldehyde and CO_2. An alternative mechanism would be for adsorbed oxygen to attack the methyl carbon, causing C-C bond cleavage to form adsorbed methoxy. However, methyl formate, which is the characteristic product of methoxy on gold [22], is not observed. Therefore, γ-CH activation and attack at the carbon center must lead directly to formaldehyde. We propose the formation of the glycolate intermediate, which is the same intermediate proposed for acetate reaction with oxygen on silver [97]. Cleavage of the glycolate C-C bond then leads to

formaldehyde and CO_2. However, the stoichiometry requires another channel for CO_2 formation (Table E.1, Fig. 3.9). As reflected in the ^{13}C data, some of the acetate methyl undergoes further H-activation to form CO_2 (Fig. 3.7). This could occur either by C-H activation of the glycolate intermediate or by secondary oxidation of the formaldehyde.

3.4.4 Comparison with reactivity of silver

The reactions of acetate on metallic gold and silver show interesting similarities and important differences. Most significantly, coadsorbed oxygen lowers the activation energy for acetate reaction on both metallic silver and gold, as manifested by the reaction temperature decreasing by well over 100 K as compared to reaction on the clean surfaces. In both cases, direct oxygen attack by adsorbed oxygen on the γ-H accounts well for the reactions observed. The main carbon-containing product of the oxygen-assisted reaction on both surfaces is CO_2. On silver the CO_2 originates from both the methyl and carboxyl carbons in separate, successive steps via conversion of the methyl to adsorbed formate, whereas on gold, CO_2 is formed primarily from the carboxyl carbon, with the methyl carbon forming primarily formaldehyde, even in the presence of excess oxygen. A glycolate intermediate is proposed on both surfaces, yielding formate and CO_2 on Ag and formaldehyde and CO_2 on Au. The explanation of this difference lies in the details of the activation energies and transition states during the attack of adsorbed oxygen on the methylenic carbon in the glycolate. If the interaction between adsorbed oxygen with this carbon is weaker on the gold surface it could be viewed as perturbative, leading to C-C bond rupture and formaldehyde

release, whereas a stronger interaction would lead to C-O bond formation resulting in adsorbed H_2CO_2, which is known to convert to formate. Further exploration of the energetics of these reaction pathways may be possible using density functional theory but is beyond the scope of the present study.

On the clean surface, it is clear that on both silver and gold, the C-C bond breaks, forming either methyl (gold) or methane (silver). This difference could be due to the inherent ability of silver (and inability of gold) to break C-H bonds and provide adsorbed hydrogen atoms, as the observed carbon deposition on silver is evidence for the liberation of hydrogen, which combines with methyl to form methane [76]. On gold, however, neither carbon deposition nor hydrogen evolution was detected; hence, there is no adsorbed atomic hydrogen with which to react to form methane. Further, no methyl acetate was observed on silver; however it is not known if this product was examined in the earlier work.

Patterns of reactivity have powerful abilities of prediction for catalytic activity. This study furthered develops the paradigm for oxygen-assisted reactions, establishing reaction principles for carboxylates on gold. Subtle differences in binding energy for the intermediates on gold and silver involved in these reactions lead to differences in reaction products, underscoring the necessity of accurate calculations for predicting relative rates of branching processes in catalytic reactions.

3.5 Conclusions

We have clearly established a pattern of low-temperature oxygen-assisted γ-C-H activation for carboxylates on gold and silver. The implications of this are two-fold.

First, coadsorbed oxygen significantly destabilizes adsorbed carboxylates on these metals by introducing a new, lower energy reaction pathway. On both silver and gold carboxylates have been implicated in surface site-blocking, thereby decreasing catalyst selectivity. By using these principles of oxygen-assisted reaction, it may be possible to decompose the unwanted carboxylates at lower temperature. Second, γ-CH activation is facile and selective when done directly by coadsorbed oxygen. This suggests, along with theory, that the same mechanism may be operative in selective, low-temperature β-CH activation on gold.

In the absence of oxygen, however, acetate undergoes C-C bond cleavage by the gold surface at higher temperature. An exciting outcome of this work is the discovery of a new route for methyl acetate synthesis. New, more complex ester formation via carboxylates maybe possible with knowledge of this new reaction pathway involving direct addition of alkyls to adsorbed carboxylates on gold.

3.6 Experimental Methods

Temperature programmed reaction spectroscopy (TPRS), which has been described in detail elsewhere [100], was done in an ultra high vacuum chamber with a base pressure of $\sim 2\text{x}10^{-10}$ torr using a triple filter Hiden quadrupole mass spectrometer (HAL-Hiden/3F). The heating rate in all experiments was 5 K/s. To prevent electron-stimulated reactions from taking place due to the mass spectrometer filament, a bias of -100 V was applied to the sample during TPRS experiments. The gold (111) single crystal was cleaned by argon ion sputtering and annealing to 900 K, followed by multiple oxidation cycles using ozone until no CO_2 desorbed from the

surface. Ozone was generated using a commercial ozone source (LG-7 CD Laboratory Ozone Generator). Approximately 15 g/(Nm^3) ozone in oxygen was constantly flowed through a gas line from which the ozone was dosed, creating adsorbed atomic oxygen on the surface. Each day, the ozone dose was calibrated using a reference saturation coverage of 1.1 ML. Acetic acid was dosed using a direct doser and doses were controlled by number of turns of the dosing valve; a background pressure rise was not observed during the acid doses.

To identify the products in each case, a rigorous method of quantitative TPRS was applied, which accounts for the mass fragments of all the species [26]. The product identities were deciphered using fragmentation patterns from neat samples or the NIST database when neat samples were unavailable, and confirmed by isotopic labeling. To calculate the yield for each product, the ionization cross section, quadrupole transmission and detection coefficients, and fragmentation patterns were taken into account. The correction factors applied are included in the Supporting Material (E), Tables E.2, E.3, and E.5. A MATLAB code was developed for the quantitative TPRS analysis, and is described in Appendix D.

Chapter 4

van der Waals Interactions Determine Selectivity in Catalysis by Metallic Gold

4.1 Abstract

To achieve high selectivity for catalytic reactions between two or more reactants on a heterogeneous catalyst, the relative concentrations of the reactive intermediates on the surface must be optimized. If species compete for binding sites, their concentrations depend on their relative binding strengths to the surface. In this chapter we describe a general framework for predicting the relative stability of organic intermediates involved in oxygen-assisted reactions on metallic gold with broad relevance to catalysis by metals. Combining theory and experiment, we establish that van der Waals interactions between the reactive intermediates and the surface, although weak,

determine relative stabilities and thereby dictate the conditions for optimum selectivity. The inclusion of these interactions is essential for predicting these trends. The concepts and methods employed here have broad applicability for determining the stability of intermediates on the surfaces of catalytic metals and specifically demonstrate the critical role of weak interactions in determining reaction selectivity among reactions of complex molecules.

This chapter has been accepted to *Journal of the American Chemical Society*.

4.2 Introduction

Controlling reaction selectivity is key to achieving energy efficiency and conserving resources in heterogeneously catalyzed, sustainable chemical processes [127]. An important determinant of reaction selectivity in heterogeneous catalysis is the competition of reactants and intermediates for reaction sites, [26] which dictates the relative concentrations of species on the surface and, hence, the reaction selectivity and overall product yield.

A striking illustration of the importance of competitive binding of reactants for surface sites in determining reaction selectivity arises in the oxidative cross-coupling of dissimilar alcohols over metallic gold; e.g., methanol and 1-butanol (Fig.4.1) [26]. In this example the reactive intermediates are formed by reaction with adsorbed atomic oxygen (O_{ads}) to yield surface-bound alkoxy by transfer of the alcoholic proton to the adsorbed O_{ads}. Competition between the alcohols and the adsorbed alkoxy moieties determines the relative concentrations of the two alkoxides (Fig. 4.2) and the

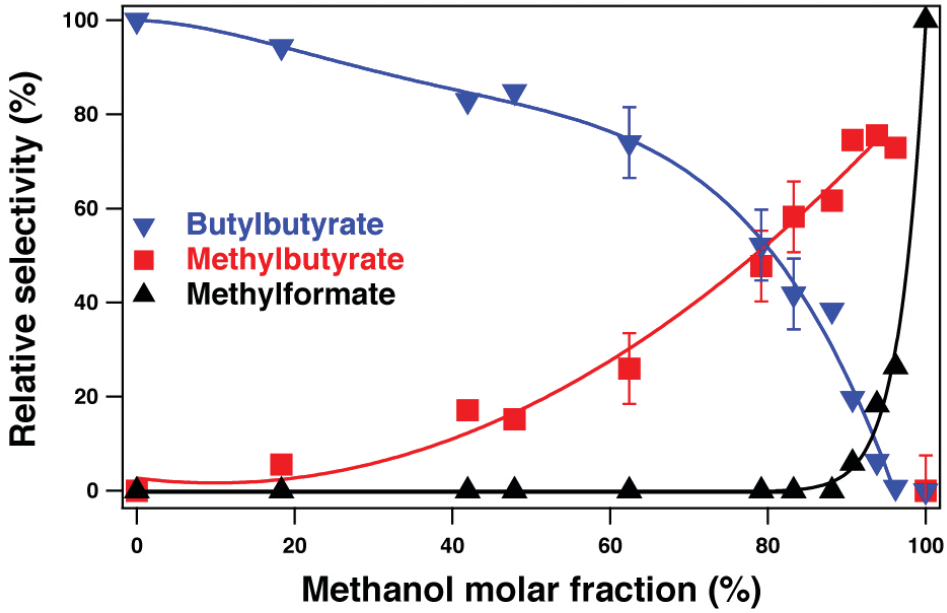

Figure 4.1: The selectivity for the esters formed from oxidative coupling of methanol and 1-butanol on O/Au(111) (θ_O=0.1 ML) depends strongly on the CH_3OH:1-C_4H_9OH due to the competition for reactive sites on the surface. Figure reprinted with permission from Xu, B.; Madix, R. J.; Friend, C. M.; J. Am. Chem. Soc., 2010, 132, 16571-16580. Copyright 2010 American Chemical Society.

distribution of esters subsequently formed by bimolecular combinations of the alkoxy species [26]. Because the binding of 1-butoxy, the adsorbed intermediate derived from 1-butanol, dominates over methoxy with an equilibrium constant for the reaction in Fig. 4.2 being ~10, the optimum selectivity for the formation of methylbutyrate requires *over 90% methanol* in the reaction mixture in order to achieve a sufficient methoxy concentration (Fig.4.1). If the two alkoxides competed equally for binding sites, the optimum ratio of methanol to butanol would be 1:1.

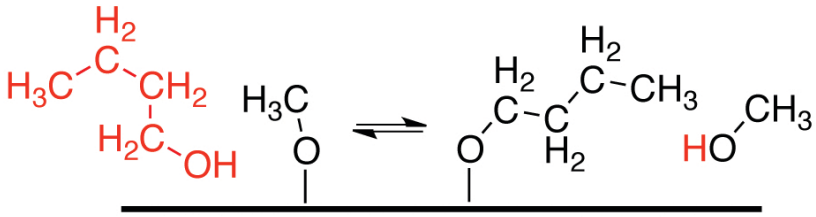

Figure 4.2: Competitive adsorption of alcohols on a catalyst surface.

Adsorbed intermediates that lead to side products, such as adsorbed carboxylates, also compete for binding sites, potentially affecting reactivity and selectivity [23, 76]. The strength of their binding to the surface is thus important in determining catalytic activity as well as selectivity. Strongly bound species, such as carboxylates, may inhibit reaction by blocking formation of other key reactive intermediates [73–75].

In this work we determine a hierarchy of stability with respect to displacement for a series of alkoxides and carboxylates on Au(111) as a first step toward understanding and predicting the competition for reactive sites and thereby controlling reaction selectivity. The underlying basis for our experimental studies is that organic acids and alcohols (generally designated as BH) selectively react with O bound to

metallic gold [61] according to

$$2\,\mathrm{BH}_{gas} + \mathrm{O}_{ads} \longrightarrow 2\,\mathrm{B}_{ads} + \mathrm{H_2O}_{ads}\,. \tag{4.1}$$

On Au(111), the conjugate base, B_{ads}, can usually be isolated on the surface by heating the surface to 200 K to desorb the water, because below this temperature no further reactions occur. Most of the adsorbed intermediates studied here have been identified in previous studies [22, 23, 26, 119, 128, 129] by a combination of vibrational and electronic spectroscopies and temperature programmed reaction.

A hierarchy of competitive binding strengths of the intermediates B_{ads} is established here by investigating displacement reactions [129] on the metallic Au surface,

$$\mathrm{B}_{ads} + \mathrm{B'H}_{gas} \rightleftharpoons \mathrm{BH}_{gas} + \mathrm{B}_{ads}\,. \tag{4.2}$$

The displacement reactions establish a scale for the surface stabilities of intermediates key to oxygen-assisted coupling reactions on Au(111), Bads that serves as the basis for predicting the relative concentrations of adsorbed intermediates in reactive environments. Notably, reaction 4.2 relates to the relative stability of adsorbed B and B′ and does not require the presence of adsorbed O to proceed. DFT+vdW was employed to a subset of these molecules to clarify the origin of the relative stabilities. *The inclusion of the relatively weak van der Waals (vdW) interactions is critical to predicting the order of stability of adsorbed oxygenates on Au(111).* This paradigmatic approach has broad applicability to other classes of molecules on coinage metals (Cu, Ag and Au) and to other metallic surfaces for predicting competition for binding sites that strongly affects catalytic activity and selectivity.

4.3 Methods

4.3.1 Experimental

All experiments were performed under ultra-high vacuum conditions in a chamber with a base pressure of $\sim 1 \times 10^{-10}$ torr. General procedures for crystal preparation and temperature programmed reaction (TPRS) have been described previously [100, 103] (see supporting information for details). The heating rate was constant at 5 K/s in all cases. Our experimental design included the collection of traces in the range m/z =2 to m/z = $2m$, where m is the molecular mass of the heaviest compound. Extensive calibrations and careful control of conditions were used to ensure that reproducible doses of the species were delivered to the surface (Fig. E.7).

Experiments were generally performed on a Au(111) surface covered with 0.05 ML O. Atomic oxygen was generated by introducing ozone to the surface [26, 46]. Ozone was produced using a commercial ozone generator (Ozone Engineering, LG-7) fed by an O_2 flow, generating a mixture of ~10% O_3 in O_2 which was then introduced to the surface using a directed doser. The coverage of adsorbed O was calibrated by comparison of the integrated O_2 signal due to O atom recombination above 500 K to the integrated signal for the saturation coverage of 1.1 ML [26, 46].

Two types of experiments were performed to determine the relative adsorption strengths of different molecules–displacement reactions and competitive adsorption reactions. Common to both, the surface was first dosed with ozone to prepare a surface containing 0.05 ± 0.01 ML of adsorbed O, hereafter referred to as O/Au(111). For displacement reactions a monolayer of BH was adsorbed on the 0.05 ML O/Au

surface at 140 K and the temperature was increased rapidly to a predetermined temperature to completely react the O_{ads} and desorb H_2O and excess molecular BH, isolating ~0.1 ML B_{ads}. This method was used if only reaction 4.1 occurred below the predetermined temperature. Isolated B_{ads} was identified by subsequent cooling to 140 K and performing TPRS to ensure the absence of residual molecular species as well as to confirm the presense of B_{ads} by monitoring its reaction (for example, Fig. E.8). The amount of residual adsorbed O following reaction this procedure was 0.0025 ML or less. After isolating B_{ads}, an excess (0.5 - 1.0 ML) of a second species, B′H, was dosed at 140 - 200 K onto the surface to test the occurrence of reaction 4.2 above. The relative amounts of B_{ads} and B_{ads} were distinguished by TPRS on the basis of the their signature products.

Alternatively, competitive adsorption was studied by dosing a mixture of BH and B′H onto the surface in excess of the pre-adsorbed 0.05 ML O/Au at ~140 K (by dosing the equivalent of a full monolayer of BH and B′H combined). The relative stabilities of B_{ads} and B_{ads} were judged by the competition of the two acids for the preadsorbed O, as determined by quantitative analysis of the product distribution measured subsequently by TPRS. This method was used when reactions of B_{ads} alone occurred at sufficiently low temperatures to preclude its isolation by annealing.

4.3.2 Theory

The calculations were carried out using the DFT+vdW^{surf} method [130], which extends pairwise vdW approaches to modeling of adsorbates on surfaces by a synergetic combination of the DFT+vdW method [131] for intermolecular interactions

with the Lifshitz-Zaremba-Kohn theory [132, 133] for the non-local Coulomb screening within the bulk. Semi-local PBE functional [134] was used throughout the paper. We employed the "tight" settings for integration grids and standard numerical atom-centered orbitals basis sets in FHI-aims code [135]. We used the "tier2" basis set for light elements (such as H, C, O, and F), and "tier1" for Au. The atomic zeroth-order regular approximation (ZORA) [136] was used to treat relativistic effects for metal atoms. We utilized 6-layer Au slabs with a (4×4) unit cell, and each slab was separated by a 40 Å vacuum. The bottom four metal layers were constrained, whereas the uppermost two metal layers and the adsorbate were allowed to fully relax during geometry relaxations. For slab calculations, we used a $3 \times 3 \times 1$ k-points mesh.

4.4 Results

The methodologies described above were used to determine the relative stability of specific intermediates (B_{ads}) utilizing their signature surface reactions. The species examined and the characteristic reaction products employed for the identification of B_{ads} are listed in (Table 4.1). The two methods described above are illustrated here with (1) the displacement of formate by trifluoroacetic acid and (2) the competitive reactions of co-adsorbed formic acid and methanol with O/Au(111). These methodologies were used for other pairs of BH and B′H to establish the scale of stabilities for a broad range of adsorbed species; the data for which are in the supporting information.

Organic acid, BH (Adsorbed conjugate base, B_{ads})	Characteristic reaction products	Peak temperature for products (K)
CF_3COOH (CF_3COO_{ads})	CO_2, CF_3	570
$HCOOH$ $(HCOO_{ads})$	CO_2	300
CH_3COOH (CH_3COO_{ads})	CO_2, CH_2CO	580
$CH_3(CH_2)_2COOH$ $(CH_3(CH_2)_2COO_{ads})$	CO_2, CH_3CHCH_2	530
CF_3CH_2OH $(CF_3CH_2O_{ads})$	$CF_3COOCH_2CF_3$	240
$c{-}C_6H_5{-}CH_2OH$ $(c{-}C_6H_5{-}CH_2O_{ads})$	C_6H_5CHO	250
$CH_3(CH_2)_3OH$ $(CH_3(CH_2)_3O_{ads})$	$C_3H_7COOC_4H_9$	300
CH_3CH_2OH $(CH_3CH_2O_{ads})$	$CH_3COOCH_2CH_3$	220
$HCCH$ (CCH_{ads})	$HCCH$	400

Table 4.1: Characteristic reactions for surface species B_{ads} on Au(111), which are derived from organic acids, BH.

4.4.1 Displacement of formate by trifluoroacetic acid

The reaction pair of formic acid (HCOOH) and trifluoroacetic acid (CF_3COOH) exemplifies the displacement reaction; trifluoroacetate (CF_3COO_{ads}) is more strongly bound to the surface (Fig. 4.3). By testing both orders of adsorption, we demonstrate that thermodynamic, *not* kinetic factors control the displacement process. The net reaction is:

$$CF_3COOH_{ads} + HCOO_{ads} \rightleftharpoons HCOOH + CF_3COO_{ads} \tag{4.3}$$

CF_3COO_{ads} was created by exposure of an excess of CF_3COOH to O/Au(111) (θ_0=0.05 ML) at 140 K, followed by rapid heating to 400 K to desorb unreacted CF_3COOH and water in order to isolate CF_3COO_{ads}.

$$2CF_3COOH_{ads} + O_{ads} \longrightarrow 2CF_3COO_{ads} + H_2O \tag{4.4}$$

The use of low surface concentrations of O guarantees the complete consumption of O during the reaction. Subsequent exposure of an excess of HCOOH at 200 K and heating showed only a minor amount of displacement of the trifluoroactate (Fig. 4.3).

Similarly, formate was isolated by reaction of formic acid with adsorbed O:

$$2HCOOH_{ads} + O_{ads} \longrightarrow 2HCOO_{ads} + H_2O \tag{4.5}$$

The adsorbed formate is displaced by exposure to excess CF_3COOH at 200 K (reaction 4.3). The near complete displacement of $HCOO_{ads}$ by CF_3COOH was demonstrated by the absence of the signature products of formate decomposition (water and CO_2 at 280 K) and the presence of those of CF_3COO_{ads} decomposition (CF_3 and CO_2 above

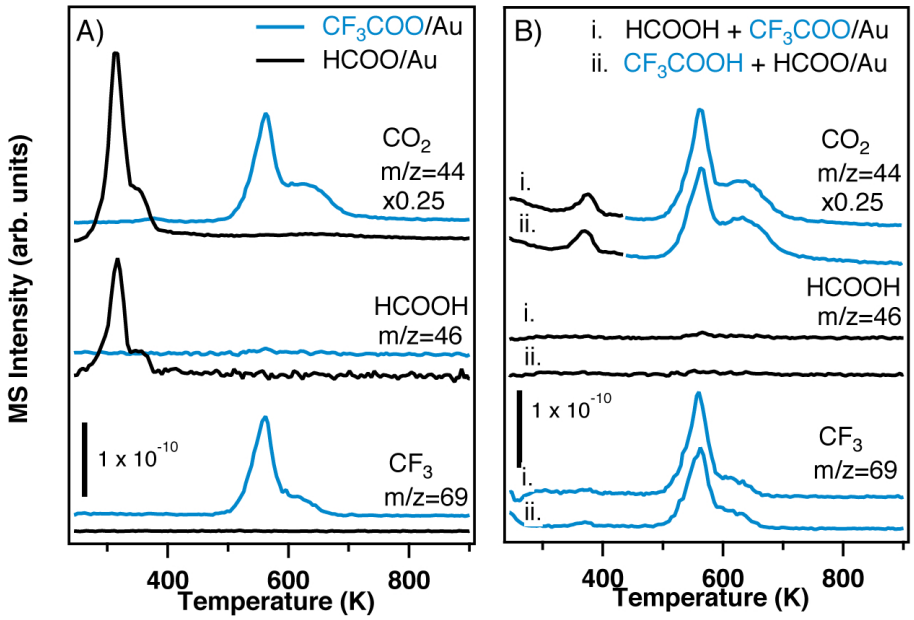

Figure 4.3: The displacement of formate by trifluoroacetic acid on Au(111) is demonstrated by monitoring characteristic decomposition reactions using temperature programmed reaction. (A) The characteristic "fingerprint" reaction products for reactions of the isolated formate (black) and trifluroacetate (blue) yield different products and occur at very different temperatures. Formate decomposes to CO_2 and HCOOH at 300 K, whereas trifluoroacetate yields CO_2 and CF_3 at 580 K. (B) The exposure of adsorbed formate to excess trifluoroacetic acid yields products characteristic of adsorbed trifluoroacetate (at 580 K). The product amounts and temperatures are independent of the order of adsorption as show, clearly showing that trifluoroacetate binding is stronger.

550 K) (Fig. 4.3; Table 4.1). These data unequivocally demonstrate that CF_3COO_{ads} readily displaces $HCOO_{ads}$ from Au(111).

Further, the integrated intensities of the characteristic CF_3 and CO_2 signals above 550 K for CF_3COO_{ads} decomposition are the same to within experimental error ($\pm$ 20%) for pure CF_3COO_{ads} created from CF_3COOH reaction on O/Au(111), for exposure of the formate-covered surface to CF_3COOH, and for exposure of HCOOH to Au covered with the trifluoroacetate (All derived from 0.05 ML O/Au(111). The small amount of CO_2 formed at 280 K is, however, indicative of a small amount of residual formate. Its presence does not affect any conclusions of this paper. On the basis of their relative gas phase acidities (4.6, Fig. 4.6), CF_3COOH (1351 kJ/mol) is expected to displace $HCOO_{ads}$ to form trifluoro acetate and formic acid (1448 kJ/mol) [129,137], whereas the opposite reaction is not expected.The gas phase acidity is defined as the enthalpy of the gas phase reaction,

$$BH_{gas} \longrightarrow B^-_{gas} + H^+_{gas} \qquad (\Delta H_{acid}) \cdot \tag{4.6}$$

4.4.2 Competitive adsorption of formic acid and methanol

The second method used to establish the relative stabilities of conjugate bases is co-adsorption, which is illustrated here by the competition between methanol and formic acid for reaction with O/Au(111). This methodology was used to investigate intermediates that themselves react or decompose below 200 K, precluding their isolation by annealing. For example, methoxy forms from methanol on O/Au(111) and reacts to form methyl formate below 200 K, preventing the isolation of methoxy by annealing to temperatures sufficient to desorb water.

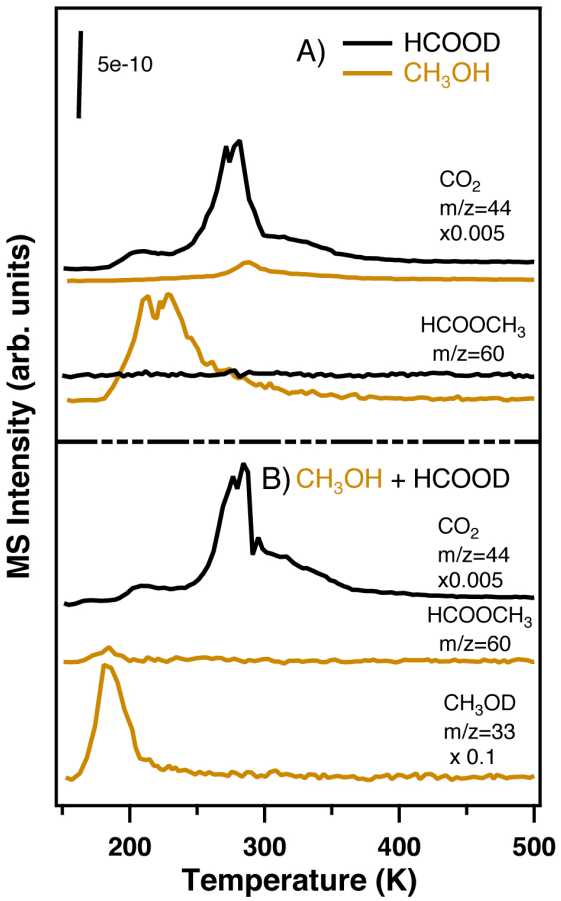

Figure 4.4: Temperature programmed reaction demonstrates the predominance of formate binding to the surface when CH_3OH and HCOOH are co-adsorbed on O/Au(111) (O = 0.05 ± 0.01 ML) at 140 K. A) The characteristic reactions of formic acid (black) alone and pure methanol (orange). B) The products observed from dosing a mixture of the two. Products characteristic of formate decomposition (CO_2) predominate in the mixture. Exposures were controlled to dose ~0.5 ML of each reactant.

The signature of methoxy in temperature programmed reaction is methyl formate (m/z 60), produced at 220 K [22], whereas the fingerprint for formate is CO_2 production near 300 K (Fig. 4.4). When methanol and formic acid are co-adsorbed onto O/Au at 140 K, formate is formed exclusively, the dominant product being CO_2 near 300 K (Fig. 4.4). The results of the competition of formic acid and methanol for adsorption on Au(111) is in accord with their respective gas phase acidities (1448 vs. 1598 kJ/mol) [137].

$$CH_3O_{ads} + HCOOD_{ads} \rightleftharpoons CH_3OD_{ads} + HCOO_{ads} \tag{4.7}$$

This experiment also shows that methoxy is *reversibly* formed on the surface in the competitive reaction, since CH_3OD is formed when CH_3OH and HCOOD are co-adsorbed. This could occur by methoxy reaction with OD/D_2O (Reactions 4.8-4.10), or methoxy directly reacting with HCOOD as in reaction 4.7.

$$CH_3OH_{ads} + O_{ads} \longrightarrow CH_3O_{ads} + OH_{ads} \tag{4.8}$$

$$HCOOD_{ads} + O_{ads} \longrightarrow HCOO_{ads} + OD_{ads} \tag{4.9}$$

$$CH_3O_{ads} + OD/D_2O_{ads} \rightleftharpoons CH_3OD_{ads} + O/OD_{ads} \tag{4.10}$$

That gas phase acidities provide an overall guide to the displacement reactions was shown using acetylene and methanol competition. Their relative gas phase acidities predict that acetylene should dominate methanol in competition for binding sites on Au(111). Whereas, for example, based on their C-H (~120 kcal/mol) and O-H

(~100 kcal/mol) bond strengths [129] or their relative pKa's, 26 and 15.5 respectively [129], the reaction

$$CH_3O + C_2H_2 \longrightarrow CH_3OH + C_2H \tag{4.11}$$

is highly unfavored. Acetylene binds reversibly, without reaction, to Au(111), but in the absence of preadsorbed O, as for methanol, hydrogen abstraction and chemisorption is effected by O_{ads}. When acetylene and methanol were co-dosed onto 0.05 ML O/ Au(111) at 140 K, preferential reaction of acetylene dominated (Fig. E.9). According to their relative gas phase acidities, reaction 4.12, this preference for adsorbed acetylide *is* reasonable,

$$CH_3O^-_{gas} + C_2H_{2gas} \longrightarrow CH_3OH_{gas} + C_2H^-_{gas} \qquad \Delta H = \text{-17 kcal/mol.} \tag{4.12}$$

We thus conclude that the relative reactivity of these adsorbed intermediates on Au(111) can be correlated to their gas phase acidities and that the surface acetylide is, correspondingly, more stable than methoxy. This conclusion supports the hypothsis that the relative stabilities of the intermediates we have studies may be guided by the gas phase acidities of their parent molecules.

4.4.3 Reversible displacement as a probe of competitive binding

When the stability of two surface intermediates is similar, their relative surface concentrations can be varied by controlling the relative exposure of their precursor molecules using reversible displacement. These experiments demonstrate that the relative concentrations of adsorbed reactive intermediates can be tuned by adjusting

their relative concentrations in a reactant mixture, taking advantage of small differences in their surface stabilities. This effect is illustrated for acetic acid and formic acid (Fig. 4.5), which compete for surface binding according to the equilibrium:

$$\mathrm{HCOOH}_{ads} + \mathrm{CH_3COO}_{ads} \rightleftharpoons \mathrm{HCOO}_{ads} + \mathrm{CH_3COOH}_{ads} \tag{4.13}$$

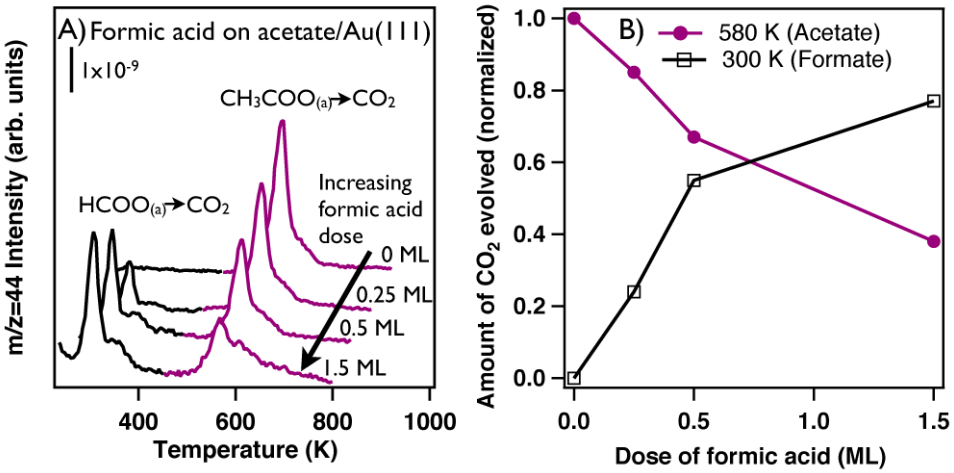

Figure 4.5: A) CO_2 evolution from coadsorbed formate (300 K) and acetate (580 K) on Au(111) initially precovered with 0.1 ML acetate (CH_3COO_{ads}/Au) and exposed to 0.0 - 1.5 ML formic acid at 140 K. The acetate-covered surface was prepared by dosing excess acetic acid on 0.05 ML O/Au and annealing to 210 K to eliminate water and unreacted acetic acid. B) The amounts of CO_2 evolved at 300 and 580 K are normalized to the amount of CO_2 for 0.1 ML of formate or acetate decomposition, respectively, found in separate experiments.

The total amount of $HCOO_{ads}$ and CH_3COO_{ads} is dictated by the amount of adsorbed O present prior to exposure to the mixture. Adsorbed acetate was formed initially by reaction of 0.05 ML O/Au(111) with acetic acid; it then was exposed to formic acid to form the mixed formate/acetate adsorbed layer. The amount of acetate remaining on the surface decreases with increasing formic acid exposure, based on the decrease in the amount of CO_2 produced from acetate decomposition (580 K) and

the corresponding increase in the CO_2 yield due to formate decomposition (300 K) (Fig. 4.5a). Within experimental control of the initial oxygen coverage (± 0.01 ML), the sum of the formate and acetate coverage is constant. Acetate is never completely displaced by formic acid; ~40% of the adsorbed acetate remains even for formic acid doses fifteen times the acetate surface concentration (Fig. 4.5b). This result indicates that surface bound acetate is more stable than formate.

Increasing surface stability ↑

Conjugate Base	Gas Phase Acidity* (kJ/mol)	Bond Dissociation Energy† (kJ/mol)	Probe Reaction‡
Butanoate	1451 ±8	439.8	1-$CH_3(CH_2)_2COOH$ + $CF_3COO_{(a)}$ → *1-$CH_3(CH_2)_2COO_{(a)}$* + CF_3COOH
Trifluoro acetate	1351 ±12	452.3 ±12	CF_3COOH + $CH_3COO_{(a)}$ → *$CF_3COO_{(a)}$* + CH_3COOH
Acetate	1456 ±9	468.6 ±12	*$CH_3COO_{(a)}$* + HCOOD ← CH_3COOD + $HCOO_{(a)}$
Formate	1445 ±9	468.6 ±12	C_6H_5OH + $HCOO_{(a)}$ ⇌ $C_6H_5O_{(a)}$ + HCOOH
Benzyl alkoxy	1548 ±8	442.7 ±8.8	C_6H_5OH + 1-$CH_3(CH_2)_3O_{(a)}$ → *$C_6H_5O_{(a)}$* + 1-$CH_3(CH_2)_3OH$
Butoxy	1570 ±8	432.3	1-$CH_3(CH_2)_3OH$ + *$HCOO_{(a)}$* ← HCOOH + 1-$CH_3(CH_2)_3O_{(a)}$
Ethoxy	1580 ±8	441 ±6	1-$CH_3(CH_2)_3OH$ + $CH_3CH_2O_{(a)}$ → *1-$CH_3(CH_2)_3O_{(a)}$* + CH_3CH_2OH
Trifluoro ethoxy	1513 ±10	447.7 ±10	$CF_3CH_2O_{(a)}$ + CH_3CH_2OH → *$CH_3CH_2O_{(a)}$* + CF_3CH_2OH
			1-$CH_3(CH_2)_3OH$ + $CF_3CH_2O_{(a)}$ → *1-$CH_3(CH_2)_3O_{(a)}$* + CF_3CH_2OH
Acetylide	1580 ±20	557.8 ±0.3	*$HCC_{(a)}$* + CH_3OH ← HCCH + $CH_3O_{(a)}$
Methoxy	1597 ±6	440.2 ±3	CH_3CH_2OH + $CH_3O_{(a)}$ → *$CH_3CH_2O_{(a)}$* + CH_3OH

Figure 4.6: Ordered stabilities of surface intermediates, the gas phase acidity of their parent acid (BH), and the reactions used to test their relative stabilities. Lower values of gas phase acidity (ΔH) indicate stronger gas phase acids. (*) Gas phase acidity (taken from NIST database) [137] is defined as ΔH for BH $\longrightarrow B^- + H^+$ (kJ/mol). Outliers to the gas phase acidity trend are indicated in bold. (†) The homolytic bond dissociation energy is defined as ΔH for BH $\longrightarrow B_{(g)} + H_{(g)}$ (kJ/mol). The recommended values from the Comprehensive Handbook of Chemical Bond Energies are included here [138]. (‡)The probe reactions are represented here as a dominant direction of equilibrium. Red arrows indicate a reversible but dominant direction. Black arrows indicate an irreversible reaction. As noted in the text, some probe reactions were displacement of an isolated intermediate, while others were competition experiments. The specific reaction data and conditions are provided in the supporting information (Section E.3, Figs. E.10-E.18).

4.4.4 Hierarchy of binding

Overall, the stabilities of the surface intermediates studied increase as the gas phase acidities of their precursors (BH) increase, similar to previous studies on O/Ag(110) [129]. Conversely, the relative stabilities do not correlate well with the homolytic bond dissociation energies (Figure 4.6) [138, 139]. Since reaction 4.6 is the heterolytic bond cleavage of BH, the reaction is endothermic, and smaller values of $\delta \mathrm{H}_{(}acid)$ correspond to higher gas phase acidity. Further, H^{+}_{gas} is common to all such reactions, so the relative gas phase acidities scale directly with the electron affinity of B_{gas}. The fact that the gas phase acidities have been correlated with the polarizability of B for similar species suggest that weaker physical interactions of B_{ads} with the surface may play an important role in its stability [140].

Relative gas phase acidities strictly employed would predict the equilibrium concentrations for the gas phase reaction

$$\mathrm{B}^{-}_{gas} + \mathrm{B'H}_{gas} \rightleftharpoons \mathrm{BH}_{gas} + \mathrm{B'}^{-}_{gas} \cdot \tag{4.14}$$

Reactions 4.2 and 4.14 differ critically in that B^{-}_{gas} and $\mathrm{B'}^{-}_{gas}$ are gas phase anions (reaction 4.14), whereas B_{ads} and $\mathrm{B'}_{ads}$ are bound to the surface (reaction 4.2). Thus, the heats of adsorption of B^{-}_{gas} and $\mathrm{B'}^{-}_{gas}$ may, in some cases, be sufficiently different to alter the order of surface stability (and displacement) predicted by the gas phase acidities.

On O/Au(111) the stabilities progress from methoxy ($\Delta \mathrm{H}_{acid}$ = 1597) to butanoate ($\Delta \mathrm{H}_{acid}$= 1451) in general agreement with the gas phase acidities of their parent acids (Fig. 4.6) [137]. The reactions used to establish the comparative surface stabilities are listed in the right hand column of Fig. 4.6. The data used for this table

is summarized in the supporting information (Figs. E.10-E.18). Notably, there are several exceptions to the trend with gas phase acidity, e.g. the fluorinated species, and formate vs acetate. The deviations from the correlation with the gas phase acidities require a more detailed examination of the surface bond energies of the intermediates using modern theoretical methods, as anticipated in the Introduction (reactions 4.2 and 4.4).

4.4.5 Calculations of alkoxide bonding

Calculations using the PBE+vdW^{surf} method were conducted to investigate the bonding of selected conjugate bases on the surface in order to provide more insight into the origin of the trends in binding energy. The structures and binding energies for a series of alkoxides bound to Au were examined: CH_3O_{ads}, $C_2H_5O_{ads}$, $CF_3CH_2O_{ads}$, and $1-C_4H_9O_{ads}$. In all cases the structures and binding energies were calculated both with and without vdW interactions, since the widely used DFT functionals, including PBE used in the present work, fail to capture the long-range vdW interactions [141] (Table 4.2).

The trend in the bond strength of the various alkoxides to the Au(111) surface is accurately predicted *only* if vdW interactions are included (Table 4.2). For example, the bond energies of ethoxy ($CH_3CH_2O_{ads}$) and 1-butoxy ($1-C_4H_9O_{ads}$) are essentially the same when PBE functionals are used; however, the experiments show that 1-butoxy is more strongly bound (Fig. 4.6). When vdW interactions are included, both the absolute bond energies and the relative bond energies within this series are changed significantly (Table 4.2) such that CH_3O_{ads}<$CF_3CH_2O_{ads}$<

Adsorbate	BE (eV) PBE	BE (eV) PBE+ vdW	Difference due to vdW (eV)
CH_3O	1.15	1.29	0.14
CF_3CH_2O	1.11	1.41	0.30
CH_3CH_3O	1.38	1.64	0.28
$1-CH_3(CH_2)_3O$	1.33	1.80	0.47

Table 4.2: The significant effect of van der Waals (vdW) interactions on the binding energies (BE) of alkoxides on Au(111).

$C_2H_5O_{ads}$<$1-C_4H_9O_{ads}$ as measured experimentally (Fig. 4.6). In contrast, calculations using the PBE functional alone predict that methoxy ≈ trifluorethoxy < ethoxy ≈1-butoxy; i.e. they do not reproduce experimental trends.

The increase in binding energies due to the inclusion of vdW interactions ranges from 0.14 eV for CH_3O_{ads} to 0.47 eV for $1-C_4H_9O_{ads}$, accounting for ~11% and ~26% of the total binding energy, respectively. The contribution due to the long-range vdW interaction is ~0.13 eV per carbon. Note that even though the $CF_3CH_2O_{ads}$ is bound more weakly than the $CH_3CH_2O_{ads}$, the contribution due to van der Waals interactions is similar. The lower overall binding energy for the trifluoro-ethoxy is attributed to repulsion of the electron-rich CF_3 group and the surface leading to an overall lower binding energy. Note that the effect of this repulsion is also manifested even if van der Waals interactions are not included when PBE functionals alone were used (Table 4.2).

The vdW interactions also alter the structure of the adsorbed species as illustrated for the specific case of ethoxy bound to Au(111) (Fig. 4.7). As might be anticipated, the inclusion of vdW interactions increases the Au-O-C1 bond angle from

123^o to 134^o such that the alkyl chain is tilted towards the surface. This tilting results in a decrease in the distance between the Au and C2 from 3.39 Å (PBE only) to 3.16 Å (PBE + vdWsurf), reflecting the attraction between the hydrocarbon tail and the Au surface. The distance between the Au surface and the O also increases by 0.06 Å when the vdw interactions are included for ethoxy. The elongation presumably reflects an optimization of the interactions between the Au and the O atom and the alkyl group. The relatively weak Au-O bond probably leads to the relatively large change in bond distance.

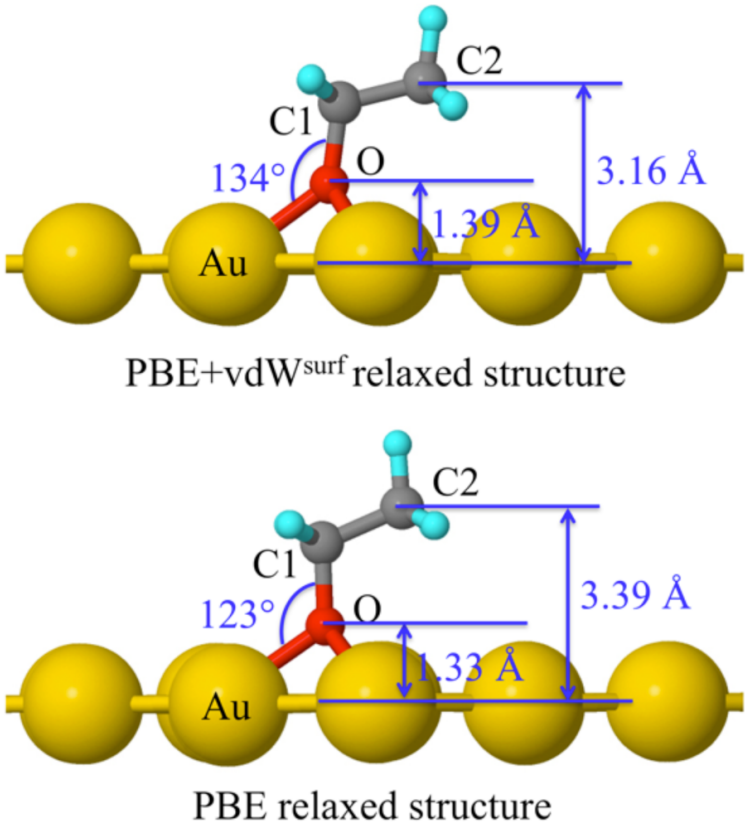

Figure 4.7: The structures of ethoxy (C_2H_5O) adsorbed on Au(111) with (top) and without (bottom) vdW interactions. Key bond lengths are changed by the vdW terms, including the Au-O, and Au-C2.

Similar structural changes occur when vdW interactions are included for the

other alkoxides bound to Au(111) (Figs. E.19-E.21). The Au-O-C1 bond angle generally increases and the distance between the terminal carbon and the surface generally decreases. Although the same trend is also observed for $CF_3CH_2O_{ads}$, the magnitude of the changes is smaller, probably due to repulsion between the electron-rich CF_3 group and the Au electrons. For example, the Au-O-C1 bond angle is smaller for $CF_3CH_2O_{ads}$ than for $CH_3CH_2O_{ads}$; the increase in this bond angle due to the inclusion of vdW interactions is also smaller–6^o vs. 11^o for $CF_3CH_2O_{ads}$ vs. $CH_3CH_2O_{ads}$. The change in the distance of O from the Au surface is also smaller for the trifluoro-ethoxyâĂŤ0.04 Å compared to 0.06 Å for ethoxy, e.g. (Figs. 4.7 and E.19-E.21). Note that the O-Au bond in the case of -CF_3 group relative to the other alkoxides stems from the direct modification of the electronic structure and is fully reproduced by the PBE functional without including vdW interactions. All of these structural differences for the trifluoro-ethoxy reflect the balance between the attractive van der Waals and the Pauli repulsion for the interaction between the CF_3 group in the trifluoro-ethoxide.

4.5 Discussion

In catalytic conditions, the hierarchy of relative stabilities can be used to guide adjustments in the partial pressures of reactants in order to achieve a desired ratio of concentration of surface intermediates, thereby affecting desired product selectivity. Here we focus on intermediates relevant to selective oxidative reactions on metals. For example, as noted in the Introduction, the selectivity for oxygen-assisted cross-esterification of different alcohols on gold can be controlled using this principle [26].

Alternatively, conditions may be designed to remove or mitigate unreactive spectator species that may inhibit reaction.

As suggested previously for metallic Ag surfaces, the adsorbed species under consideration can be classified as conjugate bases for gas phase H-acids, and the stability of these adsorbed conjugate bases generally correlates with their gas phase acidities [129]. The advantage of this correlation is that gas phase acidities are accurately known for a wide range of molecules; therefore providing a simple parameter to predict trends in reactivity and competition for reactive sites. However, though the relative stabilities of these adsorbed conjugate bases of the O-H gas phase acids generally correlate well with the gas-phase acidities of the parent acid, BH (Fig. 4.6), the notable exceptions provoke deeper analysis of the stability trends.

The DFT + vdW calculations clearly demonstrate the need to include vdW interactions for correct description of the molecular surface bonding. In the homologous series of alkoxides it is clear that weak interactions of the alkyl group significantly enhance the stability and the function of the adsorbed intermediates. For the C_1-C_4 linear alkoxides both the gas phase acidities and the binding energies calculated by DFT + vdW predict the same trend in surface stability. This is perhaps not unexpected as the effect of alkyl groups on the gas phase acidity of a set of alcohols is attributed to stabilization of the negatively charged alkoxide through polarization of the alkyl group; thus, the polarizability correlates with gas phase acidity [140]. The strength of the vdW interactions also correlates with polarizability of the alkyl groups. It is clear from Table 4.2 that these interactions must be included to account for the experimental trends, and the theory provides key insight into the underlying reason

for the correlations observed. Finally, it is notable that the binding energy trend calculated by PBE is modified and matches the experimental trend upon inclusion of the vdW interactions (Table 4.2).

There are notable exceptions to the correlation between conjugate base stabilities and gas phase acidities of the parent compounds, which are clarified by theory. Specifically, the relative stabilities of the fluorine-substituted adsorbed species, $CF_3CH_2O_{ads}$ and CF_3COO_{ads}, and of benzyl alkoxide, which contains a phenyl group, bound to Au(111) do not correlate well with their gas-phase acidities. For example, though the gas phase acidity of CF_3CH_2OH is higher than ethanol, butanol and benzyl alcohol, each of these species displaces $CF_3CH_2O_{ads}$, the reverse of the trend predicted by the gas phase acidities (Fig. 4.6). Likewise, trifluoroacetic acid (CF_3COOH) does not conform to the pattern predicted by its gas phase acidity (Fig. 4.6). Theory correctly accounts for these effects, showing that $CH_3CH_3O_{ads}$ is more strongly bound than $CF_3CH_2O_{ads}$, which in turn is more strongly bound than CH_3O_{ads}. Clearly this effect cannot be anticipated by the gas phase acidity correlation, since it does not account for differences in the heats of adsorption of the conjugate bases of the gas phase acids. The weakened bonding due to fluorine substitution is found in calculations and is attributed to repulsion of the electron-rich CF_3 group from the Au (see Table 4.2). Such substituent effects result in the larger O-Au equilibrium distance for $CF_3CH_2O_{ads}$ than for $CH_3CH_3O_{ads}$ upon adsorption on the Au(111) surface (1.45 vs. 1.39 Å), leading to a weaker chemical bonding for the $CF_3CH_2O_{ads}$/Au(111) system. The inclusion of vdW interactions is nevertheless important, increasing the binding energy of $CF_3CH_2O_{ads}$ by 0.30 eV, an amount slightly larger than that for

$CH_3CH_3O_{ads}$ (0.28 eV). This is due to the fact that the dispersion coefficient of F is somewhat larger than that of H (7.89 vs. 2.42 Hatree Bohr) [142]. We also note that the vdW interactions must be included in order to predict that the bonding of $CF_3CH_2O_{ads}$ is stronger than that of CH_3O_{ads}. The same conclusion was also found in the case of the $CF_3CH_2O_{ads}$ and $1-CH_3(CH_2)_3O_{ads}$ pair (see Table 4.2).

The relative stabilities were also compared with the homolytic bond energies, and there is no obvious guideline from their relative values. Recent work on platinum [139] shows an elegant example of a correlation between surface bond strength and the homolytic B-H bond energy. For comparison the homolytic bond energies are listed in Figure 4.6. Overall, the surface bond energies are approximately half the BH bond dissociation energy for a few select oxygenates on Pt(111). Though the results reported in that paper would predict that water would not spontaneously displace methoxy, as would be predicted on the basis of their gas phase acidities, application of the same scaling would not predict that acetylene would displace methoxy on gold. The binding energy of the acetylide to gold would have to be a substantially higher fraction of the bond dissociation energy of acetylene than was found for the correlation for the surface bond strengths of the oxygenates on Pt(111). In order to predict displacement from such information both the bond dissociation energy and the surface bond energy must he known (see Supporting Information). For the coinage metals, where dissociative adsorption of BH does not occur in the absence of adsorbed oxygen, these values may be hard to determine calorimetrically. Here we have shown that the displacements correlate well with the relative gas phase acidities, with understandable exceptions, as described.

Notably, the experimental trend in stability for carboxylates ($RCOO_{ads}$) is similar to the alkoxides: $HCOO_{ads}$<CH_3COO_{ads}<$CH_3(CH_2)_2COO_{ads}$. The stability increases as a function of alkyl chain length. The gas phase acidity of the corresponding acids–formic, acetic, and 1-butanoic–are all quite similar (Table 4.1), suggesting that van der Waals interactions between the surface and the alkyl group affect the surface stability of the carboxylate. The carboxylates are more stable on the surface that the alkoxides investigated. This result is also in accord with the general observation that the carboxylates bind in a bidentate configuration to metal surfaces at low surface concentrations. The effect of the primary bonding interaction with the surface, of course, also affects the overall stability relative to other intermediates listed in Fig. 4.6. Future theoretical studies are required to address this point. Further, it can be shown that if the homolytic bond dissociation energy of the displacing molecule, B′H, exceeds that of the parent molecule of the species being displaced (BH, B_{ads}) (Eqn. 4.2) the heat of adsorption of B'_{gas} is greater than that of B_{gas}; ie, B′ is more strongly bound (see Supporting Information). Thus, the data reveal that the carboxylate-Au interaction is stronger than the bonding of the alkoxides to the gold.

The other exception to the correlation between gas phase acidity and the stability of adsorbed conjugate base is benzyl alcohol ($c-C_6H_5CH_2OH$), which contains a phenyl ring that can interact with the surface. The gas phase acidity of benzyl alcohol lies between 1-butanol and formic acid (Fig. 4.6). Although it does displace 1-butanoate, consistent with the relative gas phase acidities, it is *not* displaced by formic acid. Instead, the stability of adsorbed formate and $c-C_6H_5CH_2O_{ads}$ are similar (Fig. 4.6, Fig. E.13). Based on the calculations for the linear alkoxides (Table 4.2)

we suggest that the higher stability of the benzyloxy ($c-C_6H_5CH_2O_{ads}$) compared to 1-butanoate is due to weak bonding interactions of the phenyl ring with the surface. Calculations are necessary to elucidate this point.

While the effect of van der Waals interactions is clearly important for predicting the binding strength of various intermediates to gold, it will be interesting to test for the magnitude of these effects on other surfaces. Generally, intermediates are bound relatively weakly to Au; thus the van der Waals interactions will naturally account for a larger percentage of the binding energy. In the case of 1-butoxide bound to Au(111), the van der Waals interaction accounts for ~25% of the total bond energy (Table 4.2). On a per carbon basis the increase in binding energy of the linear alkoxides due to van der Waals interactions is ~0.13 eV (~3 kcal/mol). For a homologous series of adsorbed species, which may be involved in competitive catalytic reactions of similar reactants, these interactions may significantly affect relative surface concentrations because of the exponential dependence of the surface coverage on the heat of adsorption.

The demand and desire for reaction selectivity prediction has driven efforts to develop simple scaling relationships for rates of elementary surface reactions based on binding energies of specific atoms to metals surfaces using density functional theory (DFT) studies [143, 144]. While these scaling relationships have been relatively successful for predicting periodic trends in the bonding and reactivity of small molecules, e.g. diatomics, NH_3, CH_4 and CH_3O, they are less successful in predicting differences in binding for analogous species with different functional groups, e.g. binding of alkoxides (RO_{ads}) with alkyl groups with different chain lengths. These structural differences between molecules can be important in competitive binding of reactants

in complex reaction environments [129, 145] and are, therefore, important to understand.

It is very likely that the contributions of van der Waals interactions on the binding of intermediates such as the alkoxides will also be dependent on the metal surface, leading to periodic trends that will be superimposed on the scaling in the O-metal binding energy calculated using standard DFT methods. Additional experimental and theoretical studies are necessary to establish these trends in the contribution of weak interactions to bonding to other surfaces so as to adjust scaling relationships for this critical factor. We also plan to further investigate similar trends in the binding of other functional groups to the surface in order to deepen our understanding of competitive binding in more complex reaction media.

4.6 Conclusions

A framework for predicting the relative stability of reaction intermediates important for selective oxidation on metallic gold has been developed from molecular gas phase acidities and DFT analysis including van der Waals interactions. The hierarchy was determined experimentally using displacement and competitive adsorption reactions of the parent molecules, and insight into the observed trends was provided by theory. The gas phase acidities of the parent molecules of these intermediates, BH, provide a general guide for the stability of the adsorbed intermediate, B_{ads}. Within that framework, however, notable exceptions arise, predominantly with molecules that have either significant surface binding energy increases due to vdW interactions or specific interactions due to other functional groups in the molecule. By includ-

ing these interactions in the DFT calculations, the experimentally observed trend in these stabilities is understood. These conclusions and techniques provide a general approach toward predicting the relative stability of reaction intermediates on transition metal surfaces, which is crucial for the optimization of reaction selectivity in complex reaction environments.

Chapter 5

The Effect of Fluorination on the Stability of Adsorbed Primary Alkoxy Species on Gold: Equilibrium Binding and the Rate of β-H Elimination

5.1 Abstract

The fundamental reactivity principles governing alcohol oxidation selectivity on gold were extended to 2,2,2-trifluoroethanol, in order to evaluate the influence of the -CF_3 group on stability of an alcohol in a reactive setting. Though 2,2,2-trifluoroethanol alone self-couples on O-covered Au(111), in the presence of methanol or ethanol it preferentially cross-couples to form the respective 2,2,2-trifluoroethoxy-esters. This result indicates that the rate of β-H elimination from the adsorbed

trifluoro-alkoxy is slower than for either adsorbed methoxy or ethoxy. This observation is consistent with the relative estimated beta-C-H bond strengths for these molecules. The equilibrium constants governing the formation of the adsorbed alkoxy species in the presence of both 2,2,2-trifluoroethanol and either ethanol or methanol were also calculated for these mixtures to be 2.4 and 0.38, respectively. The equilibrium constants are qualitatively in agreement with differences in binding energy calculated previously using density functional theory including van der Waals forces.

Planned submission to *Angewandte Chemie*.

5.2 Introduction

Recently, there has been a surge in interest in using hydrofluoroalcohols and hydrofluoroethers for industrial use in lubricants, electronic components, and refrigeration as more environmentally friendly alternatives for chlorofluorocarbons, which cause stratospheric ozone depletion. While hydrofluorocarbons and hydrochlorofluorocarbons have been in use as alternatives to chlorofluorocarbons in the last two decades, they retain global warming potential [146]. Hydrofluoroalcohols and hydrofluoroethers, however, cause less greenhouse warming and have even shorter atmospheric lifetimes due to higher reactivity [147, 148]. In order to develop fundamental understanding of hydrofluoroalcohols in catalytic reactions, which may lend insight into their degradation as well as possible production routes of hydrofluoroethers, we have examined the fundamental nature of the stability of adsorbed 2,2,2-trifluoroethoxy relative to other primary alkoxides on gold, which serves as a model catalyst surface.

Previous studies have shown that on gold surfaces alcohols require the presence of adsorbed atomic O to initiate reaction, [22, 115, 117, 146, 149] the first step being hydrogen transfer from the O-H to adsorbed O, yielding an adsorbed alkoxide (RO_{ads}) and hydroxyl. β-C-H scission in the adsorbed alkoxide then yields the corresponding aldehyde, which can either couple to remaining alkoxide to form an ester, desorb from the surface or react with excess adsorbed O along the pathway to combustion.

Following this mechanism, coupling of dissimilar alcohols can be achieved on gold, leading to the synthesis of various esters. The selectivity for production of specific esters from a mixture of different alcohols depends on two main factors in both model (eg, low pressure ultrahigh vacuum conditions) [26, 146–149] and flow reactor systems under catalytic conditions: (1) the relative rate of β-H elimination from the adsorbed alkoxy species to form the aldehyde, which determines the identity of the cross-coupling product, and (2) the relative concentrations of the reactant alkoxides, which is, in turn, determined by the equilibrium between the adsorbed intermediates and the ambient reactant gas. The second factor has been used to optimize the reaction selectivity for coupling of methanol with ethanol and 1-butanol on gold by adjusting the composition of the reaction mixture. [26, 146]

Here, the reactivity and relative stability of 2,2,2-trifluoroethoxide, derived from the corresponding alcohol, is investigated in order to ascertain the influence of the $-CF_3$ group on the reactions of alcohols. This work was motivated in part by our recent study of the relative stability of surface intermediates (Chapter 4), in which the surface stability of 2,2,2-trifluoroethoxide formed from 2,2,2-trifluoroethanol was compared to intermediates formed from reaction of other primary alcohols and acids with

adsorbed O on Au(111) using displacement reactions (Fig. 5.1). Density functional theory results, including van der Waals forces, predicted that 2,2,2-trifluoroethoxy would be more stable than methoxy and less stable than ethoxy and butoxy, in agreement with experiment. The binding of all of these alkoxides to Au(111) is significantly influenced by van der Waals forces; however, the binding of the trifluoro-ethoxy is also weakened by repulsive interactions between the surface and the electron-rich CF_3 group. In this work the effect of the CF_3 group on the surface binding strength is quantified; the effect of fluorination on the rate of β-C-H dissociation is also examined.

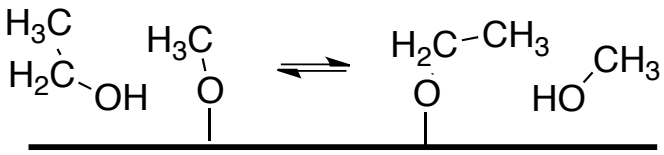

Figure 5.1: Competitive equilibrium of alkoxides on a gold surface, shown for methanol and ethanol.

A quantitative measurement for the relative stability of alkoxides on the surface was obtained by measuring the equilibrium constant between pairs of alkoxides and an ambient phase of known composition. In order to do this, a mixture of two alcohols of known composition was dosed on oxygen-covered gold at a low oxygen coverage such that all the oxygen was consumed and excess alcohol remained; it was assumed that equilibrium was reached on the surface, according to Fig. 5.1. Then the surface was heated, and the species leaving the surface were measured by quantitative temperature programmed reaction spectroscopy. Molecularly adsorbed species desorb intact, and each alkoxy species were identified and quantified on the basis of their well known product distributions and temperatures. The equilibrium constants were then computed over a wide range of ambient compositions. [26, 147, 148] The relative

rate of β-H elimination of the different alkoxy species is reflected in the identity of the coupling productsâĂŤthe alcohol which undergoes faster β-H elimination makes up the acyl portion of the alkyl-ester product (Fig. 5.2). [22, 26, 115, 117]

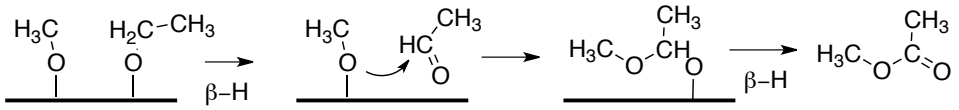

Figure 5.2: Cross-coupling between different alkoxides depends on relative rates of beta-H elimination, shown for methanol and ethanol.

In this work we observe significantly different equilibrium constants for each pair of species resulting from the relative surface stabilities of the alkoxy species on gold according to ethoxy > 2,2,2-trifluoroethoxy > methoxy. These measurements agree with the previously reported density functional theory results for the binding strength of the alkoxide intermediates. Also the $-CF_3$ group impedes β-H elimination relative to ethoxy and methoxy. While this trend correlates with the β hydrogen bond dissociation energies of the alcohols, further calculations to investigate the transition state and energy barrier for the β-H elimination would be helpful to fully understand this phenomenon.

5.3 Results and Discussion

5.3.1 Relative rates of β-H elimination

First, the products of the coupling reactions between the three pairs of alcohols were investigated to determine the relative rates of β-H elimination. It has been observed previously that the alcohol with the faster rate of β-H elimination provides

Bond broken (**bold**)	Bond dissociation energy (kJ/mol)	Distance between C1 of alkoxide and Au surface (Å) (from Chapter 4)
H_2**C-H**OH	402	2.83
H_3CH**C-H**OH	401	2.81
F_3CH**C-H**OH	409	2.86
$H_3CH_2CH_2$CH**C-H**OH	397	2.83

Table 5.1: Homolytic bond dissociation energies for relevant β-C-H bonds. Bond dissociation energies taken from [138] except for F_3CH_2COH, which was estimated using calculated enthalpies of formation from [148].

the ester of the coupled ester product, with the opposite alcohol then making up the alkoxy portion of the coupled ester [26]. Hence, the product distribution serves as a basis for determining the relative β-H elimination rate.

In the case of ethanol and 2,2,2-trifluoroethanol, the coupling product 2,2,2-trifluoroethylacetate indicates that β-H elimination from the ethanol is significantly faster than from 2,2,2-trifluoroethanol, as illustrated by temperature programmed reaction data for a mixture of 2,2,2-trifluoroethanol (31%) and ethanol (69%) on 0.1 ML O/Au(111) (Fig. 5.3).

The fact that $CF_3CH_2O{-}C(CH_3){=}O$ and $CH_3CH_2O{-}C(CH_3){=}O$ are produced, but not $CF_3CH_2O{-}C(CF_3){=}O$ or $CH_3CH_2O{-}C(CF_3){=}O$ in temperature programmed reaction for a mixture of 2,2,2-trifluoroethanol (31%) and ethanol (69%) on 0.1 ML O/Au(111), shows that β-C-H scission from the ethoxy is significantly faster than from 2,2,2-trifluoroethoxy. If β-C-H bond breaking occurred at a similar rate for the two alkoxides, all coupling products

would be observed.

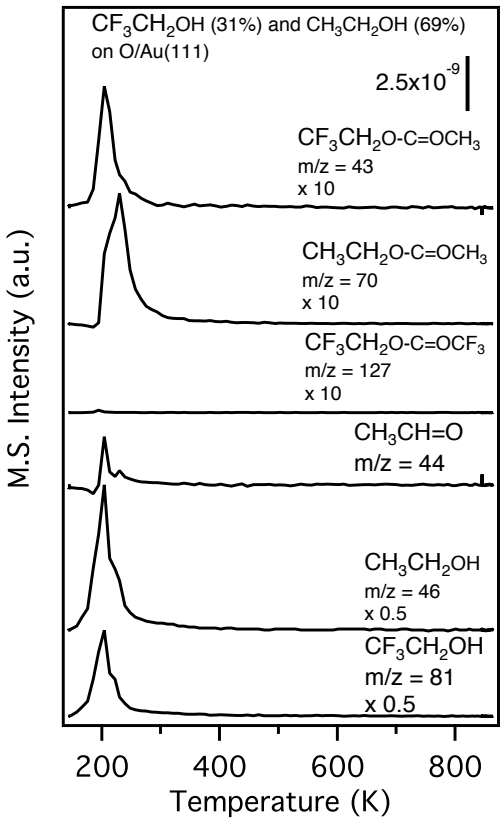

Figure 5.3: Oxidation of a mixture of 2,2,2-trifluoroethanol (31%) and ethanol (69%) on 0.1 ML O/Au(111). The mixture of alcohols was dosed in excess at 120 K, to ensure equilibrium could be reached between the alkoxides and the alcohols. The heating rate was 5 K/s. The relative amounts of the alcohols were determined from a condensation experiment of the alcohol mixture.

Similar results are observed for methanol 2,2,2-trifluoroethanol mixtures. In this case the cross-coupling product was 2,2,2-trifluoroethylformate, even for 2,2,2-trifluoroethanol and methanol on O/Au(111) (0.1 ML initial O coverage) dilute in methanol (Fig. 5.4). Therefore, the rate of β-H elimination is faster for methanol than 2,2,2-trifluoroethanol. This result is again consistent with the gas phase bond dissociation energies for the β-C-H bonds, as well as a possible influence of the â Ă Ş CF_3

group on the proximity of the β-H to the surface. Further calculations into the energy barriers and the transition states for β-H elimination would be helpful in further clarifying this reactivity trend.

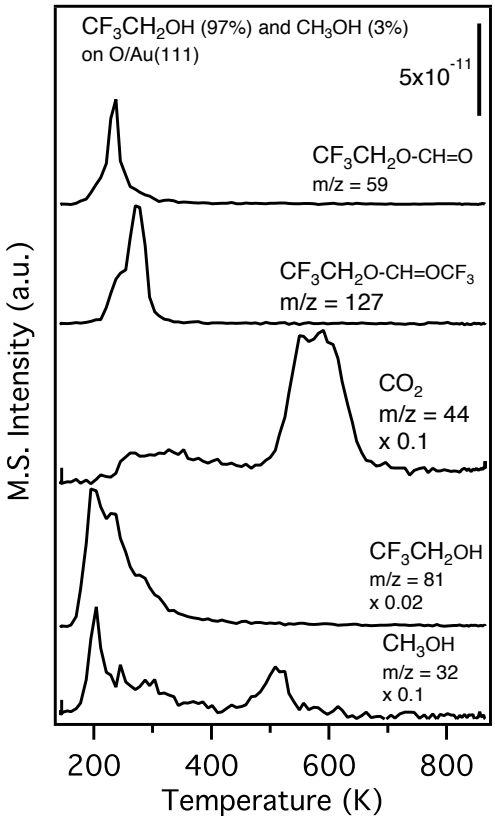

Figure 5.4: Oxidation of a mixture of 2,2,2-trifluoroethanol (97%) and methanol (3%) on 0.1 ML O/Au(111). The mixture of alcohols was dosed in excess at 120 K, to ensure equilibrium could be reached between the alkoxides and the alcohols. The heating rate was 5 K/s. The relative amounts of the alcohols were determined from a condensation experiment of the alcohol mixture.

There are two principal factors that are expected to affect the rate of C-H bond breaking: (1) the proximity of the β-H to the surface; and, (2) the β-C-H bond strength. The proximity to the surface is important because the abstraction of the β-H requires interaction with the surface or another surface-bound species. [77] Based

on the recent density functional calculations that include van der Waals interactions, the distance between the β-H and Au surface is closer in the non-fluorinated alkoxy species (as measured by the distance from the C1 carbon of the alkoxide to the Au surface (Table 5.1) because of repulsion between the CF_3 group and the surface,. Hence, the rate of β-C-H dissociation should be faster for ethoxy and methoxy in comparison to the trifluoro-ethoxy. The second factor, β-C-H bond strength, is not experimentally known for the $CF_3CH{-}HOH$ bond; however, recent calculations for ΔH_f for CF_3CHOH and CF_3CH_2OH [148], the bond dissociation energy for the $CF_3CH{-}HOH$ bond is estimated to be 409.3 kJ/mol, compared to 401 and 402 kJ/mol for methoxy and ethoxy, respectively (Table 5.1). Although these relative β-C-H bond energies are generally consistent with the more rapid elimination from ethoxy and methoxy, the differences may be too small relative to the error in the calculated energies to be definitive, and refinement of these values would be useful.

As a check for consistency with previous results, ethanol and 1-butanol reacted together in the presence of oxygen on gold. As predicted, 1-butoxy β-H eliminates faster, and the cross-coupling product observed is ethyl butyrate (Fig. 5.5). Also observed are the self-coupling products, butyl butyrate and ethylbutrate, as well as trace amounts of butanal and acetaldehyde (not shown). This confirms the previous conclusion that 1-butanol β-H eliminates at a faster rate than ethanol. This is consistent with the slight decrease in β-C-H bond strength (Table 5.1), although it is possible that other factors, like proximity to a surface $O_{(a)}$, which is enhanced by van der Waals interactions in the case of butoxy, could also play a role, although this is not evidently the primary reason, as the distance between the C1 of butoxy and

the gold surface is actually greater than the distance between the C1 of ethoxy and the gold surface. Further calculations to evaluate the energy barrier to the transition state might elucidate the reason for this discrepancy.

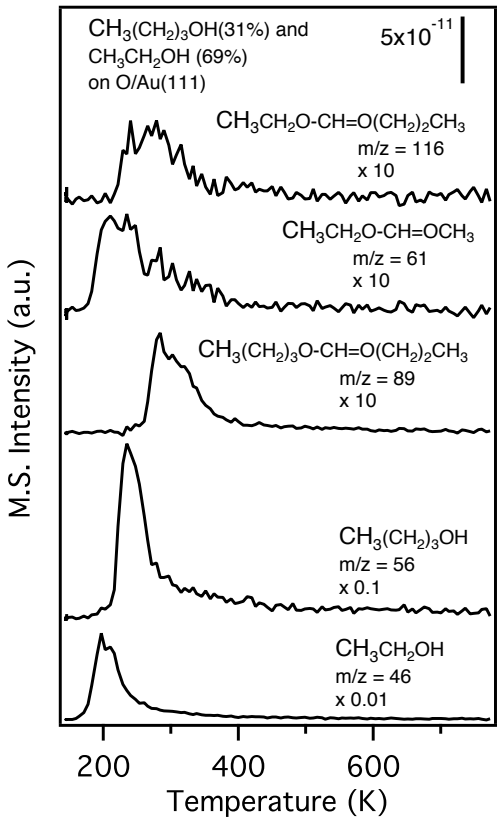

Figure 5.5: Oxidation of a mixture of butanol (31%) and ethanol (69%) on 0.1 ML O/Au(111). The mixture of alcohols was dosed in excess at 120 K, to ensure equilibrium could be reached between the alkoxides and the alcohols. The heating rate was 5 K/s. The relative amounts of the alcohols were determined from a condensation experiment of the alcohol mixture.

5.3.2 Determination of equilibrium constants

The equilibrium constants for the pairs of alcohols binding to the Au(111) surface were determined by systematically varying the composition of the mixtures of

the alcohols. A series of mixtures of two alcohols was dosed in excess on gold surface with 0.1 monolayers of pre-adsorbed atomic O. The alcohols then form an equilibrium mixture consisting of adsorbed alcohols and alkoxides (Fig. 5.1). The relative amounts of the surface alkoxides were calculated by quantitative analysis of the products using temperature programmed reaction. The equilibrium constants were then calculated for the reaction

$$\mathrm{RO}_{ads} + \mathrm{R}'\mathrm{OH} \rightleftharpoons \mathrm{ROH} + \mathrm{R}'\mathrm{O}_{ads} \tag{5.1}$$

either as a value at each point using the equation

$$\mathrm{K}_{eq}=[\mathrm{RO}][\mathrm{R}'\mathrm{OH}]/[\mathrm{R}'\mathrm{O}][\mathrm{ROH}], \tag{5.2}$$

or as a fit of the form

$$[\mathrm{RO}]=[\mathrm{ROH}]/(\mathrm{K}_{eq} + (1 - \mathrm{K}_{eq}) \cdot [\mathrm{ROH}]), \tag{5.3}$$

in a plot of alkoxide molar fraction vs. alcohol molar fraction. The concentrations of [ROH] and [ROH] dosed were determined by condensation and subsequent desorption of the mixture of alcohols without pre-adsorbed O. In this study, CF_3CH_2OH is always treated as ROH, whereas ethanol and methanol are identified as ROH. This way, a K_{eq} value greater than 1 indicates that the equilibrium lies to the right and favors the unfluorinated alkoxy, whereas a K_{eq} less than 1 indicates that the equilibrium lies to the left, favoring $CF_3CH_2O_{(a)}$. We use the same method as previously reported for determining the K_{eq} value between methanol and ethanol or butanol. [26]

The equilibrium constants for ethanol and 2,2,2-trifluoroethanol (Fig. 5.6a) and 2,2,2-trifluoroethanol and methanol (Fig. 5.6b) were calculated to be 2.4 and 0.38,

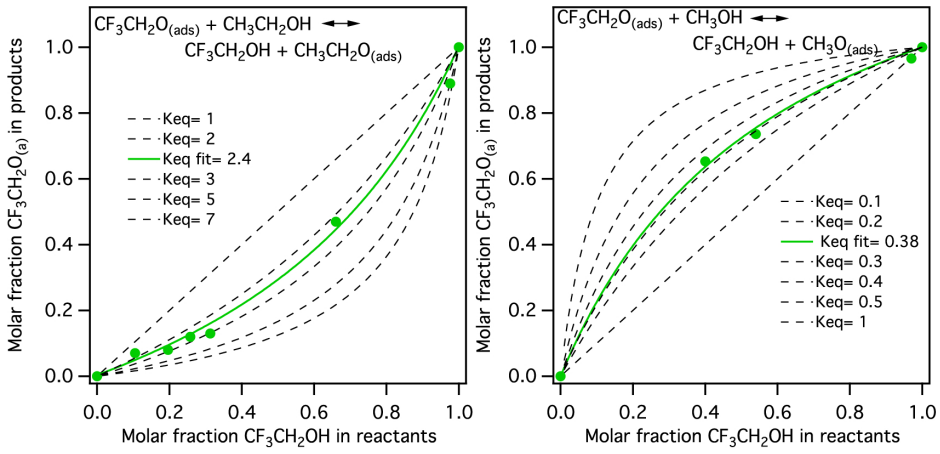

Figure 5.6: Equilibrium constant determinations for 2,2,2-trifluoroethoxide with methoxide or ethoxide on Au(111).

respectively (Table 5.2), in agreement with the trend in binding energies of the different alkoxide intermediates previously calculated by DFT including the van der Waals interactions: 1-butoxide > ethoxide > trifluoro-ethoxide > methoxide. The K_{eq}'s for methanol and ethanol can then be estimated by taking the ratio of these numbers (2.4/0.38), which gives K_{eq}~6. This is quite close to the previously measured value of 5, indicating that our results are internally consistent. Though the relative K_{eq} values are qualitatively consistent with the relative differences in calculated binding energies for the adsorbed alkoxide intermediates (Table 5.2), when including van der Waals forces, the energetic differences are larger than those expected from the measured equilibrium constants. These differences appear too large to be accounted for by the inclusion of entropic factors. Certainly there is some experimental error in the value of the equilibrium constants, but must lie in the range of 10 to 0.1 since formation of the alkoxy species is competitive at all binary concentrations studied. Nevertheless, the trend for the relative binding of this set of species is predicted using

Alcohol Pair	Difference in BE of alkoxides (eV) (from Chapter 4)	K_{eq}
Butanol, methanol	0.51	10
Ethanol, methanol	0.35	5
Butanol, ethanol	0.16	2.5
Ethanol, 2,2,2-trifluoroethanol	0.23	2.4
2,2,2-trifluoroethanol, methanol	0.12	2.6

Table 5.2: K_{eq} values are consistent with difference in BE's of the alkoxides.

electronic structure calculations if van der Waals interactions are included, whereas their exclusion gives qualitatively incorrect predictions.

5.4 Conclusions

2,2,2-Trifluoroethoxy has a slower rate of β-H elimination than both methoxy and ethoxy. These results are consistent with the estimated β-H bond dissociation energies of the alcohols and with the geometric structures of the adsorbed alkoxides predicted by DFT including van der Waals forces. The binding energy of adsorbed 2,2,2-trifluoroethoxy lies between ethanol and methanol, manifesting dramatically differences between the equilibrium constants for formation of the 2,2,2-trifluoroethoxy in the presence of ethanol or methanol, respectively.

Chapter 6

Direct Selective Oxygen-Assisted Acylation of Amines Driven by Metallic Silver Surfaces: Dimethlyamine with Formaldehyde

6.1 Abstract

Facile, direct acylation of dimethylamine with formaldehyde to N, N-dimethylformamide proceeds with a selectivity approaching 100% at low oxygen concentrations on metallic silver surfaces; the reaction proceeds via nucleophilic attack of adsorbed dimethylamide on formaldehyde with subsequent β-H elimination from the adsorbed hemiaminal.

This paper was published in *Chemical Communications*, **2010**, *46*, 704-706.

6.2 Introduction

Acylation of amines is a fundamentally important synthetic process in chemistry and biology [150]. The amide group, important in natural products, polymers, and pharmaceuticals, can be introduced by reactions of carboxylic acids or their derivatives with amines [151], modified Staudinger reactions [152], aminocarbonylation of halides with CO and amines [153], mercury-catalyzed rearrangements of ketoxime [154], and transition-metal-catalyzed carbonylation of alkenes [153] and alkynes [155] with amines. These processes, however, often involve complex procedures and produce toxic chemical waste [156]. Recently, direct synthesis of amides by reacting alcohols [157,158] or aldehydes [159,160] with amines has attracted growing interest, because of the more environmentally benign nature of these reactions, as well as the wide availability of the starting materials. A few homogeneous transition metal complexes [157–159] have been reported to effectively catalyze this class of reactions, although the mechanism remains unclear. Alternatively, recent studies of supported gold catalysts in direct synthesis of amides [71, 72] suggest that a greener heterogeneous catalytic process may be possible. We report here for the first time the direct acylation of an amine mediated by metallic silver, the elementary surface reaction steps that comprise this transformation, and the underlying chemical character of the reaction intermediates that selectively drive the reaction.

The acylation of the amine is facilitated by oxygen (O) adsorbed on the silver surfaces, and the specificity of the reaction originates in the chemical nature of this oxygen. On both Ag(110) and Ag(111), adsorbed oxygen atoms form structures into which added silver atoms are incorporated. On Ag(110) this structure

takes the form of extended -O-Ag-O- chains [161], whereas on Ag(111) an hexagonal, honeycomb structure forms [162]. Further, it is well established that oxygen adsorbed on silver surfaces (O/Ag) behaves both as a Brønsted base and a strong nuceophile [10, 96, 145, 163–167]. As a Brønsted base O/Ag selectively activates gas phase acids, BH, to produce the adsorbed anion of the conjugate base, B^-_{ads} and eliminate water [129, 167]. Subsequent reactions are then dictated by the reactivity of B^-_{ads}. Alcohols, for example, are intitally deprotonated by O/Ag to form alkoxides, which then β-H eliminate to yield aldehydes with extremely high selectivity [10, 168]. Aldehydes may also be attacked at the electron deficient carbon by O/Ag acting as a nucleophile to yield adsorbed carboxylates [10, 163, 169], which ultimately produce carbon dioxide and water in an oxidizing environment. The explication of these reactions, obtained entirely using ultra high vacuum studies, affords complete understanding of the industrial conditions used for formaldehyde production on silver catalyst [170, 171].

Further, metallic silver is known to effect the oxygen-assisted esterification of alcohols [10]. This reaction is initiated via selective O-H activation in the alcohol to form the surface alkoxides. Under appropriate conditions as the aldehyde is formed by β-H elimination from the alkoxide, it undergoes nucleophilic attack by coadsorbed alkoxide to form the hemiacetal, which β-H eliminates to form the ester. Previous research indicates that the alkoxide can be considered to be anionic and, thus, it can react as a nucleophile [129].

Earlier studies have established that ammonia and amines are also deprotonated by O/Ag, as is expected from the general pattern of reactivity described above.

Ammonia reacts with O/Ag to form adsorbed N and NH [59], and ethylamine reacts similarly to form adsorbed CH_3CH_2N, which reacts further by β-H elimination to acetonitrile [58], for example. It may be anticipated that adsorbed amides, such as $RR'N_{ads}$, can react as nucleophiles as do adsorbed alkoxides. In this communication, we report the highly selective oxygen-assisted acylation of dimethylamine with formaldehyde mediated by metallic silver surfaces. The coupling product, N, N-dimethylformamide was formed on both Ag(111) and Ag(110) single crystal surfaces with nearly 100% selectivity, under controlled, low oxygen coverages. In exact analogy with esterification via the alkoxide intermediate, the nucleophilic character of the adsorbed amide, selectively formed by O activation of the N-H bond, drives the acylation of the amine.

6.3 Results and Discussion

The reactions were conducted by dosing dimethylamine and formaldehyde sequentially on oxygen-covered single crystal silver surfaces and subsequently heating the surface in vacuum. This procedure affords maximum definition of the reaction conditions and has been employed to study many heterogeneously catalyzed reactions [87]. Deuterated formaldehyde and dimethylamine were also employed to establish the product identity by mass spectrometry. Fig. 6.1a shows the evolution of reaction products from perhydrido dimethylamine and a mixture of d_0- and d_2-formaldehyde (1.8:1) on Ag(111) initially covered with 0.1 monolayer (ML) oxygen. Aside from the adsorbed reactants (not shown), H_2O desorbs at 180 K, followed by the simultaneous evolution of N,N-dimethylformamide ($(CH_3)_2NC(H)=O$), H_2, and

H_2O at 270 K, and d_1-N,N-dimethylformamide ($(CH_3)_2NC(D)=O$), D_2, and HDO at 285 K. Experiments with d_6-dimethylamine and d_2-formaldehyde as well as quantitative mass fragmentation analysis show the water at 180 K to arise from the selective deprotonation of the N-H bond in the amine. N,N-dimethylformamide was identified by quantitative comparison of the mass fragmentation pattern of the product to that measured for a condensed neat sample desorbed from the clean surface (Table 6.1). No CO_2 (m/z 44), NO_2 (m/z 46), or other secondary oxidation products were detected above the noise level, which for CO_2 was 0.01 monolayer. Further, no residual carbon or nitrogen species was detectable by X-ray photoelectron spectroscopy on the surface after completion of temperature programmed heating to 700 K to complete the reactions. Reaction of d_6-dimethylamine ($(CD_3)_2NH$) and d_0-formaldehyde yields H_2O at 180 K, and d_6-N, N-dimethylformamide ($(CD_3)_2NC(H)=O$) (indicated by the mass shift of the parent ion from 73 to 79 amu and the corresponding mass shifts of the primary mass fragments), as well as H_2, and H_2O at 270 K (Fig. 6.1b). Clearly, the facile production of N, N-dimethylformamide with ~100% selectivity is achieved on Ag(111) under the conditions employed. The temperature at which these products form suggest an activation energy of approximately 17 kcal/mol for the rate-limiting step.

The absence of deuterated water (D_2O and DHO) below 250 K strongly suggests the selective activation of the N-H bond in $(CD_3)_2NH$ by O/Ag to form the $(CD_3)_2N_{ads}$ intermediate, as anticipated from previous work. The isotopic substitutions also clearly show that the methyl groups in the dimethylamine and the carbonyl group in the formaldehyde are preserved and that the only C-H bond breaking is from the

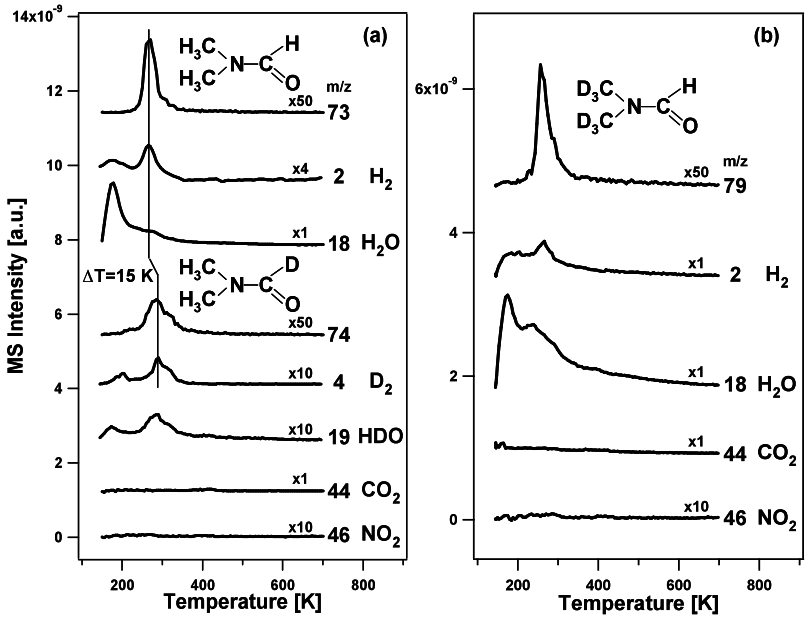

Figure 6.1: Temperature programmed reaction spectra of (a) dimethylamine and a mixture of d_0/d_2-formaldehyde on 0.1 ML O-covered Ag(111) initially at 140 K, and (b) d_6-dimethylamine and formaldehyde on 0.1 ML O-covered Ag(111) initially at 140 K, respectively. The contributions from fragmentation of N,N-dimethylformamide and dimethylamine to the m/z 44 signal, and of dimethylamine to the m/z 46 signal were subtracted for clarity.

m/z	Product at 270 K	Multilayer of N, N-dimethylformamide condensed on clean surfaces at 120 K
73	45	45
72	4	4
45	9	11
44	100	100
42	69	69

Table 6.1: The relative intensities of mass fragments for N, N-dimethylformamide formed in by reaction of dimethylamine and formaldehyde on the oxygen-covered Ag(111) and (110) surfaces at 270 K and that of the condensed neat sample. This quantitative comparison was used to identify the product. The other products in the reactions (CO_2, NO_2 and H_2O) were identified on the basis of their corresponding fragmentation patterns in the NIST database.

aldehyde. Thus, it is clear that the adsorbed $(CD_3)_2N$ group adds to the formaldehyde or a derivative thereof. The C-H bond in formaldehyde is not activated by silver itself, and adsorbed HCO is not formed [10]. An oxidized intermediate of formaldehyde can be ruled out, as it is known that formaldehyde is selectively oxidized to formate on silver, which yields CO_2 and H_2 at $\sim$ 400 K [96]. In fact, there is not a trace of formate formation at the low initial oxygen coverages. Further, reaction of dimethylamine with formate on O/Ag(111) at 140 K produced no N,N-dimethylformamide (Fig. E.22). Thus, the adsorbed amide appears to add directly to the carbonyl carbon of the formaldehyde. Notably, $(CH_3)_2NC(D)=O$ (and D_2) evolves at $\sim$ 15 K higher than $(CH_3)_2NC(H)=O$ and $(CD_3)_2NC(H)=O$ (and H_2) in the acylation reactions involving D_2CO and H_2CO (Fig. 6.1a), respectively. This is a clear kinetic isotope effect (KIE) [94], suggesting that breaking the C-H bond originally associated with

the aldehyde group is involved in the rate-limiting step. This KIE, coupled with the fact that hydrogen, water and N, N-dimethylformamide form simultaneously, strongly suggests that N, N-dimethylformamide is formed from rate limiting β-H elimination from the adsorbed hemiaminal intermediate, $(CH_3)_2NC(H_2)O_{ads}$ (Fig. 6.3).

N, N-dimethylformamide was also formed with ~ 100% selectivity in the reaction of dimethylamine and formaldehyde on the Ag(110) surface initially covered with 0.25 ML O (Fig. 6.2a). When the initial oxygen coverage was increased to 0.5 ML, combustion products, CO_2, NO_2, and H_2 were also detected (Fig. 6.2b). These products appear to be formed via direct oxidation of dimethylamine and formaldehyde, as they also appear at identical temperatures in the separate oxidation of dimethylamine or formaldehyde on O-covered Ag(110) (Figs. E.23 and E.24). Clearly, the selective O-assisted acylation of dimethylamine by formaldehyde on silver surfaces requires control of the oxygen coverage and the relative reactant concentrations in order to suppress secondary oxidation reactions.

Catalytic cycles have been successfully derived from mechanistic studies of partial oxidation of methanol to formaldehyde on silver single crystals in ultrahigh vacuum [10]. The surface methoxy group is the rate-limiting reaction intermediate for formaldehyde production. As noted earlier, recently microkinetic models using this cycle, with its accompanying combustion reactions via the formate intermediate, have been shown to accurately account for choices of operating conditions for methanol oxidation under industrial conditions [171].

In order to provide a framework for microkinetic modeling of the acylation reaction reported here, a catalytic cycle for silver-mediated acylation of dimethylamine

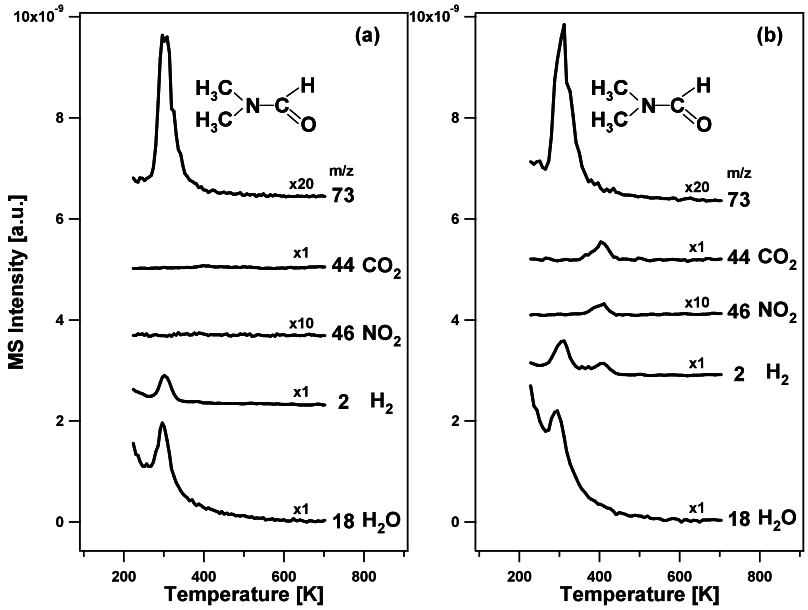

Figure 6.2: Temperature programmed reaction spectra of dimethylamine and formaldehyde on (a) 0.25 ML O-covered Ag(110), and (b) 0.5 ML O-covered Ag(110) initially at 120 K, respectively. The contributions from fragmentation of N, N-dimethylformamide and dimethylamine to the m/z 44 signal, and of dimethylamine to the m/z 46 signal were subtracted for clarity.

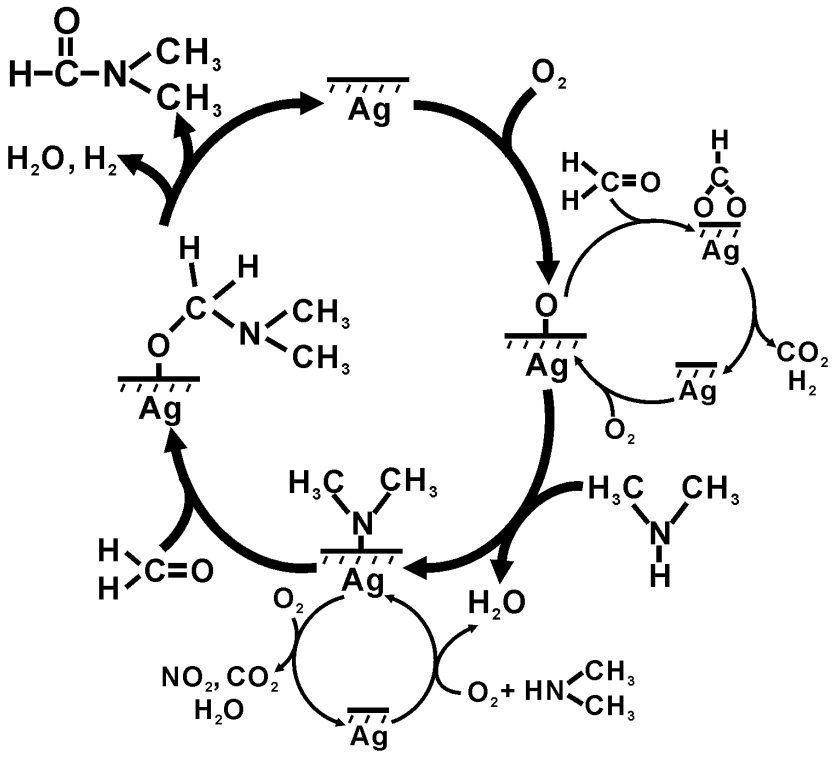

Figure 6.3: The catalytic cycle for silver-mediated acylation of dimethylamine with formaldehyde. Two competing pathways leading to the combustion products are also included in the scheme.

with formaldehyde, as well as two competing combustion pathways (Figs. E.23 and E.24), is proposed in Fig. 6.3. Dioxygen dissociates on the silver surfaces to form chemisorbed oxygen [88]. The first reaction step is selective, oxidative deprotonation of dimethylamine to form adsorbed amide, $(CH_3)_2N_{ads}$ and water. Nucleophilic attack by adsorbed $(CH_3)_2N$ at the aldehydic carbon in formaldehyde forms the adsorbed hemiaminal intermediate, $(CH_3)_2NC(H_2)O_{ads}$. The following β-hydride elimination is the rate-limiting step for the formation of N, N-dimethylformamide. This reaction mechanism, which is analogous to that proposed on transition metal complexes [157], and is analogous to esterification of alcohols by aldehydes [10] should be applicable to the oxygen-assisted acylation of amines mediated by metallic silver in both the vapor and liquid phases if conducted under appropriate conditions.

6.4 Conclusions

In conclusion, we have demonstrated the highly selective oxygen-assisted, silver-mediated synthesis of N, N-dimethylformamide via acylation of dimethylamine with formaldehyde on silver single crystals. The oxygen coverage and the relative reactant concentrations can be controlled to achieve 100% selectivity towards N, N-dimethylformamide. Further investigations into the generality of silver catalysts in acylation of amines and the synthetic application of this catalytic process are in progress.

Chapter 7

Nucleophilic Reactivity of Hydroxyl Adsorbed on Metallic Silver: Formaldehyde Oxidation on Ag(110)

7.1 Abstract

Many oxidative catalytic reactions take place in the presence of adsorbed hydroxyl. This is because hydroxyl can be formed when adsorbed oxygen is in the presence of water or an organic acid, or when base is added in solution. Yet the specific reactive role of adsorbed hydroxyl remains unclear. We find that adsorbed hydroxyl on Ag(110), like atomic oxygen, reacts nucleophilically with formaldehyde, ultimately forming the same H_2COO precursor to adsorbed formate. A mechanism is proposed in which $OH_{(a)}$ directly interacts with the positive carbon center of formaldehyde, forming an intermediate which decomposes to form H_2COO and releases water. The

H_2COO then releases hydrogen in two steps, forming first adsorbed formate and later CO_2.

Planned submission to *Chemical Science*.

7.2 Introduction

Group IB metals, particularly silver and gold, have high selectivity for oxygen-assisted partial oxidation and coupling reactions. These reactions are generally initiated by the abstraction of a hydrogen atom from a reactant by adsorbed oxygen atoms to form water and the adsorbed conjugate base of the organic reactant [61,96,172]. In this capacity the adsorbed atomic oxygen is viewed as a Brønsted base. The surface-bound intermediate thus formed can then undergo further reaction. This chemistry has been exploited in catalytic cycles to yield many useful products, including aldehydes [10,24,105,173], esters [22,26,27,67,81,113,115], and amides [69,70,72,84,174], in both model and reactor studes. Alternatively, the adsorbed oxygen can react nucleophilically, as in epoxidation of alkenes or CO oxidation [19, 55, 63, 175, 176]. The nucleophilic character of surface-bound atomic oxygen is perhaps most evident in highly selective reactions with aldehydes to form adsorbed carboxylate groups [177].

In virtually all oxygen-assisted reactions on metals, adsorbed hydroxyl ($OH_{(a)}$) is present to some extent, but although it has been observed to enhance many reactions, its reactive nature is not well understood. $OH_{(a)}$ results from the initial hydrogen abstraction from the reactant (eg. an alcohol, amine, alkyne) or from water. It will also be present in chemistry in basic solution. In excess reactant it has been assumed that $OH_{(a)}$ can also abstract the acidic hydrogen from the reactant. Also, $OH_{(a)}$ has

been suggested to play an important role in oxidation of alcohols and CO on gold, particularly under basic conditions in solution [178]. Evidence for direct reactions by OH, however, remains indirect. We have chosen to specifically study the reactivity of OH on silver (110) instead of gold because it can be isolated, is stable below 300 K [60, 179], and is a well-studied system [57, 180–189].

The fact that on both metallic silver and gold surfaces adsorbed atomic O and methoxy ($OCH_{3(a)}$) add nucleophilically to formaldeyde [10, 22], suggests that similar nucleophilic reactivity may occur for adsorbed OH. On one hand, $OH_{(a)}$ is expected to exhibit properties similar to, but perhaps weaker than $O_{(a)}$, and on the other hand it is homologous with OR. In this work the nucleophilicity of $OH_{(a)}$ was demonstrated by its reactivity with co-adsorbed formaldehyde to produce adsorbed formate.

7.3 Results and Discussion

7.3.1 Formation of isolated OH on Ag(110)

Hydroxyl adsorbed on a silver single crystal (OH/Ag(110)) was prepared by dosing water onto an oxygen covered surface (O/Ag(110)) at 225 K, above the temperature of molecular water desorption (180 K), but below the temperature of OH disproportionation (320 K) (Fig. 7.1). $OH_{(a)}$ disproportionation results in water desorption centered at 320 K and oxygen recombination at 575 K. The small water peak at 240 K has been previously attributed to adsorbed water stabilized by OH [57]. Therefore a small amount of excess water is present, which ensures that there is no residual $O_{(a)}$.

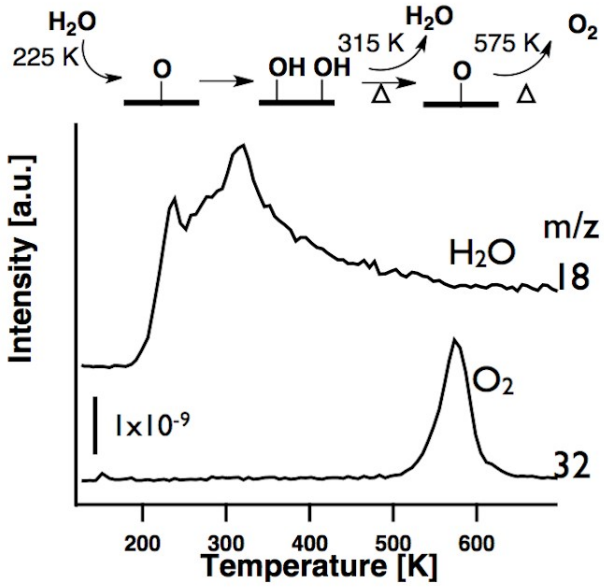

Figure 7.1: Schematic and temperature programmed reaction spectra of formation and disproportionation of 0.2 ML OH/Ag(110). Water was dosed on 0.1 O/Ag(110) at 225 K and cooled to 130 K before heating. The small feature at 240 K has been previously attributed to hydroxyl-stabilized water [57].

The conversion of $O_{(a)}$ to $OH_{(a)}$ has been previously observed using STM, where complete conversion occurs after dosing water on the surface below 250 K on oxygen coverages similar to the ones in our experiments [182]. The conditions used in reactivity experiments here were intentionally similar to the STM experiments, in order to further state with confidence presence of $OH_{(a)}$ and absence of residual $O_{(a)}$ on the silver surface.

The added row reconstruction of O/Ag(110), which consists of O-Ag-O chains in the [001] direction, changes to an ordered $OH_{(a)}$ structure in the orthogonal [1-10] direction [184]. This allows identification and verification of the change of the surface species using low energy electron diffraction (LEED) (Fig. 7.2). It should be noted that LEED spots are in reciprocal space, so a pattern or streaks in one direction indicates the appearance of added features, in this case O or OH rows, in the orthogonal direction.

The appearance of the characteristic (1x2) OH/Ag(110) LEED pattern and the disappearance of the (4x1) features characteristic of 0.25 monnolayer (ML) of $O_{(a)}$ verified the complete conversion of adsorbed O to adsorbed OH (Fig. 7.2). Water was dosed onto 0.25 $\pm$ 0.02 ML $O_{(a)}$ at 225K to create 0.50 ML $OH_{(a)}$, which is the saturation coverage on the Ag(110) surface. The expected (4×1) spots exhibit streaks in the [1-10] direction, which can be attributed to the coverage of being slightly lower than 0.25 ML. While the (1×2) $OH_{(a)}$ reconstruction spots are faint in the [001] direction, it is clear that the (4×1) spots or streaks of the $O_{(a)}$ reconstruction have completely disappeared, indicating conversion of the $O_{(a)}$ to $OH_{(a)}$.

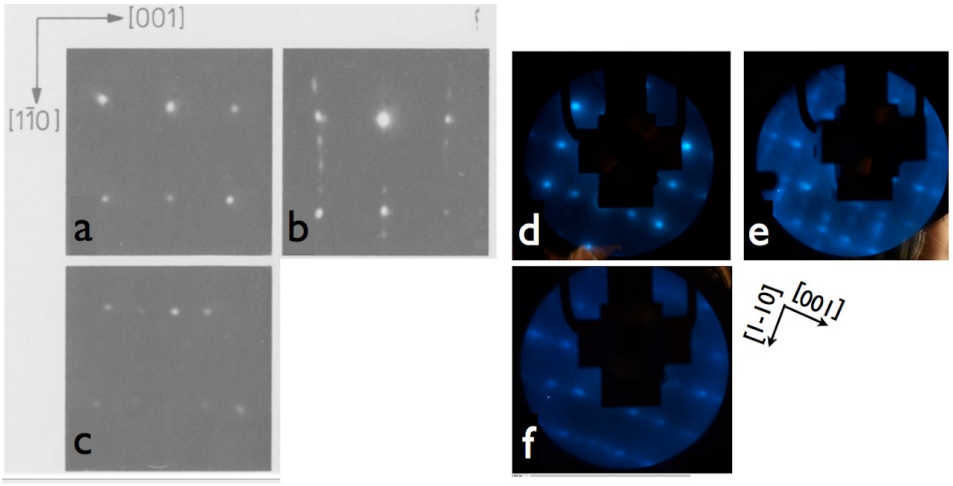

Figure 7.2: Confirmation of isolation of OH on the silver (110) surface by comparing LEED with previous work. From Bange et al, 1985, a) LEED of clean Ag(110) surface, b) LEED of 0.25ML O (4×1) pattern, c) LEED of 0.5 ML OH (1×2) pattern. D) LEED of clean Ag(110), e) LEED of 0.25ML O (4×1) pattern, f)LEED after dosing water on 0.25 ML O at 225K, confirming transformation to 0.5 ML OH by (1×2) LEED pattern.

7.3.2 Reaction of OH with formaldehyde

D_2-formaldehyde reacts with $OH_{(a)}$ to form adsorbed formate via the D_2CO_2 intermediate exactly like $O_{(a)}$, ultimately yielding $D_2$and CO_2 (Fig. 7.3). For comparison, D_2CO was reacted with 0.1 ML O/Ag(110), 0.2 ML O/Ag(110), and 0.2 ML OH/Ag(110). In all three cases, $D_2$is released at ~235K from adsorbed D_2COO, signaling the formation of formate, DCOO. H_2 and HD formation is negligible. This demonstrates that OH reacts with the formaldehyde, because formate is formed well below the temperature of OH recombination. Subsequently CO_2 and D_2 form from the decomposition of formate at 400K. The identical peak shapes and temperatures for the reactions of adsorbed O and OH demonstrate that the overall reaction of adsorbed with formaldehyde is similar to that of $O_{(a)}$.

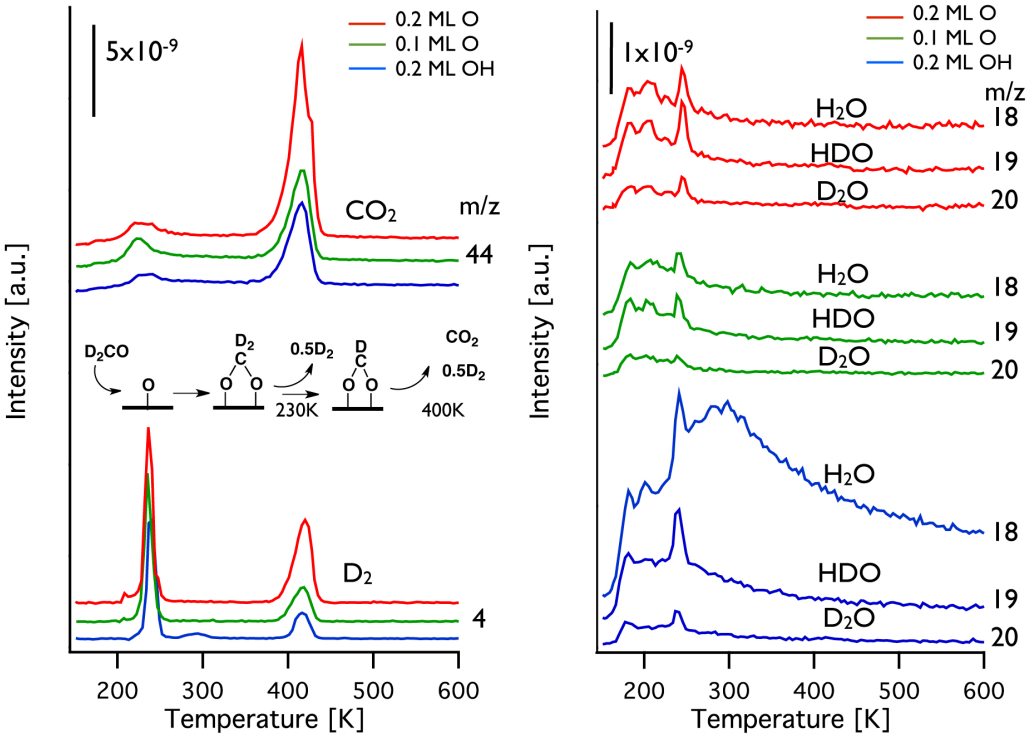

Figure 7.3: Temperature programmed reaction spectra for the reaction of d_2-formaldehyde with 0.2 ML O/Ag(110) (red), 0.1 ML O/Ag(110) (green), and 0.2 ML OH/Ag(110). The fragments for the products, CO_2 and D_2 are shown on the left panel, while the traces for the various water isotopes are grouped together on the right for ease of comparison. Approximately 6 L of formaldehyde was dosed at 150 K onto 0.1 and 0.2 ML O and 0.2 ML OH, prepared as described above. The long tail for the water features is attributed to pumping speed limitations for water. A schematic is included for the reaction of formaldehyde with O/Ag(110).

Reaction Conditions	CO_2 area
0.1 MLO	1.5
0.2 MLO	3
0.2 ML OH	1.4

Table 7.1: Amount of CO_2 evolved from formate decomposition on O(OH)/Ag(110). Area is calculated from the area under the m/z=44 TPRS peak, given in arbitrary units.

Reaction with 0.2 ML OH yields exactly the same amount of products as 0.1 ML adsorbed O, demonstrating that two OH's are consumed in the formation of one formate. Comparison of the areas under the product peaks shows that the same amount of formate forms for the 0.2 ML OH surface as the 0.1 ML O surface, both being half that of the 0.2 ML O surface (Table 7.1).

In addition to the D_2 and CO_2, water is evolved in a sharp peak at 240 K coincident with deuterium elimination from adsorbed D_2CO_2 (Fig. 7.3), indicating that some of the deuterium released reacts with adsorbed OH. D_2CO was reacted with both adsorbed O and OH in order to ascertain the origin of the hydrogen (H) in the water. The isotopic purity of the D_2CO was determined to be above 97.5%, so release of hydrogen (H) cannot account for the amount of hydrogen seen in the water. However, even when D_2CO is reacted with 0.1 and 0.2 ML O a mix of 20, 19, and 18 water forms when deuterium atoms are released from D_2CO_2 at 240 K, due to their reaction with adsorbed OH, which is present in small amounts due to reaction of $O_{(a)}$ with unavoidable background water and a small amount of water introduced while dosing the formaldehyde. We attribute the observed isotopic distribution to

rapid isotopic scrambling between D, OH, and water molecules.

Broad water peaks are observed at 200 K in reactions with $O_{(a)}$ and $OH_{(a)}$ and at 295 K only for reaction of formaldehyde with $OH_{(a)}$, the latter being below the temperature expected for OH disproportionation (320 K). The low temperature water peaks observed for reaction with pre-adsorbed O indicate the presence of background H_2O and D_2O during dosing; as mentioned, background water is expected from the preparation of the OH surface and the dosing of formaldehyde.

However, following reaction of D_2CO with adsorbed OH, only H_2O is evolved in the 295 K peak. The total amount of water is difficult to quantify. However, the amount of water desorbing at 295K is essentially the same as amount of water that desorbs in OH recombination of 0.2 ML OH (Fig. 7.4), although the peak shape and temperature is shifted. These facts can be understood by taking into account the total stoichiometry of the reaction and the conservation of hydrogen. For the reaction of OH disproportionation, as noted above,

$$2\,OH_{(a)} -> H_2O + O_{(a)}\,\cdot \tag{7.1}$$

And for the reaction of formaldehyde with OH,

$$2\,OH_{(a)} + D_2CO \longrightarrow CO_2 + D_2 + H_2O\,\cdot \tag{7.2}$$

Therefore, for the same initial coverage of OH, the resulting water desorption should be the same.

Furthermore, although there is some recombination of D with OH and isotopic scrambling to form water, the amount of D_2 released is the same for reaction of formaldehyde with both the 0.1 ML O and 0.2 ML OH covered surfaces. Therefore,

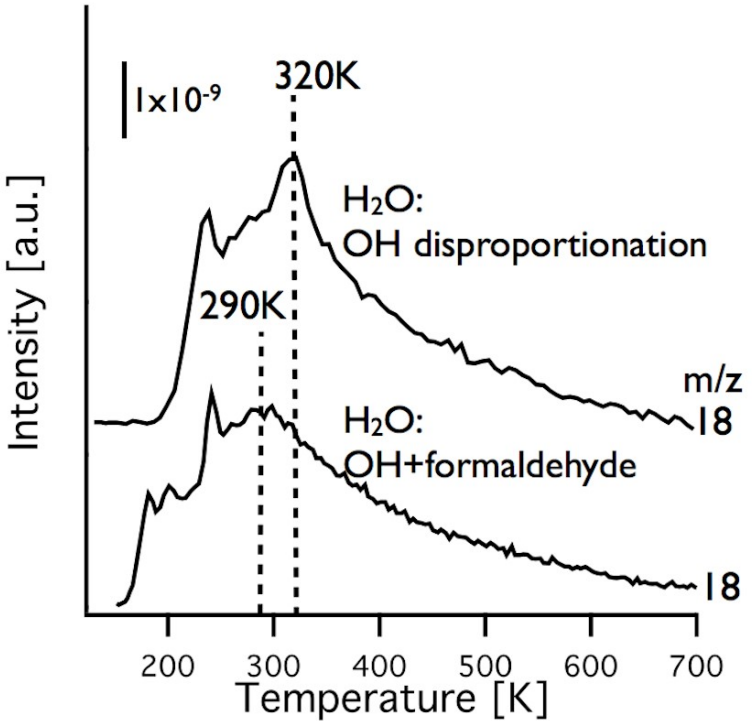

Figure 7.4: Comparison of the peaks for water in 0.2 ML OH disproportionation and in 0.2 ML OH reaction with formaldehyde.

we expect the total amount of water to be very similar, and indeed, we see that that is the case. The small amount of low temperature water desorption in the reaction of oxygen with formaldehyde could be due to water introduced with the dosing of the formaldehyde.

7.3.3 Oxygen isotope experiments

To further show that formate forms via reaction of formaldehyde with adsorbed OH, adsorbed ^{18}OH was created by reacting $H_2{}^{18}O$ with 0.1 ML O at 225K and then exposed to formaldehyde. According to the following reactions,

$$H_2{}^{18}O + O_{(a)} \longrightarrow {}^{18}OH_{(a)} + {}^{16}OH_{(a)} \tag{7.3}$$

$${}^{16}OH_{(a)} + H_2{}^{18}O{->}H_2{}^{16}O + {}^{18}OH_{(a)} \tag{7.4}$$

the preadsorbed oxygen readily exchanges with the oxygen in the water with sufficient exposure to $H_2{}^{18}O$. This result was confirmed by TPRS; a ratio of 4:1 $^{18}OH_{(a)}$:$^{16}OH_{(a)}$ was achieved, reflecting the measured isotopic purity of the $H_2{}^{18}O$ (Fig. 7.5).

Indeed, after exposure of the ^{18}OH-enriched surface to $H_2C^{16}O$, both $C^{16}O2$ and $C^{16}O^{18}O$ evolve at 400 K with an $^{18}O/^{16}O$ ratio close to that expected based on the isotopic composition (Fig. 7.6). There is a slight deficiency in the amount of ^{18}O evolved, which is attributed to two effects: (1) background $H_2{}^{16}O$ unavoidably dosed with the formaldehyde, which dilutes the ^{18}O content of the surface; and (2) exchange of the oxygen into the desorbing formaldehyde, yielding $H_2C^{18}O$ in addition to the $H_2C^{16}O$. This is indicative of the reversibility of the H_2COO formate precur-

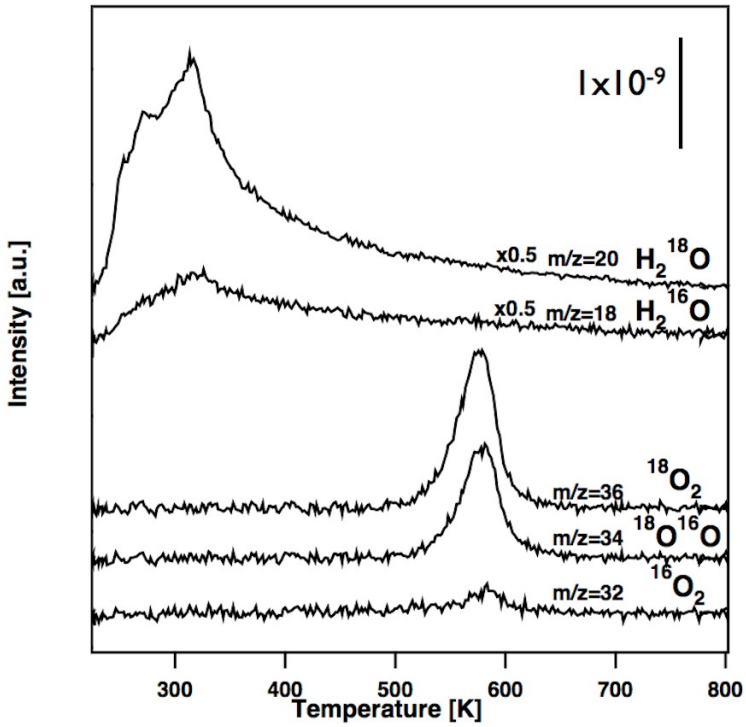

Figure 7.5: TPRS of 0.4 ML of ^{18}OH, which was made by dosing H2^{18}O water on 0.2 ML O(a) at 225 K. The surface oxygen completely exchanges with the oxygen in the water, and the isotopic ratio of both the water desorbing at 315K due to OH recombination and the oxygen desorbing at 575 K due to oxygen recombination is ~4:1 ^{18}O: ^{16}O.

sor, which then facilitates exchange of the formaldehyde oxygen with the oxygen on the surface. Regardless, this experiment proves that formate is formed from oxygen originating from $^{18}OH_{(a)}$, because formate is formed well below the temperature of OH recombination.

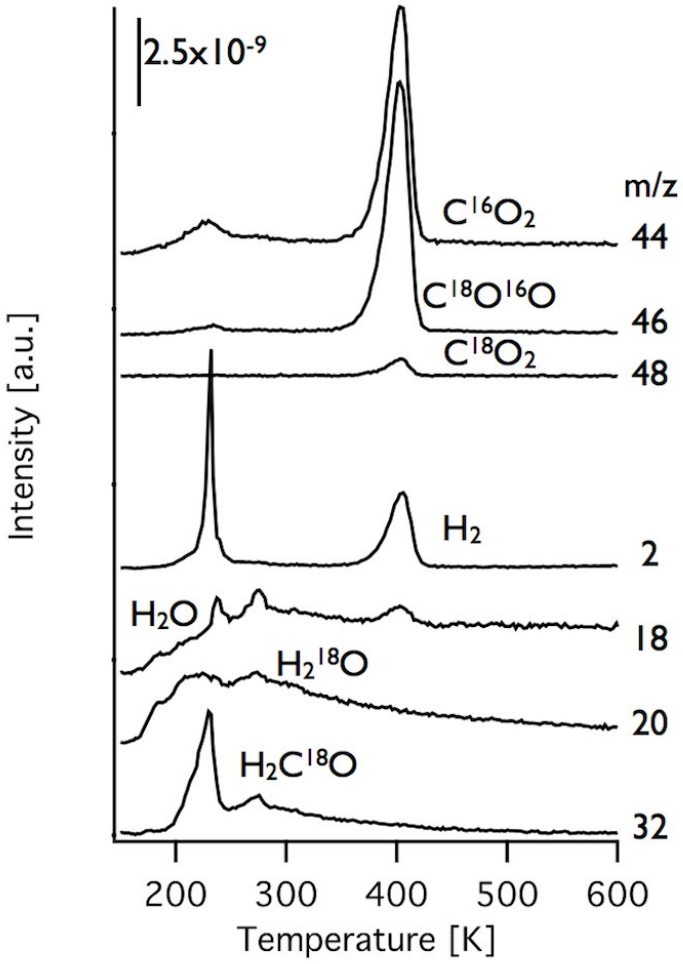

Figure 7.6: Temperature programmed reaction spectra for the reaction of formaldehyde on 0.4 ML $^{18}OH/^{16}OH$. ^{18}O is incorporated into the carbon dioxide and water products, as well as exchanged into the molecular formaldehyde, which desorbs. Approximately 6 L formaldehyde was dosed at 150 K onto 0.4 ML $^{18}OH/^{16}OH$, which was prepared as described above.

7.3.4 Mechanism

Before discussing possible mechanisms, first we will review two obvious constraints placed by the experimental results. First, the mechanism must account for the participation of two OH molecules. This suggests that interactions among the adsorbed OH species contribute somehow to formation of the H_2COO intermediate. Second, the H_2COO intermediate must be formed below 215 K, the temperature at which it decomposes to formate. (Note that while the temperature of D_2 release noted here is 230 K, the temperature of H_2 release for the analogous reaction with H_2CO is 215 K, not shown.)

One possible reaction mechanism that can be ruled out is OH dissociation. OH dissociation to adsorbed hydrogen and oxygen would produce formate by reaction of the oxygen with formaldehyde. The absence of mixing between the OH proton and the protons of formaldehyde in the hydrogen evolution at 230 K precludes this mechanism. Whether reacting D_2CO on OH/Ag(110) (Fig. 7.3) or H_2CO on OD/Ag(110) (not shown), the hydrogen evolution consists only of the isotope originating from the formaldehyde.

Taking into account the experimental evidence and what is known about O/OH reactions on silver, we present two likely mechanisms: (1) The interaction of the oxygen atom in $OH_{(a)}$ with the electron deficient carbon of formaldehyde may induce proton transfer from one $OH_{(a)}$ to a neighboring $OH_{(a)}$ well below the normal disproportionation temperature, facilitating formation of the O-CH_2-O intermediate. In the case, while this low temperature $OH_{(a)}$/ $OH_{(a)}$ interaction is novel, the rest of the intermediates are familiar. (Fig. 7.7a); (2) The $OH_{(a)}$ nucleophilically directly

attacks the carbonyl carbon, forming HO-CH_2-O, a surface-bound formaldehyde hydrate. This precursor would likely be unstable on the surface, forming H_2O and O-CH_2-O by interacting with a neighboring OH. (Fig. 7.7b) This water then must be released to the surface below 215 K, because at 215 K the H_2CO_2 decomposes to formate.

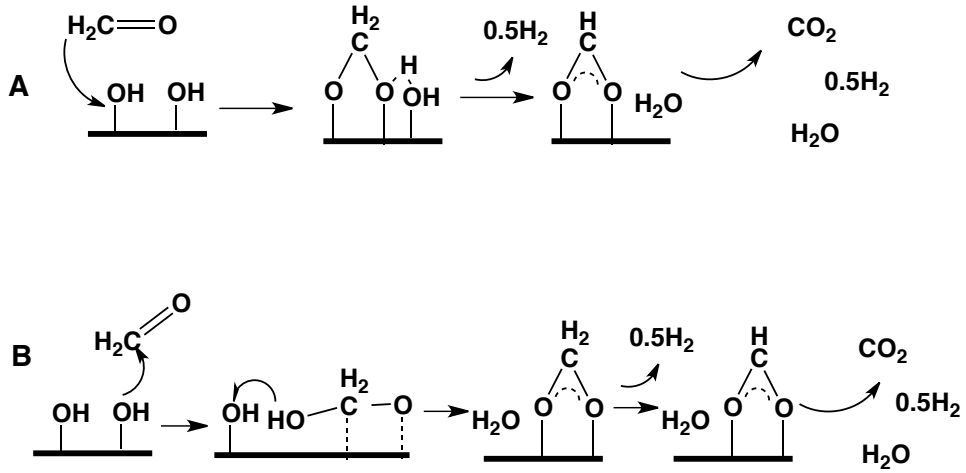

Figure 7.7: Two possible mechanisms of formaldehyde reaction with OH/Ag(110).

In either mechanism one molecule of formaldehyde reacts with two adsorbed OH species. A reversible $H_2COO_{(a)}$ intermediate forms either directly or indirectly, liberating H_2O. The hydrogen release by formate formation occurs at exactly the same temperature for the O/Ag surface as for the OH/Ag surface, indicating that it arises from the same intermediate, strongly supporting the formation of the non-hydrated H_2COO intermediate below 215 K. The $H_2COO_{(a)}$ then forms formate, which decomposes at ~400K. While we cannot directly disprove the proton shift mechanism, we believe that the direct nucleophilic attack is more likely. Formaldehyde hydration is a well-known reaction, and it is likely that OH could facilitate an analogous reaction

as well.

7.3.5 Implications

The interaction of adsorbed atomic oxygen as a nucleophile toward electron deficient carbon centers has been well established. In mechanisms of oxidative reactions on silver, OH has been seen as a generally passive intermediate and has not been directly studied. One exception is in the case of propene epoxidation on silver, where addition of water to the system promotes epoxidation by OH passivation of the surface [190]. So while it is clear that OH and O do not behave in exactly the same way, here we see that OH can indeed behave as a nucleophile toward the partially positive carbon in formaldehyde. This idea may also extend to other positive centers, such as other aldehydes or CO.

These results can be related to activity of OH seen in the literature on gold surfaces. Recently, OH has been suggested to be the active intermediate for oxidation on gold nanoparticles in aqueous solution [89, 178]. Our results agree that hydroxyl can play the part of an oxidative nucleophile, in a similar manner as atomic oxygen. DFT results also indicate that hydroxyl can play the role of aldehyde hydration in the generation of an acid from ethanol [89], which is similar to what we see experimentally here, although the acid was not observed under our conditions. Finally, a COOH intermediate has been proposed for the oxidation of CO on gold nanoparticles [191], which is directly analogous to the reaction that we have observed on silver. It would be ideal to be able to isolate hydroxyl on gold to study this mechanism experimentally, but since that is not feasible, we believe that we have gained some insight into the

general chemical character of OH reaction on IB metals by isolating it on silver.

7.4 Conclusions

Isolated hydroxyl was formed on Ag(110) in order to study the nucleophillic reactivity of adsorbed OH. The reaction of formaldehyde with $OH_{(a)}$ on silver forms $HO_{(a)}-CH_2-O_{(a)}$. At ~215 K hydrogen is released, forming adsorbed formate which decomposes near 400K to H_2 and CO_2. This reaction is analogous to reactions of $O_{(a)}$ and $OR_{(a)}$ on both metallic silver and gold. This result gives insight for OH interactions with other electrophiles on gold as well. Our results give direct experimental evidence for concept that OH can be involved in oxidation reactions of CO and aldehydes on coinage metals.

Chapter 8

The Role of Surface-bound Intermediates in the Oxygen-Assisted Synthesis of Amides by Metallic Silver and Gold

8.1 Abstract

A general mechanism for the oxygen-assisted synthesis of amides over metallic gold and silver surfaces has been derived from the study of acetaldehyde and dimethylamine in combination with previous work, allowing detailed comparison of the two surfaces' reactivites. Facile acetylation of dimethylamine by acetaldehyde occurs with high selectivity on oxygen-covered silver and gold (111) crystals via a common overall mechanism with different rate-limiting steps on the two metals. Ad-

sorbed atomic oxygen activates the N-H bond of the amine leading to the formation of an adsorbed amide, which attacks the carbonyl carbon of the aldehyde, forming an adsorbed hemiaminal. Because aldehydes are known to form readily from partial oxidation of alcohols, our mechanism also provides insight into the related catalytic coupling of alcohols and amines. The hemiaminal β-H eliminates to form the coupled amide product. On silver β-H elimination from the hemiaminal is rate-limiting, whereas on gold desorption of the amide is the slow step. Silver exhibits high selectivity for the coupling reaction for adsorbed oxygen concentrations between 0.01 and 0.1 monolayer, whereas gold exhibits selectivity more strongly dependent on oxygen coverage, approaching 100% at 0.03 monolayer. The selectivity trends and difference in rate-limiting steps are likely due to the influence of the relative stability of the adsorbed hydroxyl groups on the two surfaces. Low surface coverages of oxygen lead to the highest selectivity. This study provides a general framework for the oxygen-assisted coupling of alcohols and aldehydes with amines over gold and silver based catalysts in either the vapor or liquid phase.

This paper was published in *Journal of the American Chemical Society*, **2012**, *134*, 12604-12610.

8.2 Introduction

Oxidative coupling reactions, including production of amides from amines, are among the most important industrial chemical processes. Traditionally, amides are synthesized from carboxylic acids and amines, often by activating the acid to an acyl

chloride, which generates HCl waste [192]. Other processes also produce toxic waste; thus there has been a recent surge in research toward simple, green amide production [71, 72, 84, 157, 158, 160, 193, 194]. The ease and simplicity of dimethylacetamide production over metallic gold or silver reported here suggest that these noble metals, and alloys therefrom, may be effective catalysts for greener chemical synthesis of amides.

Silver is an established industrial catalyst for the selective oxidation of methanol to formaldehyde [195] and for the epoxidation of ethylene, while gold has recently shown exciting promise for many selective oxidation and coupling processes [196]. N-alkylation of primary amines with alcohols has been reported over both gold [86, 197] and silver [198] supported nanoparticles. In addition there are previous reports of alcohol coupling on metallic silver [10, 199] and of alcohol coupling with amines to form amides on single crystal surfaces of gold [85]. Further, direct acylation of dimethylamine with formaldehyde occurs on oxygen-covered Ag(111) [70] and Au(111) [69] surfaces; silver and gold nanoparticles also catalyze amide formation from nitrile oxidation [193] and the coupling of alcohols and amines [71, 72, 84].

Establishing reactivity patterns on the surfaces of catalytic metals is a crucial step in the rational design of novel catalytic pathways for chemical production. Usually, the best catalyst for a given reaction is found empirically. Ideally, however, patterns of reactivity would allow a rational choice of catalyst. In order to evaluate the relative merits of catalytic noble metals, as well as enable rational design of potential alloy systems, a deeper understanding of the mechanism and kinetics of coupling reactions on each surface is vital.

In this work we identify the elementary steps comprising the mechanism of the reaction, determine the rate-limiting steps on both silver and gold, and take the first step toward generalizing the mechanism for this class of coupling reactions on these noble metals. We observe the highly selective oxygen-assisted coupling of acetaldehyde and dimethylamine to form dimethlyacetamide on the (111) surface of both silver and gold. The differences between metallic gold and silver for these reactions are critically compared, developing more subtle reactivity patterns of the two surfaces.

8.3 Experimental Methods

Gold and silver were studied in two separate ultra high vacuum (UHV) chambers, each with a base pressure of 2×10^{-10} torr. Clean Au(111) and Ag(111) were prepared with Ar^+ sputtering and annealing, as well as cleaning with oxidation cycles. On Au the initial surface concentration of adsorbed atomic oxygen was reproducibly varied by dosing a controlled flux of ozone [46]. On Ag adsorbed oxygen was prepared by dosing a controlled flux of NO_2 at 500 K [200]. The exposures reported here in Langmuirs (1L = 1×10^{-6} torr s) take into account an enhancement factor of 100 due to direct dosing, which was estimated by taking into account the geometry of the system and previous measurements of the enhancement factor by the group. Temperature programmed reactions were conducted with well-established protocols [100]. The reaction products were identified by quantitative mass spectrometry (Ag: Prisma QMS 200, Au: Hiden HAL/3F) using fragmentation patterns obtained from authentic samples, unless otherwise stated.

Since prior studies have shown that low oxygen coverage increases the selectivity for coupling product between alcohols [23, 26], alcohols and aldehydes [27], and formaldehyde and dimethylamine [69, 70], we focus here on low oxygen coverages.

It should be noted that the observed differences in reactivity between silver and gold are not due to the oxygen preparation techniques (NO_2 on silver, O_3 on gold). This was confirmed by using O_3 to prepare the oxygen on silver. The reaction results (not shown) were in agreement with the NO_2 data, so the NO_2 technique was used on silver for its high precision and reproducibility.

Selectivity for the dimethylacetamide product is calculated with respect to amine-derived products, using quantitative mass spectrometry analysis [26]. The selectivity does not include oxidation of the aldehyde. It also does not include reformation of the dimethylamine, which is small and difficult to quantify due to overlap with desorption of the reactant dimethylamine.

8.4 Results

8.4.1 Dimethylamine (DMA) and acetaldehyde on $O_{(a)}$ covered Au(111) and Ag(111)

No reaction of dimethylamine and acetaldehyde occurred on the clean Au(111) surface; however, prior adsorption of atomic oxygen led to dimethylacetamide ($(CH_3)_2N{-}C(=O)CH_3$) formation. Dimethylamine was dosed onto approximately 0.1 ML of adsorbed O at 150K to form adsorbed dimethylamide [69]. Subsequent dosing of acetaldehyde and heating at 5 K/s yielded several products, including the coupling

product, dimethylacetamide, which evolved at 250K by a desorption-limited process (Fig. 8.1a). Water evolved between 200-300 K, but, except for a gradual rise in pressure near 600 K, no hydrogen evolution was detected. Methylimine ($CH_3N{=}CH_2$), methylformamide ($CH_3NHC(=O)H$), and methylisocyanate ($CH_3N{=}C{=}O$), originating from the oxidation of dimethylamine ($(CH_3)_2NH$), evolved at 255 K, 300 K and 415 K, respectively, with methylimine being the dominant product. We deduced the identity of methylimine by its mass fragmentation and the previous reports of imine formation by oxidation of amines on gold [71,109]. There is however, the lesser possibility that the product could be the cyclic amine of the same mass, ethylenimine. Significantly, products characteristic of acetaldehyde oxidation via an acetate intermediate (acetic acid, ketene, CO_2 [23]) were not detected. Based on the peak temperature of the desorption profile, the upper bound to the activation energy for dimethylacetamide and methylimine evolution is 73 kJ/mol, assuming first order kinetics and a pre-exponential factor of 10^{15} [31]. The selectivity for dimethylacetamide formation increased to nearly 100% when the initial oxygen coverage was lowered to 0.03 ML, in sharp contrast to the selectivity observed at 0.1 ML O, where the oxidative dehydrogenation of dimethylamine to methylimine dominated.

Dimethylamine and acetaldehyde also couple facilely on O/Ag(111), but with significant differences. Following a similar procedure as with Au(111), we observed dimethylacetamide at 250 K with 80% selectivity (Fig.8.1b) for an initial oxygen coverage of 0.1 ML. Methylimine formation is not significant, and there is less dependence of the selectivity on the initial oxygen coverage. Water and hydrogen evolve coincident with dimethylacetamide, whereas there was no hydrogen evolution on gold. The

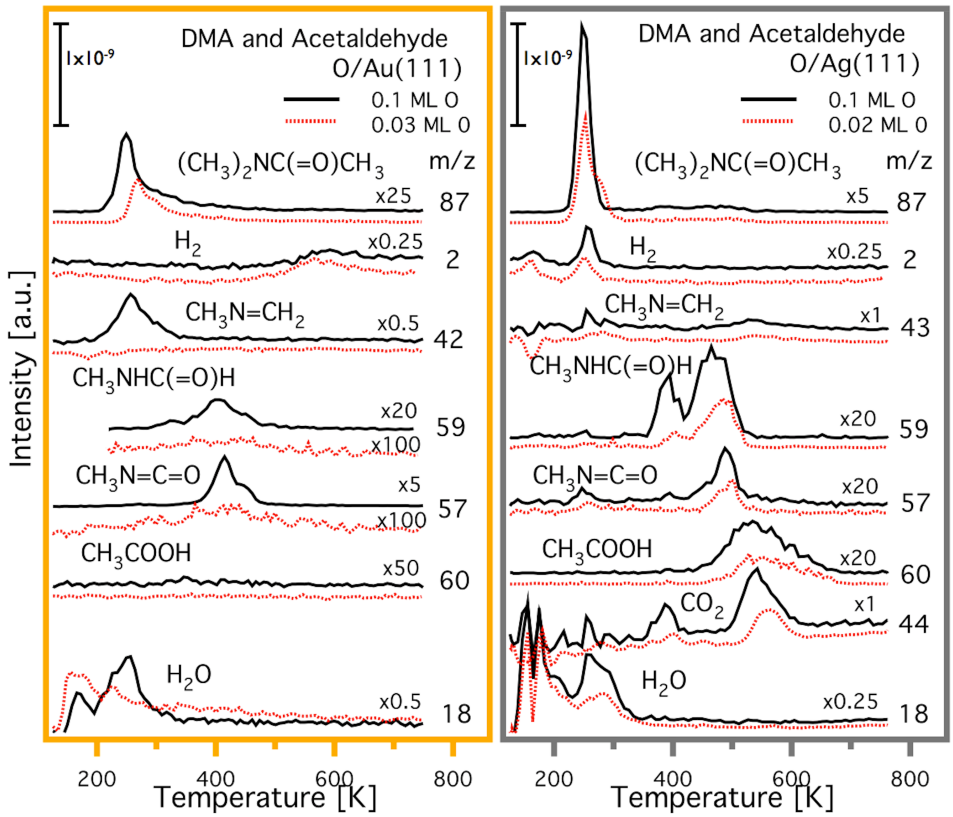

Figure 8.1: Temperature programmed reaction spectra of (a) dimethylamine and acetaldehyde dosed sequentially (1.5 L) at 150 K on 0.1 ML and 0.03 ML O/Au(111), and (b) dimethylamine and acetaldehyde dosed sequentially (1.5 L) at 125K on 0.1 ML and 0.02 ML O/Ag(111). On each surface, dimethylamine and acetaldehyde couple to form dimethylacetamide, along with secondary oxidation products. Molecular desorption of the reactants dimethylamine and acetaldehyde occurs around 200K but is not shown here. The contribution of dimethylacetamide, acetaldehyde, and dimethylamine to the m/z=44 trace is subtracted in order to see the CO_2 product. No CO_2 was observed on gold.

water and hydrogen evolve from the rate-limiting step for production of dimethylacetamide, which is β-H elimination from the hemiaminal intermediate precursor, rather than desorption of the amide (see section 3.2).

Although the dominant product on Ag(111) remains dimethylacetamide for all oxygen coverages studied, the route to secondary oxidation is clearly more diverse on Ag(111) than on Au(111). Methylformamide (375-500 K), CO_2 (400K) and methylisocyanate (500 K) form from the oxidation of dimethylamine [201]; acetic acid (450-650 K), CO_2 (500 K) and ketene (coincident with acetic acid, not shown) form from acetaldehyde oxidation [76].

Secondary oxidation of the amine is suppressed on silver by using d_6-dimethylamine. Because of the difference in zero point energy, the C-D bond is stronger than a C-H bond, which will result in a kinetic isotope effect if there is significant C-H bond breaking in the transition state. At 0.01 ML oxygen coverage, the adsorbed amide [201] intermediate $(CD_3)_2N_{(a)}$ does not undergo secondary oxidation, demonstrating that C-H(D) bond breaking is clearly important in limiting the secondary oxidation pathway. Coupling of d_6-dimethylamine with acetaldehyde on 0.01 ML O/Ag yields d_6-dimethylacetamide at 285 K without secondary oxidation of the adsorbed amide (Fig. 8.2). While a small amount of CO_2 is present at 550K due to oxidation of the acetaldehyde, neither of the amine oxidation products, methylformamide (m/z 64) or methylisocyanate (m/z 60) is observed. (Traces of m/z 60 were detected but were too small to be quantified.)

As the initial oxygen coverage was decreased from 0.1 ML to 0.01 ML on the silver surface, the overall yield decreased. Also, though the rate-limiting step appears to

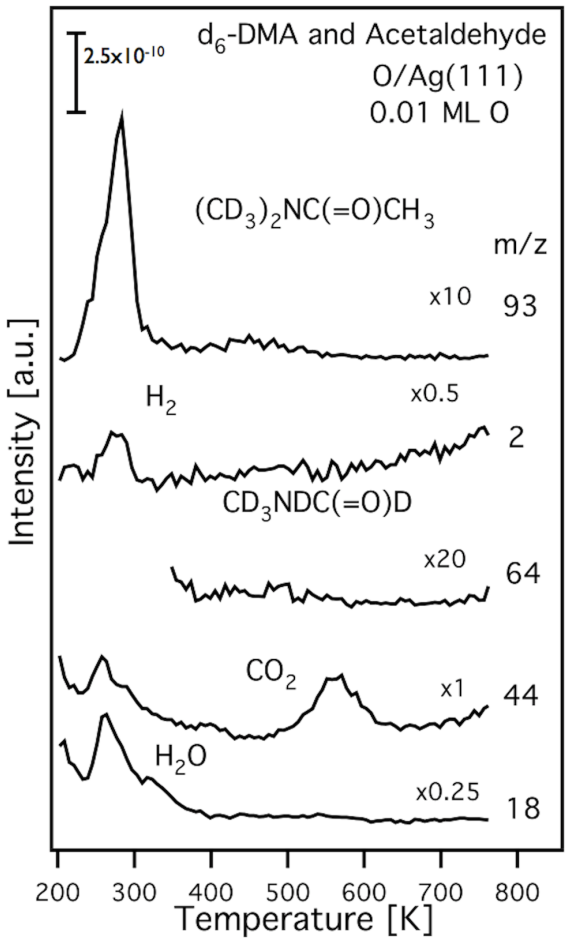

Figure 8.2: Temperature programmed reaction spectra of d_6-dimethylamine and acetaldehyde dosed sequentially (1.5 L) at 125 K on 0.01 ML O/Ag(111). The reactants couple to form dimethylacetamide, and secondary oxidation of the amine is eliminated. Molecular desorption of the reactant d_6-dimethylamine occurs at 170 K but is not shown here. M/z 64 was present at low temperature due to contamination of the acetaldehyde, so it was removed.

remain the same, the dimethylacetamide peak shifted to higher temperature, forming an additional peak approximately 30 K above the peak seen initially for an oxygen coverage of 0.1ML (Fig. E.25a,b). The same effect occurs for desorption of the neat product at low coverages (Fig. E.26).

8.4.2 Isotopic labeling: product identity and the kinetic isotope effect

Isotopic labeling of the reactants was used to confirm the identity of the coupling product on both O/Au(111) and O/Ag(111). Reacting d_0- and d_6-dimethylamine with d_0-acetaldehyde yielded d_0-dimethylacetamide (m/z=87) and d_6-dimethylacetamide (m/z=93), respectively. This increase in mass confirms that all six C-D bonds in dimethylamine are retained in the dimethylacetamide product. Reacting d_0- and d_6-dimethylamine with d_4-acetaldehyde produced d_3-dimethylacetamide (m/z=90) and d_9-dimethylacetamide, (m/z=96)) respectively (Fig. 8.3), clearly showing that one of the hydrogens in acetaldehyde is lost in forming the coupled product.

A kinetic isotope effect for the rate-liming step was clearly observed on Ag(111) but not Au(111). On the gold surface the slight shift in the peak temperature observed with d_4-actetaldehyde in place of d_0-acteldehyde was within the experimental reproducibility of the measured peak temperature (± 5 K) and temperature shift due to slightly lower coverage on the surface, which is determined by the oxygen coverage (± 10%) (Fig. 8.3a)). Further, no shift in peak temperature for dimethylacetamide was observed when reacting d_6-dimethylamine (compared to d_0-dimethylamine) with d_0-acetaldehyde on either surface. However, the reproducible shift of 20 K observed

on silver when using d_4-acetaldehyde in place of d_0-acteldehyde is indicative of a kinetic isotope effect for the formation of dimethylacetamide [70, 94].This difference indicates clearly that the rate-limiting step on silver is loss of a hydrogen from the carbonyl carbon originally associated with the aldehyde.

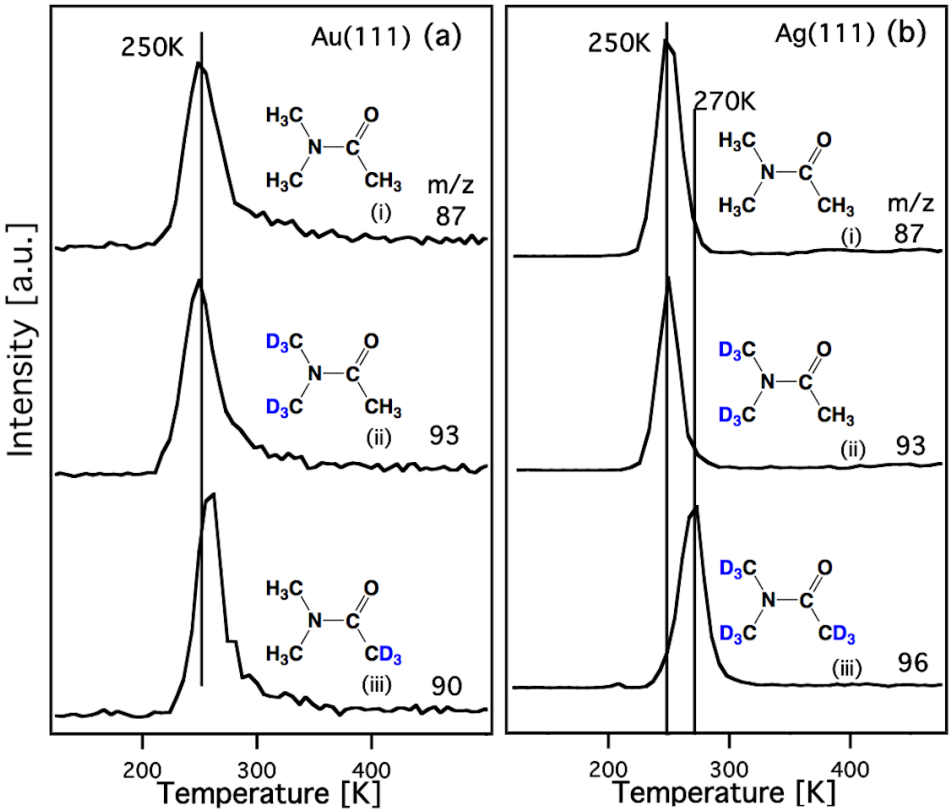

Figure 8.3: (a) Dimethylamine and acetaldehyde (1.5 L) were dosed sequentially at 150K on 0.05ML O/Au(111) with the following isotopic labels: (i) d_0-dimethylamine and d_0-acetaldehyde, (ii) d_6-dimethylamine and d_0-acetaldehyde, and (iii) d_0-dimethylamine and d_4-acetaldehyde. (b) Dimethylamine and acetaldehyde (1.5 L) were dosed sequentially at 125K on 0.1ML O/Ag(111) with the following isotopic labels: (i) d_0-dimethylamine and d_0-acetaldehyde, (ii) d_6-dimethylamine and d_0-acetaldehyde, and (iii) d_6-dimethylamine and d_4-acetaldehyde. Peaks are scaled to the same size to see differences in peak shape and temperature.

The absence of a clear kinetic isotope effect on Au(111) suggests that the pro-

duction of dimethylamide is desorption limited (Fig. 8.3a). As an independent test, d_0-dimethylamine, d_4-acetaldehyde and d_0-dimethylacetamide were co-adsorbed on 0.05 ML O/Au(111) prior to the temperature programmed reaction. The temperatures of evolution of the d_3-dimethylacetamide formed in the coupling reaction and d_0-dimethylacetamide initially adsorbed on the surface were identical to within experimental uncertainties (Fig. E.27), confirming that this product is desorption-limited on Au(111).

8.5 Discussion

8.5.1 General reaction mechanism

Oxygen adsorbed on coinage metals exhibits patterns of reactivity which provide guidelines for predicting new reaction sequences [202]. In particular, adsorbed oxygen acts as a Brønsted base toward gas phase acids and also exhibits strong nucleophilicity. Prior studies show that adsorbed atomic oxygen activates O-H, C-H and N-H bonds in a variety of molecules, a guiding factor being their gas phase acidities. In this activation process water is released, and the conjugate base of the acid is bound to the surface and itself can act as a nucleophile. For example, the O-H bond in alcohols is readily activated to water and surface-bound alkoxy. This adsorbed alkoxy group nucleophilically attacks the electron-deficient carbon in aldehydes to form the corresponding esters via an adsorbed hemiacetal [10, 26]. The reactive coupling between the dimethylamine and acetaldehyde reported here was anticipated from these principles, illustrating their predictive utility.

On both silver and gold surfaces adsorbed atomic oxygen is essential for initiating the sequence leading to coupling. The adsorbed oxygen activates N-H bonds in amines [24, 58] and ammonia [59, 203] on the group 1B metals to form adsorbed amides. We predicted, by analogy with reactivity of the adsorbed alkoxy, that the adsorbed amide would react as a nucleophile toward an aldehyde to form a hemiaminal, which would subsequently undergo β-H elimination to form an amide product. This reaction pathway was initially verified by coupling dimethylamine and formaldehyde to form dimethylformamide with high selectivity on the oxygen-activated (111) surface of silver and gold under controlled conditions in ultra high vacuum [69, 70].

The results reported here indicate that the mechanism for the reaction between secondary amines and aliphatic aldehydes is general on oxygen-activated metallic gold and silver. The complexity introduced by the alkyl functionality in the acetaldehyde appears to be primarily the competing oxidation pathways not found with formaldehyde.

The mechanism for dimethylacetamide formation on Ag(111) can be deduced from isotope experiments (Figs. 8.3a, E.25). The temperature shift observed when using d_4-acetaldehyde in the place of d_0-acetaldehyde is as expected for C-H vs. C-D bond cleavage on metal surfaces [94]. A similar kinetic isotope effect was also observed for dimethylamine and formaldehyde coupling on this surface [70]. The kinetic isotope effect shows that the C-D bond breaking from the carbonyl carbon is rate-limiting. Furthermore, deuterium and dimethylacetamide evolve at the same temperature, which indicates they are produced from the same intermediate (Fig. E.25b). Therefore, β-H elimination from a hemiaminal intermediate appears to be

the rate-limiting step. We conclude that the reaction mechanism is identical on both gold and silver, but is reaction-limited on silver and desorption-limited on gold. The fact that the β-H elimination must happen at a lower temperature on gold than silver (because the product evolves at 250 K on both surfaces, but is desorption limited on gold) indicates that the β-H elimination from the hemiaminal is more facile on gold. We postulate that greater ease of β-H elimination from the hemiaminal on gold suggests that the adsorbed O aids in the β-H elimination on gold, but on silver, the β-H elimination is surface-mediated (see Section 8.5.2).

This mechanism, along with differences between the reaction on silver and gold, is depicted in Fig. 8.4. The coupling between dimethylamine and aliphatic aldehydes on gold occurs by (a) amine activation by $O_{(a)}$ to form the surface-bound amide, (b) nucleophilic attack of the adsorbed amide on the electron deficient aldehydic carbon accompanied by rearrangement to form a surface-oxygen bond, (c) β-H elimination from a hemiaminal intermediate to yield the dimethyl amide, and (d) product desorption.

These studies provide mechanistic insight into recently reported catalytic reactions on gold nanoparticles [71, 72, 84, 109]. Angelici et al. [109] observed formation of imines over both alumina-supported gold and bulk gold powder. For cyclic and primary amines they also observed the coupling product. They proposed that under the conditions of their experiments an imine first forms, which then couples with another amine. Our results suggest that this imine comes from an adsorbed amide intermediate. Christensen et al. [72] reported coupling in alcohol solution between alcohol and amines over a supported gold catalyst, which is consistent with

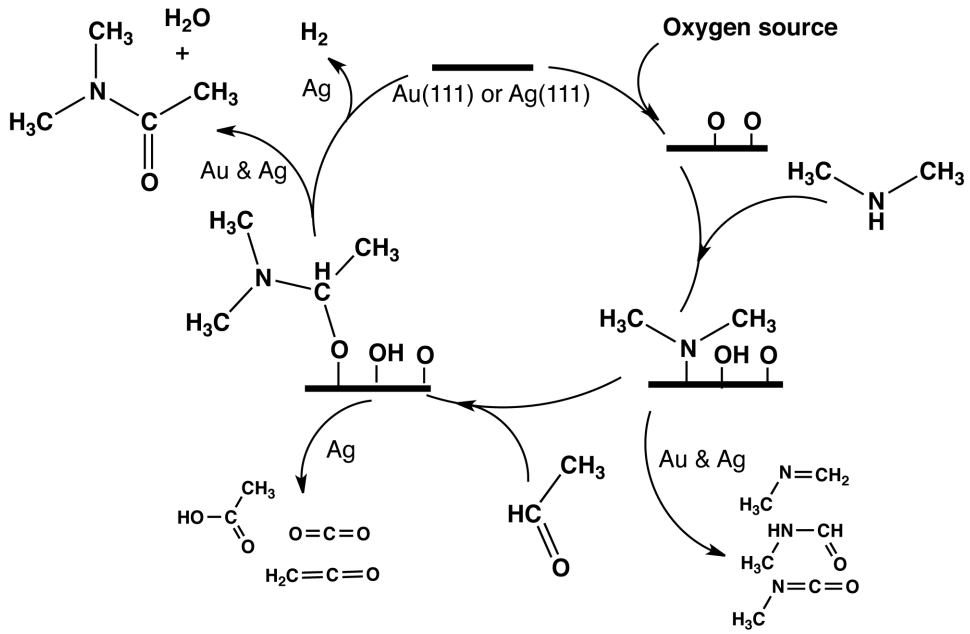

Figure 8.4: Direct acetylation of amines on both silver and gold.

the mechanism elucidated here: the alcohol first forms the alkoxy, which is known to eliminate H to yield the aldehyde; then the aldehyde can couple with an adsorbed amide. We have specifically demonstrated the coupling of methanol and dimethylamine on gold via this mechanism [85], and, in general, aldehydes are known to form from partial oxidation of alcohols on both metallic gold and silver [10, 26, 118, 204]. Ishida and Haruta [71] reported N-formylation of amines in methanol solution over gold nanoparticles. They deduce a mechanism via aminolysis, where methlyformate is formed from the methanol over gold and then interacts with the amine to form the amide. To investigate whether this aminolysis pathway occurs in our studies, we condensed ethylacetate with dimethylamine on O/Ag(111), but did not detect any dimethylamide product (not shown). Thus, though this reaction may proceed in methanol solution, we conclude that this mechanism does not occur on the surface in our vapor-phase conditions.

In a comprehensive study Kobayashi et al. [84] recently expanded the range of catalysts for the amine-alcohol coupling system using gold and gold/nickel,-iron,-cobalt nanoparticles. To explain the coupling process they invoke a tandem oxidative process via a carbinolamine formed by reaction of the amine and an aldehyde (the aldehyde being produced by catalytic oxidation of the alcohol), which they suggest is then further catalytically oxidized to the amide. Their mechanism involves a series of steps with no specific recognition of the role of the surface, each step producing a molecular intermediate, the carbinolamine being the immediate precursor to the amide. However, the mechanism we describe in this paper is more direct, involves reactions on the surface dictated by clear principles of surface reactivity, and it is entirely compatible with the reactions they observe. The adsorbed hemianimal we identify is the immediate precursor to the amide, not the carbinolamine. In fact, both the N-H and O-H bond in the carbinolamine would be expected to be activated by oxygen on the gold surface, severely limiting the selectivity for amide production. The results presented here appropriately focus attention on the surface-bound reaction intermediates affected by the heterogeneous catalyst.

Overall, the partial oxidation and coupling reactions observed in solution phase catalysis using molecular oxygen as the oxidant appear to follow the same acid-base reaction and coupling patterns as seen in our model studies using O-activated gold. To the best of our knowledge, no similar studies have been undertaken on metallic silver catalysts. In solution the added dimension is the possibility of homogeneous reactions between an intermediate product and one of the reactants, as exemplified by others [71].

8.5.2 β-H elimination on Ag(111) and Au(111)

On Ag(111) the rate-limiting β-H elimination from the hemiaminal intermediate appears to occur via reductive elimination to the silver surface, whereas on the gold surface it appears to be assisted by adsorbed oxygen, because H_2 is evolved from Ag(111) during amide evolution, whereas only water forms on Au(111) (Fig. 8.1a,b). The water and hydrogen peaks from Ag(111) usually lag the dimethylacetamide by 5-15 K, indicating that the surface reactions involving the hydrogen are not instantaneous [10]. This fact suggests that on Ag(111) hydrogen is transferred to the surface, and then combines with $O_{(a)}$, $OH_{(a)}$ or $H_{(a)}$ to yield both hydrogen and water (if excess adsorbed oxygen is present). The absence of H_2 evolution observed on Au(111) for this reaction as well as in other oxidation and oxidative couping reactions on Au(111) involving β-H elimination [26, 69, 118], suggests that if there is excess oxygen, an oxygen-assisted β-H elimination pathway is favored on Au(111). To date there are no conclusive experiments to prove this hypothesis, but experiments to examine these reactions in the absence of excess adsorbed oxygen are planned.

This role of adsorbed oxygen or OH in facilitating β-H elimination on gold is suggested by recent theoretical work, which demonstrates the thermodynamic favorability of direct H-transfer to adsorbed O or OH, forming OH or water, as opposed to H-transfer to the Au surface [77,89]. An alternative explanation is that in the presence of excess oxygen on gold, all released hydrogen immediately reacts to form water due to the high activation barrier for recombinative desorption of H_2 on Au [205]. Other factors such as the different structures of the adsorbed O on Ag(111) and Au(111) could also strongly influence the selectivity toward H_2 and H_2O. These factors remain

Intermediate on Ag	β-H bond cleavage T (E_a)	Reference
Methoxy	310 K (90 kJ/mol)	[10]
Ethoxy	285 K (83 kJ/mol)	[204]
Dimethylformamide precursor	270 K (78 kJ/mol)	[70]
Dimethylacetamide precursor	250 K (73 kJ/mol)	This work

Table 8.1: Temperatures and activation energies (by Redhead analysis, assuming a preexponential factor of $\nu = 10^{15}$ [31]) for β-H elimination from similar intermediates on silver surfaces.

to be studied.

The temperature at which β-H elimination from the hemiaminal occurs on silver is consistent with other, similar reactions (Table 8.1). Metallic silver is known to cleave β-C-H bonds from methoxy at 310 K [10] and from ethoxy at 285 K [204] in the low coverage limit, in general agreement with a decrease in activation energy with increasing carbon chain length. Similarly, for the hemiaminal precursor to dimethylformamide, β-H elimination takes place at 270 K [70], whereas β-H elimination of the dimethylacetamide precursor occurs at 250 K (this work), indicative of a difference of approximately 5 kJ/mol in the activation energy. We attribute this difference to the presence of the methyl group in the latter case. The energy for β-H elimination decreases from a primary to secondary (alkoxys) or secondary to tertiary (hemiaminals) carbon. These β-H elimination reactions occur around or below room temperature, indicating that silver could be a facile low-temperature catalyst for these synthetic reactions, provided the buildup of more stable intermediates due to the secondary oxidation does not occur and block reactive sites.

The stoichiometry of the coupling reaction could be different for silver and gold catalysts depending on whether or not surface oxygen participates in β-H elimination, particularly at low oxygen coverages: For example, on Ag,

$$2\,(CH_3)_2NH + O_{(a)} + 2\,CH_3CHO \longrightarrow 2\,(CH_3)_2NC(=O)CH_3 + H_2O + H_2 \qquad (8.1)$$

and on Au,

$$(CH_3)_2NH + O_{(a)} + CH_3CHO \longrightarrow (CH_3)_2NC(=O)CH_3 + H_2O \cdot \qquad (8.2)$$

This difference does not affect the yield of dimethylacetamide, although the percent conversion of dimethylamine would be affected under oxygen-limiting conditions.

8.5.3 Secondary oxidation and selectivity

Gold and silver exhibit distinct differences with regard to both the extent and type of secondary oxidation. In order to appreciate the differences, we must first understand the secondary oxidation process for each reactant on both surfaces (Fig. 8.5).

Both O/Ag(111) and O/Au(111) activate dimethylamine to form an adsorbed amide, which can dehydrogenate to methylimine or further oxidize to methylformamide, methylisocyanate and, with excess oxygen, to CO_2 [85, 201]. (NO and N_2 would be expected products with higher oxygen coverage, but were not observed here.) Acetaldehyde reacts with O/Ag(111) or O/Au(111) to form adsorbed acetate, which leads directly to acetic acid and CO_2, as well as ketene [23, 76]. Methane has also been previously reported [76] as a product of acetaldehyde oxidation on silver, but was not detected in this study.

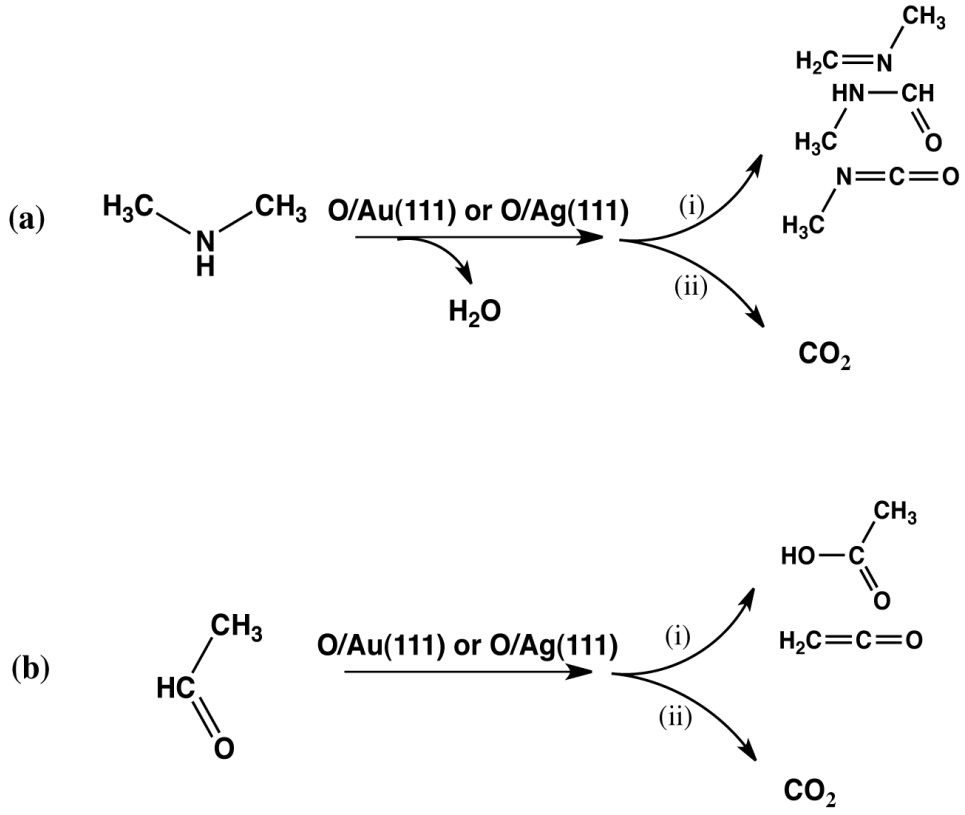

Figure 8.5: Oxidation pathways for (a) dimethylamine and (b)acetaldehyde on oxygen activated Au(111) and Ag(111). (i) and (ii) designate more selective and less selective oxidation, respectively.

The main differences in secondary oxidation during the coupling reaction are twofold: (1) on gold methylimine was the dominant amine oxidation product at both 0.1 and 0.05 ML O, but only occurred in trace amounts on silver, and (2) on silver products of acetaldehyde oxidation were observed; they were never detected on gold. The conspicuous absence of acetaldehyde oxidation on gold suggests that the acetate intermediate does not form or is formed reversibly under these conditions.

On gold, there is a dramatic change in selectivity with respect to conversion of the amine with oxygen coverage, favoring the coupling product at the lowest oxygen coverages (0.02 ML), but favoring methylimine at higher oxygen coverage (Fig. 8.6). In stark contrast, the selectivity for the amide on silver was 70% even at the higher oxygen coverages studied and increased to only 80% at the lowest oxygen coverage. The reactions with d_6-dimethylamine on silver noted above (Fig 8.2, E.25) were not included in the selectivity comparison. The selectivity for coupling depends much more strongly on oxygen coverage on metallic gold, and under very specific conditions nearly 100% selectivity may be obtainable.

8.5.4 Reactivity of adsorbed oxygen species

The contrast in methylimine production on silver and gold at low oxygen coverages may be due to the difference in reactivity of the surface oxidant available under reaction conditions. The following reactions are envisioned for formation of methylimine, where O/OH is used to indicate reaction with either adsorbed O or OH:

$$(CH_3)_2NH + O_{(a)}/OH_{(a)} \longrightarrow (CH_3)_2N_{(a)} + OH_{(a)}/H_2 \tag{8.3}$$

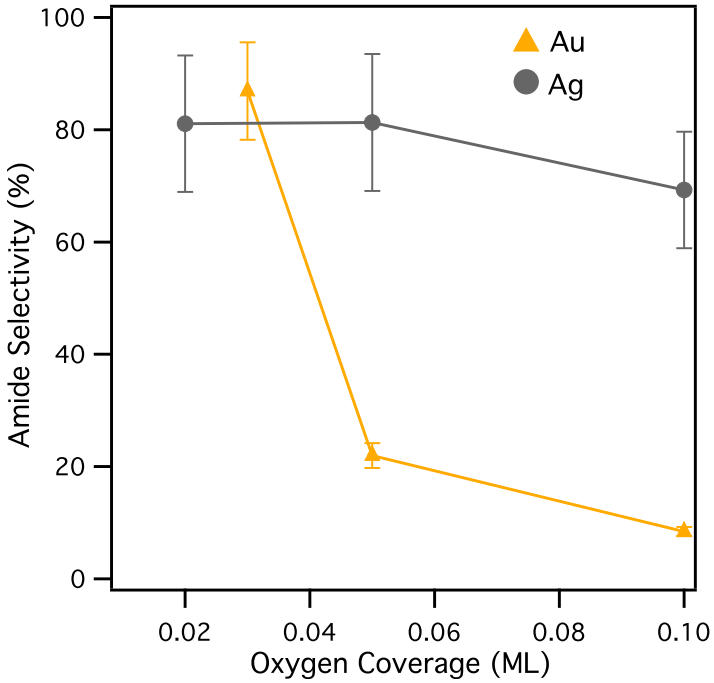

Figure 8.6: Selectivity toward dimethylacetamide with respect to the total amount of amine-derived products on O/Au and O/Ag. Not included in this calculation is reformation of dimethylamine. The error bars are estimated; the large error bars on the silver data account for possible trace amounts of methylimine.

$$(CH_3)_2N_{(a)} + O_{(a)}/OH_{(a)} \longrightarrow CH_3NCH_2 + OH_{(a)}/H_2O \tag{8.4}$$

The relative reactivity of the $O_{(a)}$ or $OH_{(a)}$ present on the surface may dictate whether or not the imine forms before the amide reacts with the acetaldehyde. It is known that on Au(111) adsorbed O and OH equilibrate to favor adsorbed O [60], leaving it free to facilitate C-H bond activation in the amide and form the imine. However on Ag(111), $OH_{(a)}$ is quite stable, disproportionating to adsorbed O and H_2O near 300K, which is well above the temperature of formation of the dimethylacetamide coupling product. Thus if adsorbed OH is ineffective in activating the C-H bond in the adsorbed amide on silver, the amide can couple with the aldehyde. There are many other factors that could also have an effect on the selectivity difference and remain to be studied, such as proximity and mobility of adsorbates and morphology of the surface.

8.6 Conclusions

Both metallic silver and gold facilitate the direct coupling of amines and primary aldehydes for amide synthesis. The oxygen-assisted reaction proceeds on the surface via activation of N-H to form adsorbed amides. Coupling then occurs via a nucleophillic attack by the amide on the carbonyl carbon of the aldehyde. At low coverages of adsorbed atomic oxygen on silver the selectivity for coupling is consistently near 80%, whereas on gold it exhibits a strong dependence on the oxygen coverage, increasing from 8% toward 100% between 0.1-0.03 ML oxygen. While the overall mechanisms on silver and gold are essentially identical, the rate-limiting step differs, indicative of greater facility of C-H bond activation on the gold surface. Differences

are also manifested in the secondary oxidation products, the selectivity for coupling, and hydrogen production. Reactivity of the adsorbed oxygen species with the amine and the relative stability of adsorbed O and OH appear to determine the differences in secondary oxidation. Finally, dominance of oxygen-assisted hydrogen abstraction on gold may contribute to the absence of hydrogen formation on gold.

Appendix A

Selective Oxidation of Dimethylamine on Ag(111)

A.1 Abstract

In this work, we describe the oxidation of dimethylamine on Ag(111), which results in the production of N-methyl methylenimine and methylisocyanate. We investigate this process using temperature programmed reaction spectroscopy, supplemented by reflection absorption infrared spectroscopy and scanning tunneling microscopy. As part of this study, the surface of the silver surface is seen to be dynamic–silver adatoms are incorporated into the surface intermediates.

This paper is in progress and will be submitted at a later date.

A.2 Introduction

Development of effective catalysts for in situ production of reactive intermediates is important for safer, more efficient chemical production [149]. Relatively unstable reactants such as unsubstituted imines and methylisocyanate are critical for chemical synthesis but present challenges of safe storage and ease of handling and use. In situ production of these substances as intermediates in a total synthesis may eliminate these challenges. An example of success in this regard is methylisocyanate produced using a silver catalyst by DuPont on an as-needed basis for insecticide production [206].

Herein, we use surface science methods to investigate the capability of silver to act as a catalyst to produce both N-methyl methylenimine and methylisocyanate as reaction intermediates to form imine- and isocyanate-derived compounds. To that end, the oxidation of dimethylamine to produce methylisocyanate and N-methyl methylenimine has been investigated by temperature programmed reaction, infrared spectroscopy, and scanning tunneling microscopy on a silver surface as a model for possible catalytic reactions.

Imines, also known as Schiff bases, are versatile and important reaction intermediates for a wide variety of chemical processes [207]. Imines are used in many organic reactions [208, 209]. Most commonly, imines are formed by condensation of an aldehyde or keytone with a primary amine; this method was discovered by Schiff [210]. However, this method does not work for particularly unstable imines, because of the difficultly in removing the water [211]. Recently, N-methyl methlenimines of aryl aldehydes have been formed using a mild, solvent free method and methylamine chloride

as the amine source [208]. N-methyl methylenimine, in the absence of aryl substituents, is an unstable imine [212], and has only been formed by heating the trimer 1,3,5-trimethylhexahydrosymtriazine [213, 214], by pyrolysis of dimethylamine [215], flash vacuum thermolysis [216] or made unintentionally as a side product in a reaction involving dehydration of dimethylamine [69, 70]. Here, in contrast, we report formation of N-methyl methylenimine below room temperature by simple oxidative dehydrogenation of dimethylamine using a silver surface to model chemical processes related to catalysis. This has been done successfully for other industrial reactions, e.g. the oxidation of methanol to formaldehyde [10, 171].

Methylisocyanate is produced worldwide and is used to make methylcarbamates and ureas, which are used for pesticides. Commonly produced from phosgene and methylamine, methylisocyanate, which is toxic and explosively reactive with water, must then stored in large quantities before being used, which has proven to be leathally dangerous [217]. Alternatively, methylisocyanate can be produced by oxydehydrogenation of methylformamide, using a silver catalyst between 300-700 C [149, 206]. Here, we report another approach: partial oxidation of dimethylamine on silver.

Using temperature programmed reaction spectroscopy, we demonstrate selective stepwise formation of N-methyl methylenimine and methylisocyanate, at 250 K and 500 K respectively. The surface intermediates in the oxidation of dimethylamine are proposed based on results derived from a combination of surface science techniques so as to provide a general understanding of the process of dimethylamine oxidation on silver. These results are discussed in the broader context of amine oxidation on Ag

and other coinage metals and possible utility of Ag as a catalyst for in situ production of methylenimine and methylisocyanate.

A.3 Experimental methods

Temperature programmed reaction spectroscopy was performed as has been described elsewhere [100] in an ultra high vacuum chamber with a base pressure of $\sim 2\times10^{-10}$ torr. It was outfitted with the Pfiffer quadrupole mass spectrometer, and the sample was capable of cooling to ~125 K using liquid nitrogen and heating to ~900 K using radiative heating with a tungsten filament. Atomic oxygen was formed on the sample by dosing NO_2 on the Ag(111) sample at 500 K. The oxygen coverage was calibrated by comparing the integral of the temperature programmed reaction peak to that of the saturation coverage of oxygen, which is equal to 0.4 ML O. The sample was prepared by argon ion sputtering and annealing cycles, followed by oxidation cycles until no residual CO, CO_2, or NO was seen in temperature programmed reaction. Dimethylamine (Sigma-Aldrich, 99%) was introduced to the surface using a direct doser, which has an estimated enhancement factor of 100, which has been accounted for in the reported doses. The heating rate for all temperature programmed reaction studies was 4 k/s. The reflection absorption infrared spectroscopy set-up was integrated into the same ultra high vacuum chamber.

Reflection absorption infrared spectroscopy was conducted with a Thermo Nicolet Nexus 670 spectrometer and MCT/A detector in the standard grazing angle reflection-absorption geometry; conflat-mounted BaF_2 windows allowed for transmission above 800 cm^{-1}. For all spectra in this experiment, 1000 scans were averaged

at 4 cm^{-1} resolution, yielding a scan time of 7 minutes per spectrum. The dimethylamine and oxygen were dosed on the silver crystal following the same technique as employed during temperature programmed reaction. Temperature programming was accomplished using identical heating filament PID controller parameters as those employed during temperature programmed reaction. During temperature programming, the sample was heated at a rate of 4 K/sec to the specified temperature point and then cooled back to the sample low temperature (~125 K) before taking the infrared spectra. Background spectra were obtained after sample acquisition for each temperature point by flashing the sample to 850K and cooling to the sample low temperature without making changes to the sample position.

Scanning tunneling microscope experiments were performed in a separate chamber with an RHK-STM with a beetle-style scanning head. In a prep 0.2 ML oxygen coverage was prepared on Ag(111) through the decomposition of NO_2 direct dosed at 2×10^{-8} torr at 500 K for 3 min. In the calibration, this procedure resulted in 50% of the mass 32 peak area as in a saturation dose. The sample was then transferred to the microscope chamber and place in the sample stage and the sample temperature was allowed to equilibrate with the cryostat. The scanning tunneling microscope chamber was at a pressure of 3×10^{-10} torr. Ninety minutes after the NO_2 dose, the sample temperature was stable at 125 K. Dimethylamine was dosed using a directed doser that was aimed slightly away from the sample in order to keep scanning during the dose and avoid contact of the doser with the scan head.

A.4 Results

A.4.1 Partial oxidation reaction products (temperature programmed reaction)

In the oxidation of dimethylamine on 0.1 ML O/Ag(111) (Fig. A.1), N-methyl methanimine, $CH_3{-}N{=}CH_2$, is produced from dehydrogenation of the adsorbed amide, $(CH_3)_2N_{(a)}$, at 240 K, simultaneous with reformation of dimethylamine. Methylisocyanate is formed and desorbs at 320 K and 500 K, with the high temperature peak dominating the methylisocyanate production. Methylformamide is produced is much lower amounts at 390K and 500K. A small amount of hydrogen is detected at 240 K. Water desorbs from 250 K-350 K. CO_2 and a small amount of NO evolve at 390 K and 450 K, respectively. These products were identified using quantitative mass spectroscopy and isotopic labelling (see A.1)

The selectivity for dimethlyamine oxidation decreases as a function of increasing oxygen coverage, illustrated for the case where the initial O coverage is 0.2 ML (Fig. A.2). The selective oxidation products are produced at the same temperatures as on the 0.1 ML O surface– imine (240 K), methylformamide (390 K, 500 K), and methlyisocyanate (320 K, 500 K). At the higher initial O coverage, no hydrogen was detected; instead, water is evolved in the range of 250-375 K. There is also formation of more CO_2, including an additional peak at 450 K and more NO at 460 K. Production of N_2 is also observed at 445 K, just prior to the NO and higher temperature CO2 peaks. Excess oxygen recombines and desorbs at 575 K.

Using isotopic labeling, the identities of all products were confirmed A.1. This

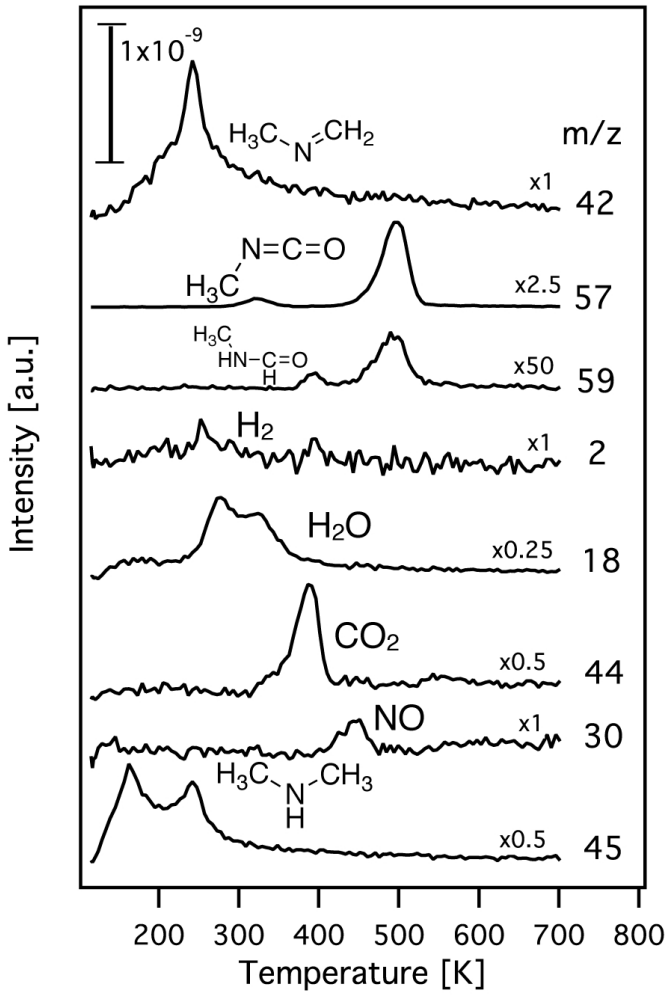

Figure A.1: Temperature programmed reaction data obtained after adsorption of dimethylamine on 0.1 ML O/Ag(111) produces the partial oxidation products, N-methyl methanimine and methyl isocyanate, in competition with combustion to CO_2. The mass traces have been corrected by subtraction to account for contributions from other products. Dimethylamine was dosed (6 L) at 125 K. The heating rate was 5 K/s.

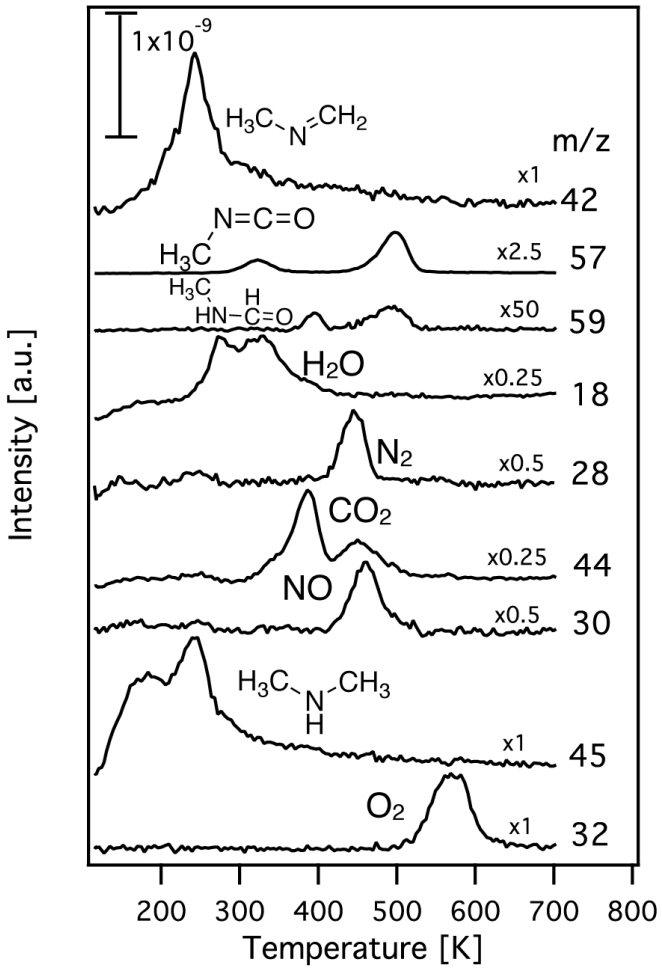

Figure A.2: Temperature programmed reaction data obtained after adsorption of dimethylamine on 0.2 ML O/Ag(111) produces the partial oxidation products, N-methyl methanimine and methyl isocyanate, in competition with combustion. The mass traces have been corrected by subtraction to account for contributions from other products. Dimethylamine was dosed (6 L) at 125 K. The heating rate was 5 K/s.

was especially useful for the 0.2 ML O coverage, as potential oxidation products can overlap in mass (i.e. m/z 44 could be CO_2 or N_2O; m/z 28 could be CO or N_2). In addition, it was discovered that there may also be contribution of the m/z 28 fragment coming from an NCH_2 group, as evidenced by the appearance of m/z=29 when using ^{15}N-dimethylamine. ^{18}O was achieved on the surface by first preparing an oxygen covered surface using NO_2 as described above. Then, 12 L of $H_2{}^{18}O$ was dosed at 125 K, at which temperature reaction occurs with the oxygen on the surface, forming surface hydroxyls. The surface was the annealed for 5 min at 300 K to desorb molecular water before cooling again to dose the dimethylamine. The excess of water leads 70% of the oxygen on the surface being labeled. This preparation decreases the oxygen coverage by ~25%. The use of isotopes also allows for some interpretation of the reaction mechanism, indicating that as expected, one nitrogen is retained in the main products, N-methyl methylenimine, and methylisocyanate. Also, one surface oxygen is incorporated into the methylisocyanate.

On 0.1 ML O, the selectivity for methylisocyanate was 20% and the selectivity for N-methyl methanimine was 50%, with CO_2 comprising most of the remaining products. On 0.2 ML O, the selectivities were much lower for methylisocyanate and N-methyl methanimine (15% and 18%, respectively), and combustion products (CO_2, N_2, NO) comprising 60% of the products.

Isotopic labeling, experimental conditions	methylisocyanate (m/z)	N-methyl methyl-enimine (m/z)	Methyl formamide (m/z)	CO_2 (m/z)	NO (m/z)	N_2 (m/z)	N_2O (m/z)	NCH_2 (m/z)	NO_2 (m/z)
d_0-dimethylamine 0.1 ML O	57	43/42	59	44	30	no 28	–	no 28	no 46
d_0-dimethylamine 0.2 ML O	57	43/42	59	44	30	28	–	28	no 46
^{15}N-dimethylamine 0.1 ML O	58	44/43	60	44	no 30, 31	no 30	no 46 at high T	29, small 28	no 47
^{15}N-dimethylamine 0.2 ML O	58	44/43	minor 60	44	31	30	no 46 at high T	29, no 28	no 47
d_0-dimethylamine 0.1 ML ^{18}O	59	43/42	no 61 (too small)	46/48	minor 30, 32	28	–	28	–
^{15}N-dimethylamine 0.1 ML ^{18}O	60	44/43	no 60 (too small)	46/48	no 31, 33	minor 30	–	minor 30	minor 51 @250 K
^{15}N-dimethylamine 0.2 ML ^{18}O	60	44/43	minor 62	46/48	31, 33	30	–	29	minor 51 @250 K

Table A.1: Product m/z for dimethylamine oxidation with isotopic labeling, to confirm product identification.

A.4.2 Investigating proposed intermediates using infrared spectroscopy

Infrared spectroscopy was used to probe the nature of the intermediates present on the surface initially containing 0.1 ML of O that lead to specific products (Fig. A.3). Due to the complexity of the system and to a limited signal-to-noise ratio, a full assignment of the spectra was not possible; rather signature peaks were used to monitor the development of specific functional groups. Assignments were made based on comparison to the spectrum of condensed dimethylamine and literature data for other related intermediates.

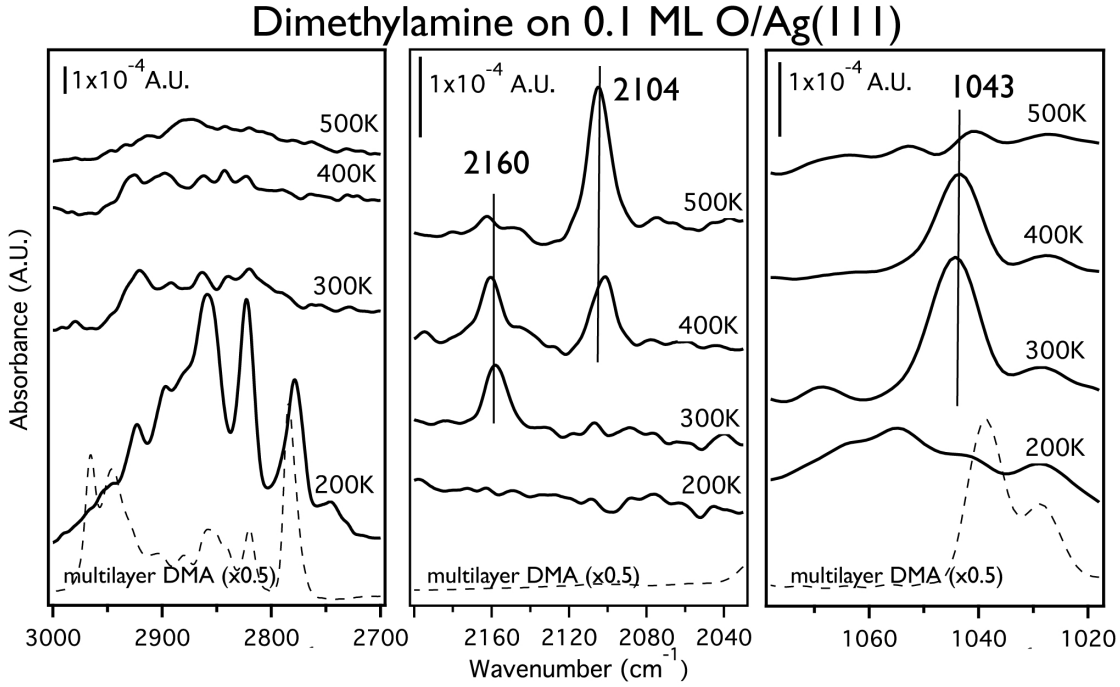

Figure A.3: Temperature programmed RAIRS of dimethylamine oxidation on 0.1 ML O. The main features are consistent with intermediates proposed from TPRS.

The first step of dimethylamine reaction is dissociation of the N-H bond, yield-

ing adsorbed dimethylamide $(CH_3)_2N_{(a)}$ species and an $OH_{(a)}$ group, based in part on the observation of a new peak at 903 cm^{-1} assigned to the Ag-O-H bend of hydroxyl (Not shown). The spectrum is otherwise similar to that for the condensed amine. There is precedence in the literature for the promotion of N-H bond dissociation by O adsorbed on silver(110), supporting this assignment [58, 59]. Two new prominent peaks were observed in the infrared spectrum at 2158 cm^{-1} and 1043 cm^{-1} (Fig. A.3) assigned to an NCO stretch and a C-N bend, after heating to 300 K –a temperature just above that required for evolution of the N-methyl methanimine. These peaks persist even after heating to 400 K, i.e. until methyl isocyanate is evolved (Fig. A.1,A.2). The C-H stretching region shows markedly fewer well-resolved features as temperature increases. Starting at 300 K, an additional peak appears at 2104 cm^{-1}, which is tentatively assigned to a C-triple-bond-N containing degradation product. While no unique C-N containing product was clearly seen above 500 K in the TPRS, it is possible that a small amount of remaining combustion products cause this peak, or that a larger CN product desorbs or is absorbed into the surface. N-methyl methylenimine is known to polymerize easily, so a polymerized product is a reasonable possibility.

On 0.2 ML O/Ag(111), the spectra are substantially similar to the 0.1 ML O/Ag(111) spectra, with peaks at 2161 and 1044 being consistent with NCO and CN bends, respectively, which appear at the appropriate temperatures for methylisocyanate, or an intermediate leading to methylisocyanate, to be formed. However at 300 K, a new peak is observed at 2087 cm^{-1} (Fig. A.4). This is potentially associated with the degradation product seen at higher temperatures on the 0.1 ML O/Ag(111) sample, indicating that the surface intermediate formed on the 0.2 ML O surface

possesses a lower barrier to total oxidation. Additionally, an O-H stretch at 3578 cm^{-1} is resolvable at 300 K (not shown). While it is curious that we do not observe the O-H stretch at other temperatures, this could be the ideal experiment to observe it: the imine and molecular dimethylamine have desorbed, but OH recombination is only just beginning to take place. The higher oxygen coverage facilitates a higher OH coverage and therefore better signal/noise as well.

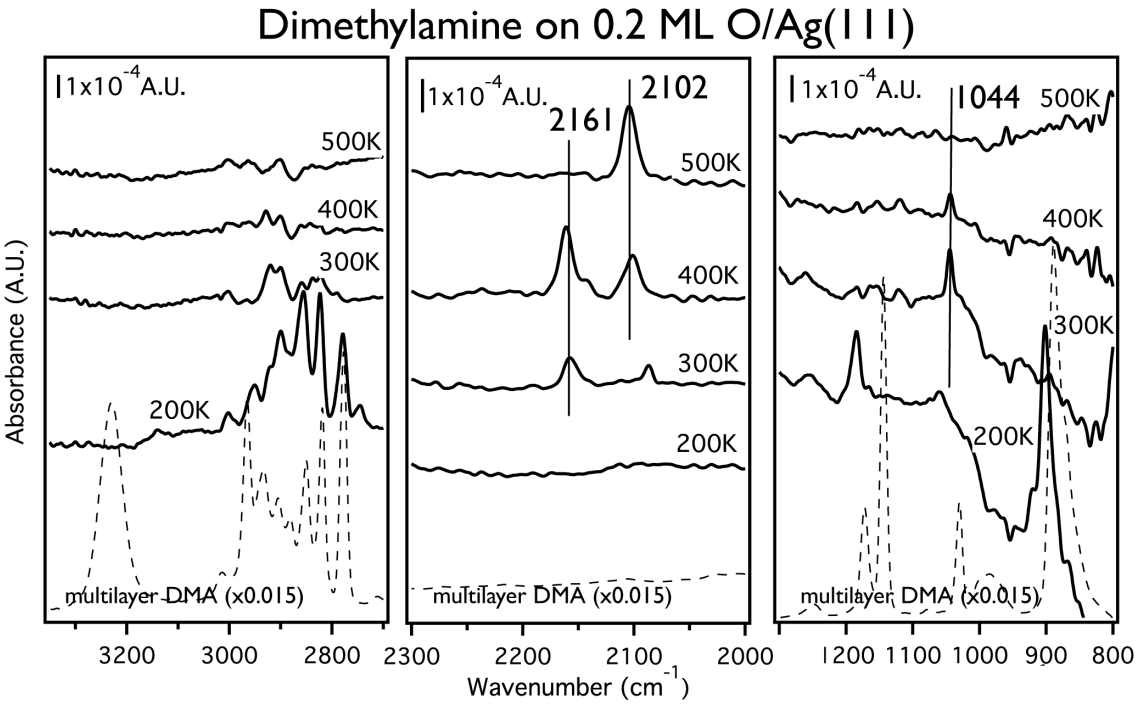

Figure A.4: Temperature programmed RAIRS of dimethylamine oxidation on 0.2 ML O. The main features are consistent with intermediates proposed from TPRS.

To compare to the spectra of the methylisocyanate formed via oxidation of dimethylamine, the IR spectra was collected for neat methylisocyanate under similar reaction conditions. Significantly, for the neat methylisocyanate on an oxygen-covered surface, the NCO stretch at 2160 cm^{-1} was not observed at any temperature point.

Instead, the NCO stretch for multilayer methylisocyanate exhibits multiplet transitions centered at 2300 cm^{-1}, as observed in prior solid-phase vibrational studies of neat methylisocyanate. Once the multilayer desorbs, no additional peaks were observed. This is in agreement with TPD of neat methylisocyanate on an oxygen-covered surface, which shows total desorption of the methylisocyanate by 150 K.

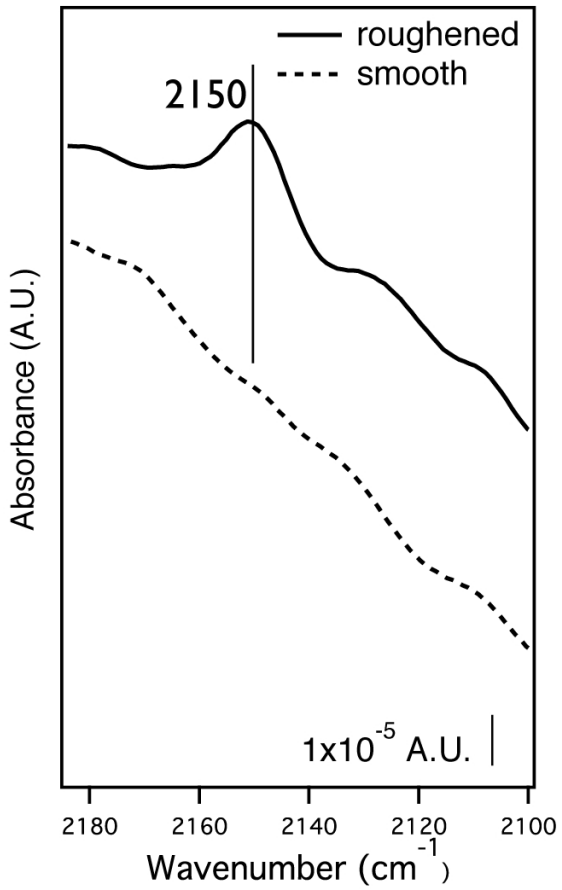

Figure A.5: IR spectrum of neat methylisocyanate on a clean, smooth and clean, roughened surface, zoomed in to see the relevant vibration area around 2160 wavenumbers, which is where the NCO stretch was identified in TP-RAIRS experiments. The roughened surface was prepared by Ar-ion sputtering at 300 K and then cooled to dose the MIC at 125 K. The smooth surface was prepared by annealing a clean surface to 800 K.

While methylisocyanate on an oxygen-covered surface did not give the expected

NCO stretch at 2160 cm^{-1}, we then considered that at the point of formation of the methylisocyanate, the oxygen from the Ag-O-Ag islands was already reacted away. However, the metal adatoms that were pulled from the bulk by the oxygen atoms could remained as adatoms on the surface, potentially bound to or incorporated into the methylisocyanate precursor intermediate. To investigate this hypothesis, neat methylisocyanate was also dosed on a surface roughened by argon ion sputtering (not shown). Roughening of the Ag(111) surface followed by dosage of neat methylisocyanate yielded a small peak at 2150 cm^{-1}, indicating that the NCO peak formed during dimethylamine oxidation is enhanced or caused by a rough surface or the incorporation of surface defects or adatoms.

A.4.3 Visualizing the surface during reaction (scanning tunneling microscopy)

Using the information from temperature programmed reaction and reflection absorption infrared spectroscopy, we know that (1) dimethylamine reacts with oxygen by at least 200 K to form the surface amides, (2) an intermediate is formed by ~275-300 K that involves an NCO stretch and can lead to production on methylisocyanate, and (3) the intermediate is likely associated with metal adatoms or surface defects. Point (3) is also consistent with the high temperature of desorption of methylisocyanate– association with surface defects or metal adatoms may make the intermediate more strongly bound. This prior knowledge is then taken into account when interpreting the results of scanning tunneling microscopy experiments.

First, the oxygen was formed using the same preparation technique as the tem-

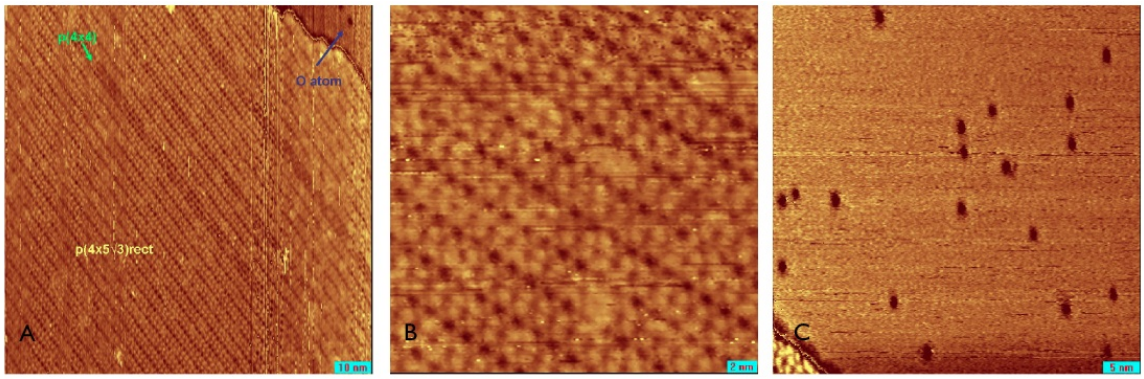

Figure A.6: The oxygen reconstruction as prepared on silver (111) was found to be mostly the p$(4 \times 5\sqrt{3})$rect structure (A), shown close-up in (B). Also, oxygen adatoms, which appear as ~1 nm depressions, are found on the terraces without the oxygen reconstruction (C). Blue scale bars at the bottom of the images are 10, 2, and 5 nm, respectively.

perature programmed reaction and RAIRS experiments. The scanning tunneling microscopy images show two types of oxygen phases: low coverage with scattered oxygen atoms and oxygen covered in a p$(4 \times 5\sqrt{3})$rect structure (Fig. A.6). The appearance of the individual oxygen atoms in the scanning tunneling microscopy images is consistent with previous observations [162, 218]. In the King study the atomic oxygen was formed using NO_2 and in the Besenbacher study with a thermal cracker. Oxygen appears as a circular depression ~1 nm in diameter and 40 pm in depth. The 1 nm diameter spot corresponds to a footprint of 12 Ag atoms. The oxygen atoms were not mobile at 125 K but are not expected to be until about 370 K [162]. The p$(4 \times 5\sqrt{3})$rect structure has been previously reported in scanning tunneling microscopy studies [162, 218, 219]. It has been formed using NO_2, O_2, and atomic O preparation methods. The phase is shows a striped pattern with the dark stripes being the p(4×4). In some areas the spacing between the bright rows is wider, allowing more p(4×4) phase in between. The King study showed the that the p(4×4)

phase can convert to p($4 \times 5\sqrt{3}$)rect by annealing at 490 K [218]. The Besenbacher work gives a nice summary of the preparation parameters using the atomic O source and found that the two phases often coexist [162]. Because of the long time needed for cooling of the scanning tunneling microscopy chamber, an oxygen coverage of 0.2 ML was used, to ensure adequate coverage even after prolonged time in the chamber. Dimethylamine was then dosed in increasing amounts and then annealed to 200 K and 280 K, at which points the dimethylamine would have reacted with oxygen and the n-methyl methylenimine would have desorbed, respectively.

Upon adsorption on 0.2 ML O/Ag(111) at 125 K, dimethylamine first associates with oxygen adatoms on the silver surface (Fig. A.7a,b). This is observed by keeping the scan head in the same position as dimethylamine is introduced into the chamber at a background pressure of 1×10^{-10} torr for 30 seconds. A new bright feature appears in the image, which is associated with an oxygen adatom. This feature is persistent over time at different scan directions and scanning parameters (not shown). Because dimethylamine was just dosed, it is reasonable to assess that this feature is either dimethylamine or a reacted derivative (i.e. the amide). However, since the oxygen adatom appears as a large depression, it is not readily possible to distinguish whether the dimethylamine is next to, bound to, or reacted with the oxygen adatom. As more dimethylamine is dosed (Fig. A.7c,d,e), the p($4 \times 5\sqrt{3}$)rect domains are still present, and more bright features can be seen at the location of the oxygen atoms on the Ag(111) terrace.

After annealing to 200K, at which point both the dimethylamine multilayer and molecular water are desorbed, the surface has restructured. At this point, clearly,

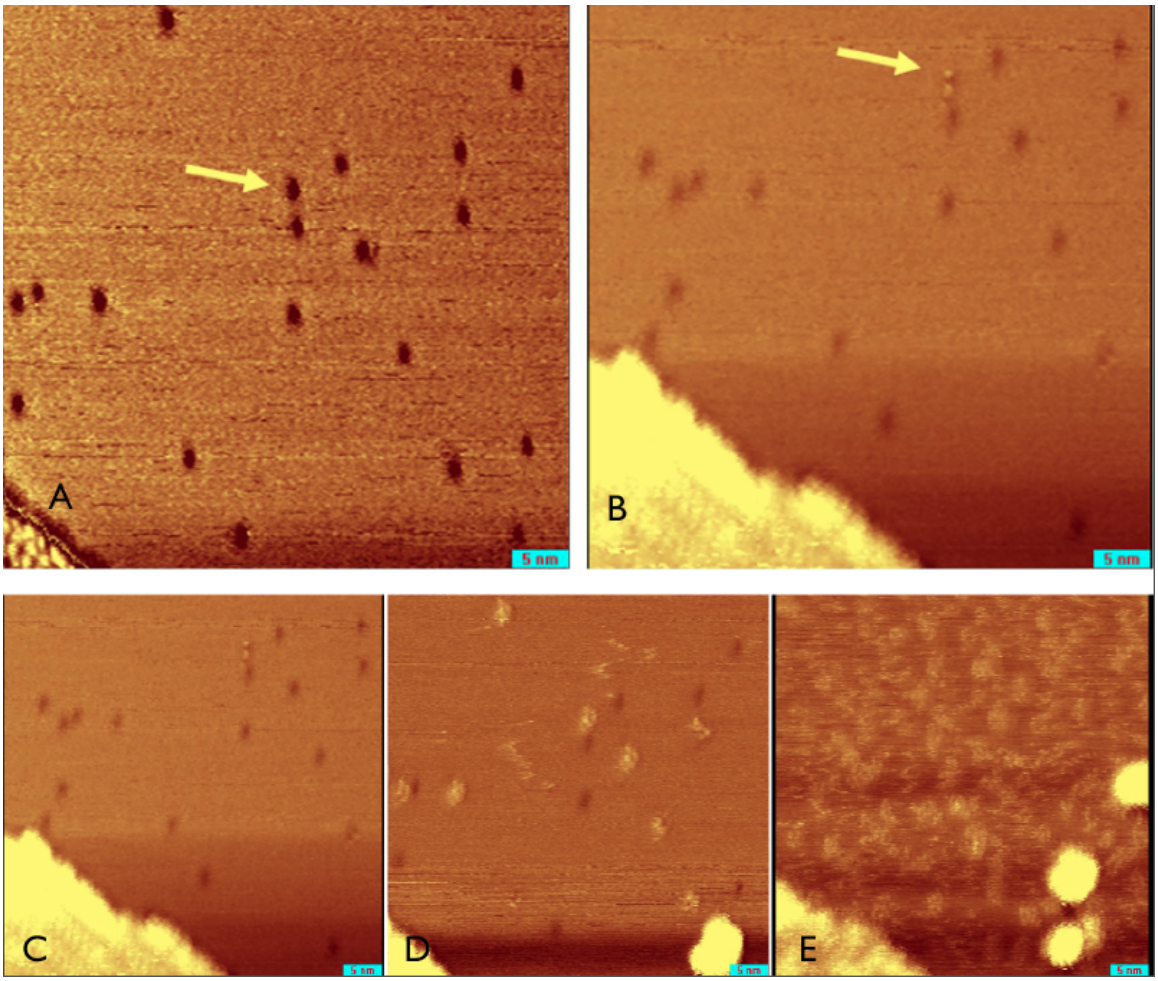

Figure A.7: Before (A) and after (B) dosing 1×10^{-10} torr dimethylamine for 30 seconds at 125 K. The yellow arrows point to the same feature before and after the dose. The image shows an Ag(111) terrace with scattered O atoms (dark spots) that are stationary at this temperature. After dosing, panel (A) shows a bright feature located at one of the O atoms. The bright features attributed to dimethylamine increase on the surface after dosing dimethylamine at 125 K for (A) 1×10^{-10} torr, 30 seconds; (B) 5×10^{-10} torr, 60 seconds; and (C) 5×10^{-10} torr, 30 seconds. The blue scale bars at the bottom of the images are 5 nm in all cases.

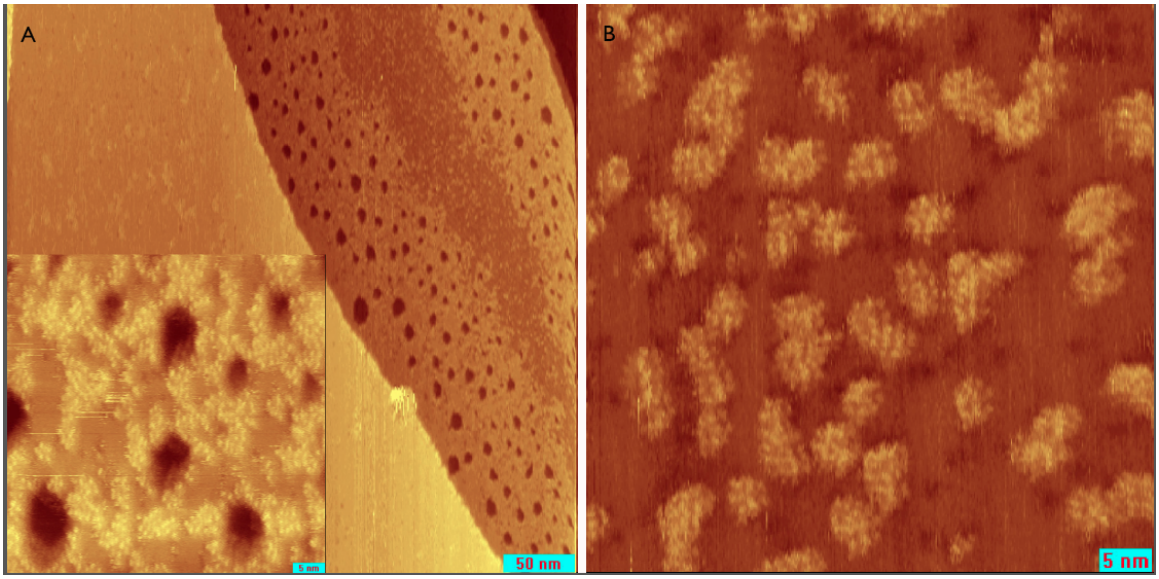

Figure A.8: The surface after reaction of dimethylamine on 0.2 ML O at 125 K, (A) annealed to 200 K, and cooled back to 125 K for imaging. The left side of the large image has a flat terrace with small bright features. The right hand side shows a terrace with large one atom deep holes. The pit size decreases with the distance to the step edge (both step up and step down). Inset shows a closer view of the pits and features, which are ~1nm in size. Blue scale bars are 50 nm for the large image and 5 nm for the inset. (B) The surface was then annealed to 280 K and cooled again for imaging. All areas looked the same: large terraces decorated with large clusters (5-10 nm) made up of ~1 nm bumps along with possible scattered oxygen atoms. Scale bar is 5 nm.

reaction has taken place with the oxygen reconstruction, and intermediates, which will lead to both n-methylimine and methylisocyanate, as well as combustion products, are on the surface. Areas of the surface have large flat terraces while other have large pits; both are covered with bright features. Pits form on only some terraces, presumably those which were previously covered with the oxygen p($4 \times 5\sqrt{3}$)rect overlayer. The pits are one Ag atom deep, and are decorated with 1 nm features (Fig. A.8). A simple explanation is that reaction of the dimethylamine with oxygen and subsequent collapse of the oxygen-silver reconstruction allowed release of the Ag adatoms, which caused formation of pits in the surface. Interestingly, the pits are larger on the edges of the terrace than in the middle, indicating a complex "reaction-front" type of chemistry, which has been observed previously on both silver and copper oxygen-covered surfaces.

Finally, upon annealing to 280 K, the pits disappeared, leaving bright features uniformly covering the surface. Sections that were formerly pitted or flat are indistinguishable. The large clusters are intermediates that will lead to both combustion products and methylisocyanate. Darker spots, similar to that of oxygen adatoms are also scattered on the surface (Fig. A.8b).

A.5 Discussion

A.5.1 Selectivity

Selectivity is improved by using a lower oxygen coverage. Selectivity for the desired partial oxidation products, N-methylmethanimine and methylisocyanate is

60% and 18%, respectively at 0.1 ML O/Ag(111), while on 0.2 ML O/Ag(111), the selectivity decreases to 18% and 15%, respectively, with over 50% of the products being combustion products (CO_2, N_2, NO).

During dimethylamine oxidation on 0.2 ML O, although methylisocyanate and N-methylimine are still produced, there is a much greater amount of oxidation products, as well as excess oxygen. This result is not intuitive, as one would expect an oxygen coverage of 0.2 ML to allow for selective formation of up to 0.4 ML of the surface amide ($(CH_3)_2N_{(a)}$), assuming that $OH_{(a)}$ formed in situ can also react in an acid-base manner to cleave another NH bond. However, the persistence of atomic oxygen, even after full oxidation of the dimethylamine, suggests that not all of the oxygen is accessible to the incoming dimethylamine.

The scanning tunneling microscopy results for the annealing to 200 K yield more insight. The pattern of the pits leads us to believe that the reaction propagates along the oxygen structure, resulting in a "reaction front" type of chemistry. With a higher initial oxygen coverage, it could be the case that the islands of the oxygen reconstruction are larger, and if the reaction occurs starting from the edges, then it could be more difficult to get to the middle and use up all of the oxygen.

Further changes in the selectivity upon annealing the surface (not shown) reveal a dynamic surface process in which rearrangement of silver adatoms plays an important role. Annealing allows intermediates and metal atoms to rearrange. The fact that this rearrangement causes a change in the selectivity demonstrates the importance of kinetics and the metal ad-atom rearrangement for this process. The greatest selectivity for methylisocyanate (30%) occurred on 0.1 ML O, when annealing to 300

K, which is when the Ag-O/Ag-OH surface is undergoing significant changes, including surface mobility and OH recombination to form water. Any annealing of the 0.2 ML O surface, however, resulted in a drop in the selectivity for methylisocyanate to 2-6%, presumably because the annealing allowed oxygen-silver islands to rearrange, giving the oxygen access to the methylisocyanate intermediates on the surface before they desorbed.

A.5.2 Metal adatom incorporation into intermediates

temperature programmed reaction desorption of methylisocyanate at 500 K indicates an extremely strong bond of the precursor intermediate to the surface, as the desorption of neat methylisocyanate (which is presumably similar to the intermediate) occurs at 150 K. Also, although there is a small shoulder of combustion products around the same temperature (510K) on the 0.2 ML O surface, on the 0.1 ML O surface, there are no other significant peaks that co-evolve with methylisocyanate, suggesting that the methylisocyanate is almost fully formed on the surface, but somehow quite strongly bound. The low temperature peak of methylisocyanate formation (at 320K) also indicates that the methylisocyanate is formed on the surface, although probably in a different binding conformation which allows its release at a lower temperature.

The NCO IR data support the hypothesis that a metal ad-atom into the structure of the methylisocyanate intermediate. The substantial bathochromic shift from the multilayer NCO stretch for neat methylisocyanate (2300 cm^{-1}) to the NCO stretch of the dimethylamine oxidation intermediate (2158 cm^{-1}) demonstrates the strong

orbital overlap of the silver surface with the NCO pi anti-bonds and indicates a strong-bonding conformation of the surface intermediate, possibly incorporating a silver ad-atom. Dosage of neat methylisocyanate on a roughened Ag(111) surface yielded at slight detection at 2160 cm^{-1}, demonstrating that the observed surface intermediate incorporates a defect site in its binding conformation.

The scanning tunneling microscopy data strongly suggests that metal adatoms play a role in the formation and reaction of the dimethylamine-derived intermediates. At the very least, the scanning tunneling microscopy demonstrates that the surface dramatically changes upon annealing, with the movement of metal atoms readily evident. Significant surface atom rearrangement, resulting in the disappearance of pits occurs at 280 K, aligns with the temperature of formation of the NCO peak in the IR. Because Ag is known to be a dynamic surface and Ag−x −Ag bonds are formed with O, the strong binding and incorporation of an Ag adatom with the methylisocyanate intermediate is quite feasible and gives the best explanation of all of the data.

A.5.3 Reaction Mechanism

As mentioned earlier, oxygen adatoms are known to react in a Brønsted-base reactivity pattern with NH bonds on coinage metal surfaces [58,59]. In previous work, dimethylamine was activated on oxygen-covered silver and gold (111) surfaces to form the adsorbed amide ($(CH_3)_2N_{(a)}$) which subsequently coupled with formaldehyde and acetaldehyde to form the corresponding amide, $(CH_3)_2NC{=}OR$ (where R=H,CH_3), proving the existence of the amide intermediate [68–70]. In this work, however, further

oxidation of the activated amide intermediate derived from dimethylamine leads to formation of N-methyl methanimine and methylisocyanate.

As evidenced by the scanning tunneling microscopy, even by 200 K, the oxygen has reacted with the adsorbed dimethylamine and the surface has reconstructed. The rest of the reaction mechanism can be best understood by analyzing what is happening as the temperature increases. Each temperature at which a product or intermediate is formed corresponds with a characteristic temperature of the silver surface, demonstrating the importance of the surface itself for these reactions. The reaction mechanism proposed here is summarized in Fig. A.9.

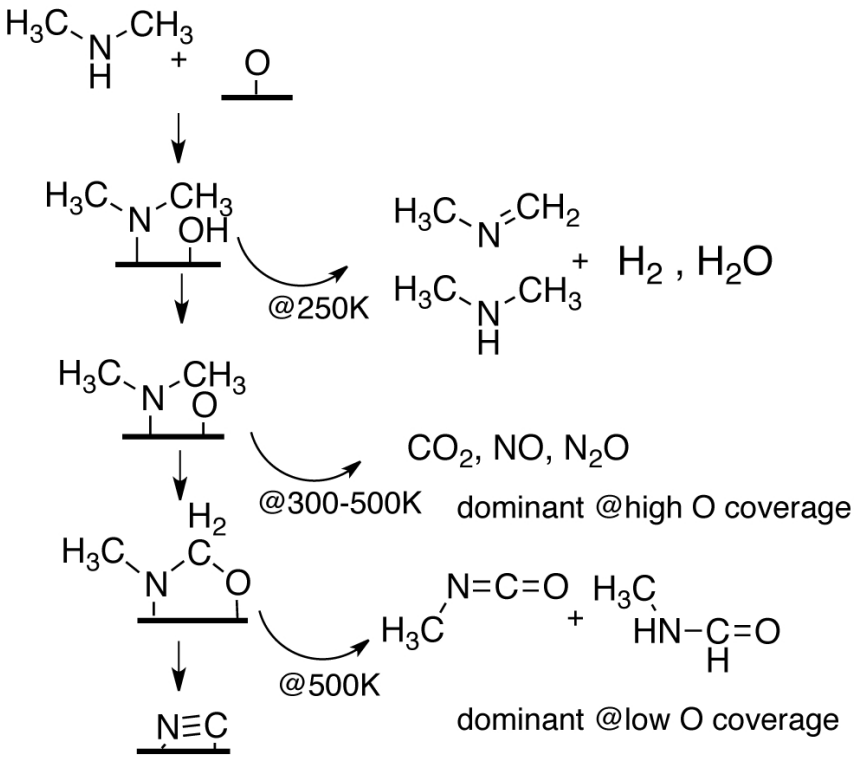

Figure A.9: Proposed reaction mechanism for the oxidation of dimethylamine on Ag(111).

At 250 K, the N-methyl methanimine is produced, requiring breaking a C-H

bond of the adsorbed $(CH_3)_2N_{(a)}$. This temperature is similar to the temperature the silver surface breaking a beta-C-H bond in similar intermediates, such as the hemiaminal $(CH_3)_2N{-}CHO_{(a)}$ (270 K) [70] Hydrogen, which would be expected to evolve due to H-atom recombination if the silver surface is breaking the C-H bond, is quite small, but there is a small amount detected, as well as H_2O produced, presumably from H recombination with a surface hydroxyl. However, the C-H bond cleavage is likely aided by a nearby $(CH_3)_2N_{(a)}$, as N-methyl methanimine and dimethylamine produced simultaneously at a ~1:1 ratio. This disproportionation reaction is particularly interesting because of the $N{-}H/C{-}H$ bond reversibility.

The formation of the NCO stretch can be seen as early as 275K in RAIRS and is quite clear by 300 K. As the scanning tunneling microscopy shows, a dramatic surface rearrangement has taken place by this temperature, and the surface is covered features, but no longer has pits. This temperature range corresponds with the range for OH recombination. Whether the surface rearrangement causes the OH recombination or vice versa, it is unknown, but these processes probably work together to enable the formation of a new surface structure as well as new intermediates, as the OH recombination results in O adatoms. The features on the surface consist of both the methylisocyanate intermediate and combustion intermediates, as well as excess oxygen. The methylisocyanate intermediate must be formed by 340 K, when the low temperature methylisocyanate peak occurs. At this point, the metal atom-intermediate complex which keeps the methylisocyanate intermediate on the surface until 500 K is likely formed.

From 350 K until 510 K, combustion products evolve, with amount and identities

of the products depending on the oxygen coverage. At 500 K, the methylisocyanate is released from the surface, and the only thing that remains is excess oxygen and the possible decomposition product, as evidence by the IR stretch at ~2100 persisting above 500 K. Finally, at 575 K, the metal atoms release any excess oxygen, annealing out and allowing excess oxygen to recombine and desorb.

In all, we have proposed and given evidence for a mechanism of dimethylamine oxidation in which the surface reconstructions and incorporation of metal adatoms play an important role. The dynamic nature of heterogeneous catalysts is often ignored, especially in model and theoretical studies of catalytic materials. However, we have shown that this is a crucial part of the chemistry in the case of dimethylamine oxidation.

A.6 Conclusions

Oxidation of dimethylamine on oxygen covered silver surfaces leads to production of n-methyl methylenimine and methylisocyanate at low oxygen coverage, as well as combustion products, which are favored at increased oxygen coverages. While n-methyl methylenimine forms in a disproportionation reaction of the surface amide at 250 K, the methylisocyanate precursor is strongly bound, not desorbing until 500 K. Using IR and scanning tunneling microscopy, it was concluded that this intermediate's NCO bond is formed by ~300 K, and the intermediate likely involved the incorporation of a metal adatom(s).

Development of catalysts to form reactive intermediates, which can be made on an as-needed basis, is crucial for chemical production to become safer and cleaner.

In this case, n-methyl methylenimine, an unstable imine, could be of immense value if available in this manner as a viable feedstock to form imine-derived molecules. Methylisocyanate, on the other hand, is an established feedstock of chemical and particularly agro-chemical industry. Safe and possibly more energy or cost effective production may be possible by developing the catalytic process we have discovered in this study by using a model silver catalyst.

Appendix B

Why Gold and not Silver?–An Exploration of Alcohol Coupling Reactivity on Silver

B.1 Introduction

Recent research on gold catalysts has revealed that selective oxidation reactions of alcohols on gold yield esters, aldehydes, and acids, depending on the reaction conditions [20, 78, 115, 220]. On gold single crystal surfaces with low oxygen coverage, alcohols self-couple and cross-couple according to predictable principles of reactivity [115]. On silver, however, alcohol oxidation under similar conditions yields predominantly the aldehyde, with self-coupling being significant only for methanol [10], and cross-coupling between alcohols being negligible. In this work, the coupling reactivity between alcohols and alcohols and aldehydes on silver is explored, in order

to elucidate differences in the governing factors of reactivity on silver and gold surfaces. This work is done in particular to support further work on silver and gold alloy surfaces, in order to have a background of reactivity knowledge on each metal.

Previous work on Ag(111) showed that while self-coupling of methanol occurs on silver, self-coupling of ethanol to form ethyl acetate did not occur. This is somewhat surprising because acetaldehyde should form somewhat more readily than formaldehyde, making it available for the alkoxide to couple with at a lower temperature. One conclusion from this is that the limitations of alcohol coupling on silver may have more to do with the alkoxide itself than the formation of the aldehyde in situ (which is the limiting step on gold).

In order to investigate the coupling abilities of the alkoxides without considering the in situ formation of the aldehyde, coupling between alkoxides and dosed aldehydes was studied on Ag(111). While coupling between methanol and formaldehyde occurred readily, coupling between methanol and any longer chain aldehydes did not. We proposed that this could be because of the lower temperature of oxidation of the aldehyde by excess oxygen to the corresponding carboxylate, after which point coupling could not occur. Using this information, the coupling temperature of methanol on Ag(111) could be pinned to between the temperatures of formation of formate from formaldehyde (215 K) and acetate from acetaldehyde (205 K), as measured by the H_2 formation when the carboxylate forms (not shown). In order to eliminate the possibility of oxidation of the aldehyde, we have done a series of experiments on Ag(110), showing that selected isolated alkoxides, in the absence of excess oxygen, can couple with aldehydes, but the ability of an alkoxide to couple depends on the

strength of the RO-Ag bond.

B.2 Results

Isolated alkoxides on Ag(110) were formed by dosing the alcohol on 0.1 or 0.2 ML O/Ag(110) and then annealing to ~200 K, ridding the surface of both water and molecular alcohol. Under these conditions, selective oxidation of the methoxy or ethoxy occurred to form the corresponding aldehydes occurred (and methylformate in the case of methoxy), indicating that excess oxygen has been eliminated (Figs. B.1, B.2).

Next, aldehydes were introduced in order to evaluate qualitatively whether the alkoxy on silver could nucleophilically couple with an aldehyde on the surface. We show that methoxy can couple with longer chain aldehydes in modest amounts in the absence of excess oxygen (Figs. B.3, B.4).

Interestingly, ethoxy can couple with formaldehyde, but not with acetaldehyde, the reason for which is still under investigation (Figs. B.5, B.6). Because the coupled product amounts are very small, this could be an artifact of the relative intensity of the unique masses measured for each product.

Butoxy, however, does not couple with formaldehyde (Fig. B.7). However, there is a very small, albeit detectable, amount of self-coupling of butanol. It is possible that a similar amount of coupling occurs between butoxy and formaldehyde, but because of overlapping fragments of the ester with butanol and butanal, any ester formed is concealed by the noise due to the subtraction.

Overall, these results indicate that the strength of the RO-M bond, which is

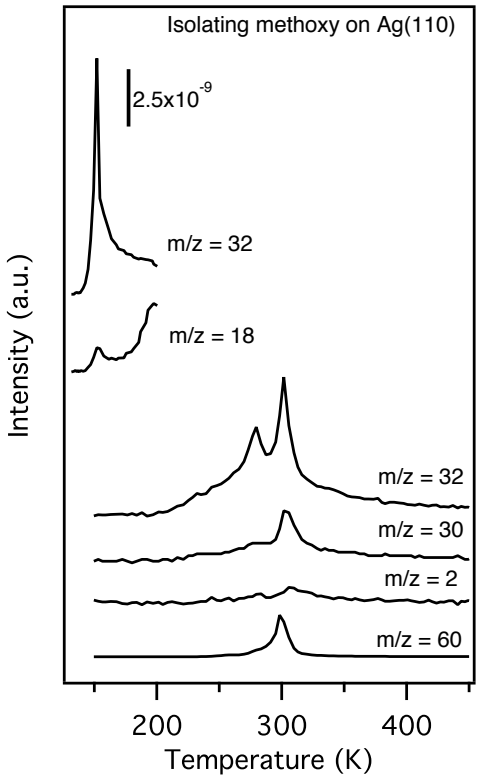

Figure B.1: Methoxy was isolated on Ag(110) by dosing ~3 L methanol on 0.2 ML O/Ag(110) at 130 K, annealing to 200 K for approximately 5 s. Then the surface was cooled to 130 K before performing temperature programmed reaction. The heating rate for both annealing and temperature programmed reaction was 5 K/s.

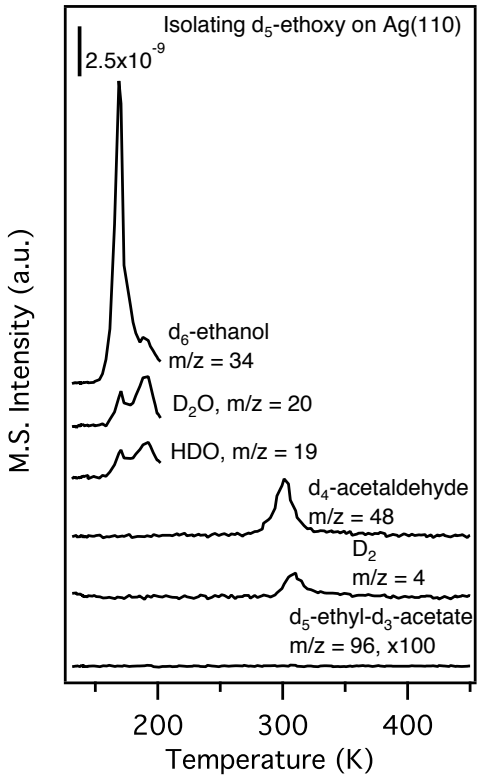

Figure B.2: D_5-ethoxy was isolated on Ag(110) by dosing ~3 L methanol on 0.2 ML O/Ag(110) at 130 K, annealing to 200 K for approximately 5 seconds. Then the surface was cooled to 130 K before performing temperature programmed reaction to observe the reaction of ethoxy on the Ag(110) surface. The heating rate for both annealing and temperature programmed reaction was 5 K/s.

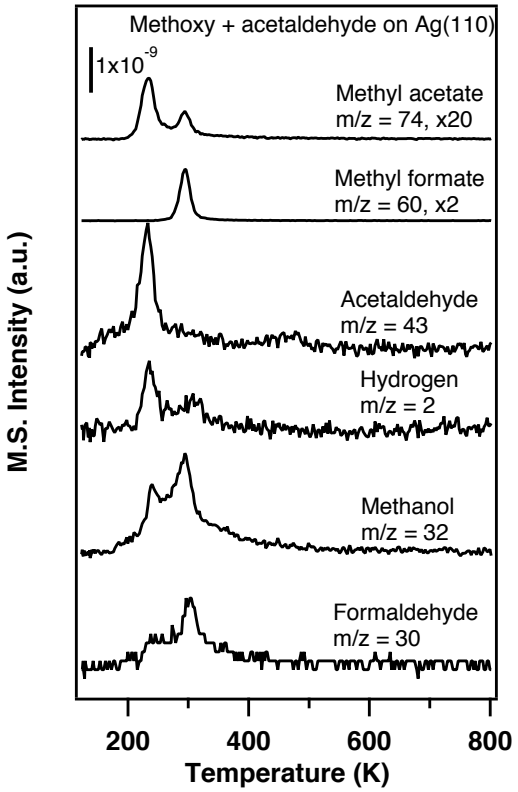

Figure B.3: Isolated methoxy can couple with acetaldehyde. After methoxy was isolated on Ag(110) by dosing ~3 L methanol on 0.2 ML O/Ag(110) at 130 K, and annealing to 200 K (see Fig. B.1), 1.5 L acetaldehyde was dosed at 130 K. The heating rate was 5 K/s.

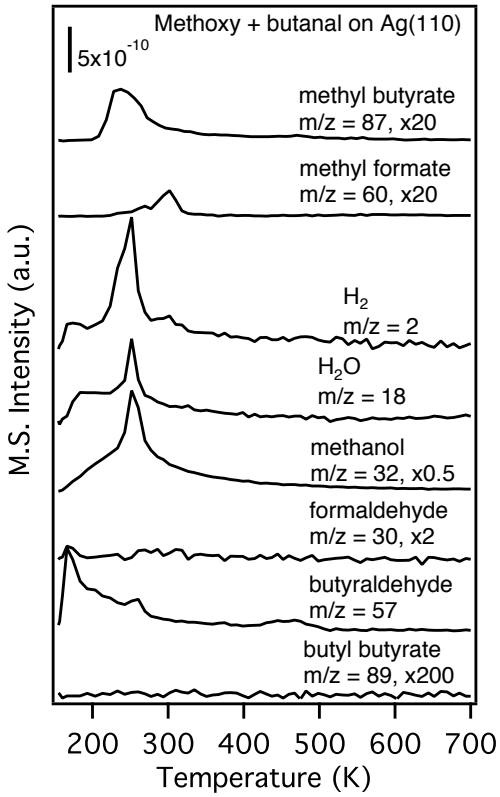

Figure B.4: Isolated methoxy can couple with butanal. After methoxy was isolated on Ag(110) by dosing ~3 L methanol on 0.1 ML O/Ag(110) at 130 K, and annealing to 200 K (see Fig. B.1), 3 L butanal was dosed at 130 K. The heating rate was 5 K/s.

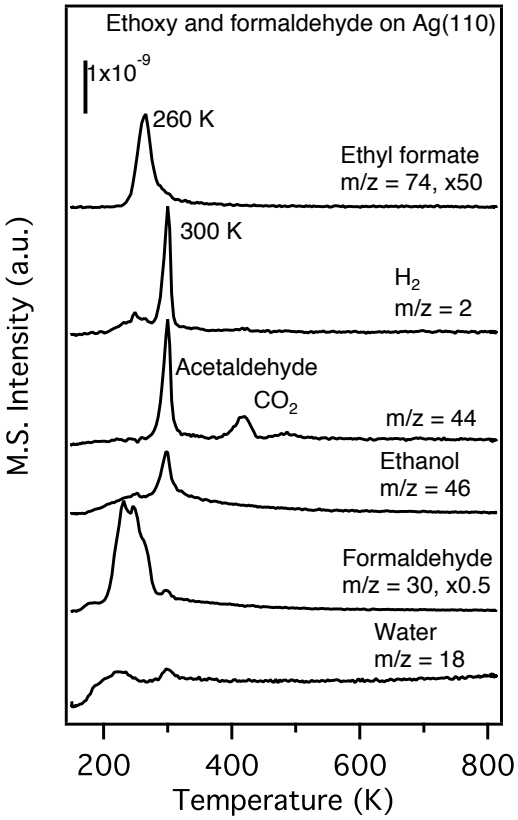

Figure B.5: Isolated ethoxy can couple with formaldehyde. After ethoxy was isolated on Ag(110) by dosing ~3 L d_6-ethanol on 0.1 ML O/Ag(110) at 130 K, and annealing to 200 K, 1.5 L acetaldehyde was dosed at 130 K. The heating rate was 5 K/s.

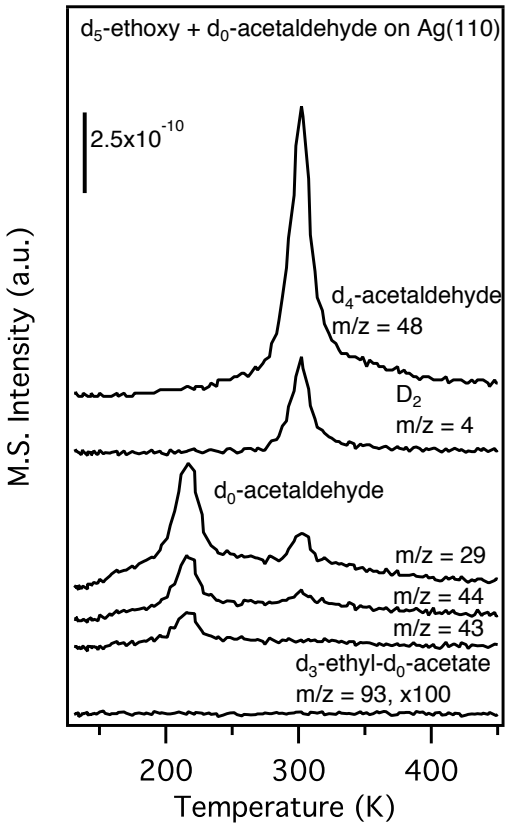

Figure B.6: Isolated d_5-ethoxy cannot couple with d_0-acetaldehyde. After d_5-ethoxy was isolated on Ag(110) by dosing ~3 L d_6-ethanol on 0.2 ML O/Ag(110) at 130 K, and annealing to 200 K (see fig 2), 3 L d_0-acetaldehyde was dosed at 130 K. The heating rate was 5 K/s.

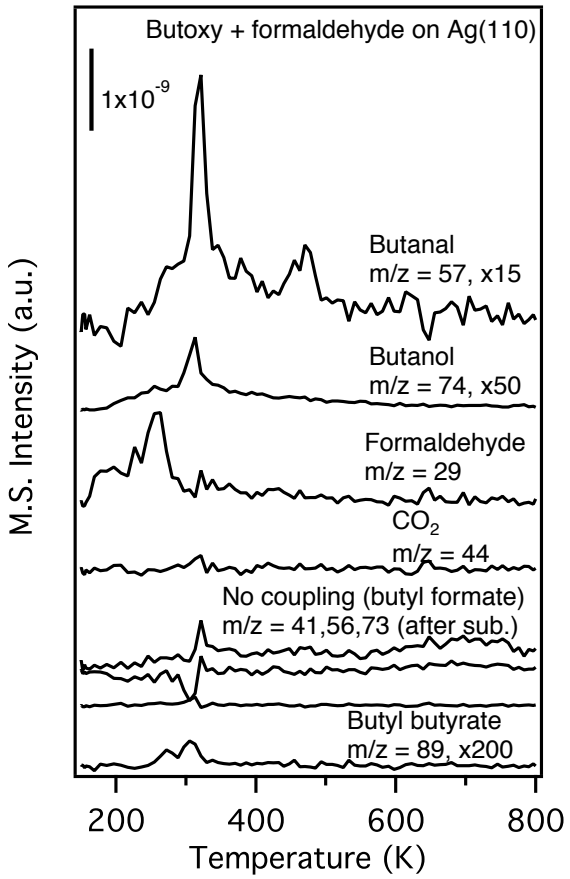

Figure B.7: Isolated butoxy cannot couple with formaldehyde. After butoxy was isolated on Ag(110) by dosing ~3 L butanol on 0.1 ML O/Ag(110) at 130 K, and annealing to 200 K, 6 L formaldehyde was dosed at 130 K. The heating rate was 5 K/s.

stronger on silver than on gold, and increases with the chain length of the alcohol, dictates the ability of the alkoxy to nucleophicially couple on silver. This is especially interesting compared to gold, for which there is apparently no barrier for the actual coupling process [77]. If we relate the coupling ability to the binding strength of the intermediate, this is a very clear example of small changes in the binding energy of intermediates having a clear and dramatic effect on the product selectivity and whether a given reaction can occur at all.

Appendix C

Brønsted Basicity of Hydroxyl on Metallic Silver

C.1 Introduction

Selective oxidation reactions are a critical technology that uses Ag-based catalysts. One major industrial process is the selective oxidation of alcohols to produce aldehydes; the methanol-to-formaldehyde process is a prime example [195].

It is well established from fundamental studies that alcohols, including methanol and ethanol, are activated by atomic oxygen adsorbed on Ag; the initial step being O-H bond breaking to yield an alkoxide and adsorbed OH [10]:

$$\mathrm{O}_{(a)} + \mathrm{ROH} \longrightarrow \mathrm{OH}_{(a)} + \mathrm{RO}_{(a)}. \tag{C.1}$$

The key methoxy intermediate has been previously identified using high resolution electron energy loss, in situ Raman, x-ray photoelectron, and ultra-violet

photoelectron spectroscopies [221–224], and microkinetic models have been developed for methanol oxidation to formaldehyde using the data derived in ultra high vacuum [170, 171]. The proclivity for the ROH activation is related to the gas phase acidity of the O-H bond in the alcohol with the adsorbed O acting as a Brønsted base [96, 129]. The aldehyde is than formed via metal-induced β-H elimination from the alkyl group–the β-H being bound to C adjacent to the oxygen in the alkoxide [10].

Herein, we test for the efficacy of adsorbed OH in promoting selective oxidation processes on Ag. Because adsorbed hydroxyl is present on the surface as a consequence of the initial reaction, the question arises as to the possible role of OH itself in driving selective oxidation reactions on Ag.

Hydroxyl on gold catalysts has been proposed to promote selective oxidation of alcohols to acids, water gas shift, CO oxidation, and epoxidation on supported gold catalysts, particularly under high pH conditions [73,78,178]. Analogously, we find that OH adsorbed on Ag(110) cleaves the hydroxyl bond of both methanol and ethanol, yielding the same products as atomic oxygen, but with different stoichiometry.

The reactions of OH can be investigated because on Ag(110), adsorbed O can be quantitatively converted to adsorbed hydroxyl by reaction with water [57, 180–189]:

$$H_2O + O_{(a)} \longrightarrow OH_{(a)} + OH_{(a)}. \tag{C.2}$$

The Ag(110) surface was utilized because prior work has established procedures for the isolation and characterization of the OH-covered surface [182, 225]. Adsorbed hydroxyl is stable on silver is stable up to around room temperature, where it disproportionates to H_2O and $O_{(a)}$ [57, 184].

C.2 Results

C.2.1 Formation of OH on Ag(110)

The structures of both adsorbed O and OH on Ag(110) system have been previously characterized, both involving the incorporation of metal atoms. The O/Ag(110) structure consists of added O−Ag−O chains along the [100] direction, and the OH covered surface has a chain-like row overlayer structure along the perpendicular [1-10] direction. As observed directly with STM, complete conversion of the O/Ag to OH/Ag occured when water was dosed onto the oxygen precovered surface below room temperature in an amount comparable to the oxygen surface coverage [182, 188]. An initial oxygen coverage of 0.25 ML results in an OH coverage of 0.5 ML, which is the saturation coverage of both adsorbed hydroxyl and atomic oxygen on Ag(110) under the conditions used in this study.

Temperature programmed desorption shows that H_2O co-adsorbed with OH on Ag(110), where the initial oxygen coverage is 0.25 ML or lower, exhibits several adsorbed states [57, 183]. The water multilayer state desorbs at 175K, a hydrogen bonded H_2O second layer desorbs at 200K, and a third water desorption peak occurs around 240K, the latter having been identified as a hydrogen-bonded H_2O:2OH phase. OH disproportionation to reform water and adsorbed O occurs over a broad temperature range, centered around 315K.

In this work $OH_{(a)}$ was formed by dosing water on 0.1 ML O/Ag(110) at 225K, preventing the build-up of multilayers of water. The existence of $OH_{(a)}$ without excess oxygen and its resulting two dimensional structure were confirmed using a

combination of temperature programmed reaction spectroscopy (TPRS) and LEED, shown in Chapter 7. For all experimental details, see Chapter 7.

C.2.2 Activation of d_6-ethanol on OH/Ag(110)

Isolated adsorbed hydroxyl promotes O-H dissociation in d_6-ethanol at low temperature, generating water and d_6-ethoxy on the surface. The evidence for ethoxy formation is the clear correspondence in the characteristic temperature programmed reaction spectra for d_6-ethanol reaction on O- and OH-covered Ag(110) (Fig, C.1a). The reaction of ethanol to ethoxy and the subsequent formation of acetaldehyde are well-understood, as discussed in the introduction; thus, the pattern for formation of acetaldehyde, water and hydrogen are a fingerprint for ethoxy formation and subsequent reaction. Specifically, d_6-ethoxy dehydrogenates to yield d_4-acetaldehyde at 290K. Note that acetate is not formed at this oxygen coverage; therefore, no CO_2 is detected. At higher O coverages, acetate forms from secondary oxidation of acetaldehyde and later decomposes to form CO_2 and hydrogen at 500 K.) D_2 evolves from the surface just after the d_4-acetaldehyde formation, as expected for β-hydrogen elimination from adsorbed ethoxy on silver. In parallel ethoxy is re-hydrogenated to d_6-ethanol coincident with the deuterium released when acetaldehyde is formed at 290K. This pattern of reactivity is the same for reaction on either O- or OH-covered Ag(110). The yield of d_4-acetaldehyde from reaction of d_6-ethanol on Ag(110) containing OH (0.2 ML) is half that for the same coverage of adsorbed O and the same as for reaction on a surface containing 0.1 ML of $O_{(a)}$ (Table C.1).

Reaction conditions	d_4-acetaldehyde (m/z=48)	re-formed ethanol (m/z=52)	total ethanol reacted
0.1 ML O	7.8	1.0	8.8
0.2 ML O	14.4	2.1	16.4
0.2 ML OH	8.9	1.0	9.9

Table C.1: Product amounts for oxidation of ethanol on oxygen or hydroxyl covered silver (110).

Reaction conditions	formaldehyde (m/z=30)	CO_2 (m/z=44)	methyl-formate (m/z=60)	re-formed methanol (m/z 32)	Total methanol reacted
0.1 ML O	3.3	0.84	2.1	0.4	8.7
0.2 ML O	4.4	1.2	4.5	3.8	18.4
0.2 ML OD	3.1	1.1	1.6	0.5	7.9

Table C.2: Product amounts for oxidation of methanol on oxygen or hydroxyl covered silver (110).

The isotopic distribution in the low temperature water for reaction of adsorbed OH with d_6-ethanol supports the assertion that OH promotes loss of the alcoholic proton. Specifically, all three isotopes of water–H_2O, HDO and D_2O–are formed in temperature programmed reaction with prominent peaks at 180 K (Fig. C.1b). These data are indicative of O−D bond breaking in d_6-ethanol induced by adsorbed OH. The ratio, D:H, in the reaction with OH is 1.5–greater than the amount expected from a 1:1 reaction of d_6-ethanol with adsorbed OH. The excess of D is attributed to reversible exchange of adsorbed OH with O−D bonds in the excess d_6-ethanol. The presence of excess d_6-ethanol is evident from the desorption peak at 175 K (Fig. C.1a). There are also mixed isotopes of water observed for the O-covered surface (data not shown), indicating some formation of OH on these surfaces due to background water. The ratios of D:H are 2.5 and 4.4, respectively, for the surfaces initially covered with 0.1 ML and 0.2 ML O, respectively.

The O-H bond in methanol is also activated by OD adsorbed on Ag(110) (Fig. C.2). The amount of methanol that reacts to form formaldehyde and methyl formate via methoxy is approximately equal on the 0.1 ML O and 0.2 ML OD surfaces, analogous to the reaction pattern seen with ethanol. Methanol reacts with 0.2 ML of adsorbed OD to generate water and methoxy on the surface. (Fig. C.2). H_2O evolves at low temperature and HDO and D_2O continue with a broad OD disproportionation peak. For the 0.2 ML OD experiment, it is strange that we do not observe large amounts of either HDO or D_2O at low temperature. However, this could simply be due to the dilution of the deuterium in the OD by the presence of excess alcohol. Deuterium is incorporated predominantly in the formation of methanol-OD, which

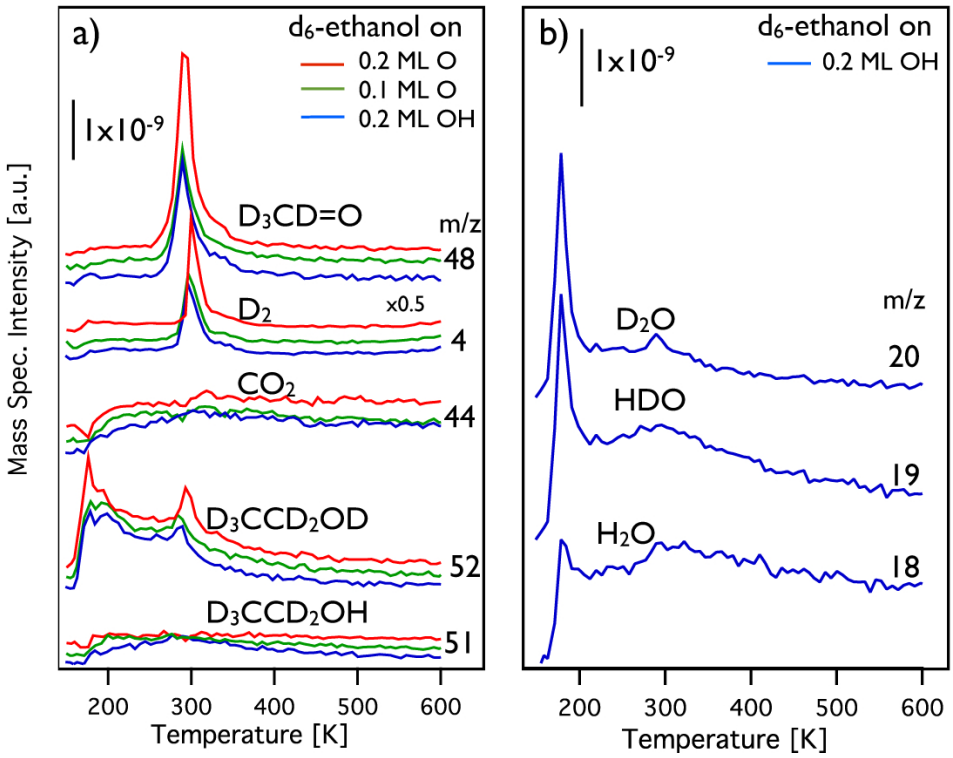

Figure C.1: Temperature programmed reaction spectra (TPRS) of 6 L d_6-ethanol at 150 K on Ag(110) with 0.2 ML O, 0.1ML O, and 0.2 ML OH shown in red, green, and blue, respectively. Panel a) primary products, b) the water isotope distribution. Fragment contributions from d_6-ethanol and d_4-acetaldehyde to other masses have been subtracted for clarity. The OH covered surface was prepared by dosing water onto 0.1 ML O/Ag(110) at 225K.

is evidence of methoxy exchanging hydrogen with surface water or OH, and in the HDO and D_2O desorption. The amount of methanol reacted, calculated as the total methoxy molecules that lead to the products detected, is approximately equal to the amount of methanol reacted on the 0.1 ML O surface, which is half as much than that reacted on the 0.2 ML O surface (Table C.2). This consistent with the results for ethanol.

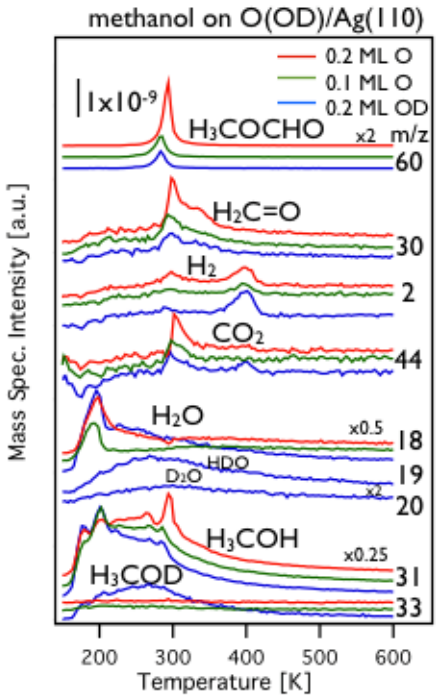

Figure C.2: Temperature programmed reaction spectra (TPRS) of 6 L d_0-methanol at 150 K on Ag(110) with 0.2 ML O, 0.1ML O, and 0.2 ML OD shown in red, green, and blue, respectively. Fragment contributions from methylformate, methanol, and formaldehyde to other masses have been subtracted for clarity. The OD covered surface was prepared by dosing D_2O onto 0.1 ML O/Ag(110) at 225 K.

Adsorbed $OH_{(a)}$ clearly reacts with the alcohols as a Brønsted base, with reactivity very similar to $O_{(a)}$ abstracting the acidic hydrogen from the alcohol to form an adsorbed alkoxy group and water on the surface. Thus, adsorbed OH has generally

the same H-abstraction capacity as half the amount of oxygen. The elementary step for hydrogen abstraction from alcohols by OH is then:

$$OH_{(a)} + ROH \longrightarrow H_2O + RO_{(a)} \cdot \tag{C.3}$$

Adsorbed hydroxyl both abstracts and exchanges hydrogen with the adsorbed molecular alcohol below 300K. Generation of both methanol-OD from dosing CH_3OH onto adsorbed OD and d_5-ethanol-OH from dosing d_6-ethanol onto adsorbed OH indicates that the alcohols can directly exchange hydrogen with an OH on the surface through hydrogen bonding and that an alkoxy can regain a hydrogen from adsorbed water or hydroxyl.

Both for ethanol and methanol the low temperature water was enhanced with the isotope of the alcoholic hydrogen. Possible reactions on the surface between d_6-ethanol and adsorbed OH are:

$$OH + Ethanol{-}OD \longrightarrow HDO + Ethanol{-}O_{(a)} \tag{C.4}$$

$$Ethanol{-}O_{(a)} + HDO \longrightarrow Ethanol{-}OH + OD_{(a)} \tag{C.5}$$

$$OD_{(a)} + Ethanol{-}OD \longrightarrow D_2O + Ethanol{-}O_{(a)} \tag{C.6}$$

Of course, all of these reactions are reversible, but the tendency to move from C.4 toward C.6 in the presence of excess alcohol explains the enhancement of low temperature water with the alcoholic hydrogen.

Taking into account these isotopic exchange reactions, we conclude that the equilibrium being maintained on the alcohol/OH/Ag(110) surface can be simplified to

$$OH + ROH \rightleftharpoons H_2O + RO_{(a)} \tag{C.7}$$

While the reaction of an alkoxy with OH to reform the alcohol and $O_{(a)}$ may be possible, the prevalence of the OH recombination peak in the reactions of both ethanol and methanol demonstrates that even if this reaction happens, it is a minor pathway.

While it is possible that a transient $O_{(a)}$ is formed in the hydrogen exchange equilibrium between OH/OH and OH/ROH, and that $O_{(a)}$ could be the active base, we believe that taking all of the data into consideration, the best and most reasonable explanation is that the OH itself is acting as a base to abstract the ROH hydrogen.

The reactivity of the adsorbed hydroxyl shows a slight sensitivity to the gas phase acidity of the alcohol, as does adsorbed atomic oxygen. Methanol does not completely consume either O or OH under the conditions of these experiments, resulting in the presence of excess oxidant and subsequent combustion of methanol, while no combustion of ethanol is observed, indicating that it is completely consumed in the creation of ethoxy. This difference from ethanol is consistent with the fact that methanol is a weaker gas phase acid than ethanol.

C.3 Conclusions

In this study, we have directly observed the Brønsted-base capability of OH toward alcohols. Therefore, in oxygen-assisted oxidation reactions, adsorbed OH is an active intermediate. Drawing analogy from other known reactions of atomic oxygen, it is likely that OH can act as a base toward other gas phase acids, abstracting acidic

hydrogens and forming the activated conjugate base on the surface. We also observe a fast equilibrium between OH on the surface and OH of alcohols, as evidenced by the isotopic dilution of the surface OH upon introduction of excess acid. This is likely facilitated by the structure of OH and alcohol or alkoxy on the surface, which could involve hydrogen bonding. While these properties to not direct answer the question of why the introduction of water can cause selectivity enhancement, they provide insight for further investigation into water as an active player in noble metal oxidative catalysis.

Appendix D

MATLAB code

D.1 Description of algorithm

The code essentially solves a classic inversion problem: quantifying product yield from mass fragment traces detected using a quadrupole mass spectrometer. The code is available on the Friend group website for use by the wider surface science community.

D.2 Code

```
function [mols,mols_tot,kernel,d_zeroed]=get_fragments5(filename,varargin)
%This version of the file works specifically for files generated by the IR
%instrument.


%filename is the input file
%varargin:{'library file names'},molecule,fragment(s)
%molecule is the # entered in varargin
```

```
%example command entry:
%[mols,mols_tot]=get_fragments4('131018-11.csv',{'CO2','H2O','H2CO'},3,[28,29]);
%will show the 28 and 29 mass contributions to the 3rd molecule entered, H2CO.
warning('off','MATLAB:rankDeficientMatrix');
close all
filterwidth=2; %e-folding width of gaussian filter put on Temperature.
               % Helps smooth things out.

t_threshold = 3; % increase in temperature, before which data is discarded

percentile = .2; % baseline signal to this percentile.
                 %ie percentile=.2 the baseline is set to the bottom 20th
                 %percentile of data points, so the noise should be around
                 %zero, not above it.

t_min = 150; %temperature for peak integration start
t_max = 250; %temperature for peak integration end

%correcting for transmission/detection- interpolation from UTI/Hiden
%manuals
delta_raw = [ % column 1 = m/z; column 2 = transmission*detection coefficient
0 2;
25 1;
35 0.9;
45 0.8;
55 0.7;
65 0.65;
75 0.588;
```

```
85 0.495;

95 0.4505;

105 0.357;

115 0.294;

125 0.2115;

145 0.084;

200 0.084;];



%load file, define m (masses), t (temperature), and d (signals)

d = dlmread(filename, ',', 1, 2);

%ignore last column if it contains zeros

if d(1,end)==0

    d=d(:,1:end-1);

end


%convert voltage to temperature and subtract off beginning and end of run

t = -73.886+178.52*d(:,1)-14.02*(d(:,1)).^2; %IR

% t = -76.883+127.71*d(:,1); %HREELS

                    %input temperature conversion here

                    %(particular to instrument, but usually a polynomial)

dummy = t(2:end);

tindex1=find((dummy-t(1:end-1))>t_threshold,1);

tindex2=find(t==max(t));

t = t(tindex1:tindex2);

d = d(tindex1:tindex2,2:end); %d is used for the signals


%file reading
```

```
fid = fopen(filename);
str = fgetl(fid);
str(end+1)=',';
fclose(fid);
colons=find(str==':');
commas=find(str==',');
quotes=find(str=='"',1);

if isempty(quotes)==0
    subtract = 2;
else
    subtract = 1;
end
%defining "M", the array of masses
m = zeros(1,size(d,2));
for nn = subtract:length(colons)
    m(nn+1-subtract)=round(str2double(str(colons(nn)+7:commas(find
    (commas>colons(nn),1))-subtract)));
end

% defining fragment transmission*detection coefficients: must be row vector
delta = interp1(delta_raw(:,1),delta_raw(:,2),m);

%populate kernel with molecule fragment data from 'library' directory
    %this has rows "mass i" and columns "molecule j"
    %entries in the kernel are fragments fij*sigma, where sigma is ionization
    %cross section
sigma=zeros(1,length(varargin{1}));
```

```
kernel=zeros(length(m),length(varargin{1}));
for nn = 1:length(varargin{1})
    if exist(['library/',varargin{1}{nn}],'file')~=2
        fprintf(2,['Error: the file ',varargin{1}{nn},' does not exist\n']);
        return
    end
    dummy =  dlmread(['library/',varargin{1}{nn}],',',0,0);
    sigma(nn)=dummy(1,1); %first line of file is the ionization cross section
    delta_dummy = interp1(delta_raw(:,1),delta_raw(:,2),dummy(2:end,1));
    dummy(2:end,2)=dummy(2:end,2)./delta_dummy;
    %account for transmission coefficients
    dummy(2:end,2)=dummy(2:end,2)./sum(dummy(2:end,2));
    %divide by total to convert to fractions, so it doesn't matter how
    you input the data (ie NIST works too)
    %populate kernel with relevant masses (ie the ones measured)
    for ii = 2:size(dummy,1)
        kernel(m==round(dummy(ii,1)),nn)=dummy(ii,2)*sigma(nn);
        %round used to ensure integer mass
    end
end



%start baseline subtraction
dummy = sort(d,1,'ascend');
dummy2= repmat(dummy(round(length(t)*percentile),:),length(t),1);

d_zeroed = (d-dummy2)./repmat(delta,size(d,1),1);
%zeroed traces, divded by transmission/detection coeffs.
```

```
%first allocate space:
d3 = zeros(size(d_zeroed));
mols = zeros(length(sigma),length(t));
mols1 = mols; mols2=mols;
d_est = zeros(size(d_zeroed)); %d_est is estimate of matrix reconstruction

%what will be included in figure?
if length(varargin)==2
    include_mols = varargin{2};%molecules that you want to include in figure
elseif length(varargin)==3
    include_mols = varargin{2};
    include_frags=zeros(size(varargin{3}));
    %fragments that you want to include in figure
    for ii = 1:length(varargin{3})
        include_frags(ii)=find(m==varargin{3}(ii),1);
    end
    include_frags = sort(include_frags,'ascend');
else
    include_mols = 1:size(kernel,2);
    %if no molecule/fragment is specified, include everything in figure
    include_frags = 1:size(kernel,1);
end

%subtract out fragments if a mass is unique for one molecule

dummy=logical(kernel);
```

```
dummy2=false(size(dummy,1),1);
for nn = 1:size(dummy,1)
    if sum(dummy(nn,:))>1
        dummy(nn,:)=false(1,size(dummy,2));
    elseif sum(dummy(nn,:))~=0
        dummy2(nn)=true;
    end
end
dummy3=sum(dummy)<=0;
dummy4=logical(dummy3-1);
kernel1=kernel.*dummy; %kernel of unique fragments
kernel2=kernel.*(1-dummy); %residual kernel

%Ideally we will be able to specify which fragment to base subtraction on
%if there is more than one unique fragment.

%SOLVING for amount of molecule at each temperature point
%mols_dummy=mols;
for nn = 1:length(t)
    filter = repmat(exp(-((t-t(nn))./filterwidth).^2),1,size(d,2));
    %gaussian filter- can do without
    (just use small number),
    but makes noise less of an issue.
    d3(nn,:) = trapz(t,d_zeroed.*filter,1)./trapz(t,filter,1); %creating
    the filtered version of d_zeroed
    mols1(dummy4,nn)=sparse(kernel1(dummy2,dummy4))\
    (d3(nn,dummy2)'); %SOLVES for the molecules with unique fragments
    %mols_dummy(:,nn)=lsqnonneg(kernel,d3(nn,:)');
```

```
    d3(nn,:)=d3(nn,:)-(kernel*mols1(:,nn))'; %subtracts contribution
    to signal from molecules with unique fragments
    mols2(dummy3,nn)=lsqnonneg(kernel2(:,dummy3),d3(nn,:)');
    %mols2(dummy3,nn)=sparse(kernel2(:,dummy3))\(d3(nn,:)');
    %SOLVES for the residual
    mols(:,nn)=mols1(:,nn)+mols2(:,nn); %total molecules
    d_est(nn,:)=(kernel(:,include_mols)*mols(include_mols,nn))';
    %estimate of reconstructed signal
end
figure
plot(t,mols','linewidth',1)
legend(varargin{1})

figure
plot(t,d_zeroed(:,include_frags),'linewidth',1);
hold on
plot(t,d_est(:,include_frags),'linestyle','--','linewidth',1)
str=cell(1,length(include_frags));
for nn = 1:length(include_frags)
    str{nn}=int2str(m(include_frags(nn)));
end
legend(str)

%find integral for molecules

%setting temperature for peak integration
tindex3=find(t>t_min,1)-1;
tindex4=find(t>t_max,1);
```

```
%find total fragment concentration (same as above, but integrated signals)
d_int = trapz(t(tindex3:tindex4),d_zeroed(tindex3:tindex4,:),1);
%integrated signals in T, divided by transmission coefficient
mols2=zeros(size(sigma')); mols1=mols2;
mols1(dummy4)=sparse(kernel1(dummy2,dummy4))\(d_int(dummy2)');
d_dummy=d_int-(kernel*mols1)';
mols2(dummy3)=lsqnonneg(kernel2(:,dummy3),d_dummy');
mols_tot=mols1+mols2;

%get residual to compare to signal and find error
res = (d_int'-kernel*mols_tot);
figure
bar(m,d_int)
hold on
scatter(m,res','r')
grid on
legend('signal','Measured-Estimated')
```

Appendix E

Supporting Material

E.1 Supporting Material for Chapter 2

Typical products for acetate reaction in the presence of co-adsorbed oxygen or on the clean surface (excess acid) are shown in Fig. E.1. Additionally, methyl acetate and a very small amount of ethane are produced on the clean surface (not shown). In the case of excess oxygen (m/z 32), there is oxygen recombination at 530 K after the reaction, whereas in the case of excess acid, there is none. While CO_2 is the main product for both reaction pathways, there are many more products on the clean surface, indicating a complex reaction pathway. A full study of the reaction mechanisms is underway (see Chapter 3).

When CH_3COOD is dosed at temperatures below the desorption temperature of water, desorption of both molecular CH_3COOD (m/z = 61) and D_2 (m/z = 20) is observed around 200 K. The fact that no O_2 (m/z = 32) desorption at $\sim$ 550 K and only the high temperature CO_2 (m/z = 44) acetate decomposition pathway are observed indicates that all of the O_{ad} is quantitatively reacted to D_2O.

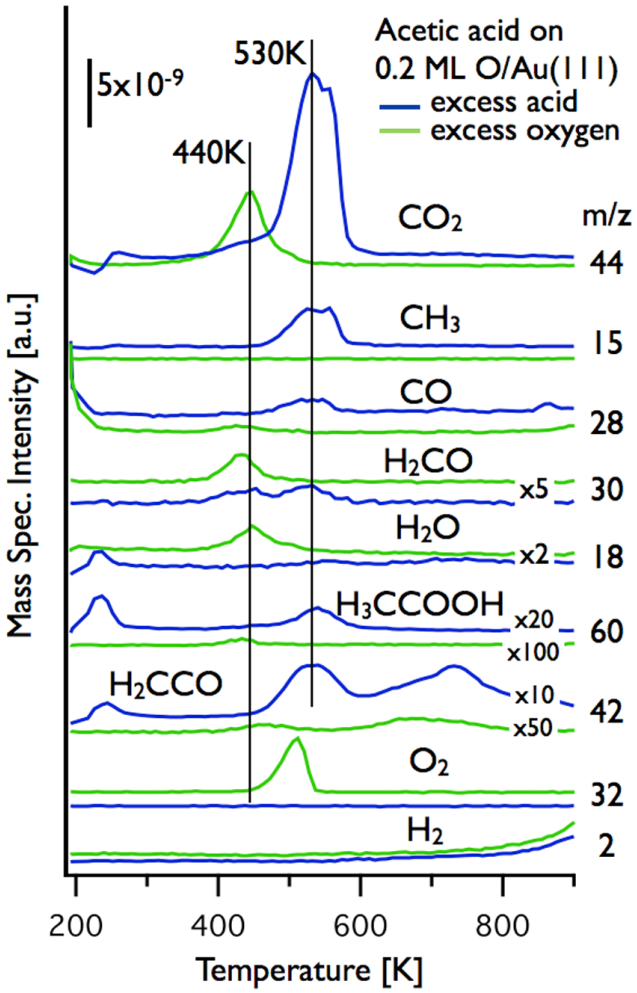

Figure E.1: Temperature programmed reaction spectra for acetate reaction on Au(111) with co-adsorbed oxygen (green/gray) or excess acid (blue/black). Fragments from other products are subtracted so that the m/z trace is representative of the molecule indicated. Dosing of both ozone to generate O/Au(111) and acid to generate the acetate was done at 200 K.

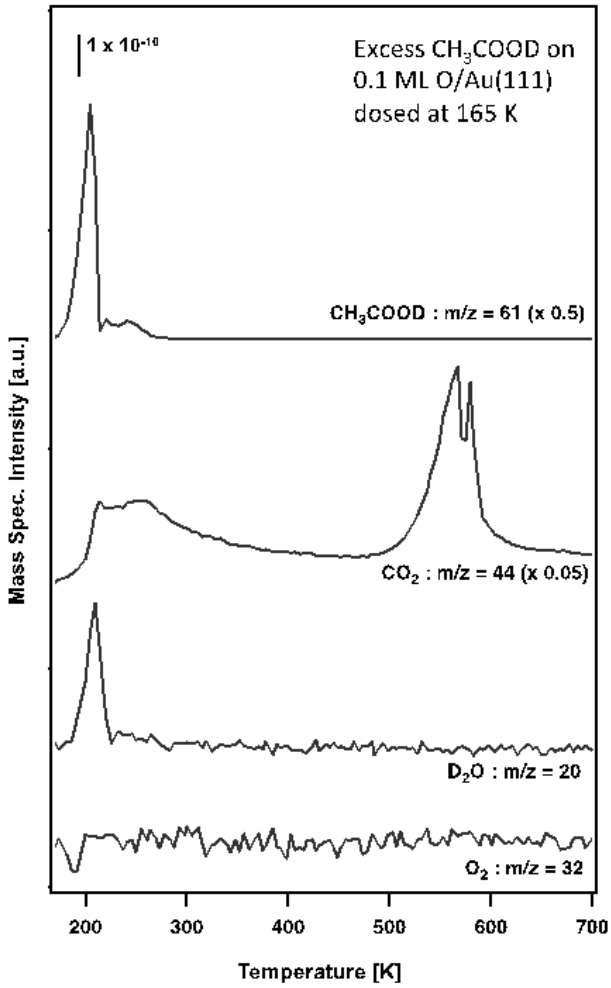

Figure E.2: Temperature programmed reaction spectra for excess CH_3COOD dosed on 0.1 ML O/Au(111). Dosing of both ozone and acid was done at 165 K.

Initial Oxygen Coverage	0.55 ML O (excess oxygen)	0.2 ML O (excess oxygen)	0.2 ML O (no coadsorbed oxygen)
CO_2	86.5 (66.5)	33.7 (75.1)	67.6 (54.0)
H_2CO	38.8 (29.9)	10.0 (22.3)	2.6 (2.1)
CH_3[a]	0 (0)	0.1 (1.0)	34.2 (27.4)
$H_3CCOOCH_3$	0 (0)	0 (0)	5.3 (4.3)
CO	2.8 (2.2)	0 (0)	8.5 (6.8)
H_2CCO	0.2 (0.2)	0.2 (0.4)	1.9 (1.5)
H_3CCOOH	1.6 (1.3)	0.5 (1.2)	4.0 (3.2)
C_2H_6	0 (0)	0 (0)	0.7 (0.6)
H_3CCO	0 (0)	0 (0)	0.3 (0.2)
H_2O	17.2 (–)	6.5 (–)	0 (–)
Excess O_2	9.0 (–)	4.1 (–)	0 (–)

Table E.1: Relative and percent yields of all products in representative cases for acetate on Au(111) with excess oxygen present and without co-adsorbed oxygen. Relative yields are given by the first number in each cell, and are calculated using quantitative mass spectroscopy, with an enhancement factor of 3.2 included for CH_3 radical. Percent yields are shown in parentheses, and are based only on carbon containing products.

E.2 Supporting Material for Chapter 3

In order to determine the identities of the products, their fragmentation patterns were compared to the fragmentation patterns of neat samples (when available) and the NIST database (when available). Then subtraction of every product's contribution to other mass fragments was performed to ensure that all products were identified. The fragmentation patterns for the products are given at the end of the Supporting Material, Table E.5.

One particularly complicated product identification was that of the m/z=28 signal. Determination of this product was confirmed to be CO using the ^{13}C experiments. Ethane has a dominant fragment at m/z=28, but also has a significant contribution to m/z= 27 and 30. At the high temperature reaction, all of these peaks were present. However, the m/z=27 peak was too small for the expected fragmentation of ethane, so we turned to isotopic labeling to figure out the product identity.

Using the ^{13}C experiment, we found that while the m/z=27 is indicative of a small amount of ethane, the m/z=28 from the unlabeled experiments was CO and not ethane or ethylene (Fig. E.3). CO from the ^{13}C methyl would have a primary fragment of 29, and either ethane or ethylene with two ^{13}C's would have a primary fragment of 30. However, almost all of the m/z=30 signal in the ^{13}C experiment was accounted for by formaldehyde, indicating only a minor amount of ethane. However, the m/z= 28/29 remained, indicating unlabeled and labeled CO.

In Fig. 3.9, the selectivity for each product is calculated on a per carbon basis (i.e. methylacetate is 3 carbons, so the absolute yield is multiplied by 3, but CO_2 is only 1) to reflect how many carbons go into forming each product. The corresponding yields for Fig. 3.9 are included here in Fig. E.4.

The total coverage acetate was calculated by taking the total number of carbons reacted, from the stoichiometry of the products and their relative yields, and calibrating to 0.2 ML O, a coverage on which there is no residual oxygen, indicating 0.2 ML of acetate reacted. Then the amount of co-adsorbed oxygen was calculated by subtracting the total acetate reacted from the initial oxygen coverage, which gives the additional oxygen that must have been on the surface. Because acetate is generally bound in a bidentate manner, the total oxygen coverage on the surface can be calculated

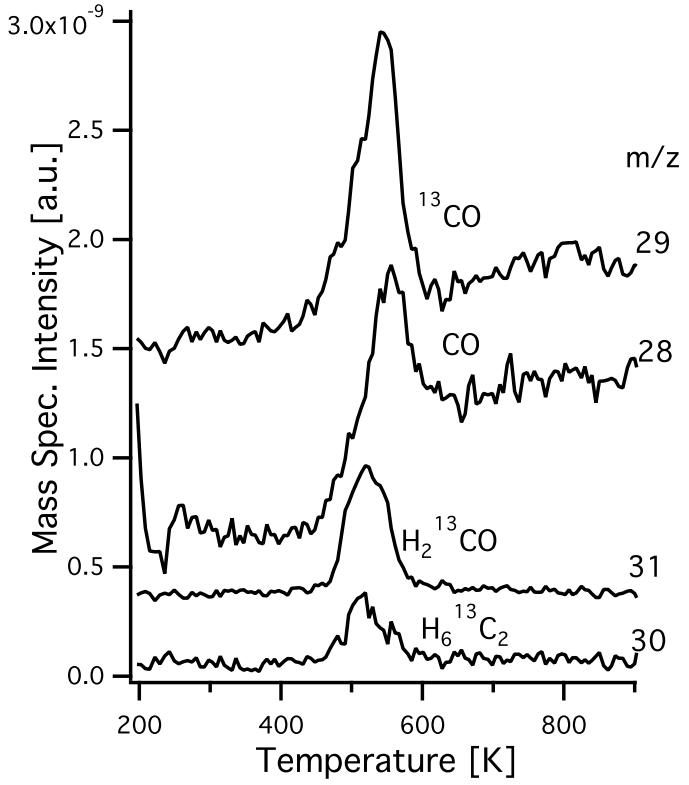

Figure E.3: Determination of the identity of m/z 28 using ^{13}C labeling on the methyl of the acetate. Excess ^{13}C acetic acid was reacted on an initial oxygen coverage of 0.2 ML O/Au(111), resulting in the characteristic clean-surface reactivity of acetate. Fragment contributions from other products (including formaldehyde) are subtracted from m/z 28, 29, and 30.

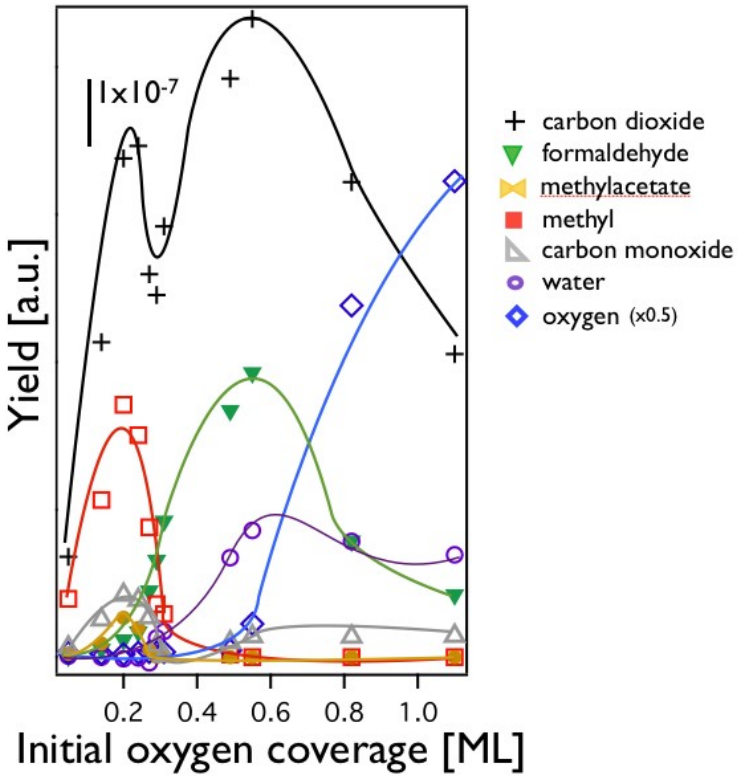

Figure E.4: The relative yield, as calculated using the MATLAB code for quantitative mass spectroscopy, for each product as a function of initial oxygen coverage.

Initial Oxygen Coverage ML	Dominant Reaction Temperature (K)	Co-adsorbed oxygen	Total acetate coverage	Total O coverage (acetate x 2 + O)
0.05-0.24	530	None	0.10-0.4 ML	0.20-0.8
0.27	440, 530	0.12 ML	0.30 ML	0.7
0.29	440, 530	0.16 ML	0.25 ML	0.7
0.31	440, 530	0.16 ML	0.30 ML	0.8
0.49	400	0.28 ML	0.41 ML	1.1
0.55-1.1	400, excess O	0.30-0.69 ML	0.45 ML- 0.19 ML	1.2-1.1

Table E.2: Comparing acetate coverage to reaction pathway.

by: 2 × acetate coverage + oxygen coverage (Table E.2). It was determined that there are three different saturation states for the acetate/oxygen system on gold: saturation of acetate itself (~0.8 ML), saturation of acetate + $O_{(a)}$(~0.8 ML) and a further saturation of acetate + $O_{(a)}$ (~1.1 ML), at which point closer packing or a shift in acetate binding may account for the greater coverage. Here, a monolayer is defined one oxygen atom per surface atom.

In order to calculate the relative yields for the products, overlapping fragments from different molecules must first be deconvoluted, usually by manual subtraction, before assessing the total amount of the product by taking the area of the TPRS peak. A MATLAB code, discussed in Appendix D, was developed to deconvolute the mass fragmentations and calculate the relative contributions for each product. For this study, both manual and automated calculations were done for deconvolution of several representative experiments and the relative contributions of fragments were within tolerable error (1-5%) between the two methods.

In the quantitative analysis, which has been written about elsewhere [26], the fragmentation pattern of each molecule, the transmission and detection coefficients in the mass spectrometer, as well as its ionization cross-section is taken into consideration. The constants used for this analysis are listed in Table E.2 and E.3 and have been adapted from previous studies [26, 226]. Here, the "total correction factor", TCF_k, is calculated as follows:

$$TCF_k = \frac{1}{T_k D_k} \frac{\epsilon}{\sigma}, \tag{E.1}$$

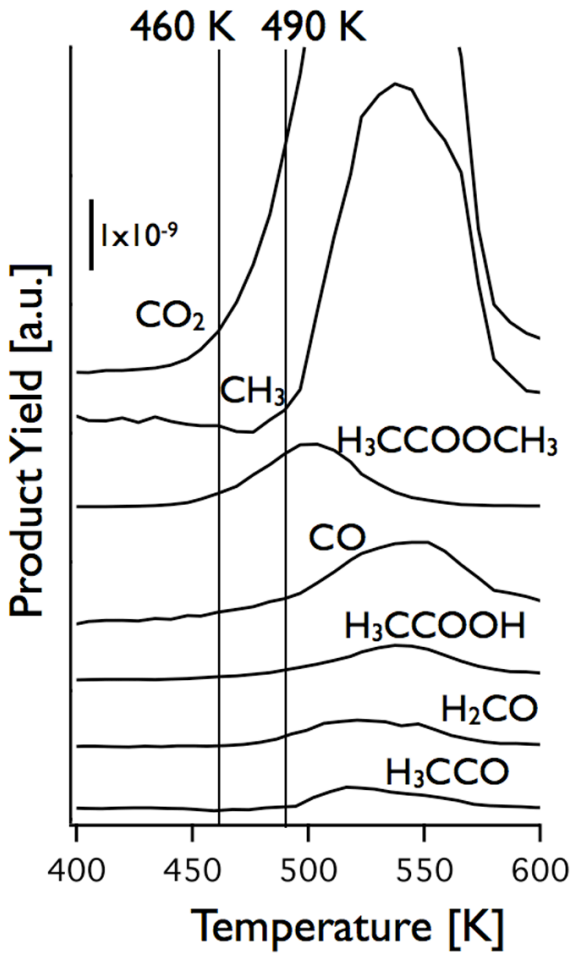

Figure E.5: Detailed illustration of the leading edges from the desorption traces in the high temperature, oxygen-free pathway on an initial oxygen coverage of 0.2 ML O taken from Fig. 3.2b. The order of appearance of the products during temperature programmed reaction aids in determining the reaction mechanism. For details, see main text.

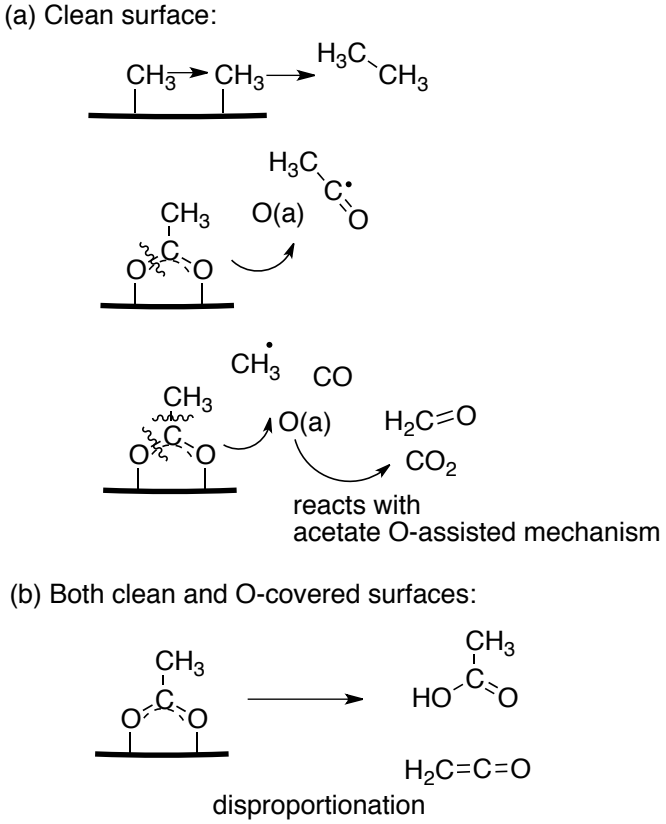

Figure E.6: Reaction mechanisms for minor products of acetate on Au(111). For disscussion see main text.

m/z	Transmission Coefficient	Detection Coefficient
0-20	1	1.5
21-30	1	1
31-40	1	0.9
41-50	1	0.8
51-60	1	0.7
61-70	1	0.65
71-80	0.98	0.6

Table E.3: Transmission Coefficient (adapted from Hiden Manual) and Detection Coefficent (adapted from UTI Manual) for given mass fragments. Adapted from [26].

where T_k and D_k are the transmission and detection coefficients for the signature mass, s_k; σ is the ionization cross section for the molecule; and ϵ is the correction for the total ion current,

$$\epsilon = \frac{s_k}{T_k D_k} \sum_{j \neq k} \frac{s_j}{T_j D_j}. \tag{E.2}$$

Here s_j, T_j, and D_j are the signals, transmission coefficients and detection coefficients for all masses other than the signature mass for the molecule. The TCF_k can then simply be multiplied by the area of the TPRS peak for the signature mass, k, (after contributions from other molecules have been subtracted) to get the relative yield of a given molecule. It should be noted that the TCF will change depending on the signature mass used.

A factor of 3.2 is applied to the total correction factor for methyl detection (originally 0.365), which is broken down as follows: additional factor of 0.7 for production of methane, which is attributed to methyl picking up hydrogen in the background, and a factor of 2.5 for detection inefficiency due to radical reaction on the mass spectrometer shroud walls. The methane factor was calculated using the peak ratios for m/z 14, 15, and 16 from an experiment at 0.2 ML with no coadsorbed oxygen. The factor of 2.5 was calculated using the isotopic distribution for the 0.2 ML,

Product	Ionization cross-section	Signature Mass	Total Correction Factor
CO_2	3.521[b]	44	0.405
H_2CO	4.14[b]	30	0.78
CH_3[a]	3.098[b]	15	1.168
$H_3CCOOCH_3$	10.4[c]	74	3.08
CO	2.5[b]	28	0.429
H_2CCO	7.25[c]	42	0.297
H_3CCOOH	7.68[c]	60	1.99
C_2H_6	6.42[b]	27	1.136
H_3CCO	7.25[c]	43	0.297
H_2O	2.275[b]	18	0.352
Excess O_2	2.441[b]	32	0.471

Table E.4: Ionization cross-sections and calculated Total Correction Factor for each product. (a) An enhancement factor of 3.2 is applied for methyl radical detection, detailed in the following paragraph. (b) Values taken from the NIST database, calculated at an incident electron voltage of 70 eV. (c) Adapted from [226].

no coadsorbed oxygen ^{13}C data, to maintain the 1:1 stoichiometry of the ^{12}C and the ^{13}C. Given that radicals are notoriously difficult to detect and more easily trapped on the walls of the mass spectrometer shroud, we believe that this multiplication factor is reasonable.

E.3 Supporting Material for Chapter 4

The ultra high vacuum chamber was outfitted with a mass spectrometer (Hiden, HAL301) for the detection of products of temperature-programmed reaction, Auger electron spectroscopy (AES) to verify the cleanliness of the surface, and low-energy electron diffraction (LEED) for determining the surface order. The Au(111) crystal was mounted on a manipulator capable of heating to 1000 K and of cooling (via liquid nitrogen) to 100 K, as measured by a thermocouple inserted into a pinhole in the side of the Au crystal.

The gold surface was cleaned by argon ion bombardment followed by cycles of ozone dosing at 200 K and flash annealing to 900 K to remove surface impurities (as judged by CO and CO_2 production from adsorbed C and NO from nitrogen). Surface cleanliness was also confirmed by AES and observation of the satellite structure due to the herringbone reconstruction with LEED [227].

The purities of the organic compounds employed were established after freeze-pump-thaw cycles by measuring the fragmentation patterns obtained from sublimation after condensation at 140 K. In all cases, the fragmentation patterns were in good agreement with those reported in the NIST database. Furthermore, we found that the traces for all fragments could be superimposed after scaling, indicative of the purity of the compound.

Control of dosing for reactants

Control of reactant dose was performed by adjustment of the dosing time, usually at very low or undetectable background pressures. Careful control experiments were performed to ensure reproducibility of the dose of each reactant. An example of the degree of control achieved is presented in Fig. E.7, for different coverages of acetylene.

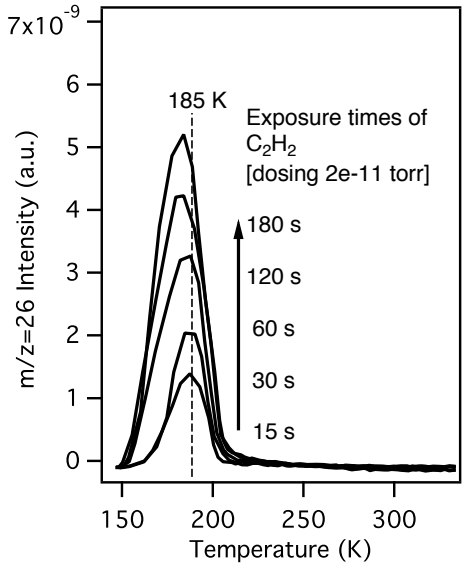

Figure E.7: Control of acetylene dose by changing the time of dosing for a low background pressure of 2×10^{-11} torr.

Mass	CO_2	H_2CO	CH_3	$H_3CCOOCH_3$	CO^*	H_2CCO	H_3CCOOH	C_2H_6	H_3CCO	H_2O^*	O_2
12	0.04										
13			0.09				0.13				
14			0.30	0.10		1	0.34				
15			1	0.60			0.78				
16	0.12			0.011	0.02		0.28				0.06
17										0.20	
18				0.012			0.77			1	
26								0.16			
27				0.006				0.25			
28	0.07	0.62		0.12	1		0.41	1			
29		1		0.09			0.12	0.23			
30		0.85		0.03				0.19			
31				0.03			0.02				
32											1
41				0.011			0.04				
42				0.10		0.65	0.16				
43				1			0.68		1		
44	1			0.04			1				
45				0.008			0.39				
59				0.04							
60							0.36				
61							0.04				
74				0.08							
75				0.003							

Table E.5: Fragmentation patterns for each product, normalized to the fragment of highest intensity for each molecule. Asterisk indicates values taken from NIST; otherwise all values were taken from a neat sample.

Isolation of B_{ads}

The isolation of B_{ads} was verified by running a control experiment in which BH was dosed at 140 K, the surface was annealed to ~200 K to desorb water and molecular BH. Then the surface was cooled back to 140 K, after which TPRS was used to verify the presence of B_{ads} on the surface by monitoring the reaction products. For example, this process is shown explicitly for trifluoro acetate in Fig. E.8. For all cases in which the isolation of B_{ads} was used (as opposed to the competitive co-adsorption experiments), the experiments of isolated B_{ads} are shown in the figures. Another confirmation of isolated B_{ads} is that B_{ads} can be titrated off by the B'_{ads} that is displacing it, forming the original BH, as shown in several of the displacement reaction experiments.

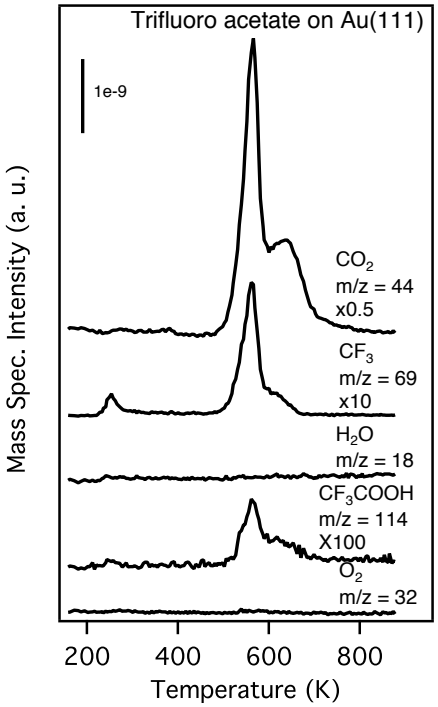

Figure E.8: The isolated intermediate trifluoro acetate was formed by dosing trifluoro acetic acid on 0.05 ML.

Competitive adsorption of methanol and acetylene

The competition between methanol and acetylene was used to demonstrate the fact that -CH acids fall into place with the -OH acids in terms of how their stability on the surface correlates with their gas phase acidity. In the case of methanol and acetylene, when acetylide was isolated on the surface and methanol was introduce, no displacement was observed, as the signature products of methoxy, formaldehyde and methyl formate, were not observed. Additionally, methanol and acetylene were dosed sequentially on 0.05 ML O/Au(111) in a competitive adsorption experiment, and again, no products indicative of methoxy were observed. This demonstrates the stronger binding of acetylene.

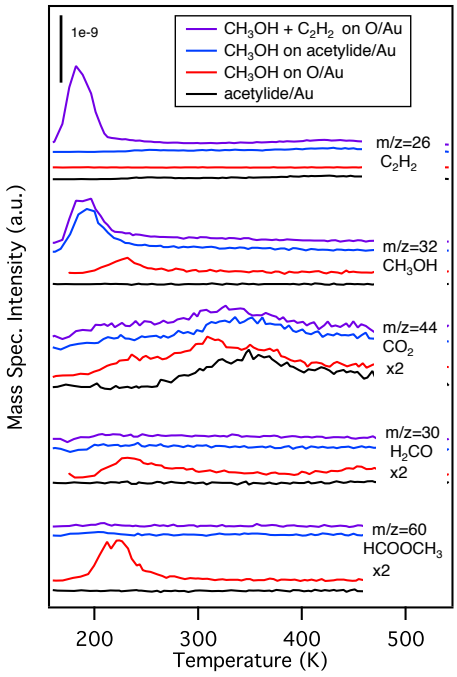

Figure E.9: Competitive adsorption of methanol and acetylene. In separate experiments, methanol and acetylene were dosed (1 ML) on 0.05 ML O/Au(111) at 140 K to establish their reactivity (red, black respectively). Then methanol was introduced on isolated acetylide/Au(111) at 140 K (blue), and methanol and acetylene were co-dosed (0.5 ML each) on 0.05 ML O/Au(111) at 140 K (purple).

Experimental results for the stability hierarchy presented in Fig. 4.6

The crucial experiments used to establish the order of surface intermediate stabilities are listed below, in the same order as presented in Fig. 4.6. The data and experimental details or references to previous work are provided for all experiments not presented in the paper.

Butanoic acid + Trifluoro acetic acid

In the competition experiments between butanoic acid and trifluoro acetic acid, the product distribution is indicative of a greater amount of butanoate on the surface, as evidenced by formation of propene and the CO_2 temperature, as well as only a minor amount of CF_3. Therefore, butanoic acid binds more strongly than trifluoro acetic acid.

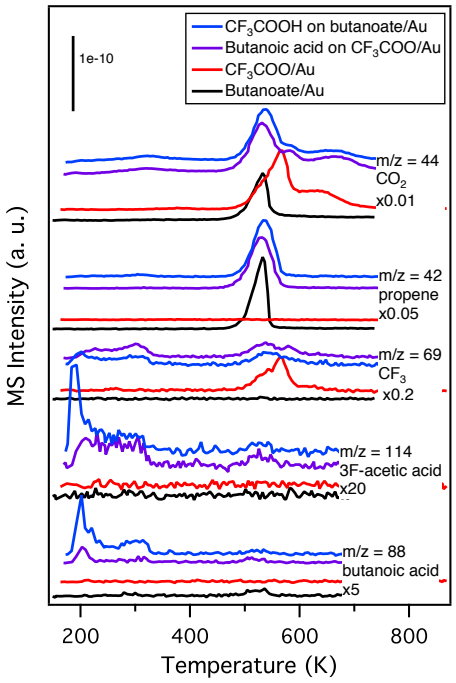

Figure E.10: In separate experiments, trifluoro acetic acid and butanoic acid were dosed (1 ML) on 0.05 ML O/Au(111) at 140 K to establish their reactivity (red, black respectively). Then trifluoro acetic acid was introduced on isolated butanoate/Au(111) at 140 K (blue), and butanoic acid was introduced co-dosed (0.5 ML each) on 0.05 ML O/Au(111) at 140 K (purple).

Trifluoro acetic acid + acetic acid

In the competition experiments between acetic acid and trifluoro acetic acid, the product distribution is indicative of a greater amount of trifluoro acetate on the surface, as evidenced by CO_2 and CF_3. In particular, the amount of CF_3 is only slightly diminished in the competition experiments, indicating that almost all of the trifluoro acetate remained, or displaced almost all of the acetate on the surface. Therefore, trifluoro acetic acid binds more strongly than acetic acid. This confirms the general effect of fluorine substitution increasing the acidity.

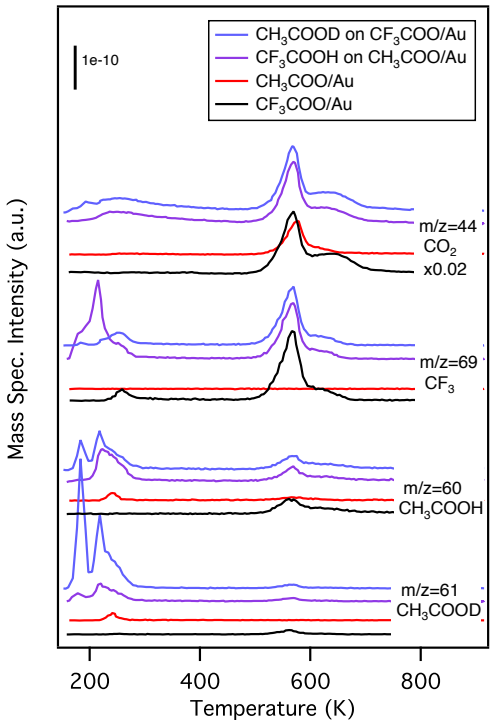

Figure E.11: In separate experiments, acetic acid and trifluoro acetic acid were dosed (1 ML) on 0.05 ML O/Au(111) at 140 K to establish their reactivity (red, black respectively). Then acetic acid (CH_3COOD) was introduced on isolated trifluoro acetetate/Au(111) at 140 K (blue), and trifluoro acetic acid was introduced on isolated acetate/Au(111) at 140 K (purple).

Acetic acid + formic acid

In the competition experiments between acetic acid and formic acetic acid, the product distribution reveals an equilibrium between the carboxylates, which strongly favors acetate. This is portrayed most clearly by the temperature of the CO_2 production, which is 580 K for acetate and 300 K for formate. Although acetic acid can completely displace formate on the surface, an excess of formate only displaces part of the acetate on the surface. This effect is explored more in the main text of the paper.

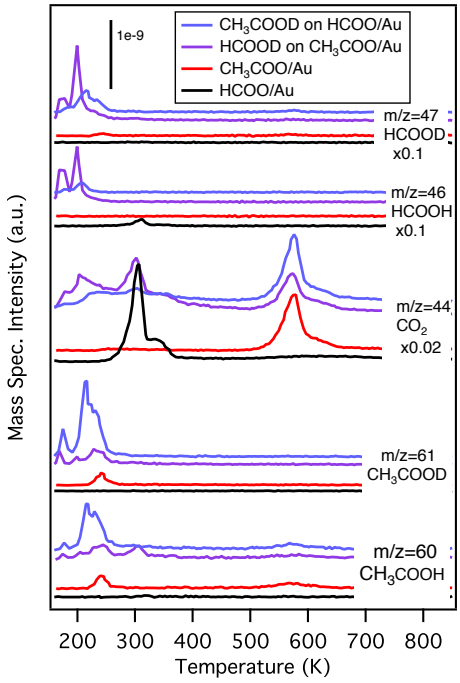

Figure E.12: In separate experiments, acetic acid and formic acid were dosed (1 ML) on 0.05 ML O/Au(111) at 140 K to establish their reactivity (red, black respectively). Then acetic acid (CH_3COOD) was introduced on isolated formate/Au(111) at 140 K (blue), and formic acid (HCOOD) was introduced on isolated acetate/Au(111) at 140 K (purple).

Formic acid + benzyl alcohol

In the competition experiments between benzyl alcohol and formic acetic acid, the product distribution reveals an equilibrium between the intermediates, in which they have comparable acidities. The presence of remaining formate is clear from the CO_2 production, and the presence of remaining benzyloxy is clear from production of benzyl alcohol, as well as the post oxidation CO_2. In the post oxidation experiments, ozone is dosed after the reaction at 200 K in order to clean the surface. While formic acid reacts cleanly on O/Au(111), so no CO_2 is formed in post oxidation experiments, there is some decomposition of the benzyloxy, resulting in surface carbon. The amount of CO_2 generated in the post oxidation experiments of the competition between benzyl alcohol and formic acid is slightly lower than the CO_2 for post oxidation of only benzyl alcohol.

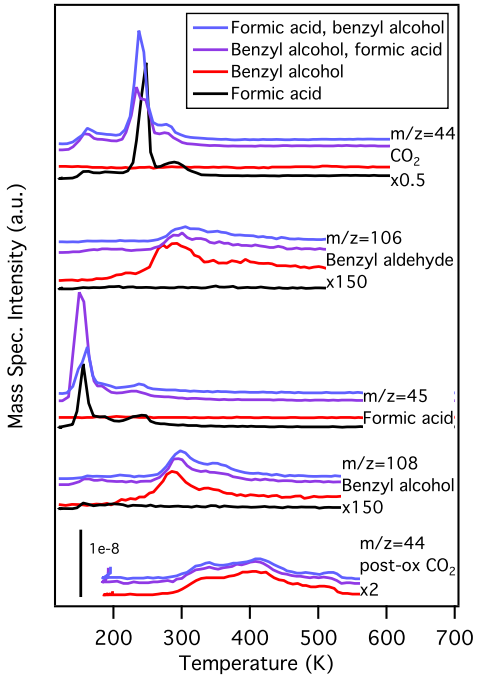

Figure E.13: In separate experiments, benzyl alcohol and formic acid were dosed (~1 ML) on 0.1 ML O/Au(111) at 150 K to establish their reactivity (red, black respectively). Then benzyl alcohol and formic acid were used in competitive adsorption experiments, in which they were sequentially dosed (~1 ML each) on 0.1 ML O/Au(111) at 150 K: formic acid before benzyl alcohol (blue), and benzyl alcohol before formic acid (purple).

Benzyl alcohol + 1-butanol

In the competition experiments between benzyl alcohol and 1-butanol, the product distribution reveals that benzyl alcohol binds more strongly. This is shown firstly by the m/z=106, benzyl aldehyde, is formed in both of the co-adsorption experiments. The clearest evidence, however, is the absence of the 1-butanol signature product, butylbutyrate. The small m/z=89 signal in the co-adsorption experiments can be accounted for by fragmentation of the benzyl alcohol. As seen in the benzyl alcohol oxidation experiment, some m/z=89 is present and matches the peak shape of the benzyl alcohol. Additionally, the carbon deposition see in benzyloxy decomposition is clearly present in the post oxidation experiments. See Fig. E.13 for the control post oxidation of benzyloxy.

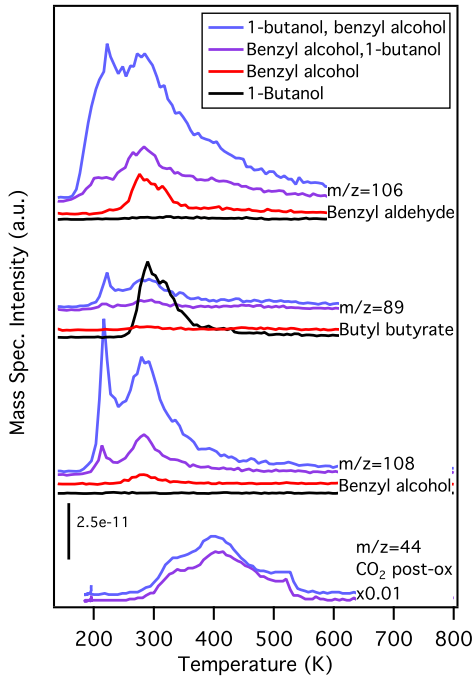

Figure E.14: In separate experiments, benzyl alcohol and 1-butanol were dosed (~1 ML) on 0.1 ML O/Au(111) at 150 K to establish their reactivity (red, black respectively). Then benzyl alcohol and 1-butanol were used in competitive adsorption experiments, in which they were sequentially dosed (~1 ML each) on 0.1 ML O/Au(111) at 150 K: 1-butanol before benzyl alcohol (blue), and benzyl alcohol before 1-butanol (purple).

1-butanol + formic acid

In the competition experiments between formic acid and 1-butanol, the product distribution formic acid binds more strongly, although there is an equilibrium in which a small amount of butoxy stays on the surface. This is evidenced by the formation of a small amount of butanal. However, the more prominent butoxy product, butylbutyrate (measured here by major fragment m/z=71) is not produced in the competition experiments. The amount of CO_2 formed from formate, while diminished in total area, is the dominant product. This indicates that formic acid displaces butoxy to form formate on the surface.

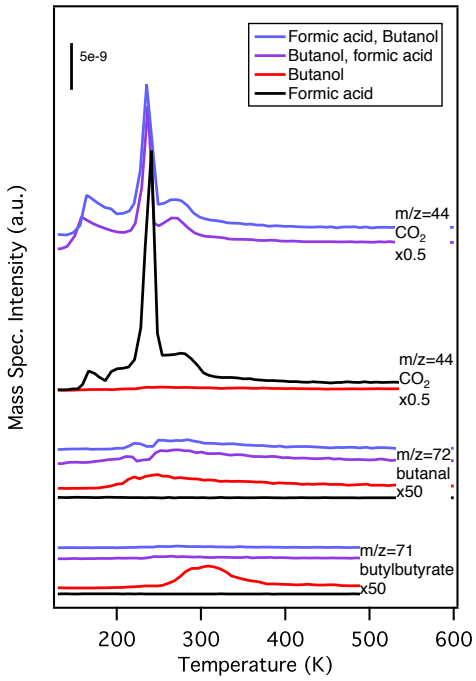

Figure E.15: In separate experiments, 1-butanol and formic acid were dosed (~1 ML) on 0.1 ML O/Au(111) at 130 K to establish their reactivity (red, black respectively). Then formic acid and 1-butanol were used in competitive adsorption experiments, in which they were sequentially dosed (~1 ML each) on 0.1 ML O/Au(111) at 100 K: formic acid before butanol (blue), and butanol before formic acid (purple). The lower temperature was used to ensure that 1-butanol did not have a chance to react to form the butylbutyrate ester before the formic acid was dosed.

1-butanol + ethanol

In the co-adsorption experiment between ethanol and 1-butanol, an excess of the alcohols was used to ensure that both alcohols had an adequate reservoir on the surface. These can be seen in the m/z=46 and m/z=56 traces. In this slightly different experimental design, the more strongly bound intermediate will yield quantitatively more products than the other, compared to their concentration in the reactant mixture. For this experiment, a prior condensation experiment was performed showing that there was more ethanol (~70%) than butanol (~30%) in the mixture. However, the products from butanol are found in greater yield: butylbutyrate from butanol self-coupling and butanal. There is a small amount of ethyl acetate from ethanol self-coupling, although there is error due to the need for subtraction of m/z=70 contribution from 1-butanol fragmentation. Additionally, there is a small amount of the cross-coupling product, ethylbutyrate. In all, butoxy dominates the product yield, showing that it is more strongly bound than ethoxy. The conclusion that butanol would displace ethoxy can also be drawn from prior work which shows that butanol displaces methoxy more efficiently than ethanol does [26].

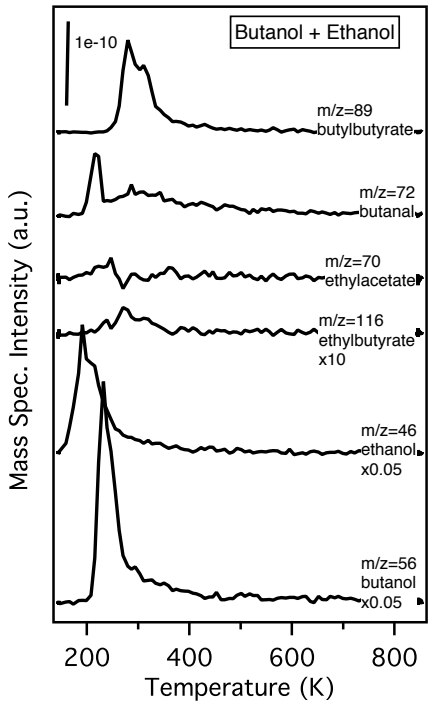

Figure E.16: Ethanol and 1-butanol were co-dosed from a mixture of the alcohols onto 0.1 ML O/Au(111) at 150 K. Analysis of the relative product yields shows that 1-butoxy is bound more strongly than ethoxy. The contributions to masses shown here from other product fragments have been subtracted for clarity.

Trifluoro ethanol + ethanol

To compare the displacement between trifluoro ethanol and ethanol, we look at the signature products of each alkoxy, which are the self-coupling products, F_3-ethyl F_3-acetate and ethylacetate, respectively. A small amount of the aldehyde from each alcohol was also formed (not shown). In the competitive adsorption experiment between trifluoro ethanol and ethanol, there is no self-coupling of the trifluoro ethanol, and there is a large amount of ethylacetate formed. This shows that ethoxy binds more strongly than trifluoro ethoxy on the surface. Interestingly, this does not correspond with the relative gas phase acidities where the fluorine substitution dominates. A very minor amount of cross-coupling may have also occurred, but was difficult to deconvolute from the fragments of the aldehydes and therefore is not shown.

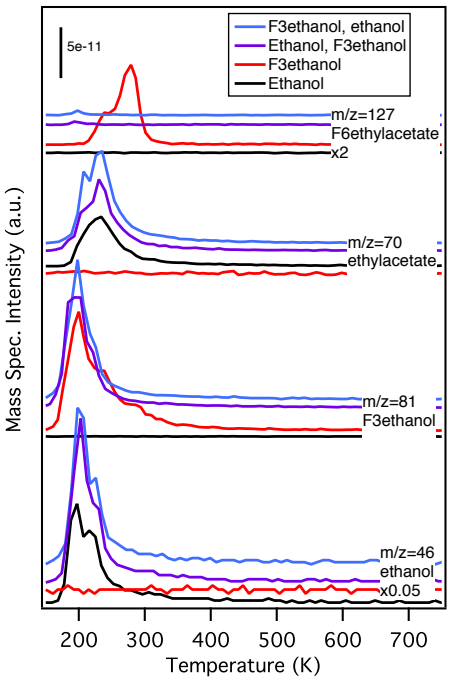

Figure E.17: In separate experiments, trifluoro ethanol and ethanol were dosed (~1 ML) on 0.1 ML O/Au(111) at 150 K to establish their reactivity (red, black respectively). Then trifluoro ethanol and ethanol were used in competitive adsorption experiments, in which they were sequentially dosed (~1 ML each) on 0.1 ML O/Au(111) at 150 K: trifluoro ethanol before ethanol (blue), and ethanol before trifluoro ethanol (purple). Fragment contributions from molecules other than the ones indicated for each mass are subtracted for clarity.

Trifluoro ethanol + 1-butanol

In the competition experiments between trifluoro ethanol and butanol, the signature product from butanol oxidation, butylbutyrate (m/z=89) is the dominant one. While there is a slight amount of cross-coupling to form trifluoro ethyl butyrate, almost no self-coupling of the trifuloro ethanol takes place. This shows that butanol binds more strongly than trifluoro ethanol.

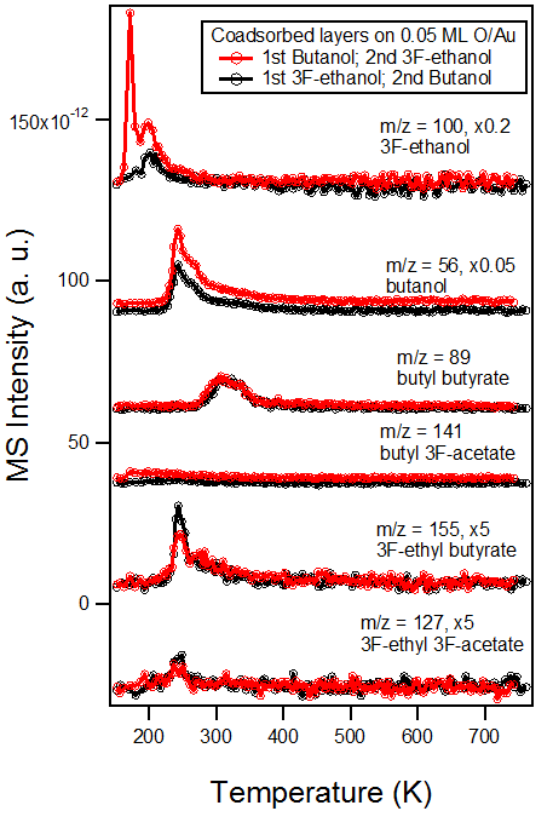

Figure E.18: In two co-adsorption experiments, trifluoro ethanol and butanol were dosed (~0.5 ML each) on 0.05 ML O/Au(111) at 140 K. They were sequentially dosed: butanol before trifluoro ethanol (red), and trifluoro ethanol before butanol (black). The control experiments for each reactant can be seen above in Figs. E.17, E.15, and E.14.

Acetylene + methanol

Shown above in Fig. E.9.

Ethanol + methanol

This was established by Xu et al [26]. Ethanol displaces methanol in cross-coupling experiments, in which the alcohols are simultaneously dosed from a mixture. This is like the competitive co-adsorption experiments in this study. The equilibrium constant between ethanol and methanol is ~5.

E.3.1 Structural changes due to van der Waals interactions

Methanol

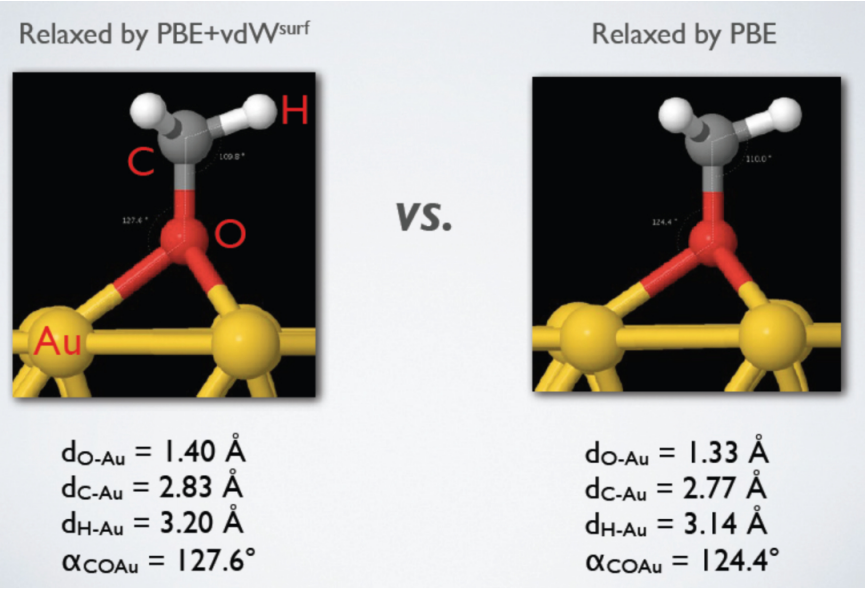

Figure E.19: Binding structure for methanol when relaxed by PBE+vdWsurf vs. PBE alone. The van der Waals forces only slightly change the adsorption structure.

1-butanol

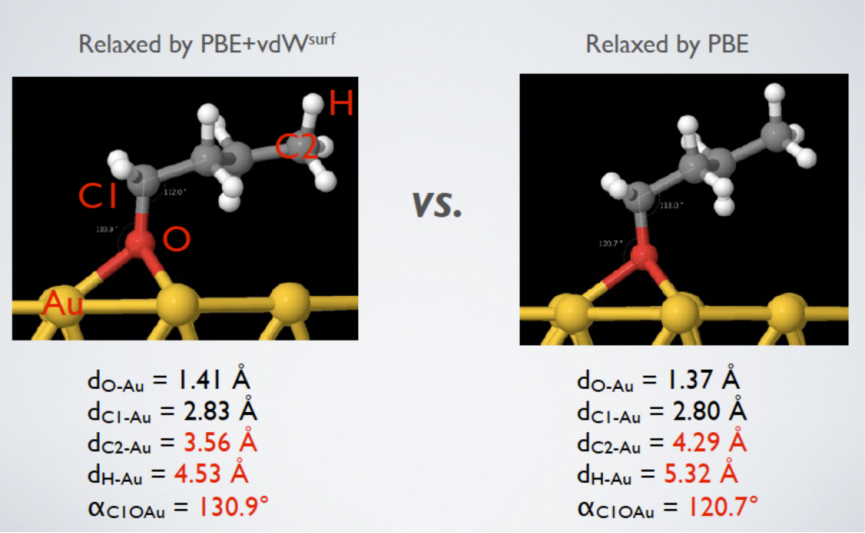

Figure E.20: Binding structure for 1-butanol when relaxed by PBE+vdWsurf vs. PBE alone. The van der Waals forces significantly alter the adsorption structure.

Trifluoro ethanol

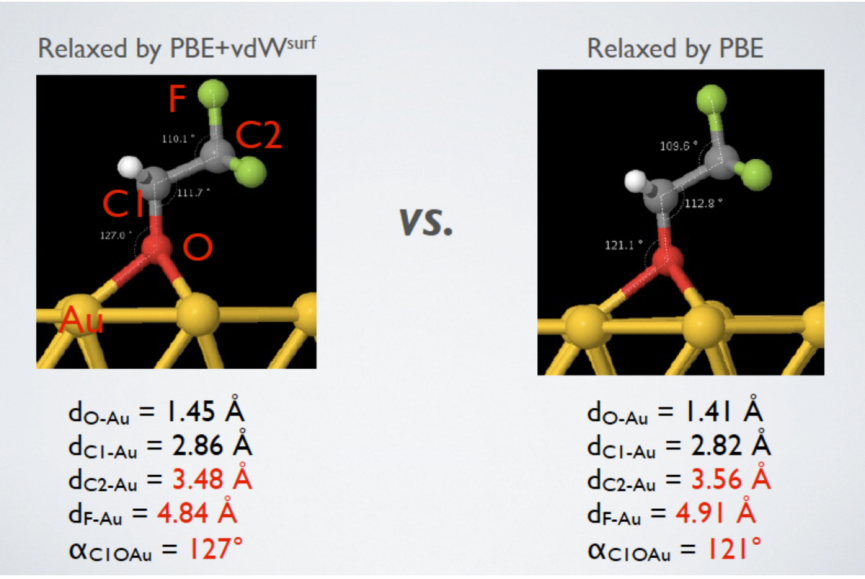

Figure E.21

E.3.2 Analysis of energetics

Relation of ΔH of dissociative adsorption (ΔH_{da}) to displacement

$$\Delta \mathrm{H}_{da} \equiv \Delta \mathrm{H} \text{ for } \mathrm{BH}_{(g)} \longrightarrow \mathrm{B}_{(a)} + \mathrm{H}_{(a)} \tag{E.3}$$

Consider $\mathrm{B'H}_{(g)}$ and $\mathrm{BH}_{(g)}$.

$$\Delta \mathrm{H}'_{da}\text{: } \mathrm{B'H}_{(g)} \longrightarrow \mathrm{B}'_{(a)} + \mathrm{H}_{(a)} \tag{E.4}$$

$$\Delta \mathrm{H}_{da}\text{: } \mathrm{BH}_{(g)} \longrightarrow \mathrm{B}_{(a)} + \mathrm{H}_{(a)} \tag{E.5}$$

Combining reactions E.4 and E.5 yields

$$\Delta \mathrm{H}'_{da} - \Delta \mathrm{H}_{da}\text{: } \mathrm{B'H}_{(g)} + \mathrm{B}_{(a)} \longrightarrow \mathrm{BH}_{(g)} + \mathrm{B}'_{(a)}\,. \tag{E.6}$$

If $\Delta \mathrm{H}'_{da}$ is more negative than $\Delta \mathrm{H}_{da}$, then B′H displaces $\mathrm{B}_{(a)}$. Therefore, displacement directly measures the relative magnitudes of $\Delta \mathrm{H}_{da}$, provided that ΔS is negligible or negative (i.e., $\mathrm{B'H}_{(g)}$ is molecularly more complex (larger) than $\mathrm{BH}_{(g)}$).

Relationship of displacement to the relative binding energies of $B_{(a)}$ and $B'_{(a)}$

Definitions:

D_0, the homolytic bond dissociation energy:

$$\mathrm{D}_0 \equiv \Delta \mathrm{H} \text{ for } \mathrm{BH}_{(g)} \longrightarrow \mathrm{B}_{(g)} + \mathrm{H}_{(g)} \tag{E.7}$$

Heats of adsorption:

$$\Delta \mathrm{H}_{ads} \equiv \Delta \mathrm{H} \text{ for } \mathrm{B}_{(g)} \longrightarrow \mathrm{B}_{(a)} \tag{E.8}$$

$$\Delta \mathrm{H}_{Hads} \equiv \Delta \mathrm{H} \text{ for } \mathrm{H}_{(g)} \longrightarrow \mathrm{H}_{(a)} \tag{E.9}$$

Then for

$$\mathrm{B'H}_{(g)} \longrightarrow \mathrm{B}'_{(a)} + \mathrm{H}_{(a)},\ \Delta \mathrm{H} = \mathrm{D}'_0 + \Delta \mathrm{H}'_{ads} + \Delta \mathrm{H}_{Hads}, \tag{E.10}$$

$$\mathrm{BH}_{(g)} \longrightarrow \mathrm{B}_{(a)} + \mathrm{H}_{(a)},\ \Delta \mathrm{H} = \mathrm{D}_0 + \Delta \mathrm{H}_{ads} + \Delta \mathrm{H}_{Hads}. \tag{E.11}$$

Combining Reactions E.10 and E.11 yields

$$\mathrm{B'H}_{(g)} + \mathrm{B}_{(a)} \longrightarrow \mathrm{BH}_{(g)} + \mathrm{B}'_{(a)}, \tag{E.12}$$

$$\Delta H=(D_0'-D_0)+(\Delta H_{ads}'-\Delta H_{ads})\equiv\Delta. \tag{E.13}$$

If B′H displaces $B_{(a)}$, then $\Delta<0$. If $D_0'\geq D_0$, then $\Delta H_{ads}'<\Delta H_{ads}$ (i.e., adsorption of $B_{(g)}'$ is more exothermic than that of $B_{(g)}$). More generally, if B′H displaces $B_{(a)}$, then

$$\Delta H_{ads}'-\Delta H_{ads}<D_0-D_0' \tag{E.14}$$

$$\Delta H_{ads}'<D_0-D_0'+\Delta H_{ads} \tag{E.15}$$

If $D_0-D_0'<0$, then

$$\Delta H_{ads}'-\Delta H_{ads}<0 \tag{E.16}$$

Conversely if $D_0-D_0'>0$, then all that can be said is

$$\Delta H_{ads}'<D_0-D_0'+\Delta H_{ads}. \tag{E.17}$$

$$\Delta H_{ads}'-\Delta H_{ads}<D_0-D_0' \tag{E.18}$$

$$\Delta H_{ads}'<D_0-D_0'+\Delta H_{ads} \tag{E.19}$$

Entropy discussion

Taking the equilibrium between two adsorbates,

$$B'H_{(g)}+B_{(a)}\longrightarrow BH_{(g)}+B_{(a)}' \tag{E.20}$$

The expression for the equilibrium constant is

$$K_{eq}=e^{-\Delta G/RT}=\frac{[BH_{(g)}][B_{(a)}']}{[B'H_{(g)}][B_{(a)}]} \tag{E.21}$$

Taking a simple case for illustration, if $[BH_{(g)}]=[B'H_{(g)}]$, then

$$K_{eq}=e^{-\Delta G/RT}=\frac{[B_{(a)}']}{[B_{(a)}]} \tag{E.22}$$

Since $\Delta G=\Delta H$ - $T\Delta S$,

$$K_{eq}=e^{-\Delta H/RT}e^{-\Delta S/R}, \tag{E.23}$$

$$\Delta H=(D_0'-D_0+(\Delta H_{ads}'-\Delta H_{ads}), \tag{E.24}$$

and

$$\Delta S = SBH_{(g)} - SB'H_{(g)} + SB'_{(a)} - SB_{(a)}, \tag{E.25}$$

where the first term of Eqn. E.25 is the contribution from the gas phase species, and the second is the contribution from the adsorbed species.

The entropies for the adsorbed species are molecular vibrations and the frustrated rotations and translations (vibrations) resulting from the localized binding of the species. The frustrated rotations contribute most to their entropy, since the 3 degrees of freedom resulting from the frustrated translations have relatively high vibrational frequencies.

The entropy difference of the gas phase species dominates ΔS due to the mass difference in the translational entropies and the difference in rotational moment of inertia. Furthermore, note that the first and second terms in Eqn. E.25 offset one another. If B′H is molecularly more complex and has higher entropy, the same will be true of $B'_{(a)}$ vs. $B_{(a)}$.

Lastly, note that the operative temperatures for the displacement process reported here are 150-200 K. Thus the contribution of $T\Delta S$ to ΔG will be small. However, we must remember that energetic differences due to vdW interactions are small as well.

Overall, it appears that if B′H is molecularly more complex than BH, then entropy cannot be driving the displacement of $B_{(a)}$ by $B'H_{(g)}$ or account for $B'_{(a)}$ being dominant in an equimolar mixture of $B'H_{(g)}$ and $BH_{(g)}$.

E.4 Supporting Material for Chapter 6

Temperature programmed reactions (TPR) on Ag(111) and Ag(110) were performed separately in two ultra-high vacuum (UHV) systems, both equipped with Pfeiffer quadrupole mass spectrometer (Prisma QMS 200), low energy electron diffraction (LEED) optics, and X-ray photoelectron spectroscope (XPS). The Ag(111) and (110) surfaces were cleaned by cycles of Ar^+ sputtering at room temperature followed by repeated exposures to NO_2 at 500 K to remove any impurities by oxidation and annealing in vacuum at 900 K for 5 min until no impurity was detected by XPS, and a sharp (1×1) LEED pattern was observed. The chemisorbed atomic oxygen on both surfaces was

prepared by dosing NO_2 (Matheson Tri-Gas, 99.5%) at 500 K to obtain the desired oxygen coverages. One monolayer (ML) is defined as one O atom per surface Ag atom. Dimethylamine (Sigma-Aldrich, 99%) and d_6-dimethylamine (Cambridge Isotope Laboratories, 99%) were dosed through a 5 mm diameter tube pointing to the sample positioned about 30 mm from the end of the tube. Formaldehyde (d_0- and d_2-) was dosed through a capillary doser via paraformaldehyde, in which the glass tube holding the sample was immersed in a hot-water bath, and the whole dosing system was heated to ~ 50 °C to achieve a higher vapor pressure in the gas line during dosing. During the TPR experiments, the samples were biased at -100 V in order to avoid possible electron-induced reactions. The reaction products were identified by quantitative mass spectrometry using fragmentation patterns obtained from authentic samples.

E.5 Supporting Material for Chapter 8

E.5.1 TPRS details

Temperature programmed reaction spectroscopy (TPRS) was performed using well-established procedures [100]. The identification of the coupling product, dimethylacetamide, was confirmed by measuring the fragmentation pattern of the neat products and comparing it to the patterns of the product formed during the reaction as well as the NIST database. The data in Table E.6 exemplifies the use of mass fragments to identify dimethylacetamide from the reaction of DMA and acetaldehyde on Ag.

Fragment subtraction was performed in order to see the product traces more clearly. In Figs. 8.1 and 8.2, the contribution of dimethylamine, acetaldehyde, and dimethylacetamide to the m/z=18 signal was subtracted for the reactions on both surfaces. The contributions to the m/z=44 fragment for the same molecules were subtracted in the Ag experiments in order to more clearly show the CO_2 formed. Contribution to the m/z=42 and 43 traces from dimethylacetamide, dimethylamine, and acetaldehyde were subtracted, which created a large error throughout the temperature range of the imine product, particularly in the silver data. Because the m/z=42 contributions were smaller

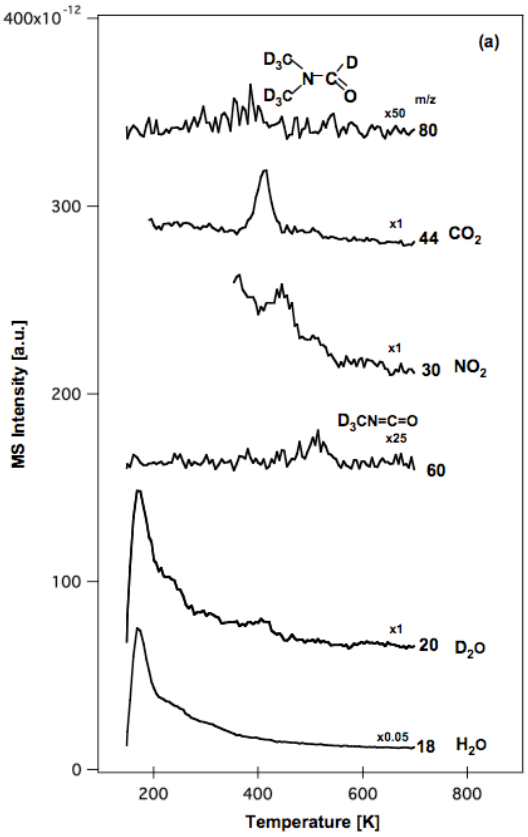

Figure E.22: Reaction of d_6-dimethylamine (DMA) with d_1-formate on O/Ag(111) at 140 K. d_1-Formate ($DCOO_{ads}$) was formed on the surface by reacting d_2-formaldehyde on a 0.4 ML O-covered Ag(111) at 140K and annealing to 325K for ten minutes to eliminate water and unreacted formaldehyde. By careful control of the dosage of formaldehyde, formate coadsorbed with atomic oxygen was achieved. This surface was then cooled to 140K and d_6-dimethylamine was dosed in order to induce formation of a mixture of coadsorbed $(CD_3)_2N$ and formate. With subsequent heating the coupling product, d_7-N,N-dimethylformamide ($(CD_3)_2NC(D)=O$, m/z 80) is not observed in significant quantity.

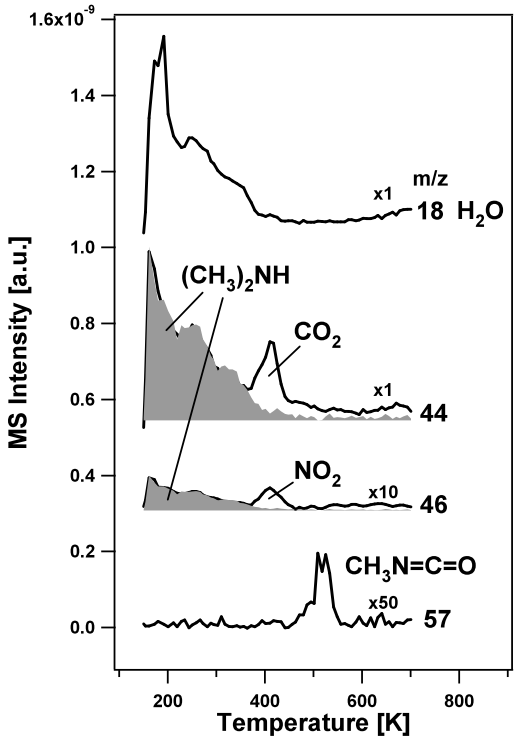

Figure E.23: Oxidation of dimethylamine on 0.1 ML O-covered Ag(110) at 150 K. In addition to H_2O, CO_2 and NO_2 are produced at 410 K, as well as a small amount of isocyanate is produced at 510 K. The shaded areas under m/z 44 and 46 spectra are attributed to the fragments of unreacted dimethylamine, according to its fragmentation pattern.

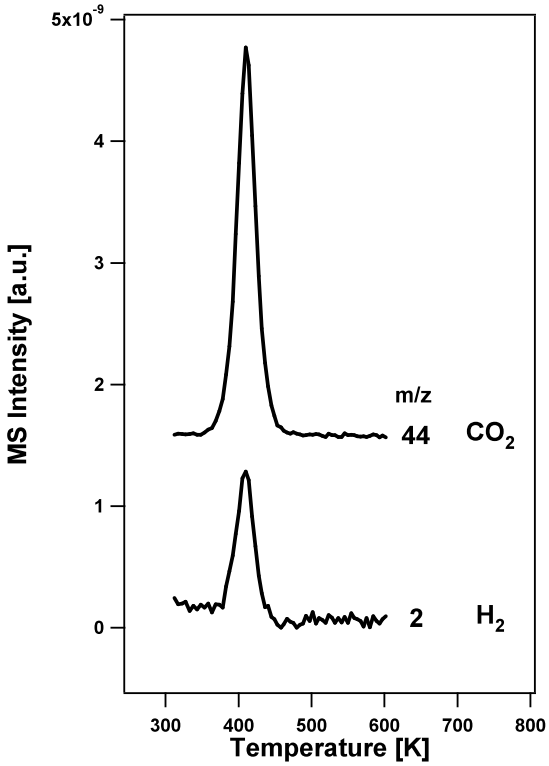

Figure E.24: Oxidation of formaldehyde on 0.1 ML O-covered Ag(110) at 300 K. CO_2 and H_2 are produced simultaneously at 410 K. Previous study has revealed that these products are formed via a formate intermediate [96].

m/z	Ag reaction	Ag neat	NIST
44	6.58	4.91	1.52
43	3.21	2.78	0.74
42	2.62	1.9	0.44
30	1.43	1.2	0.09
87	1	1	1
72	0.547	0.533	0.33
29	0.728	0.308	0.01

Table E.6: Dimethylacetamide product identification using mass spectral analysis. Signal intensities are normalized to the parent ion, m/z 87. The data in the second column are taken from a TPRS, subtracting the contribution from reactants. The data in the third column are taken from a neat sample of dimethlyacetamide adsorbed on a clean Ag(111) surface, then desorbed using TPD. The numbers here do not include correction for the transmission or detection efficiencies.

and therefore imparted less error, m/z 42 is used to measure the imine product on silver, whereas m/z 43, the parent ion, is used on gold.

In Fig. 8.1b, it is possible for the m/z=44 peak at 400 K to be N_2O instead of CO_2 (resulting from dimethylamine oxidation on silver). However, because the product was less than 10% of the amine oxidation on Ag, this matter was not studied in detail.

E.5.2 Isotope reactions on silver

Using oxygen coverage as low as 0.01 ML O/Ag(111) and d_6-dimethlyamine, it is possible to eliminate the secondary oxidation products of the amine, increasing the selectivity with respect to the amine to 100% (Fig. 8.2). However, at the extremely low oxygen coverage of 0.01 ML, the product evolved at approximately 285 K, which is about 35K higher than the product evolution at 0.1 ML oxygen coverage. As the oxygen coverage decreased from 0.08 ML to 0.01 ML, a second peak of the dimethylamide product formed, and at very low coverage, the product only evolved at the higher temperature peak (Fig. E.25a).

If the rate-limiting step were different for the 285 K product than the 250K product, the products associated with the rate-limiting step would shift as the high-temperature peak became dominant, and the kinetic isotope effect would be significantly different. However, the product distribution for hydrogen and water (which are derived from the rate-limiting step of surface-mediated H-elimination) is consistent and the kinetic isotope effect is observed across all oxygen coverages. The m/z=4, 19, and 20 (D_2, HDO, and D_2O) peak shifts were easier to observe than shifts in the peaks of m/z=2 and 18 (H_2 and H_2O), which have a much higher background signal. D_2, HDO, and D_2O formation concurrent with the dimethylacetamide is attributed to beta-hydride elimination from the hemiaminal. Clearly, the production of deuterium aligned with the peak of dimethylacetamide at all of these oxygen coverages, even portraying a doublet coinciding with the doublet product formation at 0.02 ML O (Fig. E.25b). Thus, the peak shift of dimethylacetamide on silver with decreasing oxygen coverage does not appear to be related to a change in mechanism, as the product distribution was consistent with coverage.

The isotope effect is observed at both extremes of the oxygen coverage, using d_4-actetaldehyde

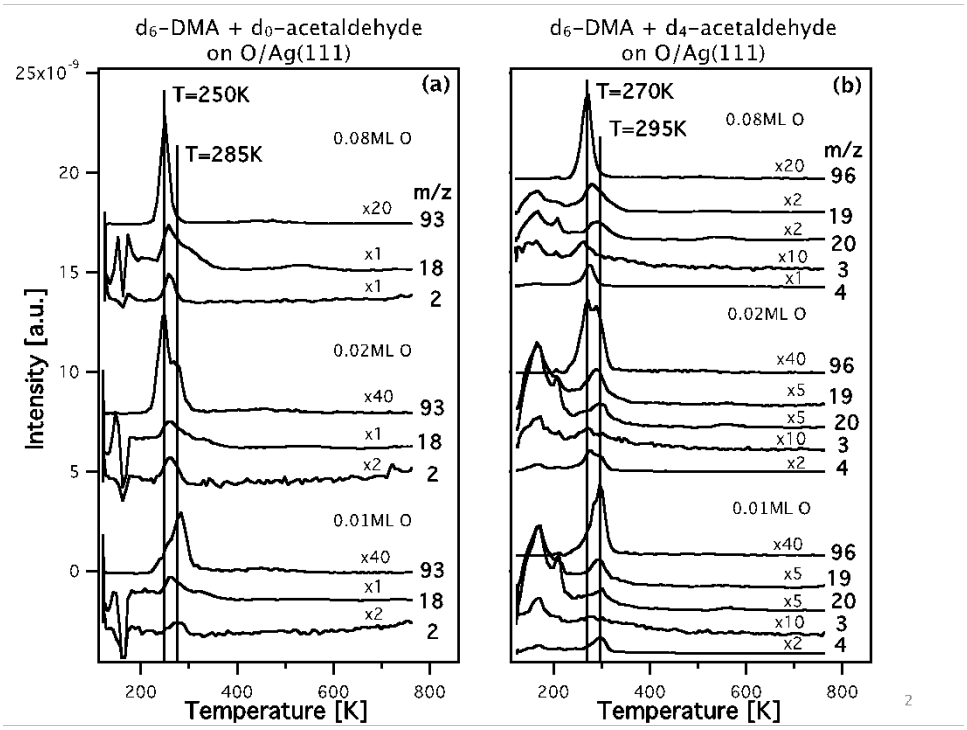

Figure E.25: (a) d_6-dimethylamine (1.5L) and d_0-acetaldehyde (1.5L) were dosed sequentially at 125K on O/Ag(111), varying the oxygen coverage. Low temperature oscillation in the m/z=18 spectra is caused by subtraction of the dimethylamine contribution. (b) d_6-dimethylamine (1.5L) and d_4-acetaldehyde (1.5L) were dosed sequentially at 125K on O/Ag(111), varying the oxygen coverage. M/z and molecule identity is as follows: (a) 93: d_6-dimethylacetamide, 18: H_2O, 2:H_2 (b) 96: d_9-dimethylacetamide, 19: HDO, 20: D_2O, 3: HD, 4: D_2.(1.5L) were dosed sequentially at 125K on O/Ag(111), varying the oxygen coverage. M/z and molecule identity is as follows: (a) 93: d_6-dimethylacetamide, 18: H_2O, 2:H_2 (b) 96: d_9-dimethylacetamide, 19: HDO, 20: D_2O, 3: HD, 4: D_2.

(Fig. E.25b). There was a 20 K kinetic isotope effect at 0.1 ML O/Ag(111) and a 10 K kinetic isotope effect at 0.01 ML O/Ag(111). This shift is not significant enough to invoke a different rate-limiting step.

Desorption of the neat product from silver at low coverages displayed a similar "double-peak" spectrum, moving to higher temperature at very low coverages (Fig. E.26). It should be noted that these desorption temperatures were still lower than the peak(s) observed for the dimethyacetamide formed by coupling reaction. Therefore, the product evolution was clearly reaction limited, supported by the persistence of the kinetic isotope effect. In the case of the neat product desorption as well as that of the coupling product, the higher temperature dimethylacetamide peak is attributed to surface defects.

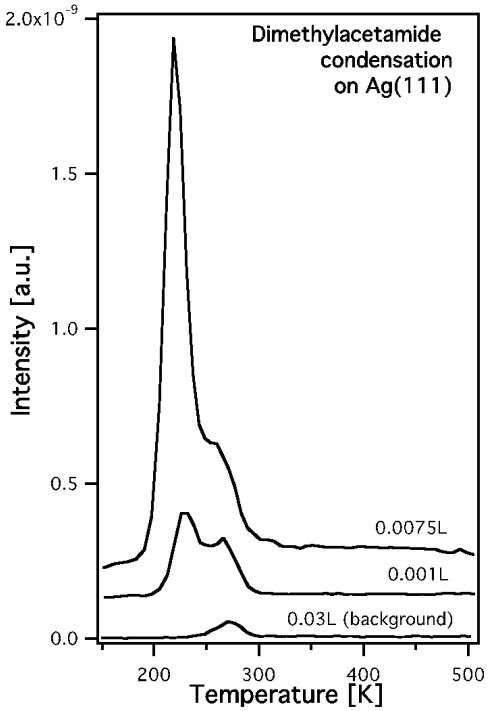

Figure E.26: Neat dimethylacetamide was condensed on clean Ag(111) at 150K with varying coverages. The desorption peak shifts from 220K at 7.5×10^{-2} L to 230K and 265K at 1×10^{-3} L to 270K using a 0.03L background dose. These doses do not account for direct dosing enhancement.

E.5.3 Dimethylacetamide desorption on gold

In order to clearly determine whether the production of dimethylamide is desorption limited on gold, as is suggested by the lack of a clear kinetic isotope effect (Fig. 8.3a), d_0-dimethylamine, and d_4-acetaldehyde and neat d_0-dimethylacetamide were co-adsorbed onto a surface with 0.05 ML O prior to the temperature programmed reaction. The desorption temperatures of the d_4-dimethylformamide formed in the coupling reaction and d_0-dimethylformamide introduced to the surface are identical to within experimental uncertainties (Fig. 8.3).

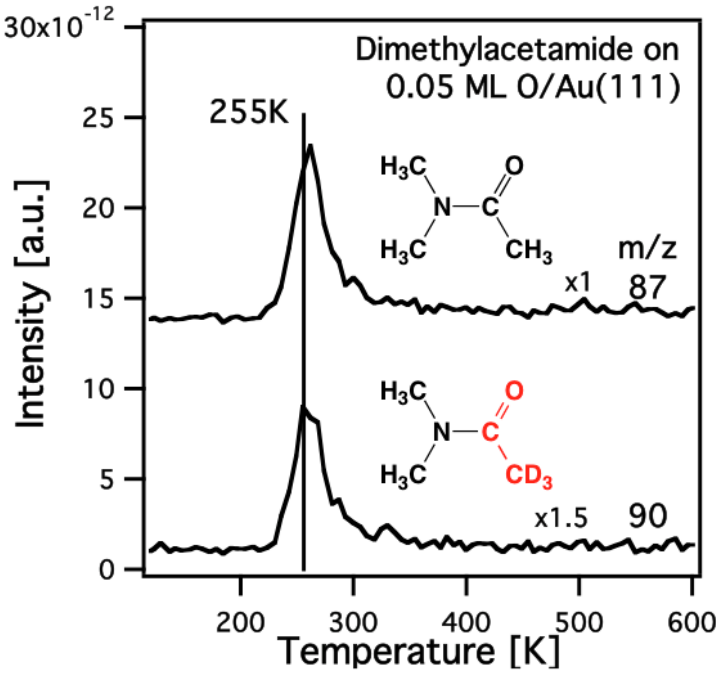

Figure E.27: (a) d_0-dimethylamine (1.5L) and d_4-acetaldehyde.(1.5L), followed by dimethylacetamide (neat product) were dosed sequentially at 120K on 0.05 ML O/Au(111).

In comparison to the temperature of evolution of dimethylformamide formed from coupling formaldehyde and dimethylamine (175 K) [69], the desorption temperature of the dimethylacetamide product from gold (250 K) was surprisingly high. However, when a smaller coverage of dimethlyformamide was produced, the temperature shifted higher, up to 250. For both dimethylformamide and dimethylacetamide, the desorption temperature from clean Au(111) increases as the coverage de-

creases (data not shown). The lower temperature for dimethylformamide evolution on gold suggests that dimethylformamide formation may be more efficient than the formation of dimethylacetamide, which leads to relatively greater amounts of dimethlyformamide product than dimethylacetamide product under similar conditions.

The expected magnitude of any kinetic isotope effect on gold due to isotopic substitution of ^{18}O for ^{16}O is far to small to measure (~1 K), because of the small difference in the reduced mass upon substitution of ^{18}O. Furthermore, since the rate of evolution of dimethylacetamide is limited by desorption from Au, no kinetic isotope effect would be observed in any event.

Bibliography

[1] I Freestone, N Meeks, M Sax, and C Higgitt, Gold Bull. **40**, 270 (2007).

[2] S Padovani, D Puzzovio, C Sada, P Mazzoldi, I Borgia, A Sgamellotti, B G Brunetti, L Cartechini, F D'Acapito, C Maurizio, F Shokoui, P Oliaiy, J Rahighi, M Lamehi-Rachti, and E Pantos, Appl. Phys. A **83**, 521 (2006).

[3] R A Wigley, in *Noble Metals and Biological Systems: Their Role in Medicine, Mineral Exploration, and the Environment*, edited by R R Brooks (CRC Press, Boca Raton, 1992), p. 277.

[4] J M Thomas and W J Thomas, *Principles and Practice of Heterogeneous Catalysis* (VCH Publishers, Inc., New York, 1997).

[5] S Golunski, JOM **53**, 22 (2001).

[6] R Kneitsch, Pop. Sci. Monthly **61**, 24 (1902).

[7] Douglas K Louie, *Handbook of Sulphuric Acid Manufacturing* (DKL Engineering, Inc., Thornhill, 1961).

[8] J Kašpar, P Fornasiero, and N Hickey, Catal. Today **77**, 419 (2003).

[9] M. A. Barteau and R J Madix, J. Am. Chem. Soc. **105**, 344 (1983).

[10] I. E. Wachs and R J Madix, Surf. Sci. **76**, 531 (1978).

[11] I. E. Wachs and S R Kelemen, J. Catal. **71**, 78 (1981).

[12] A Andreasen, H Lynggaard, C Stegelmann, and P Stoltze, Riso National Laboratory 1 (2006).

[13] C Stegelmann, N C Schiodt, C T Campbell, and P Stoltze, J. Catal. **221**, 630 (2004).

[14] C Stegelmann and P Stoltze, Surf. Sci. **552**, 260 (2004).

[15] M Haruta, S Tsubota, T Kobayashi, and H Kageyama, J. Catal. **144**, 175 (1993).

[16] E Worrell, D Phylipsen, D Einstein, and N Martin, Technical report, Berkeley (unpublished).

[17] M S Reisch, C&EN **87**, 10 (2009).

[18] D Astruc, in *Nanoparticles and Catalysis*, edited by D Astruc (Wiley-VCH, Weinheim, 2008).

[19] B K Min and C. M. Friend, Chem. Rev. **107**, 2709 (2007).

[20] A Stephen K Hashmi and Graham J Hutchings, Angew. Chem. Int. Ed. **45**, 7896 (2006).

[21] C Della Pina, E Falletta, and M Rossi, in *Nanoparticles and Catalysis*, edited by Didier Astruc (Wiley-VCH, Weinheim, 2008).

[22] B Xu, X Liu, J Haubrich, R J Madix, and C. M. Friend, Angew. Chem. Int. Ed. **48**, 4206 (2009).

[23] X Liu, B Xu, J Haubrich, R J Madix, and C. M. Friend, J. Am. Chem. Soc. **131**, 5757 (2009).

[24] J Gong, T Yan, and C. B. Mullins, Chem. Commun. 761 (2009).

[25] H Kitahara and H Sakurai, Chem. Lett. **39**, 46 (2010).

[26] B Xu, R J Madix, and C. M. Friend, J. Am. Chem. Soc. **132**, 16571 (2010).

[27] B Xu, X Liu, J Haubrich, and C. M. Friend, Nat Chem **2**, 61 (2010).

[28] C Qi, Gold Bull. **41**, 224 (2008).

[29] X Deng and C. M. Friend, J. Am. Chem. Soc. **127**, 17178 (2005).

[30] X Deng, T A Baker, and C. M. Friend, Angew. Chem. Int. Ed. Engl. **45**, 7075 (2006).

[31] P A Redhead, Vacuum **12**, 203 (1962).

[32] D. A. King, Surf. Sci. **47**, 384 (1975).

[33] M K Weldon and Cynthia M Friend, Chem. Rev. **96**, 1391 (1996).

[34] J W Niemantsverdriet, *Spectroscopy in Catalysis: An Introduction*, second, completely revised edition ed. (Wiley-VCH, Weinheim, 2000).

[35] C J Chen, *Introduction to scanning tunneling microscopy* (Oxford University Press, New York, 1993).

[36] E Lundgren, G Kresse, C Klein, M Borg, J N Andersen, M De Santis, Y Gauthier, C Konvicka, M Schmid, and P Varga, Phys. Rev. Lett. **88**, 246103 (2002).

[37] S Devarajan, J Hinojosa, Jr, and J F Weaver, Surf. Sci. **602**, 3116 (2008).

[38] B K Min, A R Alemozafar, D Pinnaduwage, X Deng, and C. M. Friend, J. Phys. Chem. B **110**, 19833 (2006).

[39] B Hammer and J K Nørskov, Adv. Catal. **45**, 71 (2000).

[40] G Zheng and E I Altman, Surf. Sci. **462**, 151 (2000).

[41] J A Hinojosa, H H Kan, and J F Weaver, J. Phys. Chem. C **112**, 8324 (2008).

[42] A Klust and R J Madix, J. Chem. Phys. **126**, 084707 (2007).

[43] M Canepa, P Cantini, F Fossa, L Mattera, and S Terreni, Phys. Rev. B **47**, 15823 (1993).

[44] I. S. Nielsen, E Taarning, K Egeblad, R Madsen, and C. H. Christensen, Catal. Lett. **116**, 35 (2007).

[45] R J Angelici, J. Organomet. Chem. **693**, 847 (2008).

[46] N Saliba, D H Parker, and B E Koel, Surf. Sci. **410**, 270 (1998).

[47] J Wintterlin, S Volkening, T V W Janssens, T Zambelli, and G Ertl, Science **278**, 1931 (1997).

[48] S Jakubith, H H Rotermund, W Engel, A Von Oertzen, and G Ertl, Phys. Rev. Lett. **65**, 3013 (1990).

[49] K McCrea, J Parker, and G Somorjai, in *Surface Chemistry and Catalysis*, edited by A F Carley, P R Davies, G J Hutchings, and M S Spencer (Kluwer Academic/Plenum, New York, 2002).

[50] J T Roberts and R J Madix, J. Am. Chem. Soc. **110**, 8540 (1988).

[51] A C Lukaski and M. A. Barteau, Catal. Lett. **128**, 9 (2009).

[52] L Zhou and R J Madix, unpublish results .

[53] L Zhou and R J Madix, J. Phys. Chem. C **112**, 4725 (2008).

[54] L Zhou and R J Madix, Surf. Sci. **603**, 1751 (2009).

[55] T Hayashi, K Tanaka, and M Haruta, J. Catal. **178**, 566 (1998).

[56] R J Madix and J. T. Robers, *Surface Reactions*, *Springer Series in Surface Science* (Springer, Berlin, 1994).

[57] E Stuve and R Madix, Surf. Sci. **111**, 11 (1981).

[58] D. M. Thornburg and R J Madix, Surf. Sci. **226**, 61 (1990).

[59] D Thornburg and R Madix, Surf. Sci. **220**, 268 (1989).

[60] R G Quiller, T A Baker, X Deng, M E Colling, B K Min, and C. M. Friend, J. Chem. Phys. **129**, 064702 (2008).

[61] D Outka and R Madix, J. Am. Chem. Soc. **109**, 1708 (1987).

[62] X Deng, B K Min, A Guloy, and C. M. Friend, J. Am. Chem. Soc. **127**, 9267 (2005).

[63] X Deng, B K Min, X Liu, and C. M. Friend, J. Phys. Chem. B **110**, 15982 (2006).

[64] X Liu and C. M. Friend, Langmuir **26**, 16552 (2010).

[65] Bingjun Xu, Jan Haubrich, Cassandra G Freyschlag, Robert J Madix, and C. M. Friend, Chem. Sci. **1**, 310 (2010).

[66] B Jørgensen, S E Christiansen, M L D Thomsen, and C. H. Christensen, J. Catal. **251**, 332 (2007).

[67] A Wittstock, V Zielasek, J Biener, C. M. Friend, and M Bäumer, Science **327**, 319 (2010).

[68] C G F Siler, B Xu, R J Madix, and C. M. Friend, J. Am. Chem. Soc. **134**, 12604 (2012).

[69] B Xu, L Zhou, R J Madix, and Cynthia M Friend, Angew. Chem. Int. Ed. **49**, 394 (2010).

[70] L Zhou, C G Freyschlag, B Xu, C. M. Friend, and R J Madix, Chem. Commun. **46**, 704 (2010).

[71] T. Ishida and M Haruta, ChemSusChem **2**, 538 (2009).

[72] S. K. Klitgaard, K Egeblad, U. V. Mentzel, A. G. Popov, T Jensen, E Taarning, I. S. Nielsen, and C. H. Christensen, Green Chem. **10**, 419 (2008).

[73] M Daté, M Okumura, S Tsubota, and M Haruta, Angew. Chem. Int. Ed. **43**, 2129 (2004).

[74] Y Hao, M Mihaylov, E Ivanova, K Hadjiivanov, H Knözinger, and B C Gates, J. Catal. **261**, 137 (2009).

[75] M M Schubert, A Venugopal, M J Kahlich, V Plzak, and R J Behm, J. Catal. **222**, 32 (2004).

[76] M. A. Barteau, M Bowker, and R J Madix, J. Catal. **67**, 118 (1981).

[77] B Xu, J Haubrich, T A Baker, E Kaxiras, and C. M. Friend, J. Phys. Chem. C **115**, 3703 (2011).

[78] J Gong and C. B. Mullins, Acc. Chem. Res. **42**, 1063 (2009).

[79] X Liu, L He, Y-M Liu, and Y Cao, Acc. Chem. Res. **47**, 793 (2014).

[80] A K Sinha, S Seelan, S Tsubota, and M Haruta, Top. Catal. **29**, 95 (2004).

[81] E Taarning and C. H. Christensen, Chim. Oggi **25**, 70 (2007).

[82] T. Ishida, N Kinoshita, H Okatsu, T Akita, T Takei, and M Haruta, Angew. Chem. **120**, 9405 (2008).

[83] B Xu, R J Madix, and C. M. Friend, J. Am. Chem. Soc. **133**, 20378 (2011).

[84] J-F Soule, H Miyamura, and S Kobayashi, J. Am. Chem. Soc. **133**, 18550 (2011).

[85] B Xu, R J Madix, and C. M. Friend, Chem. - Eur. J. **18**, 2313 (2012).

[86] L He, X-B Lou, J Ni, Y-M Liu, Y Cao, H-Y He, and K-N Fan, Chem. - Eur. J. **16**, 13965 (2010).

[87] X Liu, R J Madix, and C. M. Friend, Chem. Soc. Rev. **37**, 2243 (2008).

[88] R J Madix and J. T. Robers, in *Surface Reactions*, edited by R J Madix (Springer, Berlin, 1994), Vol. 34.

[89] B N Zope, D D Hibbitts, M Neurock, and R J Davis, Science **330**, 74 (2010).

[90] Xiaoying Liu, Thomas A Baker, and Cynthia M Friend, Dalton Trans **39**, 8521 (2010).

[91] Daniel Torres, Nuria Lopez, Francesc Illas, and Richard M Lambert, Angew. Chem. Int. Ed. Engl. **46**, 2055 (2007).

[92] Robert L Brainard and Robert J Madix, J. Am. Chem. Soc. **111**, 3826 (1989).

[93] Thomas A Baker, Bingjun Xu, Xiaoying Liu, Efthimios Kaxiras, and Cynthia A Friend, J. Phys. Chem. C **113**, 16561 (2009).

[94] R J Madix and S. G. Telford, Surf. Sci. **328**, L576 (1995).

[95] M Yata and R J Madix, Surf. Sci. **328**, 171 (1995).

[96] M. A. Barteau, M Bowker, and R J Madix, Surf. Sci. **94**, 303 (1980).

[97] A Sault and R Madix, Surf. Sci. **172**, 598 (1986).

[98] Robert L Brainard and Robert J Madix, J. Am. Chem. Soc. **109**, 8082 (1987).

[99] Robert L Brainard and Robert J Madix, Surf. Sci. **214**, 396 (1989).

[100] Robert J Madix, Surf. Sci. **299-300**, 785 (1994).

[101] Jiahui Huang, Tomoki Akita, Jérémy Faye, Tadahiro Fujitani, Takashi Takei, and Masatake Haruta, Angew. Chem. Int. Ed. **48**, 7862 (2009).

[102] Cristina Della Pina, Ermelinda Falletta, and Michele Rossi, J. Catal. **260**, 384 (2008).

[103] Juan Carlos F Rodríguez-Reyes, Cynthia M Friend, and Robert J Madix, Surf. Sci. **606**, 1129 (2012).

[104] Claus H Christensen, Betina Jørgensen, Jeppe Rass-Hansen, Kresten Egeblad, Robert Madsen, Søren K Klitgaard, Stine M Hansen, Mike R Hansen, Hans C Andersen, and Anders Riisager, Angew. Chem. Int. Ed. **45**, 4648 (2006).

[105] Takashi Takei, Norihiko Iguchi, and Masatake Haruta, Catal. Surv. Asia **15**, 80 (2011).

[106] Silvio Carrettin, Paul McMorn, P Johnston, Ken Griffin, Christopher J Kiely, Gary A Attard, and Graham J Hutchings, Top. Catal. **27**, 131 (2004).

[107] Laura Prati and Michele Rossi, J. Catal. **176**, 552 (1998).

[108] C Bianchi, F Porta, L Prati, and M Rossi, Top. Catal. **13**, 231 (2000).

[109] Bolin Zhu, M Lazar, BG Trewyn, and RJ Angelici, J. Catal. **260**, 1 (2008).

[110] Peng Liu, Can Li, and Emiel J M Hensen, Chem. - Eur. J. **18**, 12122 (2012).

[111] Man Ho So, Yungen Liu, Chi Ming Ho, and Chi Ming Che, Chem. - Asian J. **4**, 1551 (2009).

[112] Bolin Zhu and Robert J Angelici, Chem. Commun. **0**, 2157 (2007).

[113] Kathryn M Kosuda, Arne Wittstock, Cynthia M Friend, and Marcus Bäumer, Angew. Chem. Int. Ed. **51**, 1698 (2012).

[114] Shinya Tanaka, Taketoshi Minato, Eisuke Ito, Masahiko Hara, Yousoo Kim, Yoshinori Yamamoto, and Naoki Asao, Chem. - Eur. J. **19**, 11832 (2013).

[115] Bingjun Xu, Robert J Madix, and Cynthia M Friend, Acc. Chem. Res. **47**, 761 (2014).

[116] K J Stowers, R J Madix, and C. M. Friend, J. Catal. **308**, 131 (2013).

[117] Duane A Outka and R J Madix, Surf. Sci. **179**, 361 (1987).

[118] Jinlong Gong and C Buddie Mullins, J. Am. Chem. Soc. **130**, 16458 (2008).

[119] T Cremer, CGF Siler, J C Rodriguez-Reyes, C. M. Friend, and R J Madix, J. Phys. Chem. Lett. **5**, 1126 (2014).

[120] DHS Ying and R J Madix, J. Catal. **61**, 48 (1980).

[121] DHS Ying and R J Madix, J. Catal. **60**, 441 (1979).

[122] Jeffrey G Forbes and Andrew J Gellman, J. Am. Chem. Soc. **115**, 6277 (1993).

[123] Brian E Bent, Ralph G Nuzzo, and Lawrence H Dubois, J. Am. Chem. Soc. **111**, 1634 (1989).

[124] Bingjun Xu, Robert J Madix, and Cynthia M Friend, Phys. Chem. Chem. Phys. **15**, 3179 (2013).

[125] A M Paul and B E Bent, J. Catal. **147**, 264 (1994).

[126] Ilona Kretzschmar, Joshua A Levinson, and Cynthia M Friend, J. Am. Chem. Soc. **122**, 12395 (2000).

[127] Alexis T Bell, B C Gates, and Douglas Ray, U.S. Department of Energy Report 1 (2008).

[128] B Xu and C. M. Friend, Farad. Discuss. **152**, 307 (2011).

[129] M. A. Barteau and R J Madix, Surf. Sci. **120**, 262 (1982).

[130] Victor G Ruiz, Wei Liu, Egbert Zojer, Matthias Scheffler, and Alexandre Tkatchenko, Phys. Rev. Lett. **108**, 146103 (2012).

[131] Alexandre Tkatchenko and Matthias Scheffler, Phys. Rev. Lett. **102**, 073005 (2009).

[132] E M Lifshitz, Soviet Physics- JETP **2**, 73 (1956).

[133] E Zaremba and W Kohn, Phys. Rev. B **13**, 2270 (1976).

[134] JP Perdew, K Burke, and M Ernzerhof, Phys. Rev. Lett. **77**, 3865 (1996).

[135] Volker Blum, Ralf Gehrke, Felix Hanke, Paula Havu, Ville Havu, Xinguo Ren, Karsten Reuter, and Matthias Scheffler, Comput. Phys. Commun. **180**, 2175 (2009).

[136] E van Lenthe, E J Baerends, and J G Snijders, J. Chem. Phys. **101**, 9783 (1994).

[137] M Mautner, in *Ion Thermochemistry Data*, *NIST Chemistry WebBook, NIST Standard Reference Database Number 69*, edited by P J Linstrom and W G Mallard (National Institute of Standards and Technology, Gaithersburg, YEAR).

[138] Yu-Ran Luo, *Comprehensive Handbook of Chemical Bond Energies* (CRC Press, Boca Raton, 2007).

[139] Eric M Karp, Trent L Silbaugh, and Charles T Campbell, J. Am. Chem. Soc. **136**, 4137 (2014).

[140] John I Brauman and Larry K Blair, J. Am. Chem. Soc. **92**, 5986 (1970).

[141] Alexandre Tkatchenko, Lorenz Romaner, Oliver T Hofmann, Egbert Zojer, Claudia Ambrosch-Draxl, and Matthias Scheffler, MRS Bull. **35**, 435 (2010).

[142] O Anatole von Lilienfeld and Alexandre Tkatchenko, J. Chem. Phys. **132**, 234109 (2010).

[143] Frank Abild-Pedersen, Jeff Greeley, F Studt, J Rossmeisl, T R Munter, P G Moses, E Skulason, T Bligaard, and J K Nørskov, Phys. Rev. Lett. **99**, 016105 (2007).

[144] J K Nørskov, F Abild-Pedersen, F Studt, and T Bligaard, Proc. Natl. Acad. Sci. **108**, 937 (2011).

[145] MA Barteau and RJ Madix, Surf. Sci. **115**, 355 (1982).

[146] T J Wallington, W F Schneider, D R Worsnop, O J Nielsen, J Sehested, W J Debruyn, and J A Shorter, Environmental science & technology **28**, 320A (1994).

[147] Makroni Lily, Dipankar Sutradhar, and Asit K Chandra, Comput. Theor. Chem. **1022**, 50 (2013).

[148] Ying Wang, Jing-Yao Liu, Ze-Sheng Li, Li Wang, and Chia-Chung Sun, J. Comput. Chem. **28**, 802 (2007).

[149] Leo E Manzer, Catal. Today **18**, 199 (1993).

[150] John M Humphrey and A Richard Chamberlin, Chem. Rev. **97**, 2243 (1997).

[151] Richard C Larock, *Comprehensive Organic Transformations*, 2nd ed. (Wiley-VCH, New York, 1999).

[152] E. Saxon and C. R. Bertozzi, Science **287**, 2007 (2000).

[153] M. Beller, B. Cornils, C. D. Frohning, and C. W. Kohlpaintner, J Mol Catal A **104**, 17 (1995).

[154] Chennan Ramalingan and Yong-Tae Park, The Journal of Organic Chemistry **72**, 4536 (2007).

[155] Yoshitaka Uenoyama, Takahide Fukuyama, Osamu Nobuta, Hiroshi Matsubara, and Ilhyong Ryu, Angew. Chem. Int. Ed. Engl. **44**, 1075 (2005).

[156] M. B. Smith, *Compendium of Organic Synthetic Methods* (Wiley, New York, 2001), Vol. 9.

[157] C Gunanathan, Y Ben-David, and D. Milstein, Science **317**, 790 (2007).

[158] Lars Ulrik Nordstrøm, Henning Vogt, and Robert Madsen, J. Am. Chem. Soc. **130**, 17672 (2008).

[159] W. J. Yoo and C. J. Li, J. Am. Chem. Soc. **128**, 13064 (2006).

[160] SungYong Seo and Tobin J Marks, Org. Lett **10**, 317 (2008).

[161] Xing-Cai Guo and Robert J Madix, J. Phys. Chem. B **105**, 3878 (2001).

[162] J Schnadt, J Knudsen, X L Hu, A Michaelides, R T Vang, Karsten Reuter, Zheshen Li, Erik Lægsgaard, M Scheffler, and F Besenbacher, Phys. Rev. B **80**, 075424 (2009).

[163] I. E. Wachs and R J Madix, Appl. Surf. Sci. (1977-1985) **5**, 426 (1980).

[164] W. S. Sim, P Gardner, and D. A. King, J Phys Chem **99**, 16002 (1995).

[165] G Scott Jones, Mark A Barteau, and John M Vohs, J. Phys. Chem. B **103**, 1144 (1999).

[166] GS Jones, MA Barteau, and JM Vohs, Surf. Sci. **420**, 65 (1999).

[167] Chuan-Bao Wang, Goutam Deo, and Israel E Wachs, J. Phys. Chem. B **103**, 5645 (1999).

[168] A. J. Capote and R J Madix, J. Am. Chem. Soc. **111**, 3570 (1989).

[169] W. S. Sim, P Gardner, and D. A. King, The Journal of Physical Chemistry **99**, 16002 (1995).

[170] Israel E Wachs, Surf. Sci. **544**, 1 (2003).

[171] A Andreasen, H Lynggaard, C Stegelmann, and P Stoltze, Surf. Sci. **544**, 5 (2003).

[172] B Xu, C. M. Friend, and R J Madix, Farad. Discuss. **152**, 241 (2011).

[173] Z Li, J Xu, X Gu, K Wang, W Wang, X Zhang, Z Zhang, and Y Ding, ChemCatChem **5**, 1705 (2013).

[174] Ken-ichi Shimizu, Keiichiro Ohshima, and Atsushi Satsuma, Chem. - Eur. J. **15**, 9977 (2009).

[175] M Haruta, N Yamada, and T Kobayashi, J. Catal. **115**, 301 (1989).

[176] Y Lei, F Mehmood, S Lee, J Greeley, B Lee, S Seifert, R E Winans, J W Elam, R J Meyer, P C Redfern, D Teschner, R Schlögl, M J Pellin, L A Curtiss, and S Vajda, Science **328**, 224 (2010).

[177] E M Stuve, R J Madix, and B A Sexton, Surf. Sci. **119**, 279 (1982).

[178] Matthew S Ide and Robert J Davis, Acc. Chem. Res. (2013).

[179] E Stuve, S Jorgensen, and R Madix, Surf. Sci. **146**, 179 (1984).

[180] Scott W Jorgensen, A G Sault, and Robert J Madix, Langmuir **1**, 526 (2001).

[181] Zhen-Ming Hu and Hiroshi Nakatsuji, Surf. Sci. **425**, 296 (1999).

[182] L Savio, M Smerieri, L Vattuone, and A Gussoni, Phys. Rev. B 235412 (2006).

[183] K Bange, T E Madey, J K Sass, and E M Stuve, Surf. Sci. **183**, 334 (1987).

[184] K Bange, T E Madey, and J K Sass, Surf. Sci. **152**, 550 (1985).

[185] M Canepa, L Mattera, and E Narducci, Surf. Sci. **371**, 431 (1997).

[186] M Canepa, P Cantini, E Narducci, M Salvietti, and S Terreni, Surf. Sci. **343**, 176 (1995).

[187] M Borbach, W Stenzel, H Conrad, and A M Bradshaw, Surf. Sci. **337-339**, 796 (1997).

[188] L Guillemot and K Bobrov, Surf. Sci. **601**, 871 (2007).

[189] M Henderson, Surf. Sci. Rep. **46**, 1 (2002).

[190] J T Ranney, S R Bare, and J L Gland, Catal Lett **48**, 25 (1997).

[191] Andrzej Wieckowski and Matthew Neurock, Advances in Physical Chemistry **2011**, 1 (2011).

[192] Christian A G N Montalbetti and Virginie Falque, Tetrahedron **61**, 10827 (2005).

[193] Takato Mitsudome, Yusuke Mikami, Haruhiko Mori, Shusuke Arita, Tomoo Mizugaki, Kochiro Jitsukawa, and Kiyotomi Kaneda, Chem. Commun. **22**, 3258 (2009).

[194] Wei Wei, Xiao-Yu Hu, Xiao-Wei Yan, Qiang Zhang, Ming Cheng, and Jian-Xin Ji, Chem. Commun. **48**, 305 (2012).

[195] Gunther Reuss, Walter Disteldorf, Armin Otto Gamer, and Albrecht Hilt, Ullmann's Encyclopedia of Industrial Chemistry 1 (2009).

[196] C Della Pina, E Falletta, and M Rossi, Chem. Soc. Rev. **41**, 350 (2012).

[197] Tamao Ishida, Noriko Kawakita, Tomoki Akita, and Masatake Haruta, Gold Bull. **42**, 267 (2009).

[198] K Shimizu, M Nishimura, and A Satsuma, ChemCatChem **1**, 497 (2009).

[199] K Shimizu, R Sato, and Atsushi Satsuma, Angew. Chem. Int. Ed. **48**, 3982 (2009).

[200] Simon R Bare, K Griffiths, W N Lennard, and H T Tang, Surf. Sci. **342**, 185 (1995).

[201] Cassandra G F Siler, Joshua Klobas, Cynthia M Friend, and Robert J Madix (unpublished).

[202] Cassandra G Freyschlag and Robert J Madix, Mat. Today **14**, 134 (2011).

[203] Jinlong Gong, Rotimi A Ojifinni, Tae S Kim, John M White, and C Buddie Mullins, J. Am. Chem. Soc. **128**, 9012 (2006).

[204] I Wachs and R Madix, Appl. Surf. Sci. **1**, 303 (1978).

[205] B Hammer and JK Nørskov, Nature **376**, 238 (1995).

[206] Velliyur N M Rao and George E Heinsohn, Multi-stage process with adiabatic reactors for the preparation of isocyanates, US Patent, 1985.

[207] Robert W Layer, Chem. Rev. **63**, 489 (1963).

[208] Niko S Radulović, Ana B Miltojević, and Rastko D Vukićević, Comptes Rendus Chimie **16**, 257 (2013).

[209] Stephen F Martin, Pure Appl. Chem. **81**, 195 (2009).

[210] Hugo Schiff, Annalen der Chemie und Pharmacie **131**, 118 (1864).

[211] Asit K Chakraborti, Srikant Bhagat, and Santosh Rudrawar, Tetrahedron Letters **45**, 7641 (2004).

[212] Maurizio Dal Colle, Giuseppe Distefano, Derek Jones, Andrea Guerrino, Giancarlo Seconi, and Alberto Modelli, Journal of the Chemical Society, Perkin Transactions 2 789 (1994).

[213] K V L N Sastry and R F Curl, J. Chem. Phys. **41**, 77 (1964).

[214] Y G Lazarou and P Papagiannakopolous, J Phys Chem **97**, 4468 (1993).

[215] ĐŠ ĐŠak, N W Larsen, and H Svanholt, Acta Chem. Scand. A **31**, 755 (1977).

[216] J C Guillemin and J M Denis, J. Chem Soc, Chem Commun 951 (1985).

[217] Pallava Bagla, Science **329**, 19 (2010).

[218] C I Carlisle, T Fujimoto, W. S. Sim, and D. A. King, Surf. Sci. **470**, 15 (2000).

[219] R Reichelt, S Günther, M Rössler, J Wintterlin, B Kubias, B Jakobi, and R Schlögl, Phys Chem Chem Phys **9**, 3590 (2007).

[220] Alois Fürstner, Acc. Chem. Res. **47**, 925 (2014).

[221] Jinhai Wang, Xinhua Xu, Jingfa Deng, Yuanyan Liao, and Bifeng Hong, Appl. Surf. Sci. **120**, 99 (1997).

[222] Bao Xinhe, Deng Jingfa, Zhai Runsheng, Wang Dezheng, and Guo Xiexian, Catal Lett **4**, 25 (1990).

[223] T E Felter, W H Weinberg, G Ya Lastushkina, P A Zhdan, G K Boreskov, and J Hrbek, Appl. Surf. Sci. (1977-1985) **16**, 351 (1983).

[224] B Xinhe and D Jingfa, J. Catal. **99**, 391 (1986).

[225] K Bange, T E Madey, and J K Sass, Chem Phys Lett **113**, 56 (1985).

[226] J Hudson, Z F Weng, C Vallance, and P W Harland, Int. J. Mass Spectrom. **248**, 42 (2006).

[227] B K Min, A R Alemozafar, M M Biener, J Biener, and C. M. Friend, Top. Catal. **36**, 77 (2005).